

Paleoceanography and Paleoclimatology
















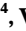
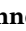

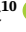
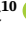

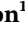
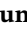
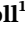

RESEARCH ARTICLE

10.1029/2020PA004037

Special Section:

The Miocene: The Future of the Past

The Miocene: The Future of the Past

M. Steinthorsdottir^{1,2} , H. K. Coxall^{2,3} , A. M. de Boer^{2,3} , M. Huber⁴ , N. Barbolini^{2,5} , C. D. Bradshaw^{6,7} , N. J. Burls⁸ , S. J. Feakins⁹ , E. Gasson¹⁰ , J. Henderiks¹¹ , A. E. Holbourn¹² , S. Kiel^{1,2} , M. J. Kohn¹³ , G. Knorr¹⁴ , W. M. Kürschner¹⁵ , C. H. Lear¹⁶ , D. Liebrand¹⁷ , D. J. Lunt¹⁰ , T. Mörs^{1,2} , P. N. Pearson¹⁶ , M. J. Pound¹⁸ , H. Stoll¹⁹ , and C. A. E. Strömberg²⁰ 

Key Points:

- Miocene floras, faunas, and paleogeography were similar to today and provide plausible analogs for future climatic warming
- The Miocene saw great dynamism in biotic and climate systems, but the reasons for these shifts are still not well understood
- The $p\text{CO}_2$ -temperature-ice relationships during major Miocene climate oscillations and transitions warrant further research

Supporting Information:

Supporting Information may be found in the online version of this article.

Correspondence to:

M. Steinthorsdottir,
margret.steinthorsdottir@nrm.se

Citation:

Steinthorsdottir, M., Coxall, H. K., de Boer, A. M., Huber, M., Barbolini, N., Bradshaw, C. D., et al. (2021). The Miocene: The future of the past. *Paleoceanography and Paleoclimatology*, 36, e2020PA004037. <https://doi.org/10.1029/2020PA004037>

Received 4 JUL 2020

Accepted 17 DEC 2020

¹Department of Palaeobiology, Swedish Museum of Natural History, Stockholm, Sweden, ²Bolin Centre for Climate Research, Stockholm University, Stockholm, Sweden, ³Department of Geological Sciences, Stockholm University, Stockholm, Sweden, ⁴Department of Earth, Atmospheric and Planetary Sciences, Purdue University, West Lafayette, IN, USA, ⁵Department of Ecology, Environment and Plant Sciences, Stockholm University, Stockholm, Sweden, ⁶The Global Systems Institute, University of Exeter, Exeter, UK, ⁷Met Office Hadley Centre, Exeter, UK, ⁸Department of Atmospheric, Oceanic and Earth Sciences and the Center for Ocean-Land-Atmosphere Studies, George Mason University, Fairfax, VA, USA, ⁹Department of Earth Sciences, University of Southern California, Los Angeles, CA, USA, ¹⁰School of Geographical Sciences, University of Bristol, Bristol, UK, ¹¹Department of Earth Sciences, Uppsala University, Uppsala, Sweden, ¹²Institute of Geosciences, Christian-Albrechts-University, Kiel, Germany, ¹³Department of Geosciences, Boise State University, Boise, ID, USA, ¹⁴Alfred Wegener Institute Helmholtz Centre for Polar and Marine Research, Bremerhaven, Germany, ¹⁵Department of Geoscience, University of Oslo, Oslo, Norway, ¹⁶School of Earth and Ocean Sciences, Cardiff University, Cardiff, UK, ¹⁷MARUM – Center for Marine and Environmental Sciences, University of Bremen, Bremen, Germany, ¹⁸Department of Geography and Environmental Sciences, Northumbria University, Newcastle upon Tyne, UK, ¹⁹Earth Science Department, ETH Zürich, Zürich, Switzerland, ²⁰Department of Biology and Burke Museum of Natural History and Culture, University of Washington, Seattle, WA, USA

Abstract The Miocene epoch (23.03–5.33 Ma) was a time interval of global warmth, relative to today. Continental configurations and mountain topography transitioned toward modern conditions, and many flora and fauna evolved into the same taxa that exist today. Miocene climate was dynamic: long periods of early and late glaciation bracketed a ~ 2 Myr greenhouse interval—the Miocene Climatic Optimum (MCO). Floras, faunas, ice sheets, precipitation, $p\text{CO}_2$, and ocean and atmospheric circulation mostly (but not ubiquitously) covaried with these large changes in climate. With higher temperatures and moderately higher $p\text{CO}_2$ (~ 400 – 600 ppm), the MCO has been suggested as a particularly appropriate analog for future climate scenarios, and for assessing the predictive accuracy of numerical climate models—the same models that are used to simulate future climate. Yet, Miocene conditions have proved difficult to reconcile with models. This implies either missing positive feedbacks in the models, a lack of knowledge of past climate forcings, or the need for re-interpretation of proxies, which might mitigate the model-data discrepancy. Our understanding of Miocene climatic, biogeochemical, and oceanic changes on broad spatial and temporal scales is still developing. New records documenting the physical, chemical, and biotic aspects of the Earth system are emerging, and together provide a more comprehensive understanding of this important time interval. Here, we review the state-of-the-art in Miocene climate, ocean circulation, biogeochemical cycling, ice sheet dynamics, and biotic adaptation research as inferred through proxy observations and modeling studies.

Plain Language Summary During the Miocene time period (~ 23 – 5 million years ago), Planet Earth looked similar to today, with some important differences: the climate was generally warmer and highly variable, while atmospheric CO_2 was not much higher. Continental-sized ice sheets were only present on Antarctica, but not in the northern hemisphere. The continents drifted to near their modern-day positions, and plants and animals evolved into the many (near) modern species. Scientists study the Miocene because present-day and projected future CO_2 levels are in the same range as those reconstructed for the Miocene. Therefore, if we can understand climate changes and their biotic responses from the Miocene past, we are able to better predict current and future global changes. By comparing Miocene climate reconstructions from fossil and chemical data to climate simulations produced by computer models, scientists are able to test their understanding of the Earth system under higher CO_2 and warmer conditions than those of today. This helps in constraining future warming scenarios for the coming

© 2020. The Authors.

This is an open access article under the terms of the [Creative Commons Attribution-NonCommercial-NoDerivs License](https://creativecommons.org/licenses/by-nc-nd/4.0/), which permits use and distribution in any medium, provided the original work is properly cited, the use is non-commercial and no modifications or adaptations are made.

decades. In this study, we summarize the current understanding of the Miocene world from data and models. We also identify gaps in our understanding that need further research attention in the future.

1. Introduction

1.1. The Case for the Miocene as a Future Climate Analog

Study of pre-Quaternary warm climates using geological records and computer simulations is an important avenue for understanding the environmental changes humanity faces in our warming future. Focus has often been on the (1) strong greenhouse climate of the early Eocene (~50 Ma) when atmospheric concentration of CO₂ ($p\text{CO}_2$) was highly elevated (>1,000 ppm) and global mean temperatures ~13°C warmer than today (Burke et al., 2018; Caballero & Huber, 2013; Inglis et al., 2020), and (2) the chronologically closer mid Pliocene Warm Period (PWP) (3.3–3 Ma), characterized by now sub-modern $p\text{CO}_2$ (~400 ppm), with average global warming of 2°C–3°C (Burke et al., 2018; Pagani et al., 2010). Different continental positions, as well as vegetation and fauna, make the much older Eocene an imperfect future analog, while $p\text{CO}_2$ of the mid Pliocene has already been surpassed ($p\text{CO}_2$ measured at Mona Loa reached 416 ppm at time of writing, see: <https://www.co2.earth/daily-co2>), with PWP-like climates predicted as soon as 2030 (Burke et al., 2018). Realistically, a middle Pliocene climate state is a near-future “best-case scenario”—modeling predicts that Pliocene-like climates could persist if emissions-reducing climate stabilization scenarios are implemented (Burke et al., 2018). This is possible only if societies succeed in meeting targets set out under the Paris Agreement, that is, to limit Earth's anthropogenic temperature anomaly to 1.5°C–2°C (Schellnhuber et al., 2016), which seems unlikely at present. More pessimistic scenarios of unmitigated greenhouse gas emissions quickly move us beyond the Pliocene state (Burke et al., 2018), pushing Earth's systems into a potentially vulnerable position where many of its “tippable” subsystems such as glaciers, sea ice, forest biomes, deserts and coral reefs will be permanently destabilized (Schellnhuber et al., 2016). Here an “intermediate” deep-time climate analog, where boundary conditions are close to modern but extreme climate changes occurred, is therefore of great interest. Recently the Miocene, and perhaps in particular the Miocene Climatic Optimum (MCO, ~16.9–14.7 Ma), has emerged as a strong candidate to serve as a future climate analog.

The range of $p\text{CO}_2$ and temperature for the Pliocene corresponds to the equilibrium climate associated with low emission future climate change scenarios such as the IPCC's Representative Concentration Pathway (RCP) of 2.6, whereas the Miocene, with a somewhat higher range of $p\text{CO}_2$ and higher estimated temperatures and sea level, spans the middle range of predicted climate states (3°C–7°C), with warming corresponding to emissions scenarios such as RCP 4.5 to RCP 6.0 (Collins et al., 2013). High range scenarios, such as RCP 8.5, formerly referred to as “business-as-usual,” appear to be less likely than once thought (Hausfather & Peters, 2020). Therefore, while no paleoclimate is the perfect analog for the future, and much can be learned by studying any period in Earth's history, there is a greater likelihood that the equilibrium future climate state will bear more in common with the Miocene than with either the Pliocene or the Eocene.

During the Miocene, including the MCO, most proxy records indicate that $p\text{CO}_2$ was near or moderately higher than modern values (Beerling & Royer, 2011; Foster et al., 2012; Sossdian et al., 2020; Steinthorsdottir et al., 2020; Super et al., 2018; Y. G. Zhang, Pagani, et al., 2013), while a host of terrestrial (Böhme, 2003; Markwick, 2007; M. J. Pound et al., 2012; Reichgelt et al., 2013; Utescher et al., 2011; Wan et al., 2009) and marine paleotemperature proxies (Lear et al., 2000; You et al., 2009; Y. G. Zhang, Pagani, et al., 2013; Y. G. Zhang et al., 2014) demonstrate a level of pervasive global warmth, sometimes unmatched since the Eocene. The MCO was ~7°C–8°C warmer than the modern world and no Miocene climate model simulation has so far reproduced that kind of warmth at less than 800 ppm, considerably higher than reconstructed $p\text{CO}_2$ (Goldner et al., 2014a). More broadly, the middle Miocene (17–11 Ma), encompasses both the MCO and a subsequent abrupt cooling and a phase of Antarctic ice-sheet expansion, termed the Middle Miocene Climate Transition (MMCT; 14.7–13.8 Ma), which appears to be associated with relatively small (~50–125 ppm) variations in $p\text{CO}_2$ (Badger et al., 2013; Super et al., 2018), although see Sossdian et al. (2018). It is possible that understanding of important physical parameters is missing to explain how these climate trends and transitions are related to these reconstructed $p\text{CO}_2$ changes. Alternatively, the climate system and carbon cycle could have been more decoupled than previously thought possible (LaRiviere et al., 2012; Pagani

et al., 1999; Shevenell et al., 2004). Such a strong decoupling has been proposed for the Pliocene, causing other, currently poorly constrained, factors to have dominated climate and environmental change. Changes in tropical monsoonal precipitation and weathering regimes and resulting nutrient and alkalinity fluxes to the global ocean likely played a fundamental role in setting internal boundary conditions for climate variability. In addition, variations in the equator to pole temperature gradient affecting atmospheric and oceanic circulation regimes would have a major impact on the marine and terrestrial carbon cycles. Answering these questions requires a whole Earth system approach where the host of possible agents and interactions with the physical, chemical, and biological components are considered. For example, applying multiple, integrating proxies for inferring paleovegetation and terrestrial climate and expanding the sampling to a broader geographic coverage is vital for constraining and testing climate models that hindcast the regional manifestation of Miocene warmth. In this review and associated special collection of papers (The Miocene: The Future of the Past), the aim is to provide such an integrative framework.

1.2. Scope of Review

This review and the associated special collection of papers grew out of two workshops (held in 2018 and 2019 in Stockholm, Sweden) that brought together an international community of researchers working on the Miocene, consisting mostly of paleoceanographers, paleontologists, geologists, and modelers. It became clear that great progress has been made in recent years, in recovering new archives, generating high-quality observational data, and simulating Miocene climates. Moreover, chronological control of the Miocene stratigraphic record is increasingly robust, allowing interrogation of the extremes and (sub)orbital-scale variability associated with Miocene dynamism at a sophisticated level. One long-term goal that emerged from this community effort was to formally evaluate the Miocene as a future warm climate analog, but furtherance of that goal requires expanded and deepened coordination of past, current, and future research on the Miocene. As one component of that effort, here we review the main accomplishments and insights gained since some of the earlier comprehensive reviews of the Miocene or parts thereof (e.g., Boyd et al., 2018; Edwards et al., 2010; Fortelius et al., 2003; Herbert et al. 2016; Janis et al., 1993; Kennett, 1985; Lyle et al., 2008; Pound et al., 2012; Shevenell et al., 2008; Strömberg, 2011). Our aim is to place what we know about the long term, broad-scale evolution of the global Miocene system in context of key scientific questions that are currently (at least partially) answered as well as those that remain unanswered to date.

The review begins with an introduction to Miocene stratigraphy, chronology, and event-related terminology (Section 2). An important part of this is the high-resolution framework provided by orbitally resolved, mostly marine sediment records that allow ticker-tape-like counting of well-defined orbital cycles for improving dating, as well as documenting Earth's environmental response to external forcings by incoming solar radiation (insolation). Section 3 sets out current understanding of Miocene tectonics and paleogeography, including topography, erosional history, as well as ocean gateways that impacted atmospheric and ocean circulation. Summaries of important marine (Section 4) and terrestrial (Section 5) biota and ecosystems follow. The next two sections deal with observational data on Miocene climate and environmental change from marine (Section 6) and terrestrial (Section 7) records, while Section 8 reviews proxy data used to trace changes in the carbon system, including progress in reconstructing atmospheric $p\text{CO}_2$. Perspectives on changes in terrestrial ice volume, including ice-sheet modeling, are gathered in Section 9. Section 10 reviews evidence for the state of ocean meridional overturning circulation (MOC) as inferred from proxies. Section 11 gives a comprehensive overview of the results of Miocene modeling, including global mean climate states and ocean circulation, with a closer inspection of sensitivity studies that explore the role of nonmodern abiotic and biotic forcing factors on the Miocene climate, including orbits, paleogeography, $p\text{CO}_2$, ice, and vegetation. The final section (Section 12: Conclusions), summarizes state-of-the-art Miocene research, including a list of some of the important unanswered Miocene climate questions for future directions. Throughout the review, we refer to the synthesis figure (Figure 1), which presents an overview of Neogene changes in physical, geochemical and biological systems, relevant to Miocene climate development. It provides a chronology, the stratigraphic framework and list of climate-event terms used, as well as the full Neogene $\delta^{18}\text{O}$ isotopic stratigraphy and current "best-estimate" $p\text{CO}_2$ curves from marine proxies and terrestrial stomatal densities, all of which are important for placing the Miocene in a wider Cenozoic context. Additional focused figures are associated with several of the paper sections.

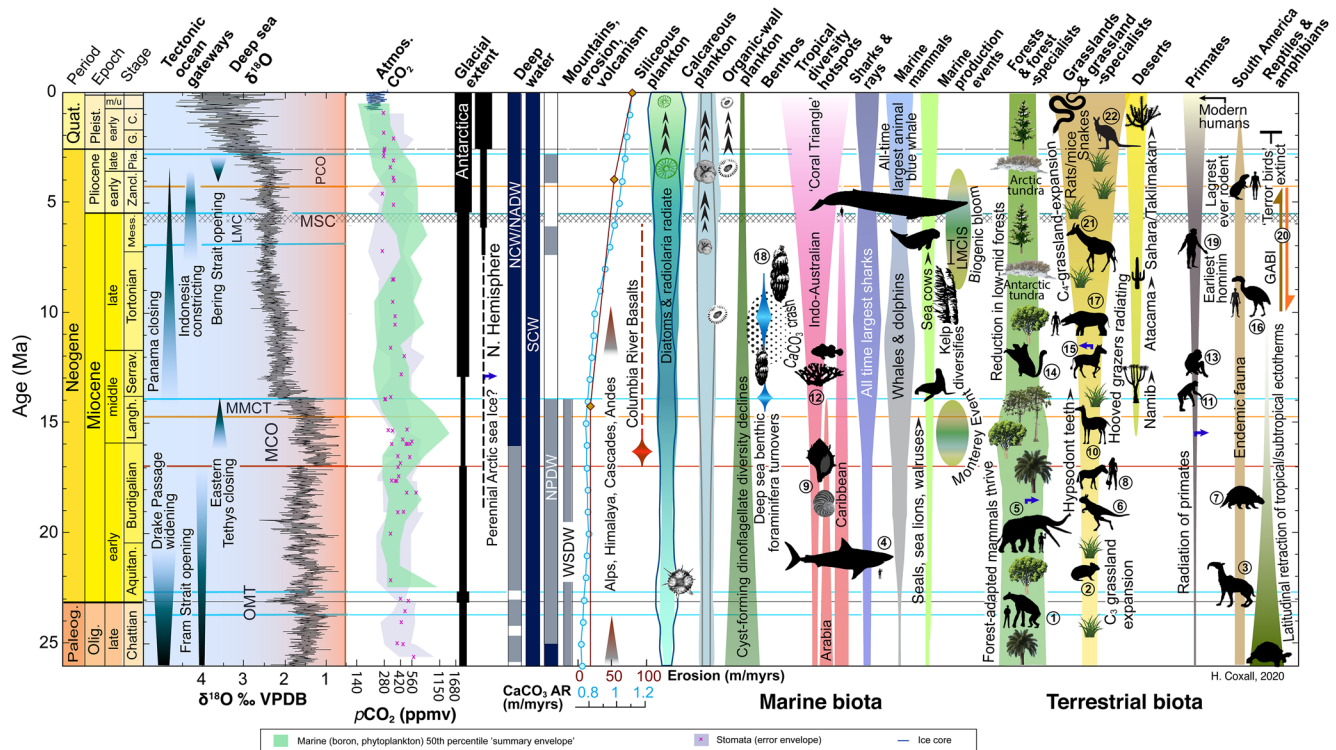


Figure 1. Miocene climatic, oceanic and tectonic changes and selected biotic developments, as summarized in this study. Stratigraphic divisions after Cohen et al. (2013, updated 2020). $\delta^{18}\text{O}$ = the “mega-splice” of De Vleeschouwer et al. (2017), provides a chemo-stratigraphic framework for identifying ocean-climate patterns, including (but not limited to) changes in deep ocean temperature and ice volume. Glacial extent = representation of mean glacial conditions across time (highly qualitative), dashed bars imply intermittent, or very small ice sheets. Summary proxy atmospheric CO_2 envelopes from marine (Sosdian et al., 2018; Stoll et al., 2019; Super et al., 2018, from two ODP sites) and stomata records; Beerling et al. (2009), Franks et al. (2014), Grein et al. (2013), Kürschner et al. (1996, 2008), Londoño et al. (2018), Reichgelt et al. (2016), Steinthorsdottir et al. (2019, 2020), Stults et al. (2011), and Y. Wang et al. (2015) (see Section 8 for further details). Pleistocene CO_2 data from Lüthi et al. (2008). Deep-water masses: NCW, Northern Component Water; NADW, North Atlantic Deep Water; AABW, Antarctic Bottom Water; NPW, North Pacific Deep Water; TISW, Tethys Indian Ocean Saline Water, (= Warm Saline Deep water). Mountain building episodes; including onset of major tectonic thrusting in the Eastern Alps to onset of major uplift in the Cascades and Altiplano (~7 Ma). Global erosion estimate (brown diamonds); Wilkinson (2005). CaCO_3 AR = marine biogenic carbonate accumulation rate, Opdyke and Wilkinson (1988). Color wedges represent generalized biotic diversity patterns (radiations and contractions) of key groups. Peak Columbia River flood basalt emplacement ca. 17–16 Ma. Biotic highlights: (1) Fruit/leaf-eating perissodactyls common in Africa, Europe, and Asia, for example, *Chalicotherium* (Oligocene–late Miocene); (2) Pika, for example *Prolagus*, ancestral rabbit, (3) litopterns, camel-like South American ungulates; (4) giant sharks for example, *Carcharocles megalodon*; (5) “Proboscidean Datum Event” gomphothere elephant dispersal (from Africa to Eurasia), mid-Burdigalian 18.5 Ma; (6) “short-faced” kangaroos radiate in Australia from ca. 20 Ma; (7) giant heavily armored armadillos; (8) appearance of hypsodont horses (*Merychippus* and relatives) ~18 Ma; (9) larger benthic foraminifera persist as important reef builders; (10) early camel *Procamelus* (16–5.3 Ma); (11) early hominids in Europe, for example, *Griphopithecus suessi* from Langhian; (12) scleractinian corals and reefs expand (14–3 Ma); (13) early hominids in Asia, for example, *Sivapithecus indicus* (ca. Langhian/Serravallian); (14) giant flying squirrel; (15) Early Late Miocene *Hipparion* steppe-adapted horse dispersal, Eurasia, North America and Africa (*Hipparion* Datum, ~12.5 Ma); (16) Phorusrhacids (terror birds) occupy South American apex predator niche; (17) an early rhinoceros *Chilotherium* (11–5 Ma); (18) peaks in high-productivity deep sea benthic foraminifera; (19) purported first hominin *Sahelanthropus tchadensis* (7–11 Ma); (20) GABI, Great American Biotic Interchange; (21) proto-giraffe *Samotherium boissieri* (9–7 Ma); (22) radiation of “true kangaroos,” Australia, from 2 Ma. LMC, Late Miocene Cooling; LMCIS, Late Miocene Carbon Isotope Shift; MCO, Miocene Climatic Optimum; MMCT, Middle Miocene Climatic Transition; MSC, Messinian Salinity Crisis; OMT, Oligocene–Miocene Transition; PCO, Pliocene Climatic Optimum. The Monterey Event = a ca. 3.4 myr-long positive $\delta^{13}\text{C}$ excursion indicative of an intense perturbation of the carbon cycle.

2. Miocene Stratigraphical and Chronological Framework

Unified chronostratigraphic nomenclature is fundamental to climate research, enabling integration of multiple types of data from the marine and terrestrial realms to assess the interplay of biotic and abiotic forcings and feedbacks (Hilgen et al., 2020). Chronostratigraphic methods and their resolution are different for activities in these different realms, and the communities tend to use somewhat different language, that is, the use of stage names, possibly regional stages by terrestrial workers, whilst marine workers, often benefiting from stronger age control, tend to use epoch and sub-epoch names and numerical ages. Translating these languages have never been more important than in the Miocene where huge signals come from the

continents. We therefore begin with stratigraphic definitions and background on the progress made in creating a robust Miocene time scale.

2.1. Miocene Chronostratigraphy

The Miocene epoch, lasted 17.7 million years (23.03–5.33 Ma), and is formally (according to the International Commission on Stratigraphy (ICS); Subcommittee on Neogene Stratigraphy: (<https://stratigraphy.org/subcommissions#neogene>) subdivided into six global stages: the Aquitanian (23.03–20.43 Ma), the Burdigalian (20.43–15.97 Ma), the Langhian (15.97–13.82 Ma), the Serravallian (13.82–11.63 Ma), the Tortonian (11.63–7.25 Ma), and the Messinian (7.25–5.33 Ma) (Figure 1). The Paleogene/Neogene Global Boundary Stratotype and Point (GSSP), which also defines the, and thus the base of the Aquitanian stage, is defined at Lemme-Carrosio in Italy. The “Golden Spike” is placed at “meter 35 below top of section” at what was identified as the base of magneto-subchron C6Cn.2n (although it has been reported that this spike has since disappeared). This horizon is bracketed by the lowest occurrence of *Paragloborotalia kugleri* (planktonic foraminifera) and the highest occurrence of *Sphenolithus delphix* (calcareous nannofossil) bio-events (Steininger et al., 1997), which provide approximations of the O/M boundary in marine records. The Miocene/Pliocene boundary (base of the Zanclean Stage) is defined in the Eraclea Minoa section in Sicily. This equates to the top of the magnetochron C3r and the lowest occurrence of the calcareous nannofossil *Ceratolithus acutus* (Van Couvering et al., 2000). The definition of other Miocene global stages and the designation of their GSSPs (some still undefined) have been summarized by Hilgen et al. (2012). Regional stages, widely applied as standard chronostratigraphic units in the Paratethys and New Zealand regions, have additionally been linked to these global stages (Hilgen et al., 2012). An Astronomically Tuned Neogene Time Scale (ATNTS2004), based on the tuning of physical property parameters and lithological variations in cyclic sediment successions from the western equatorial Atlantic Ocean and Mediterranean that have a reliable magnetostratigraphy, was developed by Lourens et al. (2004), updated (ATNTS2012) by Hilgen et al. (2012) and formulated into the formal geological time scale by Cohen et al. (2013, updated 2020). This approach constrained the ages of Miocene magnetic reversal boundaries in the Geomagnetic Polarity Time Scale (GPTS), which were previously based on seafloor anomaly profiles combined with a limited number of radio-isotopically dated tie points (Hilgen et al., 2012). However, the astronomical calibration of Miocene magnetic reversal boundaries has only been extended back to 14.9 Ma (Hilgen et al., 2012; Hüsing et al., 2007, 2009; Mourik et al., 2010) and more recently to 16.3 Ma (Turco et al., 2018). Over the interval 23–16.3 Ma, substantial incompatibilities still need to be resolved between astronomically derived ages and traditional ages based on seafloor anomalies. An astrochronozonal reference frame (Figure 2) was recently accepted by the ICS (Hilgen et al., 2020). Astrochronozones provide an orbital context for climatic and biotic events, both on land and in the marine realm. The Miocene epoch spans the following astrochronozones: long 405-kyr eccentricity Cycles 57 to 14, very long ~2.4-Myr eccentricity Cycles 10 to 3, and long ~1.2-Myr obliquity amplitude Cycles 20 to 5. These astrochronozones are concurrent with magnetochrons 6 to 3 (Figure 2).

2.2. Miocene Astronomically Calibrated Isotope Stratigraphy

Over the last decades, benthic foraminiferal stable isotopes have emerged as a powerful tool for stratigraphic correlation and for investigation of long-term fluctuations in ice volume, ocean circulation, and the global carbon cycle (e.g., Holbourn et al., 2018; Lisiecki & Raymo, 2005; Pälike et al., 2006; Shackleton & Hall, 1997; Shackleton et al., 1999). The $\delta^{18}\text{O}$ signal is closely related to astronomically controlled ice volume cyclicity, while the $\delta^{13}\text{C}$ signal provides information on deep-intermediate water circulation and carbon cycling (e.g., Holbourn et al., 2013; Mackensen, 2008; Liebrand et al., 2017). The different imprint of astronomical variations on $\delta^{18}\text{O}$ and $\delta^{13}\text{C}$ offers unprecedented insights into the pacing and drivers of long-term climate evolution and into climate-carbon cycle dynamics. In the last decades, the International Ocean Discovery Program (IODP) and its predecessors the Integrated Ocean Drilling Program (also IODP), the Ocean Drilling Program (ODP), and the Deep Sea Drilling Project (DSDP) have recovered outstanding, undisturbed sediment successions from several oceans that allowed constructions of high-resolution, astronomically calibrated timescales. Progress has been made with the Oligocene to Miocene transition (Beddow et al., 2016, 2018; Liebrand et al., 2016, 2017). However, despite a single Miocene-spanning mid-resolution

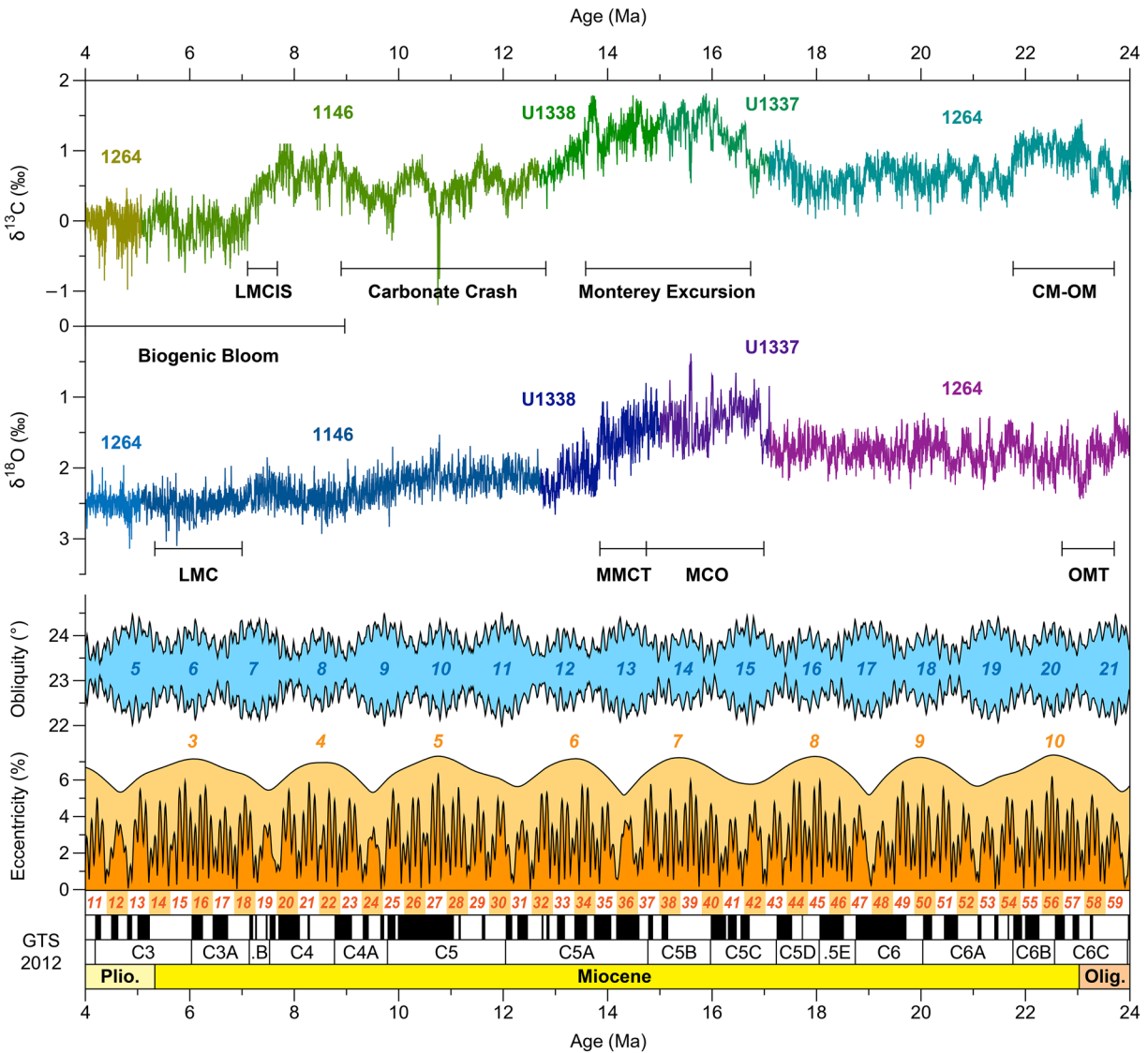


Figure 2. Compilation of high-resolution Miocene benthic foraminiferal oxygen and carbon isotopes. The records derive from ODP Site 1146 in the South China Sea (Holbourn et al., 2018); IODP Sites U1337 and U1338 in the eastern equatorial Pacific Ocean (Holbourn et al., 2014, 2015) and ODP Site 1264 in the South Atlantic Ocean (Bell et al., 2014; Liebrand et al., 2016). CM–OM, Oligocene–Miocene carbon maximum; LMCIS, Late Miocene Carbon Isotope Shift; MCO, Miocene Climatic Optimum; MMCT, middle Miocene climatic transition; OMT, Oligocene–Miocene transition. Note: 0.7‰ was deducted from the Pliocene part of the Site 1264 $\delta^{18}\text{O}$ and $\delta^{13}\text{C}$ records, and 0.5‰ was deducted from the early Miocene part of the Site 1264 $\delta^{13}\text{C}$ record to account for differences in inter-ocean isotope gradients. Astrochronozones are counted back from the present, with very long ~ 2.4 Myr eccentricity Cycle Numbers in light orange, long 405 kyr eccentricity Cycle Numbers in dark orange, and very long ~ 1.2 Myr obliquity amplitude modulation Cycle Numbers in blue. These astrochronozones are based on the La2011_ecc3L eccentricity solution (Westerhold et al., 2012) and the La2004 obliquity solution (Laskar et al., 2004). For visual purposes we added 5% to the extracted ~ 2.4 Myr eccentricity component. Magnetostratigraphy is based on the GTS2012 (Hilgen et al., 2012). We note that the stability of the ~ 20 kyr precession cycle and the 40 kyr obliquity cycle is not known for ages >10 Ma (Zeeden et al., 2014).

record from South China Sea Site 1148 (Tian et al., 2008), no high-resolution (≤ 5 kyr) standard oxygen isotope cyclostratigraphy is yet available that covers the entire Miocene from a single location, which is largely due to the fact that continuous, well-resolved records extending beyond ~ 8 Ma remain scarce. A compilation of selected Miocene, high-resolution records from the Eastern Equatorial Pacific Ocean (IODP Sites U1337 and U1338), the South China Sea (ODP Site 1146), and the South Atlantic Ocean (ODP Site 1264) is shown in Figure 2 against the Miocene astrochronozones. New, extended, Miocene records will additionally become available from recent coring efforts in the Indian and western Pacific Oceans that yielded continuous, carbonate-rich succession over the Miocene (IODP Expeditions 353 and 363). Moreover, the approach

of using carefully inter-laced benthic foraminiferal $\delta^{18}\text{O}$ and $\delta^{13}\text{C}$ “Mega Splices,” as archives for analyzing trends and “rhythms” (orbital pacing) in climate during the Cenozoic is gaining traction (De Vleeschouwer et al., 2017). These new records highlight distinct phases of Miocene climate evolution, defined by different modes of variability and changing responses to orbital forcing.

At the beginning of Miocene a phase of high $\delta^{18}\text{O}$ took place, interpreted as a brief period of Antarctic ice sheet expansion associated with transient global cooling (e.g., Beddow et al., 2016; Lear et al., 2004; Liebrand et al., 2017; Miller et al., 1991, 2020; Pfuhl & McCave, 2007; Zachos et al., 2001). The $\delta^{18}\text{O}$ maximum is commonly referred to as Mi-1, although some authors refer to it more broadly as the “Oligocene/Miocene Boundary transition” (OMB, Mudelsee et al., 2014) or, the “Oligocene Miocene (Climate) Transition” (OMT; Beddow et al., 2018; Liebrand et al., 2016, 2017); according to the original definition Miller et al. (1991), this “ $\delta^{18}\text{O}$ maximum” marks the base of an extended oxygen isotope zone “Mi-1” (similar to the definition of a biozone), that encompasses most of the lower Miocene, and excludes the increase or transition to peak values. High-resolution records now reveal that the basal Miocene has several high $\delta^{18}\text{O}$ values in close proximity such that the onset of the Mi-1 zone is not easily recognized and any discreet event-naming does not work especially well (Liebrand et al., 2011, 2016). Furthermore, the highest absolute $\delta^{18}\text{O}$ values associated with the OMT, fall in the latest Oligocene, and thus, these cannot be used to define the base of a Miocene “oxygen isotope zone” or alternatively a Miocene “event.” Liebrand et al. (2017) define the OMT as a 1-million-year long interval between ~ 23.7 and 22.7 Ma, consisting of two rapid $\sim 0.5\text{‰}$ increases in benthic foraminiferal $\delta^{18}\text{O}$ separated by an interval (405 kyr eccentricity cycle) of partial $\delta^{18}\text{O}$ recovery. We follow this definition here (Figures 1 and 2). In benthic foraminiferal $\delta^{13}\text{C}$ the Oligocene-Miocene transition is characterized by a transient carbon maximum named the Oligocene/Miocene carbon maximum, which is abbreviated to CM-OM (Figure 2; Hodell & Woodruff, 1994). This interval with high $\delta^{13}\text{C}$ values may be linked to organic carbon burial (Compton & Hodell, 1993; Compton et al., 1990).

Clear long and short eccentricity cycles (110 and 405 kyrs) in $\delta^{18}\text{O}$ and $\delta^{13}\text{C}$ characterize the early Miocene, implying strong orbitally forced climate variability (Beddow et al., 2016, 2018; Liebrand et al., 2016, 2017). The MCO (~ 16.9 – 14.7 Ma) stands out as an extended interval of sea level rise (Miller et al., 2020) and global warmth that was coupled to a major positive carbon-isotope excursion known as the “Monterey Excursion” (Figure 2; e.g., Holbourn et al., 2007; Tian et al., 2013). Climate variability generally decreased during the MMCT and after ~ 13 Ma (Holbourn et al., 2018) is suggestive of a more stable Antarctic ice sheet; however, major perturbations of the global carbon cycle coincident with climate shifts include the late Miocene biogenic bloom (Diester-Haass et al., 2005; Drury et al., 2018), the prolonged interval of reduced carbonate deposition termed the “carbonate crash” (Figures 1 and 2) and the global $\delta^{13}\text{C}$ decline known as the Late Miocene Carbon Isotope Shift (LMCIS) between ~ 8 and 7 Ma (e.g., Drury et al., 2017; Holbourn et al., 2018; Figure 2).

2.3. Anchoring the Neogene Time Scale

Intercalibration of the GPTS with the marine isotope cyclostratigraphy is a prerequisite for accurate correlation of paleoclimatic events in marine and terrestrial sequences (e.g., Abdul Aziz et al., 2003; Florindo et al., 2005; Hao & Guo, 2007; Krijgsman et al., 1994; Ohneiser et al., 2015; Sangiorgi et al., 2018). For example, the long-term variability of the Indian, East Asian, and Australian monsoonal subsystems, their sensitivity to changing climate boundary conditions such as ice volume, ocean temperatures, and greenhouse gas concentrations as well as the dynamic coupling between regional subsystems remain poorly understood, due to large uncertainties in the correlation of terrestrial and marine records. To date, none of the Miocene benthic foraminiferal stable isotope records have been directly correlated to the GPTS beyond ~ 8 Ma. The intercalibration of the marine isotope cyclostratigraphy and GPTS has been severely hampered by (1) the lack of paleomagnetic signal in Miocene sediment archives drilled using the extended core barrel (XCB) system (e.g., ODP Site 1146), (2) the absence or unreliability of magnetic signals in carbonate-rich deep sequences (e.g., IODP Sites U1337 and U1338), and (3) the incompleteness of deep-water sequences affected by carbonate dissolution and recrystallization over intervals such as the MCO and the carbonate crash (e.g., IODP Sites U1335, U1336; Kochhann et al., 2016). A further difficulty is that substantial uncertainties remain for the ages of polarity chrons between 23 and 15 Ma (Hilgen et al., 2012). However, Site U1490, recently drilled in the western equatorial Pacific Ocean, recovered a continuous succession of

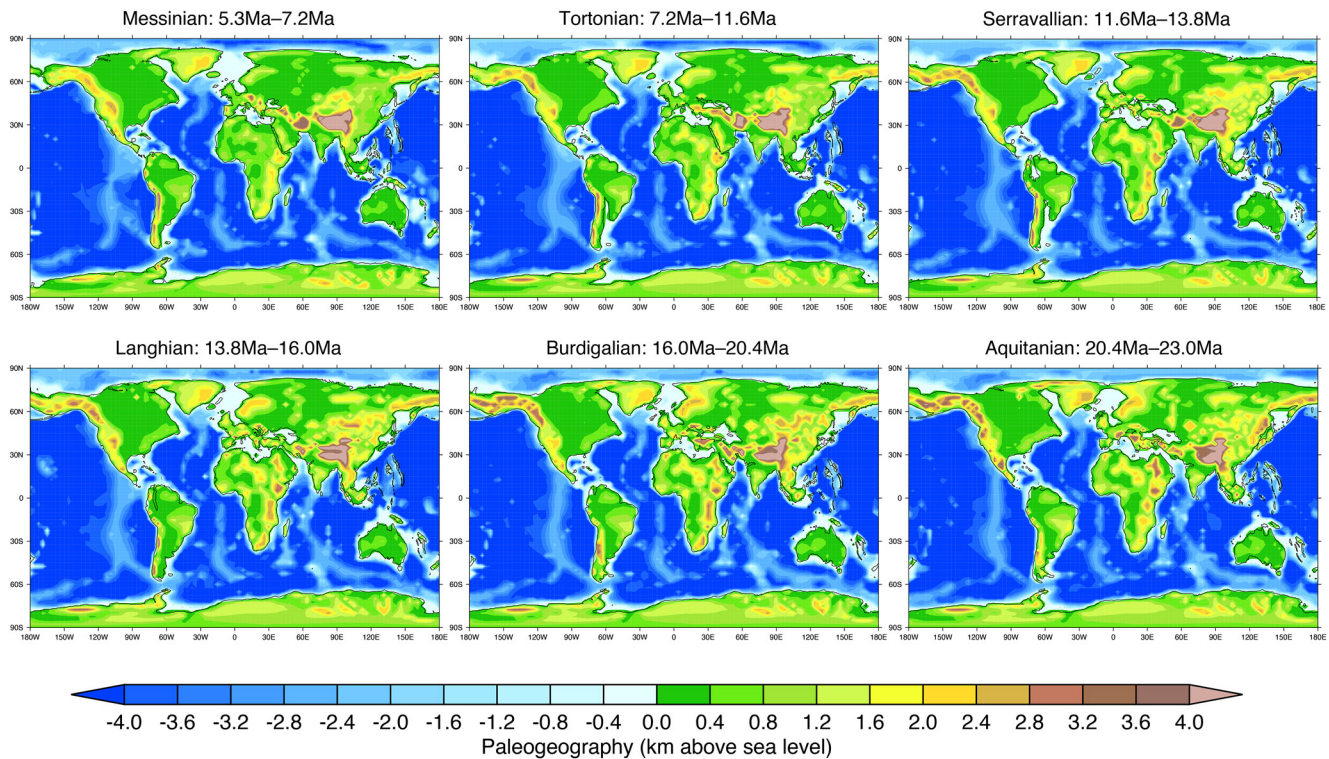


Figure 3. Paleogeographical and topographical evolution during each of the Miocene stages. Based on the reconstructions of Getech Plc, reconstructed using techniques similar to those described in Markwick and Valdes (2004), and as used in Farnsworth et al. (2019).

carbonate-rich sediment with an exceptionally well-resolved magnetostratigraphy between 18 and 9 Ma (Rosenthal et al., 2018), opening the possibility to anchor the Miocene marine isotope cyclostratigraphy to the GPTS.

3. Tectonics, Paleogeography, Erosion, and Ocean Gateways

We summarize (Figure 3) the tectonic evolution of paleogeography and topography throughout the epoch according to the Getech Plc. reconstructions (Farnsworth et al., 2019) and illustrate the boundary conditions that attend climate models (e.g., Herold et al., 2008). Tectonic activity during the Miocene shaped much of the geography we see today. Mountain building took place in circum-Mediterranean, circum-Pacific, Pontides-Caucasus-Alborz-Karakoram-Himalaya, central Asia, and the complex region in southeastern Asia to northern Australia, and plateau uplift occurred in the central Andes and Tibet. Extension initiated in the Basin and Range province of western North America and in East Africa (e.g., Atwater & Stock, 1998; Macgregor, 2015), and was ongoing through the Miocene in Turkey (Bozkurt & Mittwede, 2005), while some mountain collapse occurred in western North America (Horton et al., 2004). At the same time, sedimentary erosion rates have increased through the Neogene, as inferred from estimates of global sedimentary volumes through time (e.g., F. Herman et al., 2013; Wilkinson, 2005) and oceanic carbonate accumulation rates (from Opdyke & Wilkinson, 1988; see Figure 1). Other sedimentation data sets largely mirror these, or show even higher rates of Neogene change. While the data themselves are not controversial, the interpretations are; they are recording some yet unclear combination of tectonics and climate. The weathering data, in the context of climate-chemical weathering rates-theory, suggest that Neogene global cooling had no profound effect on average weathering rates, which instead suggest some interplay of changes in the balance of topographic relief versus rates of physical and chemical continental rock weathering and erosion.

In terms of magmatic activity, in addition to subduction along the same subduction zones present on Earth today, intense volcanism during the middle to late Miocene erupted huge volumes of basaltic lava ($\sim 210,000 \text{ km}^3$) that engulfed $\sim 210,000 \text{ km}^2$ of the Pacific Northwest in the United States to form the

Columbia River large igneous province (Reidel, 2015). The timing of the primary Columbia River Basalts (CRBs) eruptions coincides with the MCO, and a link between volcanism and climatic warming and environmental change has been suggested (Foster et al., 2012; Kasbohm & Schoene, 2018; Sosdian et al., 2020; Steinhorsdottir et al., 2020).

Miocene tectonic activity was particularly important for oceanic circulation. Ocean gateways were slowly closing in the Mediterranean, Central America, and Indonesia, whilst gateways in the Arctic, and the Southern Ocean were opening up (Figure 1). Uplift in the Himalayas and the Tibetan region commenced prior to the Miocene, after the Indian plate had collided with the Eurasian plate (e.g., Rowley & Garzzone, 2007; C. S. Wang et al., 2014), although a proto-Tibetan Highland was likely present before the collision (C. S. Wang et al., 2014). By the middle Miocene, many parts of southern and central Tibet had reached high elevations, and a high plateau began to form through compressional uplift and sediment fill (e.g., Rowley & Garzzone, 2007; Spicer et al., 2021). The concurrent projection of the Himalayas above the average elevation (~5 km) of the present-day plateau generated a strong rain shadow effect, linked with intensification of the modern South Asian monsoons (Ding et al., 2017; Spicer et al., 2017). Uplift was asynchronous, however (Garzzone et al., 2000), and other parts of Tibet began their ascent only toward the end of the late Miocene (e.g., C. S. Wang et al., 2014; W. Wang et al., 2011).

Alpine uplift also began prior to the Miocene, due primarily to the northward movement of the African/Apulian plate (Meulenkamp & Sissingh, 2003). By the early Miocene, elevations were less than half of modern elevations in the eastern Alps and remained so until at least the middle Miocene (Jiménez-Moreno et al., 2008), whereas modern or higher-than-modern elevations are reconstructed in the central Alps by the middle Miocene (Campani et al., 2012; Sharp et al., 2005) and in the western Alps by the end of the middle Miocene (Kováč et al., 1994). In South America, there was significant Miocene uplift of the Andes and the Andean Plateau, but the timing is debated. In the Central Andes, high elevations may have been attained rapidly during the late Miocene (Garzzone et al., 2006; Ghosh et al., 2006; Gregory-Wodzicki, 2002) or alternatively had already been achieved by the middle Miocene (Evenstar et al., 2015; Mamani et al., 2010; Saylor & Horton, 2014). In North America, prior to the Miocene, the Rocky Mountains may have been higher than today (Chase et al., 1998; Dettman & Lohmann, 2000; Fan et al., 2014; Sjoström et al., 2006). Orographic lowering to modern elevations is reconstructed for the middle Miocene (Wolfe et al., 1997) but subsequent late Miocene uplift is also documented (Rosenberg et al., 2014). Topographic rejuvenation of the Appalachian mountain chain of eastern North America also occurred during the Miocene (Gallen et al., 2013; Pazzaglia & Gardner, 1994).

The Drake Passage between Antarctica and South America opened during the Oligocene but tectonic changes continued to influence ocean circulation in the region during the early Miocene (Lagabrielle et al., 2009). The open Tethys gateway was a major feature of early Miocene paleogeography, connecting the Atlantic and Indian oceans, but this gateway had closed completely by the late Miocene (Rögl, 1999). Isolated from the Tethys prior to the Miocene, the Paratethys was an intracontinental sea connecting the Mediterranean Sea and the Indian Ocean until the middle Miocene (Rögl, 1999; D. Simon et al., 2018). The Indonesian Seaway connecting the Indian Ocean to the Pacific Ocean became progressively restricted throughout the Miocene as the Indo-Australian plate moved northwards. Deep-water exchange was restricted from the early to middle Miocene, and only thermocline and intermediate water exchange was allowed by the late Miocene (Christensen et al., 2017; Kuhnt et al., 2004). The Panama Gateway (also known as the Central American Seaway) connecting the Pacific and Atlantic oceans was restricting throughout the Miocene, and final closure is often thought to have been in the Pliocene (Haug et al., 2001; Keigwin, 1982; O'Dea et al., 2016). Some recent studies, however, argue for a middle or late Miocene closure (Kirillova et al., 2019; Montes et al., 2015). The Bering Strait, which today connects the Arctic and Pacific Oceans, was closed for most of the Miocene, perhaps opening only in the latest Miocene (Gladenkov & Gladenkov, 2004). The widening of the Fram Strait and the subsidence of the Greenland-Scotland Ridge, however, occurred throughout the Miocene thereby connecting the Arctic Ocean with the North Atlantic Ocean (Ehlers & Jokat, 2013; Jakobsson et al., 2007; Knies et al., 2014). The connection of these two distinct oceans had profound implications for ocean ventilation and centers of deep-water formation (Hossain et al., 2020; Hossain et al., 2021; Thompson et al., 2010; Wright & Miller, 1996). The meeting of the previously landlocked cold fresh Arctic Ocean waters (Dixon et al., 1992) with the warm saline Atlantic waters was responsible for the production of Northern

Component Water (one of the precursors to modern North Atlantic Deep Water) and its export to the abyss of the global ocean (Wright & Miller, 1996).

One of the most dramatic paleoceanographic events in Earth's history, the Messinian Salinity Crisis, occurred at the end of the Miocene ~5.96–5.33 Ma (Roveri et al., 2014; Ryan et al., 1973). At this time, two of the three connections between the Atlantic Ocean and the Mediterranean closed completely due to tectonic uplift (Flecker et al., 2015; Hsü et al., 1973; Krijgsman et al., 2018; Ryan et al., 1973). While these gateways were closed, desiccated marginal basins in the Mediterranean developed synchronous gypsum deposits and then deep basins developed kilometer-thick halite deposits as the Mediterranean received 5%–6% of global ocean salt (7–8 times the saline water received by the Mediterranean today; Haq et al., 2020; Hsü et al., 1973). Following the period of halite deposition, the Mediterranean varied between extreme brackish and hypersaline states (known as the Lago Mare) before the collapse of the sill between the Mediterranean and the Atlantic Ocean brought the Messinian Salinity Crisis to an end (Caruso et al., 2019). Since the end of the Miocene, a deep channel between the Mediterranean and the Atlantic Ocean has remained permanently open.

4. Marine Biota and Ecosystems

In this section, we review the fossil record of important groups and comment on the biological evolution of the Miocene ocean in relation to factors such as plate tectonics and ocean current realignment, ocean temperature and internal structure, ocean chemistry changes, atmospheric $p\text{CO}_2$ levels, and ocean pH. Highlights of these biotic and abiotic developments are summarized in overview Figure 1, together with perspectives on terrestrial evolution. Knowledge of the Miocene ocean biosphere is naturally limited by the nature of the fossil record. Many of the most important groups of plankton and nekton are soft-bodied and so leave little direct evidence of their history beyond what can be inferred from organic biomarkers and their evolutionary relationships and genomics. Nevertheless, there are several very important groups of marine plankton that have left a rich fossil record from the open ocean along with more sporadic fossils of many other marine organisms from mollusks, to fish (especially their teeth) and whales. The continental shelves provide a rich if more episodic record of the evolution of shallow water environments including reefs, sea-grass, and kelp biomes.

4.1. Marine Plankton

4.1.1. Diatoms

Marine planktonic siliceous diatoms are important primary producers and play an important role in ocean carbon cycling and the biological pump through their ballasting effect on organic matter (De La Rocha, 2008; Tréguer et al., 2018). At present they dominate phytoplankton assemblages in eutrophic areas including the Southern Ocean and upwelling zones. They originated in the Mesozoic (likely Early Jurassic: Lewitus et al., 2018; Nakov et al., 2018), but remained at relatively low diversity until the late Eocene. Most workers regard the Miocene as a period of rapid diatom diversification especially in the high southern (Lewitus et al., 2018) and northern (Suto, 2006) latitudes, with the largest increase in species diversity beginning in the middle Miocene around 16 Ma and continuing into the early Pliocene (Falkowski et al., 2004; Figure 1). The Neogene diversification of diatoms has been linked to high latitude cooling, the evolution of the Southern Ocean and development of the cold ocean interior (Berger, 2007; Bown, 2005; Cervato & Burckle, 2003). Hypotheses linking ocean cooling to stronger oceanic fronts, increased turbulence and enhanced nutrient availability in the photic zone likely underpin (regional) increases in diatom productivity (Falkowski et al., 2005; Katz et al., 2005; Kemp et al., 1995). However, it has also been suggested that the diversity patterns are partly a sampling artifact of the “pull of the recent” and the greater sampling of more recent sediment cores (Kotrc & Knoll, 2015; Rabowsky & Sorhannus, 2009). The most up-to-date syntheses of morphological, genetic, and fossil data (Lazarus et al., 2014; Nakov et al., 2018) indicate that speciation rates have indeed exceeded extinction rates since the early Miocene leading to significant diversification.

Miocene diversification was associated with a marked reduction in mean diatom size (Finkel et al., 2005). Despite much discussion in the literature there is no single explanation for the diversification of diatoms, which may have been related to global cooling, increasing silica availability in the ocean associated with

erosion of mountains (Cermeño et al., 2015), or the spread of grasses and associated delivery to the oceans of phytoliths (Falkowski et al., 2004), declining carbon dioxide levels (Lazarus et al., 2014), and competition with other groups of plankton (Lewitus et al., 2018). Moreover, modern-type oceanic upwelling systems important for mixing silica and other bio-limiting nutrients into the photic zone, generally became established through the Miocene (Jung & Prange, 2020; Summerhayes et al., 1992). The epoch also saw the first development of “diatom mats” in areas of equatorial and coastal upwelling in which high concentrations of diatoms sinking through the water column caused a new kind of organic-rich laminar sedimentation, potentially impacting global carbon and silica burial rates (Kemp & Baldauf, 1993; Pike & Kemp, 1999).

The success of diatoms through the Neogene, and the important ecological role they play in the ocean's biological carbon pump, has led to the idea that diatom export production/carbon sequestration contributed to the Cenozoic atmospheric $p\text{CO}_2$ reduction and consequently to changes in the global climate state (Falkowski et al., 2004; Renaudie, 2016; Tréguer et al., 2017).

4.1.2. Calcareous Nannoplankton

The calcareous nannoplankton comprise another prominent group of primary producers. During the Miocene, they supplied most of the pelagic carbonate buried in the deep sea (Si & Rosenthal, 2019; Suchéras-Marx & Henderiks, 2014). This group is dominated by coccolithophores (calcifying haptophyte algae) which had experienced a prolonged period of species diversity decline from the middle Eocene into the Oligocene, particularly among warm-adapted groups, a pattern that has been linked to global cooling (Bown et al., 2004; Dunkley Jones et al., 2008). The Miocene, by contrast, was a period of modest diversification particularly among warm-water oligotrophic groups such as the Discoasteraceae (Backman & Raffi, 1997; Backman et al., 2012; Bown et al., 2004; Raffi et al., 2006). The paleogeography and abundance of calcareous nannoplankton primarily reflect surface water conditions. This principle has been applied to track tectonic and paleoceanographic change across the Panama Gateway back to ~16 Ma (Kameo & Sato, 2000) and to quantify past levels of productivity in the incipient Benguela upwelling system during the late Miocene (Krammer et al., 2006). However, selective dissolution may superimpose differentiations in fossil assemblages that are unrelated to climate or productivity, especially in the deeper Pacific (Lohmann & Carlson, 1981) and during Miocene “carbonate crashes”—drastic reductions in carbonate accumulation rates caused by enhanced deep-sea dissolution (~12–9 Ma; Lyle et al., 1995, 2019; Roth et al., 2000; see Figure 1). Nevertheless, there are indications that the latter could also be explained by episodes of reduced pelagic carbonate production (Preiss-Daimler et al., 2013).

There is a marked decrease in coccolith size from the Paleogene into the Neogene, indicating smaller cell size (a similar pattern to diatoms; Hannisdal et al., 2012; Henderiks & Pagani, 2008; Figure 1). The long-term declines in ecological prominence and cell size have been related to decreasing levels of $p\text{CO}_2$, through direct impacts of carbon-limitation as well as indirect effects of decreased weathering rates on biocalcification (Bolton et al., 2016; Hannisdal et al., 2012; Si & Rosenthal, 2019; Suchéras-Marx & Henderiks, 2014). A global decrease in pelagic carbonate burial rates, primarily driven by calcareous nannoplankton productivity (as foraminifer-derived carbonate burial rates remained stable; Suchéras-Marx & Henderiks, 2014), may indeed relate to a decrease in alkalinity weathering input since the Pliocene (Si & Rosenthal, 2019). Guitián et al. (2020) take a closer look at the million-year scale adaptations of coccolithophore cell size and $p\text{CO}_2$ during the Oligocene to early Miocene high $p\text{CO}_2$ worlds. Global cooling at ~15 Ma following the MCO has been linked to biogeographic restriction of certain groups of calcareous nannoplankton to more tropical latitudes (Haq, 1980) and the rise in dominance of reticulofenestrads across high and low latitudes in the Atlantic (Henderiks et al., 2020). The latter are the ancestors of the important modern alkenone-producers *Emiliana huxleyi* and *Gephyrocapsa oceanica*, and this group had evolved to small and more lightly calcified forms, similar to their modern counterparts, by the late Miocene (Bolton et al., 2016; Imai et al., 2015; Young, 1990).

4.1.3. Dinoflagellates

Marine cyst-forming dinoflagellates are important primary producers in the open ocean and shelf seas. They appear to have been in decline for much of the Cenozoic, including throughout the Miocene (MacRae et al., 1996; Mudie et al., 1990; Stover et al., 1996; F. J. R. Taylor et al., 2007). One possible reason for this decline is falling sea level and the associated reduction in the area of shelf seas (MacRae et al., 1996), although

this also promoted evolution in isolated basins during the late Miocene (Mudie et al., 2019; Soliman & Riding, 2017). Evolutionary diversification of various high latitude groups has been linked to global cooling with the origination of many modern cold-water species in the Burdigalian to Langhian (Boyd et al., 2018; Mudie et al., 1990). However, these cold-water taxa only expanded their geographical ranges following the Serravallian (Boyd et al., 2018).

4.1.4. Radiolarians

Radiolarians are marine zooplankton that secrete siliceous shells which, like diatoms, prefer relatively high-productivity environments such as the polar oceans and upwelling zones. The group has been in long-term evolutionary decline since the Cretaceous. It has long been postulated that their Cenozoic decline and changes in their morphology may be linked to silica restriction and the rise of the diatoms (Harper & Knoll, 1975; Lazarus et al., 2009). Significant evolutionary turnover events among Antarctic radiolarians have been related to global cooling in the middle Miocene (15–13 Ma) and late Miocene to Pliocene (7–4 Ma) (Lazarus, 2002). There is no clear change in radiolarian test size, as is seen in the planktonic foraminifera (see below) (Lazarus et al., 2009). However, shell weights appear to decrease during the Neogene, leading to the suggestion that these plankton reduced skeletal silicification as an evolutionary response to reduced Cenozoic ocean silica availability as diatoms expanded (Lazarus et al., 2009).

4.1.5. Planktonic Foraminifera

Foraminifera are abundant zooplankton that secrete calcareous shells, many species living in association with photosymbiotic algae. Planktonic foraminifera experienced significant turnover in the late Eocene and across the EOT, leading to biodiversity reduction particularly among the warm-water groups. The early Miocene was a period of gradual diversification of various genera that are important in the modern ocean (Wade et al., 2018). Speciation was mainly in shallow water environments with little significant depth divergence up to the evolution of *Orbulina* (Pearson et al., 1997) but deeper-dwelling and high-latitude forms diversified in the middle and late Miocene and toward the present (Parker et al., 1999). Speciation and extinction rates are episodic and positively correlated (Wei & Kennett, 1986) suggesting that evolution has been partly driven by global environmental changes although biotic drivers are also important (Ezard et al., 2011). There is a general trend toward shell-size increase through the Neogene (Parker et al., 1999; Schmidt et al., 2004), which contrasts with the pattern in diatoms and coccolithophorids (see above), although there is no simple explanation for this (Schmidt et al., 2006).

4.2. Deep-Sea Foraminifera

Significant changes in deep sea foraminifera occurred in the middle Miocene around the time of the MMCT and in the late Miocene (Flower & Kennett, 1994; Holbourn et al., 2004, 2013a; Kochhann et al., 2017; Miller & Katz, 1987; Smart et al., 2007; Figure 1). Across a wide depth transect (1,200–3,500 m paleodepth) in the tropical Indian Ocean, the MMCT was characterized by an increase in epifaunal taxa at deeper sites and by increased high-productivity taxa at shallower sites (Smart et al., 2007). In the subtropical Indian Ocean, benthic assemblages suggest a late Miocene expansion in the oxygen minimum zone (Singh et al., 2012). In the tropical Indian Ocean, high-productivity taxa peak between 10 and 8 Ma (Smart et al., 2007). The deep equatorial Pacific features similar increases in abundance of benthic foraminifera characteristic of high-organic carbon delivery beginning at 13.8 Ma and coincident with increased accumulation rates of benthic foraminifera and opal (Kochhann et al., 2017). In more oligotrophic regions of the Pacific Ocean (ODP Sites 1146 and 1237) and the eastern Indian Ocean (ODP Site 761), suspension feeders (*Cibicidoides* spp.) increased markedly following global cooling at ~13.9 Ma, suggesting that global cooling and Antarctic glaciation were associated with intensification of the MOC (Holbourn et al., 2004, 2013a). This change is also coincident with Nd isotope evidence for a more isolated Pacific deep-water mass (Ma et al., 2018). In the Atlantic Ocean, accumulation rates of benthic foraminifera indicate moderate productivity levels that increased gradually across the MMCT (Diester-Haass et al., 2009). The similarity in timing of the benthic events and the mid Miocene carbonate crash (~12–9 Ma, Figure 1) suggests coupling linked to changes in export production.

4.3. Marine Mollusks

Mollusks are the most species-rich group of marine animals and also have a very wide range of morphological diversity, life habits, and geographic and bathymetric distributions (Bouchet et al., 2016). Shell-bearing mollusks, especially bivalves and gastropods, which have left a rich fossil record, diversified through the Cenozoic, though this trend seems to have slowed during the Miocene compared to the Paleogene (Crampton et al., 2006; Mondal & Harries, 2016). During the Miocene, warm-water mollusks inhabited higher latitudes compared to both their Oligocene and present-day distribution (Beu & Maxwell, 1990; Kafanov & Volvenko, 1997; Nielsen & Glodny, 2009). This also holds for the earliest Miocene of Antarctica, though most Antarctic Miocene fossil deposits have been eroded away by the glaciations (Beu, 2009).

Major biogeographic changes during the Miocene were induced by tectonic process (see Section 3). The closure of the Tethyan Seaway strengthened connections between the proto-Mediterranean Sea and the Atlantic Ocean, including deep-water connection right until the Messinian Salinity Crisis (Harzhauser et al., 2002; Kiel & Taviani 2018; Lozouet, 2014). This also led to the development of unique molluscan (and other) faunas in the vast brackish Paratethys Sea (Harzhauser et al., 2003). Collision of the Australian and Asian plates caused the development of the highly fragmented archipelagos seen in present-day Southeast Asia, apparently leading to the rise of the largest and most species-rich biodiversity hotspot in the marine realm, the so-called Coral Triangle (Renema et al., 2008). Although even a rough timing of the origins of the diverse molluscan clades in this hotspot is still controversial (Herrera et al., 2015; S. T. Williams & Duda, 2008), it is clear that since the late Miocene at the latest, the Coral Triangle has been a major source and exporter of molluscan biodiversity (Jablonski et al., 2006). Meanwhile, tropical mollusc and coral diversity decreased in the Caribbean, due to closure of the Panama Gateway which cut-off upwelled nutrient supplies from the Pacific (Johnson et al., 1995; Todd et al., 2002), as well as in Tethys and Arabia as the Tethyan Seaway finally closed (Renema et al., 2008; Todd et al., 2002).

4.4. Marine Fish

The fossil record of ichthyoliths points to a restructuring of deep-sea fish communities in the early Miocene ~20 Ma, at which time teeth increased in abundance and diversity (Sibert et al., 2016). Apart from this, the fossil record of marine fish indicates a fairly stable pattern through the Miocene with a slight increase in the diversity of actinopterygians (ray-finned fishes) and decline in elasmobranchs (sharks, rays, and skates) (Guinot & Cavin, 2016). By the start of the Miocene, the largest predatory sharks of all times (such as *Carcharocles megalodon*; Figure 1) evolved and had a worldwide distribution during the Miocene and Pliocene (Long, 2011). Shark and ray diversity was relatively high during the middle to late Miocene (Carrillo-Briceño et al., 2018), but like marine mammals these groups suffered in the Pliocene, where a global extinction of marine megafauna is observed (Pimiento et al., 2017). Certain teleost groups that are adapted to deep-water (bathypelagic) modes of life such as anglerfish (Lophiformes), fangtooths (Beryciformes), and grinnners (Aulopiformes), seem to have diversified during the Miocene to recent (Hughes et al., 2018). Most lineages of modern coral reef fish arose in the late Miocene to Pliocene with the development of the Indo-Australian Archipelago biodiversity hotspot and other reef rearrangements (Bellwood et al., 2017; Renema et al., 2008; Siqueira et al., 2020).

4.5. Marine Birds

Seabirds such as Diomedeidae (albatrosses), Oceanitidae (storm-petrels), Sulidae (boobies and gannets), Phaethontidae (tropicbirds), and the extinct Pelagornithidae (pseudo-toothed birds) all originated in the Paleogene (Mayr, 2009), and presumably occupied similar niches to their modern counterparts throughout the Miocene. The aquatic Sphenisciformes (penguins) are known from the early Paleogene onward (always in the southern hemisphere) and diversified throughout the Miocene. Crown-group penguins (that is, those belonging to modern groups down to their common ancestor assigned to Family Spheniscidae) are known only from the later part of the middle Miocene (13–11 Ma) onward (Göhlich, 2007; Jadwiszczak & Mörs, 2011), suggesting that their radiation may have followed global cooling after the MCO. Most of the penguin-like Plotopteridae, large to giant wing-propelled diving birds of the North Pacific, went extinct during the Oligocene, only *Plotopterum* survived into the early Miocene (Mayr & Goedert, 2018).

4.6. Marine Mammals and Kelp

Cetaceans evolved from terrestrial mammals in the Eocene, and for much of the Miocene they were the apex predators of the oceans (Fordyce, 2009). The two main groups of modern whales are the odontocetes (toothed whales and dolphins), which use sonar to locate individual prey, and the mysticetes (baleen whales), which filter feed. Both groups diversified during the early and middle Miocene reaching maximum diversity in the later middle or late Miocene, but subsequently declined (Marx & Fordyce, 2015; Marx & Uhen, 2010; Quental & Marshall, 2010). Long-distance migration and gigantism (at least by modern standards) of baleen whales is largely a post-Miocene development (Marx & Fordyce, 2015). It has been suggested that Cetacean diversification was linked to the development of the Southern Ocean and especially the rise of the diatoms at the base of the food chain (Berger, 2007; Marx & Uhen, 2010). This is supported by the early occurrence of mysticetes in Antarctica (Fordyce & Marx, 2018; Loch et al., 2019), although the fossil record is both sparse and biased toward the northern hemisphere, so the correlation remains controversial (Pyensen, 2017).

Kelp macroalgae may have diversified in the late Miocene associated with cooling at high latitudes (Estes & Steinberg, 1988; Estes et al., 2005) along with kelp-adapted marine mammals such as sirenians (sea cows; Figure 1), although the kelp fossil record is very incomplete and its origins may be much older (Domning, 1989). Similarly, pinnipeds such as phocids (seals) and otarioids (walruses and sea lions) seemingly originated in the Oligocene but diversified during the Miocene (Berta et al., 2018; Koretsky & Barnes, 2006). They dispersed to the Paratethys Sea by at least the middle Miocene (Koretsky & Domning, 2014) and to the southern hemisphere by the late Miocene (Churchill et al., 2014).

4.7. Carbonate Reefs

Whereas Paleogene shallow water carbonate environments were dominated by larger benthic foraminifer mounds with abundant calcareous algae, mollusks, and echinoderms, the Miocene saw the progressive development of scleractinian coral reefs as the dominant shallow-water biome of the tropics and subtropics (Montaggione & Braithwaite, 2009). There was a major increase in coral diversity in the Indo-Pacific region during the early Miocene (Wilson & Rosen, 1998), with a major biodiversity hotspot developing in the area of the Indo-Australian archipelago as Australia converged with Southeast Asia, while eastern Tethys closure to the Indian Ocean shrank the Arabian reefs (El-Sorogy et al., 2020; Renema et al., 2008; Figure 1). Major reef-dwelling groups including various types of tropical gastropods and fish diversified alongside the corals (Bellwood et al., 2017; Cowman & Bellwood, 2011; Renema et al., 2008). There was a distinct latitudinal expansion of reef extent during the middle Miocene associated with the MCO, including in the proto Great Barrier Reef on Australia's north-western margin (McCaffy et al., 2020), along the margins of the Paratethys (Perrin, 2002) and the Maldives (Betzler et al., 2018). A partial replacement of corals by other organisms better adapted to warmer and nutrient-richer waters (red algae and large benthic foraminifera), has also been reported (Halfar & Mutti, 2005).

From the later middle Miocene onward, there was a general contraction of the latitudinal range of reefs and the number of sites declined (Budd et al., 2011; Montaggione & Braithwaite, 2009), while the modern biogeographic provinces became progressively distinct (Frost, 1977). In the Caribbean, closure of the Panama Isthmus played a role in reef contraction (Reyes-Bonilla & Jordán-Dahlgren, 2017). Fully modern reef environments including, for instance, the modern Great Barrier Reef only developed in the Pleistocene. A marked increase of marine Mg/Ca during the Miocene (Evans et al., 2018), erratically declining pH (Sossian et al., 2018), and global cooling may have progressively favored aragonite producing calcifiers and framework corals such as those that structure modern reefs (Brachert et al., 2020).

Overall, the distribution of carbonate reef environments was controlled largely by plate tectonics and eustasy from ~15.5 to 9.5 Ma and thereafter by changes in global climate patterns and consequent paleoceanographic conditions (Mathew et al., 2020; Renema et al., 2008).

4.8. Summary of Marine Biota

Marine biota thrived throughout the Miocene: there were no major mass extinctions or great reorganizations and diversity among marine vertebrates appears to have been relatively high in the mid- to late-Miocene. Calcifiers such as coccolithophores, foraminifera, mollusks, and echinoderms generally thrived although a marked increase in the Mg/Ca and episodically increasing pH associated with atmospheric $p\text{CO}_2$ reduction may have gradually favored aragonite producers. The extended warm phase of the MCO coincided with a geographical expansion of “tropical” biota such as warm-adapted plankton and scleractinian reefs while closure of the Tethys Seaway resulted in shifts in global biodiversity hotspots. Subsequent global cooling and especially the progressive development of the circum-Antarctic current system, driven by plate tectonics, profoundly affected the distribution and evolution of eutrophic plankton including diatoms, dinoflagellates, and likely the whole high latitude ecosystem. Restriction of the Panama Gateway through flow in the late Miocene may have caused significant changes in tropical ocean structure and ecosystems in both the Atlantic and East Pacific, contributing to distinct phases in the evolution of open ocean ecology known as the “carbonate crash” and “biogenic bloom” (Dickens & Owen, 1999; Lyle et al., 2019; Reghellin et al., 2019; see Figures 1 and 2). The development of deep plankton niches in the tropical ocean from the middle Miocene onward may have been related to cooling and increased food supply at depth.

5. Terrestrial Biota and Ecosystems

The Miocene epoch has been heralded as marking the origins of “modern” terrestrial biomes as well as many of the world’s biodiversity hotspots (Favre et al., 2015; Herbert et al., 2016; Potter & Szatmari, 2009; Willis & McElwain, 2014). In this section, we review the palaeobotanical record, ecosystem history, and terrestrial faunas. These records show that Miocene floras underwent the most dramatic changes of the Cenozoic, in a pattern dominated by contraction of forest biomes and replacement by grasslands, a transition that may have started already by the late Oligocene (Strömberg, 2005, 2011; Figure 4). This occurred both latitudinally and within continental interiors, reflecting the overall cooling and drying of the Earth. Although temporarily reversed during the MCO, vegetation changes were paralleled by diversification and functional evolution of mammals, resulting in our familiar flora and fauna. Overarching trends and highlights of these developments are presented in overview Figure 1.

Expanding our knowledge of vegetation distributions and evolution during the Miocene is of great importance for understanding modern biodiversity, as well as providing a validation target for climate models. Vegetation feedbacks in simulations are particularly important for accurately estimating temperatures linked to $p\text{CO}_2$ levels (Bradshaw et al., 2015; François et al., 2011), which remain a topical question for the Miocene (see Section 8). Terrestrial faunas changed drastically in response to changing primary food sources. Leaf-browsing mammals were abundant in the early Miocene but declined with the forests, while rodents and hooved animals radiated as open grassland habitats became more common (e.g., Morales-García et al., 2020; Semprebon et al., 2016, 2019; Figure 1). This sequence of events occurred in many if not all continents, driving prey-predator couplings, diversification, and appearances of increasingly modern-looking biota, including primates encompassing ancestral hominins.

5.1. Miocene Floras

5.1.1. Early Miocene (Aquitanian and Burdigalian) Vegetation

In the northern hemisphere, Eurasia was dominated by subtropical evergreen and mixed mesophytic forests with many thermophilic elements, while most conifers were generally restricted to sites at elevation (Akgün et al., 2007; Ivanov et al., 2011; Kovar-Eder et al., 2008; Utescher et al., 2011; Yao et al., 2011). Turkey was dominated by laurel forest and subordinate broadleaf deciduous forest biomes (Denk et al., 2019). In contrast, an arid belt stretched across Central Asia (Caves et al., 2016; X. Sun & Wang, 2005) that impeded vegetation growth in desert intermontane basins, with semi-arid woodlands on slopes and in river valleys, and conifer forests at higher elevations (Barbolini et al., 2020). Evidence from fossil phytoliths and time-calibrated molecular phylogenies suggest that open-habitat grasses (including C_3 pooids, PACMAD grasses, and C_4 chloridoids) radiated taxonomically well before the Miocene (Christin et al., 2014; Strömberg, 2011). Fossil phytolith assemblages further show that, in many areas, such as the continental interior of North

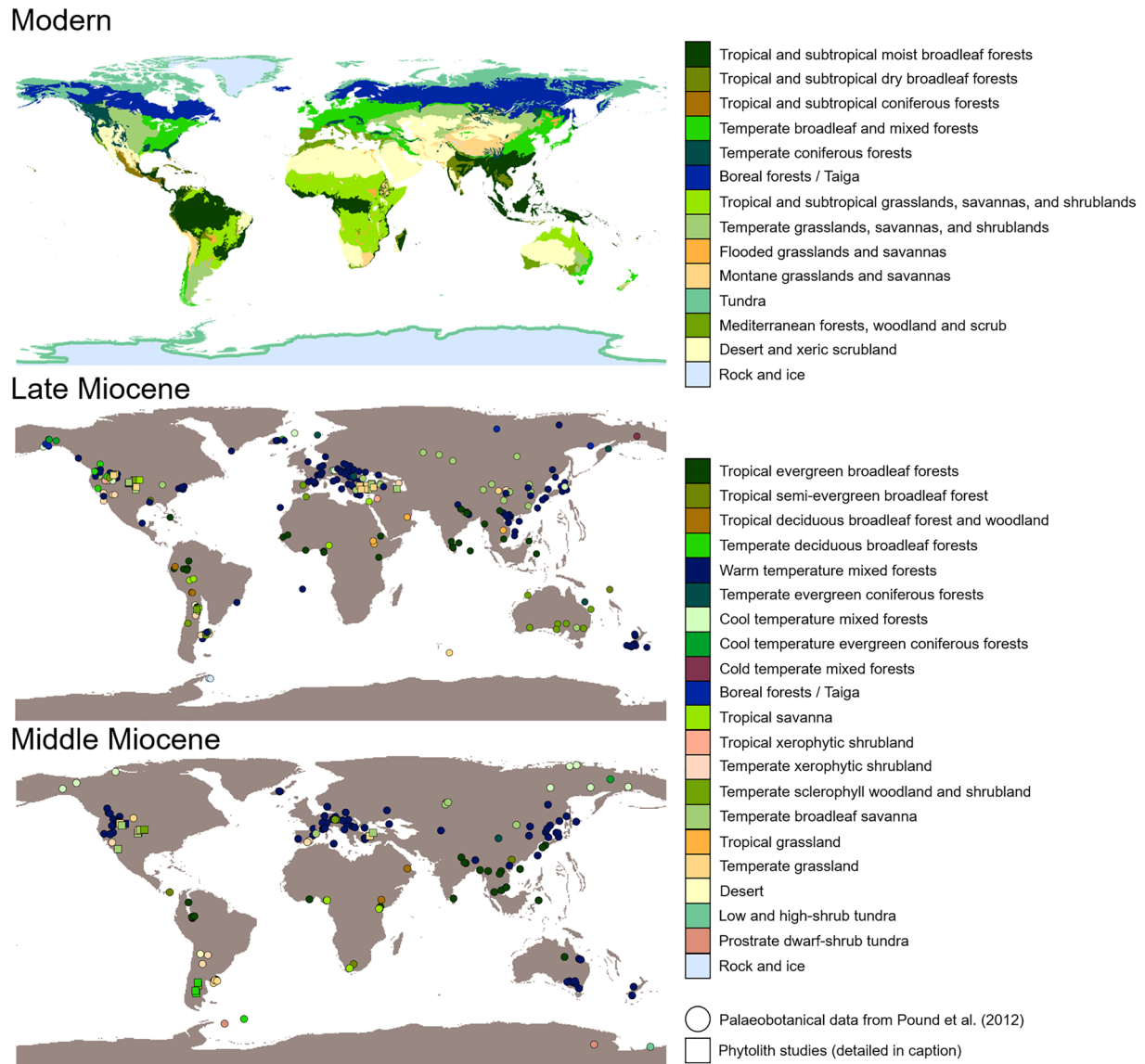


Figure 4. Global vegetation biome distribution for today (modern), the late Miocene and the middle Miocene. Modern distribution is based upon D. M. Olson et al. (2001), but recolored to match the biome classification scheme used in the Miocene reconstructions. Miocene paleobotanical data (circles) from M. J. Pound et al. (2012) and expanded with fossil phytolith data (squares) from Strömberg (2005), Strömberg et al. (2007a, 2007b, 2013), Strömberg and McInerney (2011), Cotton et al. (2014), S. T. Chen et al. (2015), Dunn et al. (2015), Harris et al. (2017), Hyland et al. (2018), Smiley et al. (2018), and Loughney et al. (2020). All colors based upon the BIOME4 vegetation model (Kaplan, 2001). Note that many of the middle and late Miocene savannas or grasslands (as reconstructed based on phytoliths) were likely nonanalog. They are labeled as “temperate” because grass communities consisted primarily of grasses that today dominate in temperate climates (pooids). However, these plant communities often also contained palms and other indicators of warmer climates.

America and Turkey, C_3 grass-dominated habitats started spreading by (at least) the earliest Miocene (Harris et al. 2017; Strömberg, 2011; Figure 1). The early Miocene of eastern North America hosted deciduous-evergreen mixed and coniferous forests rather than the more dry-adapted grassy vegetation in the continental interior, probably due to greater moisture delivery via the proto-Gulf Stream (Kotthoff et al., 2014). Further north, Arctic Canada, Siberia, and Alaska also hosted mixed conifer/northern hardwood forests (Hickey et al., 1988; Volkova, 2011; C. J. Williams et al., 2008; Wolfe, 1994).

In the southern hemisphere, xerophytic or mesophytic vegetation with megathermal affinities dominated South America (Dunn et al., 2015; Palazzesi & Barreda, 2007). Open, drier habitats across the (nonAndean) lowlands of Patagonia are suggested by the presence of pollen produced by Ephedraceae, Asteraceae, and Poaceae, and phytolith data point to open shrublands with abundant palms and patches dominated by

pooid open-habitat grasses (Dunn et al., 2015; Palazzesi & Barreda, 2007; Strömberg et al., 2013). Forests of southern beech (Nothofagaceae) probably stretched across wetter regions of western Patagonia (Palazzesi & Barreda, 2007).

Tropical East Africa contained rainforest with palms and forest grasses in the highlands and a mix of deciduous broad-leaved woodland and forest in the lowlands (Collinson et al., 2009; Currano et al., 2019; Maxbauer et al., 2013; Michel et al., 2014). In southern Africa, the Cape region and eastern shores hosted humid, subtropical forests in the early Miocene, while it is thought that a “proto-savanna” had already developed in southern Namibia (Neumann & Bamford, 2015). Forest and woodland dominated Australia during the early Miocene (MacPhail, 2007), including Casuarina and Eucalyptus forests, and woodlands around Lake Eyre in central Australia (Habeck-Fardy & Nanson, 2014). Coals in southeast Australia indicate a fire-prone heterogeneous landscape of meadow marshes and periodically flooded forests (Korasidis et al., 2017). Records from Antarctica are sparse. On the Antarctic Peninsula, a “mosaic” of tundra and woodlands of southern beech (*Nothofagus*) and conifer (*Podocarpus*) existed during the Oligocene and into the early Miocene (Anderson et al., 2011), while mainland Antarctica hosted aquatic lycopods (horsetails), mosses, and *Nothofagus* (Cantrill et al., 2017). This floral pattern might be analogous to forest biomes of modern Patagonia with temperate, alpine glaciers.

5.1.2. Middle Miocene (Langhian and Serravallian) Vegetation

The middle Miocene records the maximum advance of vegetation adapted to warm and/or wet climates to higher latitudes, as well as spreading of sclerophyllous forests, grass-dominated habitats, and initiation of modern deserts (Figure 4). Subhumid sclerophyllous forest was common in Eurasia, including west-central Europe, middle Asia, and Anatolia, where broad-leaved deciduous forest and subtropical forest also occurred (Bouchal et al., 2016; Ivanov et al., 2011; Kovar-Eder et al., 2008; Utescher et al., 2011), as well as more open, grass-dominated or steppe vegetation (Strömberg et al., 2007; Tang & Ding, 2013). Herb-dominated steppes began to spread across Central Asia, with the first significant expansion of grasslands in the region (Barbolini et al., 2020). Warm and wet-adapted floras dominated Africa (including the still-attached Arabian Peninsula) such as broadleaf woodland and mangroves along the coast of the United Arab Emirates (Jacobs et al., 2010), warm-temperate floras in Tunisia (Planderová, 1971), tropical evergreen broadleaf forest in the Niger delta (P. Simon et al., 1984), and subtropical mixed forests with palms along the southern African coast (Carr et al., 2010). However, more drought-tolerant vegetation also occurred, for example savanna in Kenya and Ethiopia (Jacobs & Deino, 1996; Wheeler et al., 2007), and the first modern desert in the Namib (Schneider & Marais, 2005; Senut & Ségalen, 2014).

North America records widespread warm-temperate evergreen broadleaf and mixed forests on the west and east coasts, whereas grass-dominated habitats continued to spread in the Rocky Mountains and continental interior (Harris et al., 2017; Loughney et al., 2020; Smiley et al., 2018; Strömberg, 2011). Tropical semi-evergreen and evergreen broadleaf forests dominated in Central America, Caribbean, and northern South America (Castañeda-Posadas et al., 2009; Kay & Madden, 1997; Pound et al., 2012; Retallack & Kirby, 2007). In non-Andean southern South America, floras typical of rainforests (e.g., tree ferns) saw an expansion during the latest early-middle Miocene, with evergreen broadleaf-mixed forests occurring to the east, followed by the spread of xerophytic and sclerophyllous vegetation, such as shrublands (Barreda & Palazzesi, 2007; Dunn et al., 2015; Palazzesi & Barreda, 2007, 2012; Pound et al., 2012).

Higher latitudes saw encroachment of vegetation types associated with lower latitudes today. These include tundra shrub with *Nothofagus* in Antarctica (Anderson et al., 2011; Lewis et al., 2008; Sangiorgi et al., 2018; Warny et al., 2009), Fagaceae-dominated forests (at 15 Ma) and conifer swamps and hummocks (at 13.5 Ma) in Iceland (Grimsson et al., 2007), cool temperate forests at >60°N (Pound et al., 2012; Wolfe, 1994), northern mixed hardwood forests in Beringia (Wolfe, 1994), and thermophilic floras along the Alaska coast (Reinink-Smith & Leopold, 2005; Reinink-Smith et al., 2018). In Australia, dry open woodlands with chenopod shrublands occupied the interior (Habeck-Fardy & Nanson, 2014; Martin, 2006), while tropical rainforest, subtropical mangroves, and warm-temperate mixed forests grew in the east (MacPhail, 2007; Pound et al., 2012).

The MCO represents a time of unusual and dynamic floras. In Austria, abrupt changes in vegetation and local paleoenvironment mark the onset of the MCO: within a few thousand years, rapid marine incursions,

accompanied by dinoflagellate and algal blooms, transformed existing salt marshes with abundant Cyperaceae into Taxodiaceae swamps (Kern et al., 2011). Pollen records from Ross Sea sediments document a massive increase (80-fold) in *Nothofagus* and *Podocarpus* at 15.7 Ma (Warny et al., 2009). This points to low tundra on coastal plains and a mosaic of tundra with shrub-like southern beech and low (maximum 50 cm) podocarp trees in sheltered areas. A second Antarctic marine record shows a dominance of pollen from members of the Podocarpaceae and *Nothofagus* (Sangiorgi et al., 2018). These indicate the presence of woody sub-Antarctic or sub-alpine vegetation, along with pollen from plants representative of shrub-tundra, and peat-lands (Sangiorgi et al., 2018).

5.1.3. Late Miocene (Tortonian and Messinian) Vegetation

The late Miocene ushered in major changes in vegetation linked to paleogeographic changes and a drying, cooling climate. Diverse biomes were present across Eurasia and East Africa, including mixed coniferous broadleaved forests, mesophytic forests, and herbaceous floras in lakeside/riverine associations, as well as steppes and C₃/C₄-dominated grasslands (Barbolini et al., 2020; Denk et al., 2018; Quade & Cerling, 1995; Strömberg, 2011; Figure 4). Forests continued to dominate parts of East Asia (Pound et al., 2012; Wu et al., 2019; Xu et al., 2008) and Central-Western Europe (Donders et al., 2009; Erdei et al., 2009; Pound and Riding, 2016; Pound et al., 2012). However, these forests progressively lost thermophilous and humid-loving elements in response to continued cooling and decreasing availability of growing season moisture (Donders et al., 2009; Martinetto et al., 2017). The youngest of these “warm-wet” floras are reported from the Plio-Pleistocene of Italy (Martinetto et al., 2017) and Pliocene of Portugal (Vieira et al., 2018) and suggest a southwards contraction in their European distribution during the late Miocene to points of refugia proximal to the coasts (Vieira et al., 2018).

In North America, boreal evergreen needle-leaf forests replaced cool-temperate mixed forests in the north, although these retained some thermophilous elements such as *Alangium*, *Magnolia*, *Nyssa*, and *Zanthoxylum* and were more diverse than modern boreal forests (Leopold et al., 1992; Pound et al., 2012; White et al., 1997; Wolfe, 1994; Reinink-Smith et al., 2018). In western North America, forests fragmented into more open habitats, as temperate xerophytic shrublands and woodlands became common in southwest North America, and the tree cover became increasingly sparse in the grassland-woodland mosaic that dominated in parts of Central and Western North America (Gabel et al., 1998; Hyland et al., 2018; Leopold & Denton, 1987; Loughney et al., 2020; Pound et al., 2012; Strömberg, 2011; Thomasson et al., 1990; Figure 4). In Central America and the Caribbean, tropical evergreen broadleaf forests persisted as they had in the middle Miocene, but warm-temperate evergreen broadleaf and mixed forest also began to develop (Graham, 1998; Pound et al., 2012). In South America, drier biomes became increasingly more prevalent, including tropical savanna (see below), tropical evergreen/deciduous broadleaf forest and woodland, temperate sclerophyll woodland and shrubland, and temperate xerophytic shrubland (Graham et al., 2001; Gregory-Wodzicki, 2002; Kirschner & Hoorn, 2020; Palazzesi & Barreda, 2007, 2012; Pound et al., 2012).

In Africa, low latitudes hosted tropical evergreen broadleaf forest, tropical savanna, and tropical grassland (Eisawi & Schrank, 2008; Médus et al., 1988; Morley & Richards, 1993; Poumot, 1989; Pound et al., 2012). To the south, fire-prone ecosystems were forming in southern Africa, and grassland expansion limited the extent of the forest biome (Mucina & Geldenhuys, 2006; Rossouw et al., 2009). Along the southwestern African coast, succulent vegetation replaced Afromontane forest dominated by *Podocarpus*, as well as subtropical coastal grasslands and thickets (Dupont et al., 2011). In Australia, temperate sclerophyll woodland and xerophytic shrubland expanded at the expense of rainforest through the late Miocene, with (C₃) grasses becoming important components of vegetation in the latest Miocene (Andrae et al., 2018; MacPhail, 2007; Martin, 2006; Pound et al., 2012).

High-latitudes saw shifts to cold-adapted floras or even floral eradication. By the late Miocene, Antarctic ice cover was extensive, possibly excluding even sparse tundra, although vegetation was still present in Wilkes Land at around 11 Ma (Anderson et al., 2011; Sangiorgi et al., 2018; Figure 4). In the Arctic, flora switched to lower diversity mixed hardwood and conifer dominated forests (Reinink-Smith et al., 2018; C. J. Williams et al., 2008; Wolfe, 1994). The diversity of thermophiles decreased further through the late Miocene of Alaska and Siberia (Reinink-Smith & Leopold, 2005; Volkova, 2011; Wolfe, 1994). Siberian pollen records suggest the appearance of steppe and semi desert floras in some regions in the latest Miocene (Volkova, 2011). The “Arctic tree line” extended up to 80°N (compared to 70°N today), and did not retreat southward until

the middle Pliocene (modern-like Arctic tundra and forest-tundra did not form until ~3 Ma; Matthews et al., 2019; Volkova, 2011). Transatlantic migration to Iceland of oaks with Eurasian and North American affinities indicates a North Atlantic Land Bridge served as a corridor for plant migration until the late Miocene (Denk et al., 2010; Grímsson & Denk, 2007).

5.1.4. The Asynchronous Rise of C₄ Grasses

Grass-dominated habitats became more common—and increasingly open—after ~10 Ma across parts of Eurasia, North and South America, Australia, and Africa (Akgün et al., 2007; Andrae et al., 2018; Barreda & Palazzesi, 2007; Bertini & Martinetto, 2011; Feakins et al., 2020; Hoetzel et al., 2015; Ivanov et al., 2011; Kovar-Eder et al., 2008; Médus et al., 1988; Pound et al., 2011; Quade & Cerling, 1995; Strömberg, 2011; Figure 4). In addition, the late Neogene saw a dramatic, cross-continental restructuring of low-mid-latitude ecosystems associated with the rise to dominance of C₄ grasses (Figure 1). Phylogenetic analyses indicate that grasses with C₄ photosynthesis, which promotes carbon fixation in hot, dry, and/or summer wet climates, evolved 22–24 times independently within a clade of tropical grasses (PACMAD) starting by at least the early Oligocene (Aliscioni et al., 2012; Christin et al., 2014, 2008; Prasad et al., 2011; Urban et al., 2010). Comparative work on the environmental preferences of modern grasses further suggest that the C₄ pathway was promoted in warm, arid and/or open habitats (Edwards & Smith, 2010; Osborne & Freckleton, 2009; S. H. Taylor et al., 2014). Nonetheless, it was not until the late Miocene to Pliocene that they became dominant, replacing forests and low-mid latitude C₃ grasslands (Cerling et al., 1997; Edwards et al., 2010; Feakins et al., 2013; Karp et al., 2018). Numerous geochemical archives document this widespread expansion of the isotopically distinctive C₄ grasses, including soil carbonates (D. L. Fox et al., 2012; Quade et al., 1995), soil organic matter (Cerling et al., 2011), the teeth of grazing mammals (Badgley et al., 2008; Cerling et al., 1997; Uno et al., 2011), phytoliths (McInerney et al., 2011), and leaf wax (Andrae et al., 2018; Feakins et al., 2005; Tipple & Pagani, 2010); these records are complemented by phytolith data adding further detail to our understanding of vegetation change during this time (Cotton et al., 2014; Hyland et al., 2018; Strömberg & McInerney, 2011). The sum of data points to substantial variation in the timing of the C₃–C₄ switch; thus, in tropical Africa, this transition started as early as 10 Ma (Feakins et al., 2013; Polissar et al., 2019; Uno et al., 2016), whereas in Australia, it did not begin until 3.5 Ma, well into the Pliocene (Andrae et al., 2018).

The drivers of this sweeping ecological shift are still debated. The original suggestion of declining atmospheric carbon dioxide as a global forcing (Cerling et al., 1997) was first rejected because of the spatial variations in the timing of C₄ expansion and the lack of pCO₂ proxy support (Pagani et al., 1999; Pearson & Palmer, 2000). More recently, Cerling et al.'s pCO₂ hypothesis has been revitalized (Herbert et al., 2016; Polissar et al., 2019) thanks to emerging evidence for a pCO₂ drop after the MCO (see Section 8), although the evidence for a proximal trigger associated with the first late Miocene C₄ expansions remains preliminary (Bolton et al., 2016; Mejía et al., 2017). The time-transient nature of regional C₄ expansions requires a more nuanced consideration of multiple and region-specific drivers (Edwards et al., 2010; Osborne, 2008). Thus, cooling, drying, and seasonality have been invoked in different areas (e.g., D. L. Fox & Koch, 2004; Y. Huang et al., 2007; Strömberg & McInerney, 2011), whereas recent evidence for paleofire regimes (Karp et al., 2018) and herbivory (Charles-Dominique et al., 2016) point to synergistic interactions of factors that promoted and sustained these ecosystems (Charles-Dominique et al., 2016; Scheiter et al., 2012). Likely the expansion of grassland and steppe ecosystems allowed for a diversification of large mammalian herbivores (see Section 5.4), and the megafauna themselves may have significantly promoted the balance of grasslands over forest by their browsing pressure (Charles-Dominique et al., 2016; Owen-Smith, 1987).

5.2. Freshwater Fish and Herpetofauna

South American and African Miocene freshwater fish faunas are dominated by archaic actinopterygians (ray-finned fishes), but the radiation of cichlid teleosts in the Great African Lakes during the late Miocene marks one of the most dramatic changes in Cenozoic freshwater fish faunas (Friedman et al., 2013; K. M. Stewart, 2001). Eurasian Miocene freshwater fish faunas are dominated by carpfishes, that had already replaced the dominating Perciformes during the Oligocene after the closure of the Turgai Strait (Hierholzer & Mörs, 2004). Early and middle Miocene European fish faunas also contain abundant tropical to subtropical toothcarps (Cyprinodontiformes) and snakeheads (Channidae) (Böhme, 2010; Reichenbacher et al., 2004).

Miocene South American herpetofaunas (reptiles and amphibians) show significant latitudinal differences. In Patagonia, helmeted frogs (*Australobatrachia*) became extinct during the Miocene, probably related to a decrease of humidity caused by the rise of the Andes, whereas the late Miocene Urumaco fauna in Venezuela is characterized by a highly diverse crocodylomorph fauna and giant pleurodire turtles (Otero et al., 2014; Sanchez-Villagra & Aguilera, 2006). Early Miocene northern hemisphere herpetofaunas, including giant salamanders (*Cryptobranchioidea*), alligators, and soft-shelled turtles, show a holarctic distribution such as in the Paleogene. By the middle and late Miocene these faunal elements disappeared in Europe together with other tropical to subtropical ectothermic tetrapods, including carettochelyne turtles, giant tortoises, monitor lizards, chameleons, cobras, boids (boas), and coral snakes (Čerňanský et al., 2017; Joyce et al., 2004).

5.3. Terrestrial Birds

Early to middle Miocene European bird faunas comprised tropical to subtropical parrots, aningas (snake birds), and flamingos, that disappeared during the late middle Miocene (Dalsätt et al., 2006; Mayr & Göhlich, 2004). Miocene parrots, aningas, and flamingos are also known from Asia, Africa, the Americas, New Zealand, and Australia (Baird & Vickers-Rich, 1998; Olson, 1985; Worthy et al., 2010, 2011; Zelenkov, 2016). In Patagonia and other open landscapes of South America, cursorial ratites (rhea relatives) were widespread and other cursorial, giant carnivorous birds (the “terror birds,” Figure 1) occupied one of the large land-predator niches (Agnolin, 2017; Degrange et al., 2019). In the early Miocene the first ostriches originated in Africa, and by the middle to late Miocene, these large cursorial birds occupied the open landscapes across the continent, and had even dispersed into Eurasia (Bibi et al., 2006; Zelenkov et al., 2019). In Australia, giant cursorial gastornithiform and casuariform birds are known from the Miocene (Boles, 1992; Worthy et al., 2016).

5.4. Terrestrial Mammals

Miocene terrestrial mammal faunas of Eurasia showed marked regional and temporal differences. While early to middle Miocene Central Asian faunas were already adapted to drier conditions, contemporaneous faunas in Europe as well as in East and South-east Asia, document tropical to subtropical rainforest environments (X. Wang et al., 2013). Characteristic tropical to subtropical elements among small mammals are marsupials, moonrats, spiny dormice, and giant flying squirrels (Mörs, 2002; X. Wang et al., 2013; Figure 1). An important faunal turnover among large mammals was the “Proboscidean Datum Event”—the dispersal of African and North American elements into Eurasia in the early Miocene (mid Burdigalian, 18.5 Ma) (Figure 1), including gomphotheres, deinotheres, chevrotains (mouse-deer), forest horses, primates, and the extinct giant hyaenodontids (Rössner & Heissig, 1999). In Europe, all of these taxa disappeared during the middle and late Miocene due to drier conditions, whereas some of the small mammals survived until today in Southeast Asia. The close relationship of these early Miocene faunas indicates an undisrupted forest belt from Europe to East/Southeast Asia at that time (Pineker & Mörs, 2011). At a similar time (~18 Ma), hypsodont horses, including *Merychippus* and relatives, evolved in North America. This is the traditional marker of the spread of grasslands in most continents, replacing closed by open habitats, although this shift is now known to have occurred well before this shift (Damuth & Janis, 2011; Strömberg, 2006, 2011). The evolution of hypsodonty (high-crowned teeth for grinding grass) in this clade is associated with a rapid taxonomic radiation reflecting a shift from a browsing diet of leaves to a grazing diet of grasses (but see, e.g., Semprebon et al., 2019). Other North American herbivores developed hypsodont teeth in parallel, such as camels, although some lineages were already hypsodont/hypselodont in the Oligocene, including some early rodents (Jardine et al., 2012). At the beginning of the late Miocene, a second North American dispersal event, the “*Hipparion* Datum,” allowed open land-adapted steppe horses to spread quickly over the whole of Eurasia, followed by canids in the late Miocene (Rössner & Heissig, 1999; Figure 1).

Due to the isolation of Africa in the Paleogene, Miocene mammal faunas there were dominated by endemic Afrotheria, with several proboscidean taxa, hyraxes, tenrecs, and primates, as well as archaic pig-like anthacotheriids and carnivorous hyaenodontids that had become extinct on other continents (Werdelin & Sanders, 2010). The early and middle Miocene dispersal of Eurasian carnivores, perissodactyls, artiodactyls, insectivorans, and rodents represents a major faunal turnover, like the dispersal of African mammals into

Eurasia at the same time (Rössner & Heissig, 1999; Werdelin & Sanders, 2010). In the middle Miocene, hippos evolved in Africa (Werdelin & Sanders, 2010). The beginning of the late Miocene in Africa is also marked by the “*Hipparion* Datum,” when open land-adapted steppe horses occur—the first horses that reached Africa (Rössner & Heissig, 1999; Werdelin & Sanders, 2010). Even later in the Miocene, the earliest camels arrived (Werdelin & Sanders, 2010). The first hominins, such as *Sahelanthropus tchadensis*, which show skeletal adaptations for habitual or obligate bipedality, diverged from the common ancestor of chimpanzees in the late Miocene (~6–7 Ma; Brunet, 2020), or possibly earlier (Lebatard et al., 2008), perhaps as African forests began shrinking.

Although linked to Eurasia, North America had its own evolution of mammalian faunas, since Beringia acted as a dispersal filter (Rössner & Heissig, 1999). Three-toed horses evolved in the Miocene, with browsing forest horses being characteristic for the early Miocene, the first grazing horses appearing in the middle Miocene, and the very successful steppe-horses radiating in the late Miocene (Janis et al., 1998). Contemporaneously, large forest-dwelling horses evolved but went extinct in the late Miocene (Janis et al., 1998). Oreodonts were still abundant in the early Miocene, and camelids had their main radiation in the Miocene (Janis et al., 1998). Native rodents were the early Miocene fossorial beavers that were replaced by fossorial mylagaulids and geomyids in the middle Miocene (Janis et al., 2008). The native mammalian carnivores were canids, with large hypercarnivorous, bone-crushing dogs evolving, occupying the niche of Old World hyenas (Janis et al., 1998). The early to middle Miocene dispersal of Eurasian mammals represents an important faunal turnover with the immigration of insectivores, lagomorphs, hamsters, a wide range of carnivores, rhinos, artiodactyls, and proboscideans (Janis et al., 2008; Rössner & Heissig, 1999).

South America was isolated from all other continents during the entire Paleogene, which resulted in unique, endemic Miocene mammalian faunas, with marsupials, xenarthrans (armadillos, glyptodonts, anteaters, and ground sloths), meridiungulates (Notoungulata, Litopterna, and Astrapotheria), caviomorph rodents, and platyrrhine primates (Vizcaino et al., 2012). Early Miocene Patagonian faunas indicate semitropical mixed forested and open habitats with grasses inhabited by insecti- and frugivorous small marsupials, large hypercarnivorous marsupials, glyptodonts, anteaters, ground sloths, and armadillos, hippo-like semiaquatic astrapotheres, horse- and gazelle-like, three- and one-toed litopterns, rabbit-like tyotheres, different families of caviomorph rodents, and the platyrrhine primates (Vizcaino et al., 2012). The middle Miocene neotropic La Venta fauna in Colombia consists also entirely of native South American mammals, including giant glyptodonts, the first pampatheres (Cingulata), anteaters, several platyrrhines, many meridiungulate species, and marsupial sabertooths (Kay et al., 1997). Furthermore, the late Miocene Urumaco fauna in Venezuela contains no North American mammals, and is characterized by giant ground sloths, armadillos, and the largest ever known rodents (Sanchez-Villagra & Aguilera, 2006; Figure 1). Nevertheless, there is evidence of gomphotheres from the late Miocene of Peruvian Amazonia, indicating a Miocene dispersal of North American mammals into South America (Campbell et al., 2009).

Like South America, Australasia (Australia and Papua New Guinea) was isolated from all other continents during the entire Paleogene, which resulted in even more unique, endemic Miocene land mammal faunas. These consisted entirely (with the exception of a few monotremes) of australidelphian marsupials (Dasyuromorphia, Peramelemorphia, Notoryctemorphia, and Diprotodontia) that occupied the herbivore, carnivore, frugivore, and insectivore, niches (Long & Archer, 2002; Vickers-Rich & Rich, 1993). The giant Miocene platypus still had teeth, in contrast with the recent platypus (Vickers-Rich & Rich, 1993). During the Miocene, mosaic riparian grasslands with many browsing marsupials (koalas, wombats, and kangaroos) gradually disappeared and were replaced by semiarid grasslands, which were occupied by macropodiforms: giant rat-kangaroos and early kangaroos (Couzens & Prideaux, 2018; Long & Archer, 2002; Vickers-Rich & Rich, 1993; Figure 1). By the late Miocene, kangaroos had evolved bipedal locomotion. The dog-like dasyuromorphs, vombatiforms, and carnivorous macropodids occupied the niche of mammalian predators (Long & Archer, 2002; Vickers-Rich & Rich, 1993).

6. Marine Climate Records

Marine records of Miocene climate rely largely on benthic foraminiferal $\delta^{18}\text{O}$ as a combined index of deep ocean temperature and global ice volume, planktonic $\delta^{18}\text{O}$ and geochemical proxies for sea surface temperatures (SSTs), such as alkenone undersaturation (UK'_{37}), TEX_{86} , and planktonic foraminiferal Mg/Ca. Absolute temperature estimates from planktonic and benthic foraminiferal Mg/Ca in the Miocene require assumptions about past seawater Mg/Ca ratios. Carbonate clumped isotope paleothermometry, which is independent of the $\delta^{18}\text{O}$ value of parent seawater, provides a viable alternative to the classic $\delta^{18}\text{O}$ paleothermometer and, thus an independent test of the Mg/Ca approach (Modestou et al., 2020).

6.1. Transitions and Variability in Deep Ocean Temperature and Ice Volume Manifest in Benthic Foraminiferal $\delta^{18}\text{O}$

The Miocene began with the OMT $\delta^{18}\text{O}$ maximum, signifying substantial ice volume (Figures 1 and 2). Increased resolution of benthic foraminiferal $\delta^{18}\text{O}$ shows that the early Miocene was characterized by high amplitude, long- and short-eccentricity-paced climate variations (Liebrand et al., 2016, 2017; Pälike et al., 2006) superimposed on longer 1.2-Ma tilt cycles (Miller et al., 2020; Figure 2). This is thought to be linked to a unipolar-glaciated climate with a dynamic East Antarctic Ice Sheet with periods of large-scale ($\sim 50\text{--}60$ m sea-level equivalent) growth and decay, during which time ice may have reached volumes greater than the modern (Liebrand et al., 2017; Miller et al., 2020; Pekar & DeConto, 2007). High-resolution benthic foraminiferal stable isotopes from IODP Site U1337 (Eastern Equatorial Pacific Ocean) revealed that the start of the MCO at ~ 16.9 Ma was marked by a relatively abrupt warming ($\sim 1\text{‰}$), coupled to the onset of a negative $\delta^{13}\text{C}$ excursion that lasted ~ 250 kyr (Holbourn et al., 2015). This abrupt $\delta^{18}\text{O}$ decrease is evident in different oceans, at DSDP Site 574 in the Central Equatorial Pacific (Woodruff & Savin, 1991), Southern Ocean (ODP Site 1090; Billups et al., 2002), South China Sea (ODP Sites 1146 and 1237; Holbourn et al., 2007), and Central Pacific (IODP Site U1335; Kochhann et al., 2016), supporting the global occurrence of this warming event. The MCO represents an extended interval of relative global warmth, characterized by high-amplitude 100 kyr climate variability ($>1\text{‰}$ variation in benthic foraminiferal $\delta^{18}\text{O}$), primarily paced by 100 kyr eccentricity (Holbourn et al., 2007, 2014). Global climate variability was mainly dependent on southern hemisphere summer insolation, thought to be amplified by a dynamic Antarctic ice sheet (De Vleeschouwer et al., 2017). Mean Antarctic ice volume was reduced and near ice-free conditions may have occurred during peak 405 ka cycles (Miller et al., 2020). One prominent hyperthermal event reflecting intense warming and/or ice volume decreases, with a benthic foraminiferal $\delta^{18}\text{O}$ decrease of $\sim 1\text{‰}$, is centered at 15.6 Ma and can be correlated across several oceans (Kochhann et al., 2016).

After ~ 14.7 Ma, there is stepwise progression (MMCT) from the period of high amplitude variability in climate and Antarctic ice cover, to an increasingly colder mode with dampened orbital-scale variability, more permanent ice sheets, and lower sea level (De Vleeschouwer et al., 2017; Holbourn et al., 2013b, 2018; Lear et al., 2015; Miller et al., 2020; Figure 2). The most prominent steps in temperature and/or ice volume occur at ~ 13.8 Ma ($\sim 1\text{‰}$ increase in $\delta^{18}\text{O}$) and at ~ 13.1 Ma ($\sim 0.5\text{‰}$ increase in $\delta^{18}\text{O}$). These distinct increases marked the base of oxygen isotope zones Mi-3 and Mi-4, originally defined by Miller et al. (1991, 2020). The dampening of orbital-scale variability and the progressive increase in $\delta^{18}\text{O}$ continues from ~ 13 to 5.5 Ma (Drury et al., 2016, 2017, 2018; Holbourn et al., 2013b, 2018). De Vleeschouwer et al. (2017) argued that this can be explained by the increasing influence of a northern hemisphere summer insolation maxima, as the Antarctic ice sheet became “too big” to be influenced by southern hemisphere precession forcing. The late Miocene record in the deep Pacific is characterized by a modest ($<0.3\text{‰}$) long term trend to more positive benthic foraminiferal $\delta^{18}\text{O}$ (Tian et al., 2018).

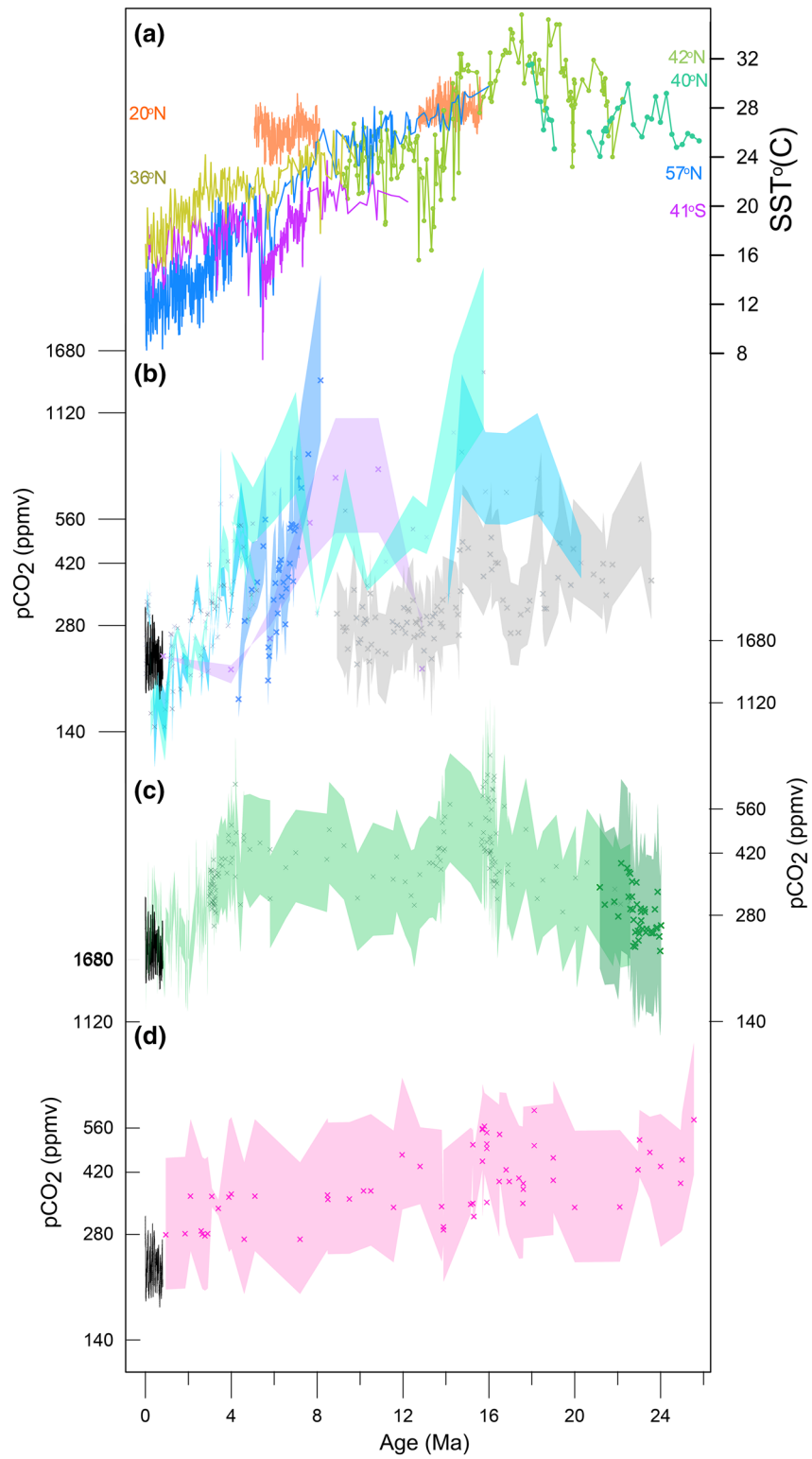
6.2. Miocene Trends in Deep Sea and Sea Surface Temperature

The existing Mg/Ca deep sea temperature records suggest that early and middle Miocene bottom water temperatures (BWTs) were $5^{\circ}\text{C}\text{--}9^{\circ}\text{C}$ warmer than present (Billups & Schrag; 2003; Hollis et al., 2019; Lear et al., 2015, 2000, 2002; Miller et al., 2020; Shevenell et al., 2008). This conclusion involves various phases of Mg/Ca temperature re-calibration as understanding of nonthermal effects on foraminiferal calcite Mg/Ca unfold, such as seawater Mg/Ca, carbonate saturation state, and diagenesis (Billups & Schrag; 2003; Hollis

et al., 2019; Lear et al., 2015). At high-southern latitudes (Tasmanian Gateway), Shevenell et al. (2008) estimated maximum temperatures of 7°C–8°C for the MCO, ~6.5°C after the MMCT (compared to 0.5°C at present) and an overall cooling across the MCT of $2 \pm 2^\circ\text{C}$. Miller et al. (2020) report a similar pattern from Pacific cores. Modestou et al. (2020) found deep-water temperatures in the Indian Ocean that are 9°C warmer based on paired clumped isotope and Mg/Ca temperature proxies, with minor discrepancies between the two methods attributed to carbonate saturation state effects on Mg/Ca. The Antarctic ice sheet was highly dynamic during the early Miocene and MCO, with a transition to a more stable ice sheet after the MMCT (De Wleeschouwer et al., 2017; Holbourn et al., 2018, 2013; Miller et al., 2020; Modestou et al., 2020). This is surprising considering the more constant and relatively warm reconstructed BWT of the time (above 5°C until the late Neogene, compared to < 1°C at present).

Estimates of early and middle Miocene SST are rather limited. Representative SST records from different latitudinal regions derived from alkenone, TEX_{86} , and foraminiferal Mg/Ca proxies are shown in Figure 5. Alkenone SST from 40°N in the western Atlantic range from 23°C to >31°C, with sub-Myr variability between the OMT and MCO (Gutián et al., 2019; Z. Liu et al., 2018). In the Central Atlantic at 42°N, TEX_{86} temperatures range from 23°C to 34°C, with peak temperatures registered just prior to the MCO, and an >8°C cooling across the MMCT (Super et al., 2018). High latitude records are especially scarce. Herbert et al. (2020) present new UK'_{37} records from the Danish North Sea that suggest Miocene SSTs were 11°C–20°C higher than modern mean annual temperature at ~55°N, with a clear maximum during the MCO evidencing the global-scale of climatic warming. Super et al., (2020) find a similar scale of MCO warming at other North Atlantic stations (10°C–15°C, 42–57°N). They find a smaller degree of MMCT cooling at the high latitude compared to the mid latitude station, suggesting a decoupling of northern subpolar compared to Antarctic temperatures, and the possibility that increased northern heat transport during this transition. TE_{x86} SSTs from the western Equatorial Atlantic are surprisingly similar in terms of absolute temperature range compared to those of the subtropical Atlantic (25°C–30°C), and show a modest 4°C cooling across the end MCO through MMCT (Y. G. Zhang, Pagani, et al., 2013); absolute temperatures from Mg/Ca are similar (27°C; Sosdian et al., 2018). Mg/Ca temperatures from the western tropical Pacific are about 30°C in the early Miocene (Sosdian et al., 2018) and, alongside a new record from ODP Site 761, show a cooling associated with the MMCT (Sosdian & Lear, 2020). These temperatures are further supported by Mg/Ca measurements from low latitude Miocene glassy foraminifera (Nairn et al., 2021). In the South China Sea, Mg/Ca surface temperatures over the interval 15.7 to 12.7 Ma range between 26°C and 30°C (values not corrected for changes in sea water chemistry) and exhibit only a slight cooling over the MMCT (Holbourn et al., 2010). By contrast, temperatures at ~55°S in the Southern Ocean show a stepwise cooling of 6°C–7°C across the MMCT (Shevenell et al., 2004). The many older SST estimates from oxygen isotopes of planktonic foraminifera (e.g., Savin et al., 1985) are now thought to be cool-biased due to diagenetic alteration (D. R. M. Stewart et al., 2004). Limited data from glassy foraminifera from the early and middle Miocene offshore Tanzania indicates water column temperatures similar to or higher than modern (Stewart et al., 2004).

During the late Miocene, alkenone SST decreased in all oceans, with high latitude sites in both hemispheres cooling by up to 8°C (Herbert et al., 2016). Many sites show steepest cooling between seven and 5.5 Ma, an episode sometimes referred to as the Late Miocene Cooling (LMC; Figure 2). Tropical upwelling sites cooled in parallel with the mid- and high latitudes. Although the magnitude of cooling is least constrained in the tropics, where temperatures exceed the sensitivity range of UK'_{37} , recent Mg/Ca analyses on glassy foraminifera support the warmest UK'_{37} estimates, indicating that the magnitude of cooling has not been significantly underestimated by this proxy (Nairn et al., 2021). However, Mg/Ca SST suggest an average cooling of nearly 4°C between seven and 5.5 Ma in the South China Sea (Holbourn et al., 2018). TEX_{86} records from the Western Pacific Warm Pool, on the other hand, suggest ~2°C cooling in the late Miocene. Available data therefore suggest a late Miocene steepening of meridional thermal gradients. Orbital-scale variation in tropical SST is also evident in the late Miocene, and intense SST cooling episodes—coinciding with planktonic $\delta^{13}\text{C}$ depletion and with planktonic and benthic foraminiferal $\delta^{18}\text{O}$ enrichments (TG isotope stages of Shackleton et al., 1995)—additionally suggest development of ephemeral northern hemisphere glaciations ~6–5.5 Ma (Holbourn et al., 2018). In the tropical Pacific, the east-west temperature asymmetry during the middle Miocene (L. Fox et al., 2021) suggests that eastern Pacific upwelling was active throughout the MCO and MMCT. However, systematic differences between paired TEX_{86} and UK'_{37}



SST estimates, raise new questions about the water-column source of these different archives, especially in oceanographically complex upwelling regions.

6.3. Spatial Gradients in Sea Surface Temperature

The Miocene has much in common with the Pliocene and Eocene, and is characterized by conditions of global warmth and much reduced meridional and zonal temperature gradients (e.g., Goldner et al., 2014a). New SST records from the Danish North Sea emphasize the view of bi-hemispheric warming during the MCO (Herbert et al., 2020). Many tropical proxy records (e.g., Chaisson & Ravelo, 2000; Medina-Elizalde et al., 2008; Wara et al., 2005) suggest the absence of the east-west (zonal) temperature difference across the equatorial Pacific Ocean between ~2 and 5 Ma, creating a "permanent El Niño" state (Cane & Molnar, 2001; Fedorov et al., 2006; Molnar & Cane, 2001, 2007) which is thought to have characterized previous Cenozoic greenhouse climates (Philander & Fedorov, 2003). Much of the tropical-to-subtropical warming in the Miocene and Pliocene is focused in ocean upwelling zones, including all four upwelling zones associated with major eastern boundary currents—California, Humboldt, Canary, and Benguela—which show anomalies of +3°C to +9°C relative to today (Brierley et al., 2009; Dekens et al., 2007; Herbert & Schuffert, 1998; Li et al., 2011; Marlow et al., 2000). These results suggest novel ocean-atmosphere interactions in a warmer world (Fedorov et al., 2013; Arnold et al., 2012; Goldner et al., 2011; Sriver & Huber, 2010; Tziperman & Farrell, 2009; Barreiro & Philander, 2008; Pierrehumbert, 2000). Yet, doubts have been raised regarding the interpretation of these proxy records (Bonham et al., 2009; Dowsett & Robinson, 2009; Galeotti et al., 2010; Groeneveld et al., 2006; Huber & Caballero, 2003; Rickaby & Halloran, 2005; Scroxton et al., 2011; von der Heydt & Dijkstra, 2011; Watanabe et al., 2011; Wunsch, 2009; Y. G. Zhang et al., 2014). Recent work (O'Brien et al., 2014; Y. G. Zhang et al., 2014) using TEX₈₆ suggests higher temperatures in the Pacific and Atlantic Warm Pools than previously inferred, indicating that the Pacific may not have been stuck in a "permanent El Niño," based on shallow zonal temperature gradients as some had suggested (e.g., Fedorov et al., 2006). This is a controversial result and more work is necessary to decipher the differences between various reconstructions (Lawrence et al., 2020).

Among the traditional mechanisms proposed to explain weakened temperature gradients, warming preferentially in the upwelling zones, and deep tropical thermoclines are: enhanced high latitude freshwater forcing (Fedorov et al., 2004, 2006), the Panama Gateway being open (Haug & Tiedemann, 1998; Klocker et al., 2005; Steph et al., 2010), and the rearrangement of the islands in the maritime continent (Dayem et al., 2007; Molnar & Cane, 2007). These processes are represented, albeit imperfectly, in the latest generation of climate models, yet while much progress has been made in modeling (for example by the Pli-oMIP effort), substantially weakened gradients are not reproduced in Pliocene (Dowsett et al., 2012; Hayward et al., 2000, 2010, 2011, 2012, 2016; Howell et al., 2014; Salzmann et al., 2013) and Miocene (Goldner et al., 2014a; Herold et al., 2011b, 2012) simulations. Fedorov et al. (2013) examined many of these mechanisms in a single modeling framework and concluded that none seems to be able to explain the observed patterns on its own. At higher latitudes, the data more clearly converge on a warming that is impossible to explain with existing models. Proxy evidence suggests that the middle Miocene Arctic, was ~11°C–19°C warmer than at present and sea ice was not perennial (see e.g., Goldner et al., 2014a; Herold et al., 2011b, 2012; Kender & Kaminski, 2013; Pound et al., 2012; Stein et al., 2016; Super et al., 2020). After the cooling of

Figure 5. Summary of SST and marine-based $p\text{CO}_2$ estimates spanning the Miocene. (a) Representative SST records from different latitudinal regions derived from alkenone, TEX₈₆, and foraminiferal Mg/Ca proxies. Alkenone records include ODP 982 (57°N in Atlantic), ODP 1208 (36°N in Pacific), and ODP 1088 (41°S in Atlantic) all from Herbert et al. (2016); and ODP 1406 (40°N in western Atlantic) from Guitián et al. (2019). TEX₈₆ record includes ODP 608 (42°N in eastern Atlantic) from Super et al. (2018). Mg/Ca records (20°N in western Pacific) from Holbourn et al. (2010), and Holbourn et al. (2018). (b) $p\text{CO}_2$ estimates derived from the phytoplankton proxy. Light turquoise and blue records are derived from alkenone isotopic fractionation in sites in the tropical Atlantic (Bolton et al., 2016; Y. G. Zhang, Pagani, et al., 2013), applying new culture-based calibrations (Bolton et al., 2016; Stoll et al., 2019; Y. G. Zhang, Pagani, et al., 2013); the dark blue curve to the left is derived from alkenone isotope fractionation in the South Atlantic applying new culture-based calibrations (Tanner et al., 2020). The purple record is derived from diatom-bound organic matter from a tropical Pacific site, applying a culture-based calibration model (Mejia et al., 2018). The gray curve shows a record from alkenone fractionation in the North Atlantic applying a classical diffusive calibration model (Super et al., 2018). (c) $p\text{CO}_2$ estimates from the boron isotope proxy, updated to homogeneous carbon system parameters, from Sosdian et al. (2018) and from Greenop et al. (2019). (d) Pink records are stomatal proxy-based $p\text{CO}_2$ reconstructions, using the stomatal ratio, stomatal index and gas exchange methods, from Beerling et al. (2009); Franks et al. (2014); Grein et al. (2013); Kürschner et al. (1996, 2008); Londoño et al. (2018); Reichgelt et al. (2016); Steinhorsdottir et al. (2019, 2020); Stults et al. (2011), and Y. Wang et al. (2015). In (b–d), black lines illustrate the ice core $p\text{CO}_2$ measurements of the last 800 ka (Lüthi et al., 2008).

the MMCT, however, proxy evidence for perennial Arctic Sea ice does occur (~13 Ma; Krylov et al., 2008), suggesting a coeval freeze in the Arctic and Antarctic regions. Thus, while past climates like the Pliocene and Miocene are clearly not a perfect direct analog of near-future warming (Huber, 2013; Lunt et al., 2009), understanding climate variability during these warmer periods can be most useful in exposing feedbacks that may be active in future warming as well.

7. Terrestrial Climate Records

Paleobotanical evidence for climate change is based primarily on megafloras and palynofloras, with the majority of the data coming from the northern hemisphere (Harris et al., 2020; Pound et al., 2012; Figure 4). Climatic interpretations rely in large part on paleoecological reconstructions of past vegetation that record ecosystem transformation and primarily a response to temperature and rainfall changes. While floral data can be inverted to estimate temperature and precipitation, many climate models also include a vegetation module that predicts distribution of plant functional types, ecosystems, or biomes. Thus, even when a flora cannot directly quantify climate conditions (e.g., a mean annual temperature) they can still provide direct validation data based on nearest-living-relative assumptions of climatic tolerance or preference. In general, warming during the MCO shifted biomes toward higher latitudes, commonly accompanied by an increase in precipitation (wet-adapted floras; Figure 4). The later Miocene witnessed cooling and the retreat of these biomes. Other floral and faunal elements of the late Miocene further indicate a general trend toward more uniformly open habitats, increased aridification, and seasonality.

7.1. Early to Middle Miocene (Aquitanian, Burdigalian, Langhian) Floral Climate Records

Overall, paleobotanical proxy data indicate that the early to middle Miocene (Aquitanian to Burdigalian, ~23–13.8 Ma) witnessed increasingly higher precipitation and temperatures, especially at mid-high latitudes, where broad-leaved or mixed forests expanded at the expense of coniferous forests, grasslands, shrublands, and deserts (Böhme et al., 2007; Dunn et al., 2015; Graham, 1999; Harris et al., 2020; Pound et al., 2012; Utescher et al., 2000, 2011; Wolfe, 1985). A particularly dramatic example of warming is in Antarctica, where shrubby trees grew and summer temperatures may have reached 10°C (Warny et al., 2009). Estimates for the MCO propose global mean annual temperatures 5°C–6°C warmer than present-day (Hui et al., 2018), with the northern high-latitudes and northern temperate zones potentially 14°C and 9°C warmer than pre-industrial (Pound et al., 2012). These higher temperatures were accompanied by increased humidity in many parts of the world (e.g., Hui et al., 2018; Trayler et al., 2020), although reconstructions from New Zealand suggest the highest drought potential during the MCO (Reichgelt et al., 2019). Tropical forests expanded and were more extensive than today (Bonnefille, 2010; Jaramillo et al., 2020), also indicating a warmer and possibly wetter climate. Sclerophyllous forests covered vast areas of northwestern Central Anatolia and indicate a humid temperate climate with a brief drier season during the winter (Denk et al., 2017).

Terrestrial ecosystems experienced substantial heterogeneity in the regional manifestation of the MCO (Harris et al., 2020). In accordance with global climate trends inferred from marine cores, many records reflect warm and wet climates either being maintained during the MCO, or shifting to a warmer and wetter climate over this period, followed by cooling and drying thereafter. This is not always the case however; some studies indicate prolonged warm climates until ~10 Ma, and precipitation records are highly variable over the MCO, reflecting aridification leading into the event, or continual dry or wet climates throughout the Miocene (Harris et al., 2020). This climatic variability is indicated by contrasting patterns of closed vs. open habitat expansion at low versus mid-to high-latitudes, with many areas of the world experiencing forest densification. In contrast, palynofloras and phytolith assemblages suggest that open, grass-dominated, mosaic habitats, or steppe vegetation continued to spread during the middle Miocene in, for example, the western interior of the United States and eastern Mediterranean as part of an ecological transition that started by at least the early Miocene (Harris et al., 2017; Leopold & Denton, 1987; Smiley et al., 2018; Strömberg, 2011; Strömberg et al., 2007; Figure 1). Paleofaunas similarly show the diversification of hoofed mammals with dental and locomotory adaptations to life in open and/or grassy habitats (Janis, 1993; MacFadden, 2005; Mihalbachler et al., 2011; Morales-García et al., 2020; Semperebon et al., 2016, 2019). Geographic variation in the manifestation of the MCO complicates understanding of whether this event was fully or partially responsible for driving middle Miocene biotic changes (Harris et al., 2020; Trayler et al., 2020).

7.2. Middle to Late Miocene (Serravallian, Tortonian, Messinian) Floral Climate Records

Terrestrial floras show an increase in latitudinal temperature gradients amidst overall global cooling. The (near) complete loss of vegetation from Antarctica during the Serravallian (13.8–11.6 Ma) with little change in vegetation elsewhere (see Section 5 above) suggests an increasing latitudinal temperature gradient for the southern hemisphere (Pound et al., 2012). By the Tortonian (11.6–7.2 Ma), the southward spread of cool-adapted needle-leaf forests in the high-northern latitudes indicates an increasing latitudinal temperature gradient in the northern hemisphere (Jimenez-Moreno & Suc, 2007) (Figure 4). Enhanced temperature seasonality and a greater proportion of summer precipitation accompanied post-MCO cooling in central Europe (Bruch et al., 2011; Utescher et al., 2000). Decreased effective precipitation (drying) promoted the expansion of increasingly open, grass-dominated ecosystems in low-mid latitudes (e.g., Strömberg & McInerney, 2011; Strömberg et al., 2007), the appearance of the first Saharan dunes at 7 Ma (Schuster et al., 2006; Z. Zhang et al., 2014), and the formation of the Taklimakan Desert near the Miocene-Pliocene boundary (Böhme, 2003; Sun & Liu, 2006; Sun et al., 2009; Figure 4). High-latitude MAT reconstructions in the northern hemisphere are 5°C–6°C higher than pre-industrial values (Pound et al., 2012), suggesting at least an 8°C cooling from the MCO. Precipitation in Europe was periodically high, with “washhouse” events identified from herpetological assemblages (Böhme et al., 2008) and confirmed by palaeobotanical based reconstructions of mean annual precipitation of up to 1,929 mm per year (Pound et al., 2012; Utescher et al., 2017).

7.3. Other Terrestrial Climate Records

Soils, sediments, and the archives they contain including soil carbonates and terrestrial vertebrate teeth provide valuable dual archives of oxygen and carbon isotopes that together can provide quantitative measures of precipitation and temperature. Combined oxygen and carbon isotope compositions of early-middle Miocene teeth (in C₃-only ecosystems) show greater precipitation (≥ 500 mm/yr) and higher temperatures ($\sim 10^\circ\text{C}$) in southern and northern mid-latitudes compared to today (e.g., Argentina: Kohn et al., 2015; Western Europe: Tütken et al., 2006). Data from central Spain suggest a 5°C–10°C decrease in MAT across the mid-Miocene cooling event (~ 14 –13.5 Ma; Domingo et al., 2012) and from 11 Ma to today (van Dam & Reichart, 2009). Distributions of ectotherms also indicate a temperature decrease of at least 7°C between the MCO and ~ 13 Ma (Böhme, 2003) and a precipitation spike (up to $\sim 3\times$ modern) at ~ 10 Ma (Böhme et al., 2008).

7.4. Monsoons, Rain Shadows, and Topographic Proxies

Monsoons have been a feature of Earth's climate since at least the early Paleogene (Spicer, 2017), but their evolution through the Miocene, and similarity to the present-day monsoon systems, remain topical questions. In particular, the roles of changing paleogeography, $p\text{CO}_2$, and land-sea thermal contrasts in modifying the monsoons are debated. Monsoon signatures are already recorded in Eocene macrobotanical remains, gastropod shells, mammal teeth, and eolian dust from Asia (Licht et al., 2014; Quan et al., 2011), but it has been argued that they were not similar to the modern-day Asian monsoon, instead being generated primarily by seasonal migrations of the Inter-tropical Convergence Zone (ITCZ) (A. B. Herman et al., 2017; Spicer, 2017; Spicer et al., 2016; Yang et al., 2020). An ITCZ-type monsoon in East Asia may have existed as far back as the Early Cretaceous, transitioning to a sea breeze-dominated monsoon by the Miocene (Farnsworth et al., 2019). Overall, Asian monsoon intensification appears to have begun in the early Miocene and continued into the middle Miocene (Clift & Webb, 2019; Clift et al., 2014), but it is now recognized that the Asian monsoons are not a purely Miocene phenomenon related to Tibetan uplift (Spicer, 2017). Modeling studies (Acosta & Huber, 2019; Boos & Kuang, 2010; Huber & Goldner, 2012) have demonstrated that the existence of the monsoon is not dependent on the Tibetan Plateau. Rather, the projection of the Himalayas from the early to middle Miocene generated a strong rain shadow effect and is linked with intensification of the South Asian monsoon (Clift & Webb, 2019; Ding et al., 2017; Spicer et al., 2017).

The modern East Asia monsoon may also have been established around this time, driven by aridification in inner Asia as well as topographic changes in northeastern Tibet (Spicer, 2017; Tada et al., 2016). The expansion of herb-dominated steppes in Central Asia at 15 Ma is strongly linked with increased environmental

moisture brought by these monsoons (Barbolini et al., 2020). At ~12 Ma, chemical weathering and erosion budgets indicate monsoonal weakening in Southeast Asia, but the late Miocene remains a controversial period for monsoonal history because of proxy record conflicts (Clift & Webb, 2019). Strengthening of the South Asian monsoon at ~8 Ma was interpreted from an increase in the foraminifer *Globigerina bulloides*, which thrives on upwelling of deep nutrient-rich waters caused today by summer monsoon winds driving surface waters offshore (Kroon et al., 1991; Prell et al., 1992). However, new studies rather argue for intensified monsoonal activity and linked oceanic upwelling beginning earlier, at ~12.9 Ma (Betzler et al., 2016; Gupta et al., 2015), and a drying and cooling climate in Asia after 8 Ma (Clift & Webb, 2019). Changing climate in the late Miocene coincided with fundamental changes in the distribution and seasonality of monsoonal precipitation over Southeast Asia, suggesting a concurrent southward shift in the average summer position of the ITCZ in the northern hemisphere at ~7 Ma (Holbourn et al., 2018).

The role of the Asian monsoon in Miocene climate is receiving renewed attention, with evidence for increased silicate weathering in the Bay of Bengal associated with strengthening monsoonal rains after MMCT at 13.9 Ma (Ali et al., 2021; Bretschneider et al., 2021), and evidence for increased monsoon driven upwelling, biological production and ocean deoxygenation in the north west Indian Ocean during the middle to late Miocene (Bialik et al., 2020). Jöhnck et al. (2020) also find increased Indian monsoon variability during the Miocene-Pliocene transition (6.2–4.9 Ma). The processes explored have the potential to interact with the carbon cycle and sequester CO₂ on long time scales, either in the subsurface ocean or marine sediment reservoirs, thus possibly contributing to the long-term Neogene cooling. Furthermore, these new results support the view that monsoons are a highly dynamic climatic feature that do not respond linearly to external insolation forcing. The Asian monsoon exhibits distinct regional expression across timescales, highlighting the amplifying role of internal feedback processes, associated, for instance, to changes in global ice volume and greenhouse gases. These emerging records will pave the way toward a synoptic understanding of the long-term evolution of the Asian monsoon and its primary forcings.

Piecing together the evolution of monsoons also requires independent estimates of topographic change, allowing us to discriminate the effect of global climatic changes from local tectonic changes encoded in a single proxy record. Much of the topographic history has already been summarized in Section 3 (Tectonics, paleogeography, erosion, and ocean gateways) and is based on stable isotopes of hydrogen and oxygen in volcanic glass, plant waxes, carbonates, and fossil teeth and shells, as linked to the meteoric water cycle. Temperature records are also developed for inferring tectonic evolution, based on microbial-branched glycerol dialkyl glycerol tetraether (brGDGT) and clumped stable isotopes (Δ_{47}) in carbonates. It is important, however, that Quade et al. (2020) question whether paleosol carbonate routinely preserves pedogenic $\delta^{18}\text{O}$ values. Because paleosol carbonate $\delta^{18}\text{O}$ has been one of the main proxies for constraining the extent and height of the Tibetan and Andean plateaus, their topographic evolution may require revision.

The topographic histories that these studies develop feed directly into climate model assumptions regarding the distribution and height of plateaus and mountain ranges. Corresponding temperature records from paleoaltimetry studies could also be used for climate model evaluation (although to date they have not been). More complex, isotope-enabled GCMs can use isotope records directly for validation, but these latter models are computationally expensive. So far, these have focused on regional rather than global climate predictions of temperature, precipitation, etc. (e.g., see Poulsen et al., 2010).

8. Atmospheric CO₂ and Carbon Cycle Dynamics

Carbon dioxide is one of the primary agents influencing climate over Earth history, with high levels of $p\text{CO}_2$ associated with higher global temperatures and decreased ice volume. Several independent methods have been applied for reconstructing Miocene paleo- $p\text{CO}_2$ using marine or terrestrial proxies. Of these, the marine alkenone-based reconstructions are perhaps the most continuous to date (Pagani et al., 1999, 2000; Super et al., 2018; Y. G. Zhang, Pagani, et al., 2013), although recent studies have greatly improved the temporal coverage also for boron isotope-based (Foster et al., 2012; Sossdian et al., 2018), and terrestrial (Kürschner et al., 2008; Reichgelt et al., 2016; Steinthorsdottir et al., 2019; Steinthorsdottir et al., 2020; Tesfamichael et al., 2017) $p\text{CO}_2$ estimates. Importantly, most recent reconstructions appear to converge on $p\text{CO}_2$ values between 400 and 600 ppm during the early Miocene and MCO (see Figure 5, which shows $p\text{CO}_2$ in relation

to reconstructed SST in panel a), although some recent estimates record peaks of close to or above 800 ppm during the MCO (Greenop et al., 2014; Sosdian et al., 2018; Stoll et al., 2019), and suggest that cooling after the MCO was paired with a drop in $p\text{CO}_2$ (~125 ppm; Super et al., 2018), contrary to earlier observations that Miocene atmospheric CO_2 levels were low overall (<350 ppm) and did not vary with temperature (Pagani et al., 1999; Pearson & Palmer, 2000).

8.1. Marine Paleo- $p\text{CO}_2$ Proxies

Two approaches have provided $p\text{CO}_2$ estimates using Miocene marine sediments: the phytoplankton proxy and the boron isotope proxy. Both proxies serve as indicators for the concentration of dissolved CO_2 $[\text{CO}_2]_{\text{aq}}$ in surface waters, which can be translated to an atmospheric $p\text{CO}_2$ estimate if the SST is accurately estimated from proxies and used to calculate CO_2 solubility (Henry's law). Recent reassessment of the SSTs as well as secondary (non- CO_2) influences on both proxies and the calibration relationships has led to significant revision, mostly upward, of $p\text{CO}_2$ estimated from both proxies compared to values reported in original publications. We summarize the rationale for these revisions and the most recent $p\text{CO}_2$ estimates and present a summary of representative Miocene values in Figure 5, current at the time of writing, recognizing that the field is moving fast as new understanding is integrated.

8.1.1. Phytoplanktonic Carbon Isotopic (“alkenone”) Derived $p\text{CO}_2$ Reconstructions

The carbon isotopic fractionation between algal organic matter and atmospheric CO_2 (ϵ_p), determined from $\delta^{13}\text{C}$ in taxon-specific biomarkers like alkenones, organic matter trapped within diatoms, or chlorophyll-derived compounds, can provide estimates of past $[\text{CO}_2]_{\text{aq}}$ when other factors influencing ϵ_p , such as growth rate, light limitation, and cell size (Henderiks & Pagani, 2008) can be constrained (Pagani, 2002; Y. G. Zhang, Pagani, et al., 2013). Because trends in secondary influences like growth rate or light can be estimated more accurately than absolute values, on both long- and short-timescales, trends in ϵ_p -derived $p\text{CO}_2$ are currently more accurate than absolute values. Previously published ϵ_p -based $p\text{CO}_2$ estimates have been substantially revised because direct SST indicators suggest much higher temperatures than those originally derived from recrystallized planktonic foraminiferal $\delta^{18}\text{O}$, so original calculations are now thought to underestimate $p\text{CO}_2$ substantially (Pagani et al., 1999; Super et al., 2018). In addition, fundamental reevaluations of the calibration of the relationship between ϵ_p and CO_2 (Badger et al., 2019; Stoll et al., 2019; Y. G. Zhang et al., 2019, 2020), suggest that ϵ_p is much less sensitive to changes in $p\text{CO}_2$ when CO_2 is low than had been assumed in previous calibrations. Constraining ancient algal physiology remains a key challenge, and this lower sensitivity could be due to the operation of cellular carbon concentrating mechanisms. Application of new calibrations based on all available laboratory experiments, leads to much higher $p\text{CO}_2$ estimates for the middle and late Miocene (Stoll et al., 2019).

For example, from classical calibrations that have revised only SST, maximum $p\text{CO}_2$ estimates are in the range of 579 ppm (95% CI is 435–865 ppm), and $p\text{CO}_2$ shows an abrupt ~30% decline from 464 to 308 ppm at the end of the MCO potentially coincident with the MMCT (e.g., mean estimate declining from 464 to 308 ppm) (DSDP 608; Super et al., 2018; Figure 5b). From revised calibrations, peak MCO $p\text{CO}_2$ is estimated at 833 ppm (ODP 925; range 657–1,287 ppm) to 1,460 ppm (ODP 999; range 1,011–2,889) with the caveat that the $[\text{CO}_2]_{\text{aq}}$ at the MCO is uncertain as it exceeds the range of modern laboratory calibrations (Stoll et al., 2019; Figure 5b). Neither of these data sets has sufficient samples to resolve the rate of change across the MMCT. A late Miocene decline in $p\text{CO}_2$ has been estimated from both alkenone (Bolton et al., 2016) and diatom-derived (Mejia et al., 2017) ϵ_p records; the latter suggest a decrease from 794 ± 233 ppm at ~11 Ma to 288 ± 25 ppm at ~6 Ma (Figure 5b). Higher resolution alkenone records suggest between 8 and 5 Ma, average $p\text{CO}_2$ declined from 600 to below 300 ppm, punctuated by substantial orbital scale variability (Tanner et al., 2020).

8.1.2. Foraminiferal Boron Isotopic Ratio ($\delta^{11}\text{B}$) Derived $p\text{CO}_2$ Reconstructions

The isotopic ratio of boron ($\delta^{11}\text{B}$) in planktonic or benthic foraminifera provides an estimation of the pH of seawater in which the foraminifera lived (Sanyal et al., 1995) when the $\delta^{11}\text{B}$ of seawater is known and any “vital effects” in foraminiferal biomineralization are accounted for. Estimation of the $[\text{CO}_2]_{\text{aq}}$ from this pH additionally requires an independent estimate of some other parameter of the ocean's carbonate system such as total dissolved inorganic carbon, alkalinity, or carbonate ion concentration (Foster et al., 2012). Both

estimations of seawater $\delta^{11}\text{B}$ and the second carbonate parameter hold considerable uncertainties moving further back in time and have recently been reassessed (Sosdian et al., 2018). A comprehensive set of sensitivity tests for both parameters suggest the lowest pH levels of the last 22 Myr occurred during the MCO ($\sim 7.6 \pm 0.1$ units) in all scenarios, which is interpreted to correspond to peak $p\text{CO}_2$ levels of ~ 800 ppm (95% CI 531–1,150 ppm; Sosdian et al., 2018). (Figure 5c) High-amplitude rapid (sub-m.y.) $p\text{CO}_2$ variability characterizes the MCO (Greenop et al., 2014; Sosdian et al., 2018). High resolution data show a rapid decrease in $p\text{CO}_2$ between 14.2 and 13.8 Ma across the MMCT (Badger et al., 2013; Sosdian et al., 2018). Because the rapid rate of the transition limits the degree of variation in the seawater $\delta^{11}\text{B}$ and carbonate systems, the relative magnitude of this transition (a 30% decrease in $p\text{CO}_2$) is much better constrained than absolute values ($p\text{CO}_2$ of $532 + 190/-157$ ppm descending to $421 + 135/-113$ ppm) (Figure 5c). SST for $\delta^{11}\text{B}$ -based $p\text{CO}_2$ calculations have relied principally on foraminiferal Mg/Ca, but SST is not considered the largest source of uncertainty in $\delta^{11}\text{B}$ based $p\text{CO}_2$ estimates for the Miocene.

8.2. Terrestrial Paleo- $p\text{CO}_2$ Proxies

Three terrestrial $p\text{CO}_2$ proxies have been applied to estimate paleo- $p\text{CO}_2$ in the Miocene–stomata-based methods, paleosol carbonate $\delta^{13}\text{C}$, and C_3 plant $\delta^{13}\text{C}$. Each is treated separately as follows:

8.2.1. Stomatal Proxy Derived $p\text{CO}_2$ Reconstructions

The stomatal proxy utilizes the empirically and experimentally tested inverse relationship of stomatal densities of plant leaves to $p\text{CO}_2$ to reconstruct past $p\text{CO}_2$ using the stomatal densities of fossil plants (Woodward, 1987). Stomatal density is defined either as the number of stomata per unit area ($\text{SD} = \text{stomata}/\text{mm}^2$) or as the percentage of stomata relative to all epidermal cells, the stomatal index ($\text{SI} [\%]$). Three methods of stomatal proxy paleo- $p\text{CO}_2$ reconstructions are currently in use: the stomatal ratio method (McElwain & Chaloner, 1996), transfer functions (e.g., Barclay & Wing, 2016) and gas-exchange modeling (Franks et al., 2014; Konrad et al., 2017, 2020). The stomatal ratio and transfer function methods are taxon dependent, whereas the gas-exchange modeling approach is taxon-independent and incorporates additional factors apart from stomatal densities, such as stomatal conductance, and $\delta^{13}\text{C}$ of the fossil leaves and atmospheres. For more detail, see McElwain and Steinthorsdottir (2017) and Steinthorsdottir et al. (2020). As applied to natural data sets, the different methods yield broadly similar results (e.g., Steinthorsdottir et al., 2020). Results of Miocene stomatal proxy data are summarized in Figure 5d and below:

- Latest Oligocene: 400–500 ppm (Reichgelt et al., 2016; Roth-Nebelsick et al., 2012; Steinthorsdottir et al., 2019; Tesfamichael et al., 2017)
- Oligocene-Miocene transition: Transient peak of 650–1,100 ppm (Reichgelt et al., 2016; Steinthorsdottir et al., 2019; Tesfamichael et al., 2017)
- Earliest Miocene (pre-MCO): 400–500 (Grein et al., 2013; Kürschner et al., 2008); bimodal: ~ 500 or ~ 900 ppm (Londoño et al., 2018)
- MCO: 400–600 ppm (Beerling et al., 2009; Kürschner et al., 2008; Royer, 2001; Steinthorsdottir et al., 2020)
- Late Miocene (post-MCO): ~ 350 ppm (Franks et al., 2014; Kürschner et al., 2008, 1996; Stults et al., 2011; Van Der Burgh et al., 1993; Y. Wang et al., 2015)

Overall, $p\text{CO}_2$ appears to have increased during the MCO then decreased, although values during the MCO were not obviously different from the latest Oligocene and Oligocene–Miocene transition. Large variations were present in the early Miocene, possibly analogous to oscillations in $p\text{CO}_2$ observed in marine records (Greenop et al., 2014). The stomatal proxy for $p\text{CO}_2$ reconstruction shows notable inter-method and inter-study consistency in the Miocene. Although the emerging record of Miocene stomatal proxy $p\text{CO}_2$ is robust, the values are low in comparison to other warm climate states such as during the Eocene. Future research should test whether climatic or environmental factors other than $p\text{CO}_2$ influence stomatal densities (and thus reconstructed $p\text{CO}_2$), leading for example, to underestimating $p\text{CO}_2$ during hothouse conditions in the past.

8.2.2. Paleosol-Derived $p\text{CO}_2$ Reconstructions

The paleosol carbonate $\delta^{13}\text{C}$ proxy introduced by Cerling (1984, 1991) is based on the carbon isotope compositions of calcite nodules and organic matter preserved in fossil soils. The proxy is sensitive to the amount

and the carbon isotope composition of atmospheric CO₂ and soil CO₂ that is released from organic matter by soil respiration. Similar to other proxies, calibrations continue to improve with increasing field-testing, thus only the more recent *p*CO₂ paleosol estimates should be considered. Significantly, Breecker (2013) and Breecker et al. (2010), provided a substantially improved calibration and error assessment based on detailed studies of the chemical processes of soil carbonate formation. This work showed that uncertainties in *p*CO₂ typically exceed −50% and +100%, although because of systematic errors, changes in calculated *p*CO₂ are considerably more reliable. To improve accuracy, Cotton and Sheldon (2012) proposed using mean annual precipitation as a proxy for the concentration of soil-respired CO₂, which is otherwise a major source of uncertainty.

At present, the most reliable interpretations correspond with paleosol sections in the Great Plains of North America (Breecker & Retallack, 2014, 5.5–23 Ma), the Beaverhead Mountains of Montana (Cotton & Sheldon, 2012; <7 Ma), and the Tianshui Basin of northern China (Ji et al., 2018, 7.1–16.8 Ma). The latter study combined carbon-, oxygen-, and clumped-isotope compositions to simultaneously infer *p*CO₂ and soil carbonate formation temperatures. Data from the Great Plains and China suggest moderately low *p*CO₂ of ~375 ppm during the MCO, a post-MCO decrease to ~200 ppm by 12 Ma, and indistinguishable values thereafter. Data from Montana suggest somewhat higher post-MCO *p*CO₂ of ~280 ppm. In summary, the paleosol *p*CO₂ proxy produces estimates that are highly variable, is based on a broad spectrum of assumptions, with large errors. For the Miocene in general, paleosols mostly indicate *p*CO₂ < 400 ppm, although with large variation in both directions. The proxy needs to be refined further before being considered robust.

8.2.3. C₃ Plant Proxy Modeling

Schubert and Jahren (2012, 2015) proposed a *p*CO₂ proxy based on a relationship between *p*CO₂ and the stable carbon isotope discrimination ($\Delta^{13}\text{C}$) of plant tissue observed in experiments and in natural data; $\Delta^{13}\text{C}$ is calculated from the $\delta^{13}\text{C}$ of leaf tissue and atmospheric CO₂ (determined from marine records: Tipple et al., 2010), then used to back-calculate the concentration of CO₂ in the past. Because absolute $\Delta^{13}\text{C}$ values are variable among plants grown in the same conditions, the C₃ proxy is calculated using the change in $\Delta^{13}\text{C}$ relative to a reference time interval (Cui & Schubert, 2016; Schubert & Jahren, 2015). Application of this approach to the extraordinarily well-preserved leaf fossils of *Clarkia*, Idaho, implies MCO *p*CO₂ of 470–600 ppm (Steinthorsdottir et al., 2020). Cui et al. (2020) reconstructed *p*CO₂ for the last 23 Ma, using a compilation of previously published $\delta^{13}\text{C}$ measurements from terrestrial organic matter and plant lipids, and recorded ~250–350 ppm, during the Miocene, with maximum *p*CO₂ reaching 343 + 191/−101 ppm (242–534 ppm; 68% CI) during the MCO. We note, however, that the approach of Schubert and Jahren (2012, 2015; see also Cui & Schubert, 2016), has been questioned because it does not account for water stress and can produce results that are unrealistically low (e.g., <0 ppm) or high (infinite; Kohn, 2016; Konrad et al., 2020; Lomax et al., 2019; Porter et al., 2019). The C₃ plant $\delta^{13}\text{C}$ proxy can produce similar results as other proxies, but the lack of an explicit dependence on precipitation or moisture availability is a weakness. Further work integrating all plant physiological factors will identify the accuracy of this proxy (e.g., Konrad et al., 2020).

8.3. Evidence of Changes in the Miocene Carbon Cycle

Variation in benthic foraminiferal $\delta^{13}\text{C}$ provides evidence of changes in the ocean carbon cycle in the Miocene. Strong 405-kyr $\delta^{13}\text{C}$ cycles with a longer term ~2.4-Myr modulation, are a persistent feature of the Miocene, a pattern that has been detected back to the Cretaceous (Holbourn et al., 2014, 2018; Liebrand et al., 2017; Woodruff & Savin, 1991; Figure 2). Superimposed on the persistent eccentricity-paced $\delta^{13}\text{C}$ rhythms is a prominent and rapid increase in $\delta^{13}\text{C}$ at ~16.7 Ma (Holbourn et al., 2015) marking the onset of the long-lasting positive carbon-isotope excursion, known as the Monterey Excursion (Vincent & Berger, 1985), which lasted until ~13.5 Ma (Figure 2). This prolonged, cyclic $\delta^{13}\text{C}$ excursion is characterized by low-frequency fluctuations (~1‰) that approximate long eccentricity cycles (Holbourn et al., 2005, 2007; Woodruff & Savin, 1991). The onset of the Monterey Excursion ~250 kyr after the beginning of the MCO (Holbourn et al., 2015) suggests that climate warming at the MCO onset was coupled to an intense perturbation of the carbon cycle (Figure 1). It has been suggested that the long-term Monterey Excursion reflects a combination of enhanced biological carbon isotope fractionation under higher CO₂ concentrations and enhanced burial of organic matter on flooded continental shelves (Sosdian et al., 2020). Meanwhile, the cyclic co-variance between $\delta^{18}\text{O}$ and $\delta^{13}\text{C}$ through the long-lasting Monterey Excursion additionally support

the hypothesis that periodic increases in organic carbon burial modulated by astronomical forcing drove $p\text{CO}_2$ drawdown and global cooling through climate feedbacks (Flower & Kennett, 1993, 1994; Holbourn et al., 2007; Sosdian et al., 2020; Vincent & Berger, 1985; Woodruff & Savin, 1991). The late Miocene climate shift occurred in the final stage of a long-term, global $\delta^{13}\text{C}$ decrease (at ~ 7 Ma, the LMCIS, Figure 2), suggesting that global cooling was connected to changes in the carbon cycle.

The surface-to-deep and interbasinal $\delta^{13}\text{C}$ gradients have also been compared as indices of variations in ocean circulation and the strength of export productivity and the biological pump. A progressive increase in the Atlantic to Pacific benthic foraminiferal $\delta^{13}\text{C}$ occurred since the middle Miocene (Tian et al., 2018; Section 10). Intensification of the $\delta^{13}\text{C}$ gradient between Pacific deep and intermediate water masses after ~ 13.9 Ma indicates invigoration of MOC following Antarctic ice expansion (Holbourn et al., 2013a). Across the MMCT, an increase in the basinal $\delta^{13}\text{C}$ gradient between Antarctic Intermediate Water and Lower Circumpolar Deep Water additionally suggests increased isolation of the Pacific Deep Water permitting greater storage of respired CO_2 , which together with evidence for enhanced shelf weathering due to sea level fall, may have facilitated CO_2 drawdown (Ma et al., 2018). Through the steepest part of the late Miocene cooling, increased surface-deep $\delta^{13}\text{C}$ gradients are interpreted to reflect strengthened biological pump and CO_2 drawdown through deep ocean storage (Holbourn et al., 2018).

Pronounced changes in the deep ocean carbonate saturation are also evidence of changes in the marine carbon cycle. Climate warming at the MCO additionally coincided with a massive increase in deep sea carbonate dissolution and substantial shoaling of the carbonate compensation depth (CCD), so that the onset of the MCO frequently corresponds to a widespread hiatus in marine sediment records (Holbourn et al., 2014; Kochhann et al., 2016). Warming pulses paced by 100 kyr eccentricity through the MCO were also associated with transient shoaling of the CCD and intense carbonate dissolution in the deep ocean (Holbourn et al., 2014; Kochhann et al., 2016). Another prolonged phase of reduced carbonate deposition, lasting 2–3 million years (~ 12 –9 Ma) was originally recognized in the tropical eastern Pacific Ocean (Mayer et al., 1985, 1986) and later termed the “carbonate crash” by Lyle et al. (1995; Figure 1). Later, intense episodes of reduced carbonate deposition from ~ 11.5 to 10 Ma (Figure 1) were identified in all major tropical ocean basins (e.g., Diester-Haas et al., 2004; Farrell et al., 1995; Luebbbers et al., 2019; Lyle & Baldauf, 2015; Peterson et al., 1992; Roth et al., 2000). Although the cause of the carbonate crash remains under debate, its global occurrence suggests that fundamental changes in the intensity of chemical weathering and riverine input of calcium and carbonate ions into the marine and terrestrial reservoirs were instrumental in driving this event (Luebbbers et al., 2019). Regional changes in ocean nutrient storage related to closure of the Central American Seaway could have also played a role, especially in the eastern equatorial Pacific (Lyle et al., 2019).

The late Miocene-early Pliocene Biogenic Bloom, which involves widespread increases in silica, carbonate accumulation, carbonate dissolution in the mid-low latitude oceans, and other evidence for increased primary production (Diester-Haas et al., 2004, 2006; Reghellin et al., 2020), is a further widespread marine sedimentation episode implying carbon system shifts. This event (or at least the initial phase) coincides with the Late Miocene Carbon Isotope Shift (LMCIS, Figures 1 and 2), which involves a $\sim 1\%$ decrease in benthic foraminiferal $\delta^{13}\text{C}$, implying decreased marine organic carbon burial. The cause of the biogenic bloom and LMCIS is uncertain. Many explanations center around transfer of organic matter from the terrestrial to marine realm and increased supply or redistribution of nutrients through enhanced terrestrial weathering and oceanic upwelling, changing atmospheric circulation and aeolian dust flux, or ocean circulation pathways (Dickens & Owen, 1999; Diester-Haas et al., 2006; Drury et al., 2016; Grant & Dickens, 2002; Herbert et al., 2016; Holbourn et al., 2018; Lyle et al., 2019). It has also been suggested that the LMCIS was primarily the result of background biological overprinting due to changes in photosynthetic pathways in marine and terrestrial primary producers that influenced $\delta^{13}\text{C}_{\text{org}}$ and therefore $\delta^{13}\text{C}_{\text{DIC}}$ (Falkowski et al., 2005; Katz et al., 2005). Zhai et al. (2021) add to this picture with the first geochemical evidence of the Biogenic Bloom in the Japan Sea.

9. Ice Sheet Dynamics

During the Miocene there was substantial variability of the Antarctic Ice Sheet (AIS), including large transitions and astronomically paced oscillations, although the exact magnitudes are still subject to debate. Perspectives on icesheets are introduced in Sections 2.2 (Miocene astronomically calibrated isotope stratigraphy), 5.1 (Miocene floras and ecosystems), and 6.1 (Transitions and variability in deep ocean temperature and ice volume manifest in benthic foraminiferal $\delta^{18}\text{O}$), but are collected here together with other types of direct polar evidence and icesheet modeling results for a more focused treatment of current knowledge. The Miocene began with a large glacial expansion event here referred to as the OMT (Mi-1; Liebrand et al., 2017; Miller et al., 1991, 2020; Zachos et al., 2001). The early to middle Miocene icesheet was highly dynamic with strong sensitivity to orbital forcing. Long- and short-eccentricity paced fluctuations in ice volume have been interpreted from $\delta^{18}\text{O}$ (De Vleeschouwer et al., 2017; Liebrand et al., 2017; Miller et al., 2020; Zachos et al., 2001), although increased sensitivity to obliquity forcing has been described for times of higher ice volume when ice-sheet margins extend into marine environments (Levy et al., 2019). During the MCO the AIS reached a minimum in volume, becoming more sensitive to changes in astronomical precession (De Vleeschouwer, 2017), before expanding and stabilizing after the MMCT (Flower & Kennett, 1993; Lear et al., 2015; Miller et al., 2020; Shevenell et al., 2008). There is limited evidence for the presence of large ice sheets in the northern hemisphere during most of the Miocene, although isolated glaciers likely existed with glaciation intensifying during the latest Miocene (Herbert et al., 2016; Holbourn et al., 2018). Ice sheet change is inferred from indirect records, principally sea level proxies and marine isotope records, and from indicators of glaciation near to the margin of the ice sheets (ice-proximal records).

9.1. Indirect Records

The modern AIS has the potential to raise sea level by 58 m and to decrease mean ocean $\delta^{18}\text{O}$ by 1.04‰ if completely melted (Fretwell et al., 2013; Lhomme et al., 2005). Reconstructions of sea level during the Miocene are principally based on sequence stratigraphy of passive continental margins and the oxygen isotope composition ($\delta^{18}\text{O}$) of benthic foraminifera. Here, we focus on efforts to determine a quantitative ice volume signal. To deconvolve an ice volume signal from benthic foraminifera $\delta^{18}\text{O}$ requires separation of the temperature-controlled fractionation signal from changes in $\delta^{18}\text{O}$ of seawater. This can be based on independent temperature estimates, an inversion method using ice sheet models or simple calibrations using independent sea level records. Measuring the Mg/Ca ratio of benthic foraminifera, which also shows a temperature dependent fractionation, is a key method of determining past deep-sea temperatures and hence past ice volumes (Lear et al., 2000). Clumped isotopes potentially offer an additional means of reconstructing Cenozoic variations in seawater $\delta^{18}\text{O}$ (e.g., Modestou et al., 2020; Petersen & Schrag, 2015) but the sample size required for adequate precision remains limiting in many cases.

Sea level reconstructions from passive margins show changes in glacio-eustasy, however, they also incorporate changes in local sea level caused by glacio-isostatic adjustment, and mantle dynamic topography that must also be considered (Kominz et al., 2008; Miller, 2005). The largest long-term change in sea level during the Miocene occurred across the MMCT, with a sea level fall of 59 ± 6 m estimated from the Marion Plateau in northeastern Australia (John et al., 2004, 2011). Another record from the New Jersey margin shows a smaller sea level fall of 23 ± 13 m for the MMCT, but may be missing the full sea level lowstand, so that the estimate is likely a minimum (Kominz et al., 2008). The MMCT is also associated with the largest change in benthic foraminiferal $\delta^{18}\text{O}$ during the Miocene (Holbourn et al., 2005; Pekar & DeConto, 2007; Shevenell et al., 2004, 2008). Based on a time series analysis of multiple records, the MMCT is associated with an average $0.88\text{‰} \pm 0.04\text{‰}$ increase in benthic foraminiferal $\delta^{18}\text{O}$ (Mudelsee et al., 2014). There was a synchronous global cooling of the deep ocean, of $\sim 1.5 \pm 0.5^\circ\text{C}$ (Billups & Schrag, 2002; Lear et al., 2000, 2010), leaving a residual change in $\delta^{18}\text{O}$ of seawater of $\sim 0.60\text{‰} \pm 0.14\text{‰}$. Using an AIS appropriate calibration of 0.014‰ m^{-1} (Lhomme et al., 2005), this produces an MMCT sea level fall of 43 ± 10 m. Model-based deconvolutions of the stacked benthic foraminiferal $\delta^{18}\text{O}$ record (Zachos et al., 2008) have been developed which use an inversion to determine both change in deep-sea temperature and ice volume using simple 1-day ice sheet models (de Boer et al., 2010; Stap et al., 2016). These model-based estimates suggest a larger change in past Antarctic ice volume, with a minimum in ice volume close to complete Antarctic deglaciation during the MCO. A recent study of this type proposes large variations in sea level over short timescales (<10 kyr),

presumably reflecting changes to the volume of the AIS (Miller et al., 2020). These variations range up to 100% AIS loss. Taken together, these data support a large expansion of the AIS during the later Miocene from a minimum during the MCO, with considerable variability over shorter time spans.

Other large glaciation events, which are marked by major increases in benthic foraminiferal $\delta^{18}\text{O}$ and sea level falls (Miller et al., 1991, 2020), occurred during the early to middle Miocene. Although earlier interpretations suggested a 1.0‰ increase in benthic foraminiferal $\delta^{18}\text{O}$ for the first glacial event at the beginning of the Miocene (Miller et al., 1991; Shevenell & Kennett, 2007), multiple records show an average 0.60‰ increase in benthic foraminiferal $\delta^{18}\text{O}$ (Mudelsee et al., 2014). An associated deep-sea cooling of $\sim 1.5 \pm 0.5^\circ\text{C}$ (Billups & Shrag, 2002; Lear et al., 2004; Mawbey & Lear, 2013) leaves a minimum residual change in $\delta^{18}\text{O}$ of seawater of $0.25 \pm 0.12\text{‰}$ (an 18 ± 9 m sea level fall). In the reconstruction of Miller et al. (2020) this event is shown as a larger sea level fall of 40 ± 10 m. This is similar in magnitude to the backstripped sea level estimates of Kominz et al. (2016) during the Early to Middle Miocene. The larger sea level contribution from the Miller et al. (2020) sea level reconstruction is a result of the use of a smoothed deep-sea temperature record, which does not capture any cooling associated with the glaciation event (Cramer et al., 2011). In addition to the large glacial events discussed above, there is a background of higher frequency changes in ice volume, driven by changes in the Earth's orbit and obliquity (e.g., Pekar & DeConto, 2007)—as discussed in Section 2.

9.2. Ice-Proximal Records

Further support for the dynamic nature of the AIS during the Miocene comes from Antarctic terrestrial records and marine records recovered close to the Antarctic continent. The first Antarctic ocean drilling expedition was DSDP Leg 28 to the Ross Sea and Wilkes Land, the data from which extended the glacial history of the AIS back through the Miocene into the Oligocene (Hayes et al., 1975). During 2018–2019 there were three IODP expeditions to the Southern Ocean, some of these campaigns have recovered material from the Miocene (McKay et al., 2018). In addition to ship-based drilling, sea ice-based platform drilling has recovered Miocene marine sediments from the Ross Sea—a recent overview of marine drilling campaigns around Antarctica is given in Escutia et al. (2019). A variety of methods are used to determine past change of the AIS.

At the beginning of the Miocene, the large glacial event of the OMT is seen as a disconformity in the AN-DRILL record from the Ross Sea, suggesting expansion of the AIS into the Ross Sea at this time. The East AIS advanced and retreated across the Sabrina Coast continental shelf during the early Miocene, with tunnel valleys providing evidence that there was melting of the ice sheet surface generating meltwater (Gulick et al., 2017). During the warmth of the MCO there were open water conditions and SSTs reached 6°C – 10°C in the Ross Sea (Levy et al., 2016). In the cooling phase of the MMCT, dinocyst assemblages show the first return of sea ice offshore of Wilkes Land since the early Oligocene (although there is a hiatus during the early Miocene; Bijl et al., 2018). Direct evidence for the expansion of the AIS during the MMCT is seen in provenance analysis of Ice Rafted Detritus (IRD) from offshore of Wilkes Land and Prydz Bay (Pierce et al., 2017) in addition to expansion in the Ross Sea (Levy et al., 2016; Passchier et al., 2011).

Terrestrial evidence from the Transantarctic Mountains show cooling of 8°C between 14.07 Ma and 13.85 Ma and the extinction of tundra vegetation (Lewis et al., 2008). The broad stabilization of the AIS during the late Miocene is supported by cosmogenic isotopes analysis of Ross Sea sediments from the AN-DRILL record. Extremely low concentrations of ^{10}Be and ^{26}Al suggests that there was no retreat onto land of EAIS ice draining into the Ross Sea during the past 8 million years (Shakun et al., 2018). Combining the ice proximal and indirect records provides a more complete reconstruction of the Miocene AIS, however it also highlights that there are large areas of the Antarctic for which there are currently no data. Filling in these gaps is extremely important as this interval is increasingly being used as a period of interest to evaluate climate and ice sheet models.

9.3. Modeling AIS Dynamism

Simulating the dynamic behavior of the AIS as shown in the proxy reconstructions has long proved challenging. This is in part due to strong stabilizing feedbacks (Huybrechts, 1993; Pollard & DeConto, 2005) and

also because of the difficulty of simulating warm poles with climate models (Langebroek et al., 2009) as discussed in Section 11. The formation of large ice sheets has a cooling effect on the Antarctic climate, because of the elevation-lapse rate (height-mass balance feedback) and albedo feedbacks (Oerlemans, 2002). Because of these feedbacks there is a strong hysteresis effect that limits AIS retreat without relatively strong regional temperature fluctuations of ~ 10 K (Huybrechts, 1993). Such temperature fluctuations require high atmospheric $p\text{CO}_2$, larger than is suggested by Miocene proxy reconstructions (Pollard & DeConto, 2005), or an increased polar amplification (Langebroek et al., 2009).

Recent advances in ice sheet model physics, oxygen isotope modeling, and climate forcing approaches has led to simulations of a dynamic AIS that is more consistent with the magnitudes of change inferred from the proxy record (Gasson et al., 2016; Langebroek et al., 2010; Pollard et al., 2015). A complication of this interpretation is that it is based on the equilibrium response of the ice sheet to climate forcing. Other work has suggested a reduced transient AIS variability in comparison to equilibrium solutions (Stap et al., 2019). Furthermore, the disequilibrium between ice volume and climate gives rise to a concurrent Antarctic ice sheet growth and $p\text{CO}_2$ rise (Stap et al., 2020). So far ice growth has been mainly linked to increased precipitation outweighing increased surface melt in a warmer climate (Oerlemans, 1991), which highlights the necessity of high-resolution proxy- $p\text{CO}_2$ records as an improved modeling constraint. Another boundary condition that is important for accurately simulating the behavior of the Miocene AIS is the bedrock topography (Colleoni et al., 2018a). Modeling studies have highlighted the sensitivity of results to differences in basal conditions (Gasson et al., 2015, 2016) and have found that the Antarctic continental shelf evolution modulates the sensitivity of the AIS to climatic forcing (Colleoni et al., 2018b). Key to resolving these issues is the recent publication of the first reconstructed bedrock topography for the Miocene Antarctic continent (Paxman et al., 2018, 2019).

9.4. Northern Hemisphere Ice Sheets?

The growth of ice sheets in the northern hemisphere is thought to have begun much later than on Antarctica and likely in several stages (Figure 1). The onset of trans-continental scale northern hemisphere glaciation (the ice ages), including growth of the massive Laurentide Ice Sheet, is typically and confidently considered to have begun during the Pleistocene ~ 2.6 Ma (Miller & Wright, 2017; Ruddiman et al., 1988). The earlier history, however, is less clear. Extensive glaciation on Greenland has been hypothesized for the Miocene and even earlier intervals based on global $\delta^{18}\text{O}$ increases and corresponding estimated ice budgets (Coxall et al., 2005; Holbourn et al., 2018; Shackleton et al., 1995). Difficulties in simulating dynamic behavior of the AIS also led to the suggestion that northern hemisphere ice sheets were contributing to changes in sea level/ice volume prior to the Pleistocene (e.g., Foster & Rohling, 2013).

Sediments from the Nordic Seas interpreted as evidence of ice-rafting have been used to suggest glaciers on Greenland as early as the Eocene (Eldrett et al., 2007; Tripathi & Darby, 2018), although this remains controversial (Edgar et al., 2007; Spray et al., 2019). From the Miocene, evidence for major northern hemisphere ice sheets is incontrovertible. Convincing ice rafted material indicates that marine-terminating glaciers existed on Greenland more or less continuously since 18 Ma (Thiede et al., 2011; Wolf-Welling et al., 1996), while lodged glacial tills dated to ~ 7 Ma on the East Greenland Shelf suggest much larger marine ice sheets from the late Miocene (Larsen et al., 1994) consistent with the $\delta^{18}\text{O}$ (Shackleton et al., 1995). Beryllium and aluminum isotope dating of glacially eroded particles and geophysical relief reconstructions of Greenland corroborate this, suggesting that a substantial and dynamic ice sheet has existed on northern and eastern Greenland from 7.5 Ma (Bierman et al., 2016; Pedersen et al., 2019). Mineral provenance studies from sediment cores suggest onset of perennial Arctic sea ice cover at ~ 13 Ma after the MMCT, coincident with AIS expansion (Krylov et al., 2008; Figure 1).

Proxy perspectives are supported by modeling that suggests the atmospheric $p\text{CO}_2$ threshold for extensive ice-sheet formation is lower for the northern hemisphere (~ 280 ppm) compared to Antarctica (~ 400 – 600 ppm) (DeConto et al., 2008), and that the “northern hemisphere ice threshold” would have been crossed during the Miocene (Pagani et al., 2005), compared to the late Eocene for Antarctica. Subsequent work suggested that these “ $p\text{CO}_2$ thresholds” are model dependent (Gasson et al., 2014). Moreover, the latest proxies imply higher $p\text{CO}_2$ values (280–420 ppm) into the late Miocene than previously thought (see Section 8). Nonetheless, Miocene continental ice records indicate that atmospheric $p\text{CO}_2$ levels hovered close to and

increasingly exceeded the threshold necessary for northern hemisphere ice sheet growth during the late Miocene (Holbourn et al., 2018).

This picture of a partially or ephemerally glaciated Greenland through the Miocene must be reconciled with parallel reconstructions of Arctic temperatures that suggest, at times, much warmer climates compared to the pre-industrial. The available palaeoclimate snapshots record SSTs of 10°C–13°C, likely a warm season bias, and diverse (fossil) flora implying terrestrial MATs of 4°C–11.5°C during the middle Miocene on fringing Arctic land masses (O'Regan et al., 2011; Weller & Stein, 2008; Wolfe, 1994). Central Arctic biomarker (IP25) constraints suggest summer sea ice-free conditions in the late Miocene (Stein et al., 2016). Improving the picture of Miocene northern hemisphere cryosphere evolution in a clearly warmer than present world with CO₂ similar to that projected for our near future remains an outstanding goal of future research that should be helped in the short term by planned future deep-sea drilling in the Arctic.

10. Overturning Circulation

The source of deep water and changing modes and rates of MOC on a warmer Earth without fully developed cryospheres is a subject of intense debate. Key proxy insights come from benthic carbon stable isotopes ($\delta^{13}\text{C}$), the Neodymium isotopic composition water mass provenance tracer (ϵNd), and the occurrence and character (mostly in seismic data) of sedimentary “drift deposits,” that is, seafloor sediment accumulations produced by deep bottom currents that are symptomatic of the vigor and geometry of overturning. Foraminiferal $\delta^{18}\text{O}$, Mg/Ca, sediment redox chemistry, and benthic foraminifera assemblages are also used to track evolving water masses and basin ventilation. During the Miocene, different continental positions, weaker latitudinal thermal gradients, warmer oceans, different wind patterns, and a stronger hydrological cycle than today, would have created differences in MOC strength and sinking regions that modulated climate patterns. As introduced in Section 3, the important ocean gateway considerations for the Miocene are: (1) a closing eastern Tethys Seaway; (2) a closing Panama Seaway; (3) changes in Nordic Seas-Arctic-Atlantic connections; (4) opening of the Bering Strait in the late Miocene to early Pliocene; and (5) constriction of the Indo-Pacific seaway (Sections 3 and 12.2.1). There is general agreement that the Drake Passage was open and a “mature” circum-Antarctic flow existed by the early Miocene (Scher & Martin, 2008). A representation of the tectonic gateways and inferred MOC modes is presented in Figure 1.

10.1. Overturning Modes Prior to the Miocene

Proxies suggest that, like today, bi-polar deep-water production was ongoing during warm periods of the Paleogene, the difference from today being that at times the North Pacific rather than the North Atlantic was the primary northern sinking center (Coxall et al., 2018; Hague et al., 2012; Mckinley et al., 2018; Thomas et al., 2014). Moreover, if North Atlantic Deep Water (NADW) or its precursor Northern Component Water (NCW), or North Pacific Deep Water (NPDW) were being produced before the Oligocene (Hohbein et al., 2012), it is likely that they did not cross hemispheres (Via & Thomas, 2003). This scenario is supported by models, which find, for instance, that the North Atlantic was too fresh to support sinking in the late Eocene due to the open connection with a warm and fresh Arctic (Hutchinson et al., 2019) and there was active NPDW production instead during the early Paleogene, NCW formed in the Atlantic but it was shallower than NADW and upwelled at the equator (Roberts et al., 2009).

10.2. Sediment Drifts

From ~25 to 26 Ma, extensive sediment drifts started growing south of Iceland, which are interpreted as evidence of more permanent Nordic overflows crossing the Greenland Scotland Ridge (GSR) and strengthening NCW (Poore et al., 2006; Wright & Miller, 1996). These drifts, and by association the overflows, are reported to have strengthened further during the MCO (Uenzelmann-Neben & Gruetzner, 2018). Interestingly, this appears to have occurred close to the opening of the Fram Strait deep-water connection between the Arctic and Greenland Seas ~17.5 Ma (Jakobsson et al., 2007). The picture from the northeastern Atlantic is consistent with downstream records, with drifts on the Newfoundland margin acquiring modern-like Deep Western Boundary Current character ~25 Ma (Boyle et al., 2017), simultaneous with nucleation of major drifts further south on the US Atlantic margin (Blake, Bahama, Chesapeake, and Hatteras), symptomatic

of strengthening and deepening NCW exports (Tucholke & Mountain, 1985). The drift data are somewhat at odds with geophysical studies of the GSR that suggest episodes of vigorous Iceland plume activity at ~25 Ma, and in the middle Miocene, that caused the igneous barriers to shallow, and has been inferred to cause considerable reduction in NCW fluxes (Abelson et al., 2008; Wright & Miller, 1996). However, rather large uncertainty exists in the timing of this activity and the exact implications for the overflow passages, such that many open questions remain.

10.3. Deep Sea $\delta^{13}\text{C}$

Geochemical proxies complement drift-sediment evidence for increasing NCW from the early Miocene to some extent but there are also some differences. Variations in intra- and inter-basin benthic foraminiferal $\delta^{13}\text{C}$ differences is routinely used as a water mass “age tracer.” Woodruff and Savin (1989) concluded that NCW was weak or absent in the early and middle Miocene and the Southern Ocean was the primary source of deep water. They attributed this to the open Eastern Tethys Seaway, sourcing warm saline intermediate waters to the Indian Ocean (Tethys Indian Ocean Saline Water (TISW), which resulted in intensified production of Antarctic Bottom Water (AABW) or its precursor Southern Component Water (SCW). The existence of TISW “in theory” is supported by modeling (although is difficult to prove using proxies). However, several modeling studies find that a wide-open Tethys typically also produces westward surface transport that helps maintain Atlantic salinity and NCW production, even with Panama open (Butzin et al., 2011; Hamon et al., 2013). Other treatments of $\delta^{13}\text{C}$ interpret discontinuous pulses of Miocene NCW production, with NCW suggested to be “on” during the early Miocene, but “off” during the middle Miocene (~15 Ma) (Lear et al., 2003; Wright et al., 1992). The analysis of Paul et al. (2000) examining early Miocene Atlantic $\delta^{13}\text{C}$ gradients concludes generally greater importance of AABW/SCW compared to today and weaker NCW. A complication here could be with the assumption that endmember NADW/NCW has always had relatively high $\delta^{13}\text{C}$ values. On the contrary, deep water production basins could have had quite different $\delta^{13}\text{C}$ in the past, or the $\delta^{13}\text{C}$ could be more similar in the different sinking regions, as implied by the surprisingly low $\delta^{13}\text{C}$ measured in Eocene to Oligocene benthic foraminifera from the Southern Labrador Sea (Coxall et al., 2018). The Miocene tropical “ocean shortcuts” would have played a role here in homogenizing global subsurface $\delta^{13}\text{C}$ (Cramer et al., 2009). The MMCT and early late Miocene (~13.9–9 Ma) saw a pivotal change, when North Atlantic and Pacific deep sea $\delta^{13}\text{C}$ signatures permanently diverged (North Pacific values becoming relatively lower) and the global system acquired a modern-like $\delta^{13}\text{C}$ distribution (Butzin et al., 2011; Cramer et al., 2009; Tian et al., 2018; Woodruff & Savin, 1989; Wright et al., 1992). This is attributed to: (i) the increasing role of well-ventilated northern-source deep water in the MOC, both through increased supply from the Nordic seas and increased Atlantic salinification due to tropical gateway closures; (ii) the longer deep-water route between the North Atlantic and Pacific imposed by tropical gateway closures, leading to increased deep-water residence times; and (iii) background changes in global carbon cycling (Section 8.3).

10.4. Deep Water Provenance From ϵNd

The ϵNd water mass tracer provides further independent insights. A long-term ϵNd decrease evident at Walvis Ridge from interval 23–11 Ma is interpreted as signaling increasing contributions of NCW to deep waters in the southeastern Atlantic from the early Miocene on (Thomas & Via, 2007). A further sharp and permanent jump to very unradiogenic ϵNd values, beginning ~10.6 Ma, may signal onset of deep convection in the Labrador Sea (Thomas & Via, 2007). Recent comparisons of eastern equatorial Pacific and Caribbean ϵNd argue that the critical event for the Atlantic Meridional Overturning Circulation (AMOC) commencement/strengthening in the Neogene was the termination of low salinity intermediate-depth Pacific inflows to the tropical Atlantic, dated to 10–11.5 Ma (Kirillova et al., 2019; Sepulchre et al., 2014). This is earlier than the prevailing view for Panama Seaway closure—impacts on the AMOC, which is typically regarded to be ~4–3 Ma (Haug et al., 2001; Leigh et al., 2014). The difference here is the definition of “closure.” These studies imply that, from a large-scale circulation perspective, it is relatively fresh intermediate depth Pacific waters that matter and it is feasible that this supply was severed during early stages of Panama restriction (Lear et al., 2003). To what extent the Nd is behaving as a conservative water mass tracer in the tectonically and oceanographically complicated Caribbean Sea seems still uncertain (McKinley et al., 2019; van de

Flierdt et al., 2016). Nd evidence has also been used to argue that the AMOC was at peak strength during the late Miocene and early PWP (also referred to as the Pliocene Climate Optimum, Miller et al., 2020; Raymo et al., 2018), and later diminished during the major intensification of northern hemisphere Glaciation 2.7–2.5 Ma (e.g., Miller & Wright, 2017), and in the Pleistocene after 1.5 Ma as AABW contributions increased (Dausmann et al., 2017). This picture generally matches interpretations of drift sedimentation in the northeastern Atlantic (Uenzelmann-Neben & Gruetzner, 2019), but not in Newfoundland where sediment drifts suggest a later final intensification of NADW in the Pleistocene (Boyle et al., 2017). A focused study on North Pacific ϵNd suggests NPDW was being produced until 14 Ma, after which a southern source takes over (Kender et al., 2018), although see Zhai et al. (2021) and Burls et al. (2017). Holbourn et al. (2013a) use ϵNd and $\delta^{13}\text{C}$ to monitor Pacific Ocean changes from the MMCT associated with Antarctic ice-sheet re-expansion. They suggest deep and intermediate water mass provenances much as today (i.e., no large scale NPDW), but find evidence for cyclic changes in ventilation in the deep North Pacific after 13.9 Ma once Antarctica re-glaciated.

11. Climate Modeling of the Miocene

The Miocene climate state is in the first instance deduced from proxy evidence, but proxy data are sparse and have uncertainties. Outputs from models also have uncertainties that are difficult to quantify, but are continuous in space and can provide details on more variables than are readily reconstructed by proxies, for instance atmospheric circulation or cloud cover. The climate states derived from existing models are synthesized and reviewed in detail in a modeling review paper in this volume (Burls et al., 2021). Here, we provide a brief summary of the mean climate (11.1) and ocean circulation (11.2) state of the Miocene as derived from models and then focus on sensitivity studies (Section 11.3) investigating the role of specific forcing mechanisms on the climate system that may have been responsible for differences between the Miocene and the pre-industrial climate.

Modeling of the Miocene has a long history, going back to the pioneering simulations carried out more than 20 years ago of Maier-Reimer et al. (1990), Dutton and Barron (1997), Mikolajewicz and Crowley (1997), Ramstein et al. (1997), and Ruddiman et al. (1997). Since then, various studies explored aspects of the Miocene climate using relatively simplified model configurations with either prescribed SSTs (e.g., Gladstone et al., 2007; Herold et al., 2010; Lunt et al., 2008a), or “slab” ocean models with prescribed heat-fluxes (e.g., Goldner et al., 2014a; Henrot et al., 2010; Herold et al., 2011a; Micheels et al., 2007; Steppuhn et al., 2007, 2006; Tong et al., 2009; You et al., 2009), or asynchronously coupled atmosphere-ocean models (Haupt & Seidov, 2012). Similarly, some studies have used offline vegetation models to explore Miocene vegetation distributions (Henrot et al., 2017; Herold et al., 2011a). However, in this review, we focus on synthesizing previous modeling work that has been carried out with fully dynamic atmosphere-ocean or atmosphere-ocean-vegetation models, because these have the most complete representation of the Earth system. Furthermore, this avoids the circularity associated with comparing model results with proxy data when the prescribed model SSTs have themselves been informed by proxies.

11.1. Modeled Miocene Surface Climate and Comparison With Data

Several atmosphere-ocean general circulation models have been used to simulate the climate of the middle Miocene (~15 Ma) and the late Miocene (~11–7 Ma) and carry out global-scale model-data comparisons. In general, models struggle to reproduce the amount of warming indicated by the temperature proxies under realistic $p\text{CO}_2$ concentrations for the Miocene as well as the reduced meridional temperature gradient. Krapp and Jungclaus (2011) simulated the middle Miocene in their MPI-ESM (ECHAM5-MPIOM-JS-BACH) and compared it to terrestrial and marine proxies (Figure 14 of Krapp & Jungclaus, 2011). For the terrestrial proxies they found best agreement with their simulations at 480 and 720 ppm, whereas for the marine proxies they found best agreement at 360 and 480 ppm.

In a different study also focusing on the middle Miocene, Herold et al. (2011b) compared their CCSM3 simulations with a terrestrial temperature data set (Table 2 of Herold et al., 2011b). Their simulation (with 335 ppm $p\text{CO}_2$) did not warm enough relative to the modern (1.4°C warming in the model compared with 6°C in the proxies). The largest biases in the model were in mid-high latitudes, indicating a too-strong

meridional temperature gradient. Herold et al. (2012) focused on the ocean component of the same fully coupled simulations and reached several conclusions, including a temperature gradient $\sim 6^{\circ}\text{C}$ lower than modern. Goldner et al. (2014a) assessed their CESM1.0 simulations of the middle Miocene relative to a proxy data set including SST and terrestrial data (Figure 1 of Goldner et al., 2014a) using the ocean heat flux convergence derived from Herold et al. (2012). Their standard Miocene simulation (with 400 ppm $p\text{CO}_2$) had global mean surface temperature 4°C lower than indicated by the proxies, with the cold bias greatest in the high latitudes and a meridional temperature gradient too strong by about 17°C . By increasing $p\text{CO}_2$ to 800 ppm they were able to better match both the global mean and temperature gradients indicated by the temperature proxies. However, this $p\text{CO}_2$ concentration is substantially greater than that indicated by $p\text{CO}_2$ proxies (see Section 8) and the mismatch was not fully resolved.

For the late Miocene ($\sim 11\text{--}7$ Ma), Micheels et al. (2011) compared their COSMOS (ECHAM5-MPIOM) simulations, with a $p\text{CO}_2$ of 360 ppm, to a terrestrial temperature data set (Figure 7a of Micheels et al., 2011). In general, their model-data agreement was reasonable and better than some previous versions of the model (Micheels et al., 2007). However, similar to the middle Miocene studies, their simulation failed to capture the observed lower meridional temperature gradient as some tropical regions (southern China) were too warm in the model and the higher latitudes (Eastern Siberia, Alaska, and Iceland) were too cold in the model. In another late Miocene study, Bradshaw et al. (2012, 2014) compared their HadCM3L simulations with a terrestrial temperature data set (Figure 9 and Table 3 of Bradshaw et al., 2012). Still, their simulation with a $p\text{CO}_2$ of 400 ppm agreed with over half (271/429) of the proxy data, but was in general too cold compared with the rest of the data, in particular outside of the Mediterranean region. Their 400 ppm simulation agreed better with the data than their 280 ppm simulation.

Independent of the global scale temperature fit, we note that all model realizations are characterized by equator to pole temperature gradients too close to modern and much greater than indicated by proxies. When compared with reconstructions this mainly reflects too low high-latitude temperatures, which echoes the principle model challenge to simulate the magnitude of high-latitude warming in a warmer-than-modern climate (e.g., Goldner et al., 2014a; Huber, 2013; Stein et al., 2017) and limited understanding or interpretation of proxy data signals (e.g., Ho & Laepple, 2016). Given recent work on the Eocene, it is possible that more recent models with improved representation of aerosols and cloud microphysics may give an improved model-data comparison (Huber, 2013; Kiehl & Shields, 2013; Kump & Pollard, 2008; Sagoo et al., 2013; Tierney et al., 2019; Unger & Yue, 2014; Zhu et al., 2019). However, the different studies mentioned here have all used different proxy data sets, the terrestrial data sets have had very few sites outside of Europe, and both marine and terrestrial data sets have large uncertainties that are not always accounted for in model-data comparisons. As such, we recommend a more systematic and consistent model-data comparison be carried out in which uncertainties in all the proxies are accounted for, before any firm conclusions are drawn.

The hydrological cycle of the Miocene is in general modeled to be more vigorous than that of the modern day because the warmer atmosphere can hold more water vapor. Krapp and Jungclaus (2011) found a 5% increase in annual mean precipitation for a middle Miocene run with $p\text{CO}_2$ at 720 ppm, compared to the control. The changes in paleogeography alone did not affect the mean precipitation but influenced the regional distribution. The rainfall increased over Eurasia, in the western Pacific warm pool, poleward of $10^{\circ}\text{N}/^{\circ}\text{S}$ in the Pacific, and large parts of the Southern Ocean. It decreased in the Equatorial Pacific, and over Africa and the Americas (Krapp & Jungclaus, 2011). In a simulation of the late Miocene ($\sim 11\text{--}7$ Ma), with unchanged $p\text{CO}_2$ compared to the present day, the mean global precipitation decreased by 4% and a prescribed low Tibetan Plateau elevation caused a general weakening of the Asian monsoon (Micheels, 2011). In contrast, a modeling study by Boos and Kuang (2010) found monsoonal circulation to be unaffected by the simulated removal of the Tibetan Plateau, with the Himalaya and adjacent mountain ranges instead acting as the primary driver of the South Asian monsoon. This result was supported by Acosta and Huber (2019) who found any high topography in the region was sufficient to cause South Asian Monsoon precipitation and that the main wind patterns in summer were relatively insensitive to topography in the region. Fully coupled climate model simulations for the late Miocene indicate that El Niño Southern Oscillation (ENSO) variability persisted, with teleconnections that extended further than today. This is attributed to the weakening of high-latitude climate modes due to a reduced meridional temperature gradient (Galeotti et al., 2010).

Regarding the role of vegetation in simulations, Zhou et al. (2018), building on the early-to-mid Miocene modeling of Herold et al. (2012) and Goldner et al. (2014a), conducted sensitivity experiments to understand Miocene vegetation dynamics. They used a version of CESM1 with advanced treatment of cloud microphysics (CAM5) similar in configuration to the studies of Zhu et al. (2019) and Tierney et al. (2019), but with the modal (3-mode) aerosol cloud microphysics treatment enabled, rather than bulk aerosol treatment. This study demonstrated that $p\text{CO}_2$ and climate both contributed to the spread of C_4 grasslands and made very specific predictions of where that innovation was favored, but the simulations were colder and had weaker temperature gradients than found in proxy data. The model finds were in general agreement with the diachronous progression of timings found in Tauxe and Feakins (2020). Improving the ability of GCMs to reproduce Miocene climates requires improved paleorecords from regions that are sensitive to CO_2 forcing, but insensitive to differences between Miocene and modern geographic configuration (Bradshaw et al., 2015). These areas include southern Europe and Middle and Central Asia, for which there are currently good to excellent records for all stages, as well as North America, northern Africa, Australia, Paraguay, southern Brazil, and northeastern Asia, for which data are currently insufficient (Bradshaw et al., 2015; Pound et al., 2012). However, good age control is lacking for some of these records, such as in many parts of Asia (Y.-S. Liu et al., 2011), and future dating may reveal some sequences, dated as Miocene on their botanical content, to in fact be older (Linnemann et al., 2017).

11.2. Ocean Circulation From Models Compared to Data

Establishing the timing of changes in MOC modes during different stages of the Miocene is useful for exploring the role of ocean heat and moisture transport in moderating Miocene climates. The strength and structure of the Miocene overturning is intimately connected to the evolution of the gateways, which control the inter-basin salt transports (Bradshaw et al., 2016; Brierley & Fedorov, 2016; Butzin et al., 2011; Herold et al., 2012; Knorr et al., 2011; Micheels et al., 2011; Sepulchre et al., 2014; von der Heydt & Dijkstra, 2006). One of the primary gateways thought to control the relative strength of deep-water formation in the Atlantic and the Pacific, is the Panama Gateway. Some modeling studies suggest that the closing of this gateway led to the startup or strengthening of the AMOC and that, from a large-scale MOC perspective, the most critical stages of seaway closure were completed by the middle Miocene, possibly as early as 18 Ma, and likely by 12 Ma, when the seaway shoaled above 500 m (Kirillova et al., 2019; Montes et al., 2015; Sepulchre et al., 2014). However, others find a strong modern-like AMOC even in early Miocene experiments with wide open Panama (Krapp & Jungclaus, 2011; Nisancioglu et al., 2003). In the case of Krapp and Jungclaus (2011), an AMOC was sustained because positive salinity in the Atlantic was maintained by higher atmospheric moisture transport to the Pacific (lower Andes topography), together with a deeper GSR allowing stronger convection at higher latitudes, something explored further by Stürz et al. (2017) and Hossain et al. (2020). Different model results, with regard to the Panama Gateway, may be partly explained by differences in the depth and location of the open ocean passageway in the model geography, since the character of incoming Pacific waters appears to be sensitive to the precise latitudinal position and configuration of the Panama Seaway, with some scenarios advecting relatively salty water from the North Pacific that supports an AMOC (Steph et al., 2006). Another noteworthy point is that while the Gulf Stream and some degree of NCW production existed at least as far back as the Eocene (Corfield & Norris, 1996; Coxall et al., 2018; Huber et al., 2003; Pinet et al., 1981), with their associated heat transport and ventilation, and both may have been vigorous at times in the Miocene (Herold et al., 2012), a significant cross-hemispheric transport typically associated with the modern AMOC may not have developed until full closure of the Panama Gateway (Lunt et al., 2008b).

Another gateway that is commonly studied with regard to Miocene ocean circulation is the Tethys Gateway. In Tethys focused experiments, the AMOC strengthens once Tethys was permanently closed ~ 14 Ma because westerly “Mediterranean Outflow” increases through the Gibraltar Strait (Butzin et al., 2011; Hamon et al., 2013). Hamon et al. (2013) also found that shoaling of the Tethys during the middle Miocene may have led to freshening of the Northern Indian Ocean and co-incident weakening of the Antarctic Circumpolar current. The Tethys Gateways can also impact the flow through the Panama Gateway; switching from Oligocene (~ 30 Ma) to early Miocene (~ 20 Ma) geography in a fully coupled climate model, involving closing the Tethys gateway and widening Southern Ocean gateways, led to the flow through the Panama Gateway reversing from westward to eastward (von der Heydt & Dijkstra, 2005, 2006). This gateway change

could therefore have allowed for cool Pacific waters to enter the Caribbean, contributing to the demise of the warm water corals there.

Brierley and Fedorov (2016) found that a closed Bering Strait had an important role in helping salinify the North Atlantic and supporting AMOC by reducing fresh water export from the North Pacific into the Arctic, thus compensating for the open Panama Seaway freshening. This condition probably applied only from the late Miocene when this gateway is thought to have opened (Gladenkov & Gladenkov, 2004). The other paleogeographic boundary condition that has been tested explicitly for the Miocene is the Weddell Sea shelf. Specifically, X. Huang et al. (2017) found that a more realistic shelf morphology, based on seismic data, with a shelf break further south, resulted in enhanced AABW/SCW formation during the middle Miocene. Finally, the opening of Fram Strait 17.5 Ma seems to be a rather under-appreciated event with respect to global ocean processes that could have initiated a critical supply of cold dense water to reinforce an early AMOC.

Different climate boundary conditions during the Miocene may also have impacted the MOC. In the early-to-mid Miocene simulation of Herold et al. (2012), the AMOC was much weaker and shallower than the modern day, which they attributed to weaker convective preconditioning in the Labrador Sea and weaker southern hemisphere Westerlies caused by the lowering of the meridional surface temperature gradient. In their simulations, southern sinking predominated, especially in the Weddell Sea. Another climate-related impact on ocean circulation is the mean ocean temperature. Higher mean ocean temperatures favors a more distributed overturning with deep water forming in the Atlantic, Pacific, and Southern Oceans while lower temperatures favor overturning in the North Atlantic (Boer et al., 2007, 2008). This is because of the nonlinearity of the equation of state, in which temperature has strong effect on density in warmer water, so that winter cooling can more easily destabilize the water column and cause deep water formation in salinity-stratified polar basins such as the Pacific. This may help explain $\delta^{13}\text{C}$ based observations of a rather weak or nonexistent AMOC during the warm climates of the Miocene. Warm climate, higher-than-modern CO_2 (>400 ppm), also generally acts to dampen or shutdown North Atlantic overturning due to an enhanced hydrological cycle leading to a fresher East Greenland Current exiting the Arctic (Bradshaw et al., 2015; Herold et al., 2012).

The different ocean states produced by the various models make it premature to conclude whether the AMOC was continuously vigorous from the early Miocene, as suggested by interpretations from sediment drift data and Nd deep water tracers or was weaker during warmer parts of the Miocene, as supported by $\delta^{13}\text{C}$. Improved salinity constraints in the northern North Atlantic basins as well as expanded databases of “ocean endmember” benthic $\delta^{13}\text{C}$ fingerprints needed to interpret inter-basin $\delta^{13}\text{C}$ with respect to ventilation patterns would certainly help with this, as would greater confidence in separating local overprinting versus “water-mass provenance and mixing effects” on the ϵNd tracer (McKinley et al., 2019; van de Flierdt et al., 2016). Where there is no or reduced AMOC, northern ocean heat transport is relatively reduced, although this may be compensated for by an increase in atmospheric heat transport (Micheels et al., 2011), emphasizing the need for coupled atmosphere-ocean modeling (Herold et al., 2012). While many models studying the sensitivity of zonal mean ocean heat transport to different Cenozoic boundary conditions robustly shows small changes in ocean heat transport, none has been able to explain high latitude warmth through differences in ocean heat transport alone (Goldner et al., 2014; Haywood et al., 2013; Huber & Sloan, 2001; Krapp & Jungclauss, 2011; Z. S. Zhang, Nisancioglu, et al., 2013).

11.3. Sensitivity Studies to Forcing Factors of the Miocene Climate

From a modeling perspective, there are five main forcing factors (or “boundary conditions”) that make the Miocene climate different from that of modern or pre-industrial: paleogeography (including orography, bathymetry and ocean gateways), greenhouse gas concentrations (predominantly $p\text{CO}_2$), vegetation distribution, ice sheets, and orbit. In reality, some of these forcings are Earth System Feedbacks, such as ice sheets, vegetation, and even $p\text{CO}_2$, but they are typically handled in climate models as imposed boundary condition changes and are therefore considered as forcings. Many Miocene modeling efforts consist of sensitivity studies to one or more of these forcings, and below we synthesize each in turn.

Caution is urged in interpreting results of model sensitivity studies such as those described here, given the weaknesses that models clearly demonstrate in reproducing Miocene mean climate states. If the system

responses are state-dependent (Caballero & Huber, 2013), the fact that these simulations are pervasively too cold and with overly strong meridional temperature gradients may give misleading results. For example, if simulations are too cold near the poles, the response to high latitude forcing might be artificially inflated by ice-albedo feedbacks because the model has substantial sea ice in a time interval which may have had none. Alternatively, thermohaline circulation responses might be dulled or artificially enhanced by being in the wrong part of parameter space for density gradients due to incorrect temperatures in a nonlinear equation of state (Boer et al., 2007). Until this key problem is solved, sensitivity studies assuming at least piece-wise linearity may be our best approach to understanding the system.

11.3.1. Impact of Paleogeography on Miocene Climate

Most Miocene climate modeling studies focus on the early to middle Miocene (~15 Ma) or the late Miocene (~8 Ma). The derivation of the boundary conditions of the middle Miocene period as well as that of the MMCT (~13 Ma) have been carefully documented and published (Frigola et al., 2018; Herold et al., 2008). The impact of paleogeographic differences on the global mean atmospheric temperature between the Miocene and today is generally found to be small but not insignificant (order of 2°C). For the middle Miocene, Krapp and Jungclaus (2011) estimated that the topography changes can explain 0.7°C of the Miocene warming compared to the present day and Herold et al. (2011b) found that paleogeographic and vegetation changes together caused a 1.5°C warming. They also found that the combined paleogeographic changes between the middle Miocene and the present day did not play a significant role in how $p\text{CO}_2$ impacts the ENSO and the Pacific Decadal Oscillation (PDO); in both geographies a doubling of $p\text{CO}_2$ from 360 to 760 ppm leads to the merging of these two oscillations (Krapp & Jungclaus, 2015). Note though that, in CCSM3, increasing $p\text{CO}_2$ does not result in merging of the modes in the Miocene or Eocene (Galeoti et al., 2010; Garric & Huber, 2003; Huber & Caballero, 2003).

Similarly, studies that investigated the climatic effect of paleographic changes between the late Miocene and today did not find a strong role for topographic boundary conditions on climate either. The most prominent paleogeographic differences between this time period and today are an open Panama Gateway, a more southward Australia, and lower elevations of most of the highest regions of the globe. Knorr et al. (2011) found that the impact of these tectonic changes on mean atmospheric temperature was 0.7°C and that this was small compared to the impact of vegetation changes of 2.5°C in their model (and the combined effect of the two was smaller than the sum of their individual contributions). Bradshaw et al. (2012) concluded a similarly small role of paleogeography for the late Miocene and computed only a small 0.3°C mean atmospheric temperature increase, which was small compared to the 2.9°C rise in temperature from increasing atmospheric $p\text{CO}_2$ (280–400 ppm).

11.3.2. Impact of $p\text{CO}_2$ on Miocene Climate

During the Miocene a relatively broad range of $p\text{CO}_2$ between ~280 and 700 ppm has been reconstructed (see Section 9). Thus, the related radiative forcing including a $p\text{CO}_2$ doubling provides a potentially dominant control on global temperature changes. The impact of atmospheric $p\text{CO}_2$ changes on the Miocene climate has been investigated for concentrations between 200 and 800 ppm (Bradshaw et al., 2012; Goldner et al., 2014a; Henrot et al., 2010; Herold et al., 2012; X. Huang et al. 2017; Knorr & Lohmann, 2014; Krapp & Jungclaus, 2011, 2014; Stürz et al., 2017). The corresponding Miocene specific equilibrium climate sensitivity (global mean warming per $p\text{CO}_2$ radiative forcing) is 1.0–1.5 K/(W/m²) (95% confidence interval), which is higher than the 0.4–1.2 K/(W/m²) (“likely” range, or >66% probability) obtained for modern climate (Knutti et al., 2017). Note that the state-dependency has not yet been understood in its full extent in earlier approaches which aimed to make sense of paleoclimate sensitivity from data of the last 65 million years (Rohling et al., 2012), and in which the Miocene was underrepresented.

11.3.3. Vegetation and Miocene Climate

Henrot et al. (2010) performed one of the first studies in which a factorization type of approach (a series of sensitivity experiments in which Miocene forcings for example, $p\text{CO}_2$, land ice, gateways, topography are imposed in isolation in order to assess their impact) was used to isolate the role of Miocene vegetation feedbacks. They use a sequential approach in which are: (1) the climate from their Earth systems Models of Intermediate Complexity (EMIC) simulation, with all Miocene forcings active, is used to force a dynamic vegetation model; (2) the vegetation parameters from this Miocene forced dynamic vegetation model are

prescribed as an additional forcing in the EMIC to assess the climate impacts of the vegetation changes. The Miocene vegetation changes seen in this study include an expansion of forest in place of grassland and desert, and expanded tundra and temperate forests in the high latitudes. The climate impacts of these vegetation changes lead to +0.5°C of global warming (less than the responses seen in the same study to $p\text{CO}_2$ and orography), a signal that is amplified over the continents and is largely the result of vegetation induced surface albedo changes. While the global mean impact was modest, regionally, these vegetation changes resulted in substantial changes.

Using a similar approach in full complexity coupled ocean-atmosphere general circulation model, Knorr et al. (2011) find a much stronger role for vegetation in supporting late Miocene warmth, largely through its direct effect on surface albedo. Acting on its own, imposing reconstructed vegetation changes gave rise to a 2.5°C increase in global mean surface temperature. Key regions in which reconstructed late Miocene vegetation lowers surface albedo are the mid-to high-latitude taiga and cold deciduous forest regions of the northern hemisphere, including Greenland, the Sahara, and Australia. Using a full complexity coupled ocean-atmosphere-vegetation model, Bradshaw et al. (2015) explicitly simulate the potential role of vegetation feedbacks during the late Miocene. They find vegetation feedbacks in response to $p\text{CO}_2$ -induced warming to be an important mechanism contributing regionally to late Miocene warmth. Furthermore, there are several regions where vegetation is particularly sensitive to changes in $p\text{CO}_2$ forcing given the greater land mass in the northern hemisphere, and the resulting differences in vegetation contribute to increased sensitivity to changes in $p\text{CO}_2$ forcing. Vegetation was also found to play a role in maintaining and being maintained by the Australian monsoon in the Miocene (Herold et al., 2011a) although CO_2 was found to be a critical mediator of that process.

11.3.4. Impact of Orbit on Miocene Climate

In the study of Goldner et al. (2014a) for the early to middle Miocene, orbital changes were found to improve the model-data mismatch, although the improvement was small and localized. The role of orbital forcing in the late Miocene climate (8 Ma) has been investigated in three coupled climate model studies (Marzocchi et al., 2019, 2015; D. Simon et al., 2017). They found that the orbital forcing does not change the mean global surface temperature greatly, but can have substantial regional impact on both precipitation and temperature. For instance, during precession minima, the North African summer monsoon is strongly intensified (Marzocchi et al., 2015) and the western Mediterranean and the Atlantic margin are influenced by enhanced winter precipitation from the Atlantic storm tracks (Marzocchi et al., 2019). The influence of precession on this monsoon was also found by D. Simon et al. (2017) who could link the orbital changes to the formation of a sapropel-bearing sedimentary record in the Mediterranean. The regional impacts of orbital forcing emphasize the importance of considering orbital timing when carrying out model-data comparison studies.

11.3.5. Impact of Ice on Miocene Climate

Sea level and ice volume estimates (see Section 10) suggest that the Antarctic ice sheet was highly dynamic prior to the MMCT with a large fluctuation potential of up to 80% of modern ice volume conditions. As yet, only few studies simulated the impact of Miocene ice sheet changes (Frigola et al., 2018; Hamon et al., 2012; Knorr & Lohmann, 2014). These studies agree that strong oceanic feedbacks represent a key to climatic responses by a complex interplay among the wind field, ocean circulation, and the sea-ice system. These feedbacks give rise to heterogeneous surface responses, with sea surface warming and a modest deep-water cooling in large parts of the Southern Ocean (Knorr & Lohmann, 2014) in spite of pronounced cooling over Antarctica. This corroborates the absence of significant cooling at major ice growth steps between 14 and 12 Ma and the Neogene decoupling of deep-water temperature and ice volume as inferred from benthic foraminiferal records of $\delta^{18}\text{O}$ and Mg/Ca ratios (Lear et al., 2015). Qualitatively, the heterogeneous surface temperature changes to Miocene Antarctic ice-sheet growth are convergent to simulated responses at the EOT (Goldner et al., 2014b; Kennedy et al., 2015; Ladant et al., 2014) although regions of Southern Ocean cooling and warming are different. Such differences can arise for example, as a consequence of simulation specific gateway characteristics in the Southern Ocean (Kennedy et al., 2015) and spin-up length (Kennedy-Asser et al., 2019a, 2019b) or the position of the continental shelf (X. Huang et al., 2017). Furthermore, it has been suggested that the transformation from a largely unglaciated (low albedo) to a largely glaciated (high albedo) Antarctic continent at earlier glaciations is the key to reconcile relatively pronounced global

cooling in glaciation scenarios at the EOT (Goldner et al., 2013, 2014b) with the MMCT responses (Knorr & Lohmann, 2014).

12. Conclusions

12.1. Synthesis of Miocene Climate and Biota

The temperature regime reconstructed for most of the Miocene, $\sim 5^{\circ}\text{C}$ – 8°C above modern, is equivalent to projected future warming in about a century under unmitigated carbon emissions scenarios. This nominates the Miocene, with its collection of “tippable” subsystems, as an important warm-climate analog for better understanding vulnerable Earth system components. However, despite the high temperatures and significantly flattened latitudinal temperature gradients, reconstructed $p\text{CO}_2$ was in the near-modern range during the Miocene. Even peak warmth of the middle Miocene was associated with $p\text{CO}_2$ levels similar or only modestly elevated compared to today (~ 400 – 600 ppm) according to most studies. These temperature patterns resemble the warmth of the Eocene, bearing a greater resemblance to that greenhouse climate in many ways than to modern conditions, yet most of the boundary conditions were close to modern. Tectonics, climate, oceanic, and atmospheric circulation, sedimentary systems, the hydrological cycle, and terrestrial and marine ecosystems are intimately connected and increased temperatures will profoundly affect familiar Earth systems. Many of Earth's critical climate subsystems have been forecast to be destabilized by warming the Earth above 4°C , and studying the Miocene world may provide some insight into what our future Earth could be like.

On land during the early and middle Miocene much of the Earth was heavily forested, and these forests extended to much higher latitudes than today. Trees grew around the Arctic and even on Antarctica in sheltered areas, while humid subtropical forest flourished in Iceland. Floras and their distribution changed significantly from the MMCT through the late Miocene. Forests and the associated leaf-browsing fauna diminished (contracting from high latitudes), while grasslands, first C_3 then C_4 types, and grazing inhabitants (and their predators), continued to spread and diversify. These faunal and floral changes reflect the interrelated effects of aridification of continental interiors (changes to the hydrologic cycle), preferential cooling of high latitudes (strengthened latitudinal temperature gradients), and changes to ocean and atmosphere circulation. These processes may have catalyzed primate evolution and the hominin lineage from which modern humans later evolved.

Closure or critical constriction of tropical gateways between 12 and 14 Ma coincides with key steps in the development of a modern-like routing of ocean currents and ocean overturning circulation mode, which may have helped drive mid to late Miocene cooling. Changes in marine ecosystems, from phytoplankton to apex predators and giant plankton feeders, occurred during the middle to late Miocene, and involved a shift in dominance of siliceous over calcareous primary producers, with co-evolution in many biotic groups, including whales and dolphins. Forcing mechanisms were likely changes in winds and nutrient supply/distribution due to global cooling, gateway reconfigurations, and related changes in MOC.

Key subsystems of our modern Earth had evolved and stabilized by the late Miocene, including but not limited to, the East AIS; the AMOC; perennial Arctic sea ice; stronger monsoon systems; the El Niño Southern Oscillation; the tundra/permafrost biome; widespread grasslands and their ecosystems; as well as modern-type forests, deserts, and their affiliated ecosystems. That these Earth system components, many of which are now viewed as “vulnerable” to anthropogenic climate change, switched on at this time, implies they have their “tipping points” in the Miocene temperature/ $p\text{CO}_2$ zone. However, important differences exist between the Miocene scenario and future warmer Earth—for example that the background climate “state” was warmer in the Miocene overall than at present, which influenced every part of the Earth system.

12.2. Future Directions

In this study, we have reviewed the state-of-the-art Miocene research, and in doing so identified a number of key unresolved questions and important areas of knowledge gaps, which may help shape the future of Miocene research. We summarize these below:

- The moderate $p\text{CO}_2$ mostly recorded during the Miocene cannot produce the elevated reconstructed temperatures in existing climate models, and this remains a paradox. Are positive feedbacks missing in the models? Did past climate forcings operate in a way we do not yet understand? Or are the proxies systematically underestimating $p\text{CO}_2$ —and if so, why? This key paradox needs to be tackled on all fronts, in order to improve our knowledge of Miocene climate and its applicability as a future analog.
- The depth of oceanic gateways, as well as the timing and rate of deepening or constriction, is still not well understood for the Miocene, but can have major impacts on ocean currents and mixing of marine reservoirs, as well as nutrient transport. Better understanding of gateway processes is essential and will improve the accuracy of GCMs.
- Understanding the long-term adaptive strategies of marine biota as well as shorter-term responses of marine ecosystems to ocean warming remains a fundamental challenge. From the Miocene fossil record, it is clear that all trophic levels, from primary producers to top predators, were impacted. However, the main driving forces need to be better understood. In combination with growing knowledge of modern marine biota and their physiologies, the Miocene fossil record could serve as a benchmark for modeling the long-term changes in a future warmer ocean.
- The drivers of the important shift from C_3 – C_4 vegetation are still not well understood. The dramatic changes to Earth's climate during the Miocene will help advance research on how physical changes (temperature, precipitation, topography, etc.) affect evolution and function. Grasslands spread at least in part in response to cooling and drying, and ungulates evolved more cursoriality to take advantage of these open habitats. But grasslands spread heterogeneously and existed long before cursoriality evolved. Why? How do biotic interactions (e.g., competition, predator-prey relationships, etc.) intersect with physical changes to drive evolution?
- Desertification occurred in various areas throughout the middle to late Miocene. Did the consequences of this, such as increased continental albedo, contribute to the cooling of the climate system during that time? Given human-driven expansion of deserts, will such a cooling effect also occur in the future?
- The number and quality of terrestrial climate proxies continues to improve, and provides direct input into GCM model validation. However, many areas of the world either lack direct proxies for, or have very sparse records of, temperature and—in particular—precipitation, for example, Africa, southeast Asia, Australia, Central America, and northern and Central South America. Improving the quality, quantity and global coverage of terrestrial climate records must remain an important goal.
- The significant waxing and waning of the Antarctic ice sheet through the Miocene represents an important but challenging target for ice sheet models. Recent improvements have reduced the historic mismatch between model simulations and proxy records for this dynamic behavior, although further work is still required, especially for transient simulations. Key questions focus on the inclusion and parameterization of certain glacial processes in ice sheet models, in addition to the need for higher resolution records of $p\text{CO}_2$.
- The existence, timing, and extent of northern hemisphere ice sheets in the Miocene is still an important unanswered issue, as it impacts the interpretation of global signals (e.g., sea level, seawater $\delta^{18}\text{O}$) as changes in Antarctic ice volume. A focused multi-faceted effort to resolve this is needed.
- Models continue to simulate polar regions that are too cold during warm climates and thus have exaggerated meridional temperature gradients—the challenge to solve this problem is ongoing in the modeling community.
- Miocene modeling studies use a wide variety of boundary conditions, making it difficult to distinguish the impact of boundary conditions versus model physics. A coordinated Miocene Model Intercomparison Project (Mio-MIP), targeting various stages in this period, is under way and will provide valuable insights.

The Miocene may be the best available analog for our future Earth under anthropogenic climate change. By studying it, many lessons can be learned, about for example the cause and consequences of highly elevated temperatures such as occurred during the MCO, and about the tipping zone for many climate subsystems (mostly occurring in the late Miocene). Improved understanding of how the Earth system operates under varying background conditions may enable us to answer such important questions as whether highly elevated temperatures can be achieved at relatively moderate $p\text{CO}_2$, a particularly pertinent question as we enter uncharted territory of elevated $p\text{CO}_2$ already at present. It can inform the ways ecosystems and individual

taxa evolve and adapt to tackle these changes (or, in some cases, not) and how this in turn may affect physical processes. Synthesizing the existing and forthcoming data on Miocene temperature, $p\text{CO}_2$, precipitation, tectonic evolution, marine and terrestrial ecosystems, atmospheric and ocean circulation, and ice sheet dynamics, within a rigorous chronological framework, allows us advance this understanding, including by simulating the various scenarios in climate models. There remains great potential to expand Miocene proxy records, requiring new dedicated ocean and continental drilling expeditions, as well as fieldwork campaigns in targeted regions, including the sensitive subsystems such as polar and subpolar regions, tropical diversity hotspots, and continental interiors. Bringing together scientific expertise from across disciplines to inspire, discuss and challenge paradigms with respect to both interpretative frameworks and methodologies, as well as to integrate and synthesize results, remains the best approach.

Data Availability Statement

Data availability statement has been published in supporting information.

Acknowledgments

The initial workshops that catalyzed this project were supported by The Bolin Center for Climate Research, Stockholm University, and the Swedish Research Council (Conference Grant nr. 2018–06,618 to M. Steinhorsdottir). The authors acknowledge funding from: the Swedish Research Council (VR starting grant nr. NT7-2016 04,905 to M. Steinhorsdottir; VR grants nr. 2016–03,912 to A. M. de Boer and nr. 2016–04,434 to J. Henderiks); the United States National Science Foundation (NSF), through the P2C2 program grant nr. 1602905 to M. Huber, the Atmospheric and Geospace Sciences program grant nr. to N.J.B (who is also supported by the Alfred P. Sloan Foundation as a Research Fellow), and the Global Change, Sedimentary Geology & Paleobiology, and Geobiology and Low-temperature Geochemistry programs grant nrs. 1349749 and 1561027 to M. J. Kohn; and the UK Natural Environment Research Council (grant NE/P019102) to C. H. Lear. E. Gasson acknowledges funding from a Royal Society fellowship. Clara Bolton, Peter Bijl, Daniel Breecker, Jeremy Caves Rugenstein, Florence Collioni, Mikael Fortelius, David Lazarus, Eelco Rohling, Francesca Sangiorgi, Maria Seton, Erik Skovbjerg Rasmussen, Appy Sluijs, Lars Werdelin, and Zhongshi Zhang are thanked for their useful comments with respect to Figure 1. M. Huber acknowledges assistance in Miocene work from Nick Herold and Ashley Dicks. No new data were created for this study, and all reviewed data sets are available through the cited original papers. The authors declare no conflict of interest.

References

- Abdul Aziz, H., Krijgsman, W., Hilgen, F. J., Wilson, D. S., & Calvo, J. P. (2003). An astronomical polarity timescale for the late middle Miocene based on cyclic continental sequences. *Journal of Geophysical Research*, *108*(B3), 2159. <https://doi.org/10.1029/2002JB001818>
- Abelson, M., Agnon, A., & Almogi-Labin, A. (2008). Indications for control of the Iceland plume on the Eocene-Oligocene “greenhouse-icehouse” climate transition. *Earth and Planetary Science Letters*, *265*(1–2), 33–48. <https://doi.org/10.1016/j.epsl.2007.09.021>
- Acosta, R. P., & Huber, M. (2020). Competing topographic mechanisms for the summer Indo-Asian monsoon. *Geophysical Research Letters*, *47*, e2019GL085112. <https://doi.org/10.1029/2019GL085112>
- Agnolin, F. L. (2017). Unexpected diversity of ratites (Aves, Palaeognathae) in the early cenozoic of south America: Paleobiogeographical implications. *Alcheringa: An Australasian Journal of Palaeontology*, *41*(1), 101–111. <https://doi.org/10.1080/03115518.2016.1184898>
- Akgün, F., Kayseri, M. S., & Akkiraz, M. S. (2007). Paleoclimatic evolution and vegetational changes during the late oligocene–Miocene period in western and central Anatolia (Turkey). *Palaeogeography Palaeoclimatology Palaeoecology*, *253*(1–2), 56–90. <https://doi.org/10.1016/j.palaeo.2007.03.034>
- Ali, S., Hathorne, E. C., & Frank, M. (2021). Persistent provenance of South Asian monsoon-induced silicate weathering over the past 27 million years. *Paleoceanography and Paleoclimatology*, *36*, e2020PA003909. <https://doi.org/10.1029/2020PA003909>
- Aliscioni, S., Bell, H. L., Besnard, G., Christin, P. A., Columbus, J. T., Duvall, M. R., et al. (2012). New grass phylogeny resolves deep evolutionary relationships and discovers C_4 origins. *New Phytologist*, *193*(2), 304–312. <https://doi.org/10.1111/j.1469-8137.2011.03972.x>
- Anderson, J. B., Warny, S., Askin, R. A., Wellner, J. S., Bohaty, S. M., Kirshner, A. E., et al. (2011). Progressive Cenozoic cooling and the demise of Antarctica’s last refugium. *Proceedings of the National Academy of Sciences of the United States of America*, *108*, 11356–11360. <https://doi.org/10.1073/pnas.1014885108>
- Andrae, J., McInerney, F., Polissar, P., Sniderman, K., Howard, S., Hall, P., & Phelps, S. (2018). Initial expansion of C_4 vegetation in Australia during the late Pliocene. *Geophysical Research Letters*, *45*(10), 4831–4840. <https://doi.org/10.1029/2018GL077833>
- Arakaki, M., Christin, P.-A., Nyffeler, R., Lendel, A., Eggli, U., Ogburn, R. M., et al. (2011). Contemporaneous and recent radiations of the world’s major succulent plant lineages. *Proceedings of the National Academy of Sciences of the United States of America*, *108*(20), 8379. <https://doi.org/10.1073/pnas.1100628108>
- Arnold, N., Tziperman, E., & Farrell, B. F. (2012). Abrupt transition to strong superrotation driven by equatorial wave resonance in an idealized GCM. *Journal of the Atmospheric Sciences*, *69*, 626–640. <https://doi.org/10.1175/JAS-D-11-0136.1>
- Atwater, T., & Stock, J. (1998). Pacific-North America plate tectonics of the Neogene southwestern United States: An update. *International Geology Review*, *40*, 375–402. <https://doi.org/10.1080/00206819809465216>
- Backman, J., & Raffi, I. (1997). Calibration of Miocene nannofossil events to orbitally tuned cyclostratigraphies from Ceara Rise. In N. J. Shackleton, W. B. Curry, C. Richter, & T. J. Bralower (Eds.), *Proceedings of the ODP, Scientific Results* (Vol. 154 (pp. 83–99)). Ocean Drilling Program.
- Backman, J., Raffi, I., Rio, D., Fornaciari, E., & Pälike, H. (2012). Biozonation and biochronology of Miocene through Pleistocene calcareous nannofossils from low and middle latitudes. *Newsletters on Stratigraphy*, *47*(2), 1–24. <https://doi.org/10.1127/0078-0421/2012/0022>
- Badger, M. P. S., Chalk, T. B., Foster, G. L., Bown, P., Gibbs, S. J., Sexton, P. F., et al. (2019). Insensitivity of alkenone carbon isotopes to atmospheric CO_2 at low to moderate CO_2 levels. *Climate of the Past*, *15*, 539–554. <https://doi.org/10.5194/cp-15-539-2019>
- Badger, M. P. S., Lear, C. H., Pancost, R. D., Foster, G. L., Bailey, T. R., Leng, M. J., & Abels, H. A. (2013). CO_2 drawdown following the middle Miocene expansion of the Antarctic Ice Sheet. *Paleoceanography*, *28*, 42–53. <https://doi.org/10.1002/palo.20015>
- Badgley, C., Barry, J. C., Morgan, M. E., Nelson, S. V., Behrensmeier, A. K., Cerling, T. E., & Pilbeam, D. (2008). Ecological changes in Miocene mammalian record show impact of prolonged climatic forcing. *Proceedings of the National Academy of Sciences of the United States of America*, *105*, 12145–12149. <https://doi.org/10.1073/pnas.0805592105>
- Baird, R. F., & Vickers-Rich, P. (1998). Palaeolodus (Aves: Palaelodidae) from the middle to late Cainozoic of Australia. *Alcheringa: An Australasian Journal of Palaeontology*, *22*(2), 135–151. <https://doi.org/10.1080/03115519808619196>
- Barbolini, N., Woutersen, A., Dupont-Nivet, G., Silvestro, D., Tardif, D., Coster, P. M. C., et al. (2020). Cenozoic evolution of the steppe-desert biome in Central Asia. *Science Advances*, *6*, eabb8227. <https://doi.org/10.1126/sciadv.abb8227>
- Barclay, R. S., & Wing, S. L. (2016). Improving the Ginkgo CO_2 barometer: Implications for the early cenozoic atmosphere. *Earth and Planetary Science Letters*, *439*, 158–171. <https://doi.org/10.1016/j.epsl.2016.01.012>
- Barreda, V., & Palazzesi, L. (2007). Patagonian vegetation turnovers during the Paleogene-early neogene: Origin of arid-adapted floras. *The Botanical Review*, *73*(1), 31–50. [https://doi.org/10.1663/0006-8101\(2007\)73\[31:PVTDTTP\]2.0.CO;2](https://doi.org/10.1663/0006-8101(2007)73[31:PVTDTTP]2.0.CO;2)
- Barreiro, M., & Philander, S. G. (2008). Response of the tropical Pacific to changes in extratropical clouds. *Climate Dynamics*, *31*(6), 713–729. <https://doi.org/10.1007/s00382-007-0363-5>

- Beddow, H. M., Liebrand, D., Sluijs, A., Wade, B. S., & Lourens, L. J. (2016). Global change across the Oligocene-Miocene transition: High-resolution stable isotope records from IODP Site U1334 (equatorial Pacific Ocean). *Paleoceanography*, *31*(1), 81–97. <https://doi.org/10.1002/2015PA002820>
- Beddow, H. M., Liebrand, D., Wilson, D. S., Hilgen, F. J., Sluijs, A., Wade, B. S., & Lourens, L. J. (2018). Astronomical tunings of the Oligocene-Miocene transition from Pacific Ocean Site U1334 and implications for the carbon cycle. *Climate of the Past*, *14*(3), 255–270. <https://doi.org/10.5194/cp-14-255-2018>
- Beerling, D. J., Fox, A., & Anderson, C. W. (2009). Quantitative uncertainty analyses of ancient atmospheric CO₂ estimates from fossil leaves. *American Journal of Science*, *309*, 775–787. <https://doi.org/10.2475/09.2009.01>
- Beerling, D. J., & Royer, D. L. (2011). Convergent cenozoic CO₂ history. *Nature Geoscience*, *4*, 418–420. <https://doi.org/10.1038/ngeo1186>
- Bell, D. B., Jung, S. J. A., Kroon, D., Lourens, L. J., & Hodell, D. A. (2014). Local and regional trends in Plio–Pleistocene ¹⁸O records from benthic foraminifera. *Geochemistry Geophysics Geosystems*, *15*, 3304–3321. <https://doi.org/10.1002/2014GC005297>
- Bellwood, D. R., Goatley, C. H. R., & Bellwood, O. (2017). The evolution of fishes and corals on reefs: Form, function and interdependence. *Biological Reviews*, *92*, 878–901. <https://doi.org/10.1111/brv.12259>
- Berger, W. H. (2007). Cenozoic cooling, Antarctic nutrient pump, and the evolution of whales. *Deep Sea Research Part II: Topical Studies in Oceanography*, *54*, 2399–2421. <https://doi.org/10.1016/j.dsr2.2007.07.024>
- Berta, A., Churchill, M., & Boessenecker, R. W. (2018). The origin and evolutionary biology of pinnipeds: Seals, sea lions, and walrus. *Annual Review of Earth and Planetary Sciences*, *46*, 203–228. <https://doi.org/10.1146/annurev-earth-082517-010009>
- Bertini, A., & Martinetto, E. (2011). Reconstruction of vegetation transects for the Messinian–Piacenzian of Italy by means of comparative analysis of pollen, leaf and carpological records. *Palaeogeography Palaeoclimatology Palaeoecology*, *304*(3), 230–246. <https://doi.org/10.1016/j.palaeo.2010.09.005>
- Betzler, C., Eberli, G. P., Kroon, D., Wright, J. D., Swart, P. K., Nath, B. N., et al. (2016). The abrupt onset of the modern South Asian Monsoon winds. *Scientific Reports*, *6*, 29838. <https://doi.org/10.1038/srep29838>
- Betzler, C., Eberli, G. P., Lüdmann, T., Reolid, J., Kroon, D., Reijmer, J. J. G., et al. (2018). Refinement of Miocene sea level and monsoon events from the sedimentary archive of the Maldives (Indian Ocean). *Progress in Earth and Planetary Science*, *5*, 5. <https://doi.org/10.1186/s40645-018-0165-x>
- Beu, A. G. (2009). Before the ice: Biogeography of Antarctic Paleogene molluscan faunas. *Palaeogeography Palaeoclimatology Palaeoecology*, *284*, 191–226. <https://doi.org/10.1016/j.palaeo.2009.09.025>
- Beu, A. G., & Maxwell, P. A. (1990). Cenozoic Mollusca of New Zealand. *New Zealand Geological Survey Paleontological Bulletin*, *58*, 1–518. <https://www.gns.cri.nz/static/Mollusca/>
- Bialik, O. M., Auer, G., Ogawa, N. O., Kroon, D., Waldmann, N. D., & Ohkouchi, N. (2020). Monsoons, upwelling and the deoxygenation of the northwestern Indian Ocean in response to Middle to Late Miocene global climatic shifts. *Paleoceanography and Paleoclimatology*, *35*, e2019PeLocator003762. <https://doi.org/10.1029/2019PA003762>
- Bibi, F., Shabel, A. B., Kraatz, B. P., & Stidham, T. A. (2006). New fossil ratite (Aves: Palaeognathae) Eggshell Discoveries from the late miocene Baynunah Foramat of the United Arab Emirates, Arabian Peninsula. *Palaeontologia Electronica*, *9*(1), 2A:13. http://paleo-electronica.org/paleo/2006_1/eggshell/issue1_06.htm
- Bierman, P. R., Shakun, J. D., Corbett, L. B., Zimmerman, S. R., & Rood, D. H. (2016). A persistent and dynamic East Greenland Ice Sheet over the past 7.5 million years. *Nature*, *540*, 256–260. <https://doi.org/10.1038/nature20147>
- Bijl, P. K., Houben, A. J. P., Hartman, J. D., Pross, J., Salabarnada, A., & Escutia, C. (2018). Paleooceanography and ice sheet variability offshore Wilkes Land, Antarctica – Part 2 : Insights from Oligocene – Miocene dinoflagellate cyst assemblages. *Climate of the Past*, *14*, 1015–1033. <https://doi.org/10.5194/cp-14-1015-2018>
- Billups, K., Channell, J. E. T., & Zachos, J. (2002). Late oligocene to early miocene geochronology and paleooceanography from the subantarctic South Atlantic. *Paleoceanography*, *17*(1), 1004. <https://doi.org/10.1029/2000PA000568>
- Billups, K., & Schrag, D. P. (2003). Application of benthic foraminiferal Mg/Ca ratios to questions of Cenozoic climate change. *Earth and Planetary Science Letters*, *209*(1–2), 181–195. [doi.org/10.1016/S0012-821X\(03\)00067-0](https://doi.org/10.1016/S0012-821X(03)00067-0)
- Boer, D. A. M., Sigman, D. M., Toggweiler, J. R., & Russell, J. L. (2007). Effect of global ocean temperature change on deep ocean ventilation. *Paleoceanography*, *22*(2), PA2210. <https://doi.org/10.1029/2005PA001242>
- Boer, D. A. M., Toggweiler, J. R., & Sigman, D. M. (2008). Atlantic dominance of the meridional overturning circulation. *Journal of Physical Oceanography*, *38*(2), 435–450. <https://doi.org/10.1175/2007JPO3731.1>
- Böhme, M. (2003). The miocene climatic optimum: Evidence from ectothermic vertebrates of central Europe. *Palaeogeography Palaeoclimatology Palaeoecology*, *195*, 389–401. [https://doi.org/10.1016/S0031-0182\(03\)00367-5](https://doi.org/10.1016/S0031-0182(03)00367-5)
- Böhme, M. (2010). Ectothermic vertebrates (Actinopterygii, Allocaudata, Urodela, Anura, Crocodylia, Squamata) from the miocene of Sandelzhausen (Germany, Bavaria) and their implications for environment reconstruction and palaeoclimate. *Paläontologische Zeitschrift*, *84*(1), 3–41. <https://doi.org/10.1007/s12542-010-0050-4>
- Böhme, M., Bruch, A. A., & Selmeier, A. (2007). The reconstruction of Early and Middle Miocene climate and vegetation in Southern Germany as determined from the fossil wood flora. *Palaeogeography Palaeoclimatology Palaeoecology*, *253*(1–2), 91–114. <https://doi.org/10.1016/j.palaeo.2007.03.035>
- Böhme, M., Ilg, A., & Winklhofer, M. (2008). Late miocene “washhouse” climate in Europe. *Earth and Planetary Science Letters*, *275*, 393–401. <https://doi.org/10.1016/j.epsl.2008.09.011>
- Boles, W. E. (1992). Revision of *Dromaius gidju* Patterson and rich, 1987 from Riversleigh, northwestern Queensland, Australia, with a reassessment of its generic position. *Los Angeles County Museum, Science Series*, *36*, 195–208.
- Bolton, C. T., Hernández-Sánchez, M. T., Fuertes, M.-Á., González-Lemos, S., Abrevaya, L., Mendez-Vicente, A., et al. (2016). Decrease in coccolithophore calcification and CO₂ since the middle Miocene. *Nature Communications*, *7*, 10284. <https://doi.org/10.1038/ncomms10284>
- Bonham, S., Haywood, A., Lunt, D., Collins, M., & Salzmann, U. (2009). ENSO, Pliocene climate and equifinality. *Philosophical Transactions of the Royal Society A: Mathematical, Physical & Engineering Sciences*, *367*, 127–156. <https://doi.org/10.1098/rsta.2008.0212>
- Bonnefille, R. (2010). Cenozoic vegetation, climate changes and hominid evolution in tropical Africa. *Global and Planetary Change*, *72*, 390–411. <https://doi.org/10.1016/j.gloplacha.2010.01.015>
- Boos, W. R., & Kuang, Z. (2010). Dominant control of the South Asian monsoon by orographic versus plateau heating. *Nature*, *463*, 218–222. <https://doi.org/10.1038/nature08707>
- Bouchal, J. M., Zetter, R., Grímsson, F., & Denk, T. (2016). The middle miocene palynoflora and palaeoenvironments of Eskihisar (Yatağan basin, south-western Anatolia): A combined LM and SEM investigation. *Botanical Journal of the Linnean Society*, *182*(1), 14–79. <https://doi.org/10.1111/boj.12446>

- Bouchet, P., Bary, S., Héros, V., & Marani, G. (2016). How many species of molluscs are there in the world's oceans, and who is going to describe them?. *Memoires du Museum National d'Histoire Naturelle*, 208, 9–24.
- Bown, P. R. (2005). Calcareous nannoplankton evolution: A tale of two oceans. *Micropaleontology*, 51(4), 299–308. <https://doi.org/10.2113/gsmicropal.51.4.299>
- Bown, P. R., Lees, J. A., & Young, J. R. (2004). Calcareous nannoplankton evolution and diversity through time. In H. R. Thierstein, & J. R. Young (Eds.), *Coccolithophores: From molecular processes to global impact*. Berlin: Springer-Verlag.
- Boyd, J. L., Riding, J. B., Pound, M. J., De Schepper, S., Ivanovic, R. F., Haywood, A. M., & Wood, S. E. (2018). The relationship between Neogene dinoflagellate cysts and global climate dynamics. *Earth-Science Reviews*, 177, 366–385. <https://doi.org/10.1016/j.earscirev.2017.11.018>
- Boyle, P. R., Romans, B. W., Tucholke, B. E., Norris, R. D., Swift, S. A., & Sexton, P. F. (2017). Cenozoic North Atlantic deep circulation history recorded in contourite drifts, offshore Newfoundland, Canada. *Marine Geology*, 385, 185–203. <http://dx.doi.org/10.1016/j.margeo.2016.12.014>
- Bozkurt, E., & Mittweide, S. K. (2005). Introduction: Evolution of continental extensional tectonics of western Turkey, *Geodinamica Acta*, 18/3-4, 153–165. <https://doi.org/10.3166/ga.18.153-165>
- Brachert, T. C., Corrège, T., Reuter, M., Wroczynna, C., Londeix, L., Spreter, P., & Perrin, C. (2020). An assessment of reef coral calcification over the late Cenozoic. *Earth-Science Reviews*, 204, 103154. <https://doi.org/10.1016/j.earscirev.2020.103154>
- Bradshaw, C. D., Lunt, D. J., Flecker, R., & Davies-Barnard, T. (2015). Disentangling the roles of late Miocene paleogeography and vegetation – implications for climate sensitivity. *Palaeogeography Palaeoclimatology Palaeoecology*, 417, 17–34. <https://doi.org/10.1016/j.palaeo.2014.10.003>
- Bradshaw, C. D., Lunt, D. J., Flecker, R., Salzmann, U., Pound, M. J., Haywood, A. M., & Eronen, J. T. (2012). The relative roles of CO₂ and paleogeography in determining late miocene climate: Results from a terrestrial model–data comparison. *Climate of the Past*, 8, 1257–1285. <https://doi.org/10.5194/cp-8-1257-2012>
- Bradshaw, C. D., Lunt, D. J., Flecker, R., Salzmann, U., Pound, M. J., Haywood, A. M., & Eronen, J. T. (2014). Corrigendum to “The relative roles of CO₂ and paleogeography in determining late miocene climate: Results from a terrestrial model–data comparison” published in *Climate of the Past*, 8, 1257–1285, 2012. *Climate of the Past*, 10(1), 199–206. <https://doi.org/10.5194/cp-10-199-2014>
- Breecker, D. O. (2013). Quantifying and understanding the uncertainty of atmospheric CO₂ concentrations determined from calcic paleosols. *Geochemistry Geophysics Geosystems*, 14, 3210–3220. <https://doi.org/10.1002/ggge.20189>
- Breecker, D. O., & Retallack, G. J. (2014). Refining the pedogenic carbonate atmospheric CO₂ proxy and application to Miocene CO₂. *Palaeogeography Palaeoclimatology Palaeoecology*, 406, 1–8. <https://doi.org/10.1016/j.palaeo.2014.04.012>
- Breecker, D. O., Sharp, Z. D., & McFadden, L. D. (2010). Atmospheric CO₂ concentrations during ancient greenhouse climates were similar to those predicted for A.D. 2100. *Proceedings of the National Academy of Sciences of the United States of America*, 107(2), 576–580. <https://doi.org/10.1073/pnas.0902323106>
- Bretschneider, L., Hathorne, E. C., Huang, H., Lübbers, J., Kochhann, K. G. D., Holbourn, A., et al. (2021). *Provenance and weathering of clays delivered to the Bay of Bengal during the middle Miocene: Linkages to tectonics and monsoonal climate*. Accepted Author Manuscript. e2020PA003917. <https://doi.org/10.1029/2020PA003917>
- Brierley, C. M., & Fedorov, A. V. (2016). Comparing the impacts of Miocene–Pliocene changes in inter-ocean gateways on climate: Central American seaway, Bering Strait, and Indonesia. *Earth and Planetary Science Letters*, 444, 116–130. <https://doi.org/10.1016/j.epsl.2016.03.010>
- Brierley, C. M., Fedorov, A. V., Liu, Z., Herbert, T. D., Lawrence, K. T., & LaRiviere, J. P. (2009). Greatly expanded tropical warm pool and weakened Hadley circulation in the early Pliocene. *Science*, 323(5922), 1714–1718. <https://doi.org/10.1126/science.1171418>
- Bruch, A. A., Utescher, T., & Mosbrugger, V. (2011). Precipitation patterns in the miocene of central Europe and the development of continentality. *Palaeogeography Palaeoclimatology Palaeoecology*, 304(3), 202–211. <https://doi.org/10.1016/j.palaeo.2010.10.002>
- Brunet, M. (2020). *Sahelanthropus tchadensis* nicknamed “Toumaï”: The earliest known Hominin. *Bulletin de l'Academie Nationale de Medecine*, 204(3), 251–257. <https://doi.org/10.1016/j.banm.2019.12.017>
- Budd, A. F., Klaus, J. S., & Johnson, K. G. (2011). Cenozoic diversification and extinction patterns in Caribbean reef corals: A review. *Paleontological Society Papers*, 17, 79–93. <https://doi.org/10.1017/S108933260000245X>
- Burke, K. D., Williams, J. W., Chandler, M. A., Haywood, A. M., Lunt, D. J., & Otto-Bliessner, B. L. (2018). Pliocene and Eocene provide best analogs for near-future climates. *Proceedings of the National Academy of Sciences of the United States of America*, 115(52), 13288–13293. <https://doi.org/10.1073/pnas.1809600115>
- Burls, N. J., Bradshaw, C. D., De Boer, A. M., Herold, N., Huber, M., Pound, M., et al. (2021). Simulating Miocene warmth: Insights from an opportunistic Multi-Model ensemble (MioMIP1). *Paleoceanography and Paleoclimatology*. Retrieved from <https://www.essoar.org/doi/10.1002/essoar.10505870.1>
- Burls, N. J., Fedorov, A. V., Sigman, D. M., Jaccard, S. L., Tiedemann, R., & Haug, G. H. (2017). Active Pacific meridional overturning circulation (PMOC) during the warm Pliocene. *Science Advances*, 3. <https://doi.org/10.1126/sciadv.1700156>
- Butzin, M., Lohmann, G., & Bickert, T. (2011). Miocene ocean circulation inferred from marine carbon cycle modeling combined with benthic isotope records. *Paleoceanography*, 26, PA1203. <https://doi.org/10.1029/2009PA001901>
- Caballero, R., & Huber, M. (2013). State-dependent climate sensitivity in past warm climates and its implications for future climate projection. *Proceedings of the National Academy of Sciences of the United States of America*, 110(35), 14162–14167. <https://doi.org/10.1073/pnas.1303365110>
- Campani, M., Mulch, A., Kempf, O., Schlunegger, F., & Mancktelow, N. (2012). Miocene paleotopography of the central Alps. *Earth and Planetary Science Letters*, 337, 174–185. <https://doi.org/10.1016/j.epsl.2012.05.017>
- Campbell, K. E., Frailey, C. D., & Romero Pittman, L. (2009). In defense of Amahuacatherium (Proboscidea: Gomphotheriidae). *Neues Jahrbuch für Geologie und Paläontologie - Abhandlungen*, 252(1), 113–128. <https://doi.org/10.1127/0077-7749/2009/0252-0113>
- Cane, M. A., & Molnar, P. (2001). Closing of the Indonesian seaway as a precursor to east African aridification around 3–4 million years ago. *Nature*, 411, 157–162. <https://doi.org/10.1038/35075500>
- Cantrill, D. J., Ashworth, A. C., & Lewis, A. R. (2017). Megaspores of an early Miocene aquatic lycophyllid (Isoetales) from Antarctica. *Grana*, 56, 112–123. <https://doi.org/10.1080/00173134.2016.1144784>
- Carr, A. S., Boom, A., & Chase, B. M. (2010). The potential of plant biomarker evidence derived from rock hyrax middens as an indicator of palaeoenvironmental change. *Palaeogeography Palaeoclimatology Palaeoecology*, 285(3), 321–330. <https://doi.org/10.1016/j.palaeo.2009.11.029>

- Carrillo-Briceño, J. D., Carrillo, J. D., Aguilera, O. A., & Sanchez-Villagra, M. R. (2018). Shark and ray diversity in the Tropical America (Neotropics)—an examination of environmental and historical factors affecting diversity. *PeerJ*, 6, e5313. <https://doi.org/10.7717/peerj.5313>
- Caruso, A., Blanc-Valleron, M. M., Da Prato, S., Pierre, C., & Rouchy, J. M. (2019). The late Messinian “Lago-Mare” event and the Zanclean Reflooding in the Mediterranean Sea: New insights from the Cuevas del Almanzora section (Vera Basin, South-Eastern Spain). *Earth-Science Reviews*, 200, 102993. <https://doi.org/10.1016/j.earscirev.2019.102993>
- Castañeda-Posadas, C., Calvillo-Canadell, L., & Cevallos-Ferriz, S. R. (2009). Woods from miocene sediments in Panotla, Tlaxcala, Mexico. *Review of Palaeobotany and Palynology*, 156(3–4), 494–506. <https://doi.org/10.1016/j.revpalbo.2009.04.013>
- Caves, J. K., Moragne, D. Y., Ibarra, D. E., Bayshashov, B. U., Gao, Y., Jones, M. M., et al. (2016). The neogene de-greening of central Asia. *Geology*, 44(11), 887–890. <https://doi.org/10.1130/G38267.1>
- Cerling, T. E. (1984). The stable isotopic composition of modern soil carbonate and its relationship to climate. *Earth and Planetary Science Letters*, 71, 229–240. [https://doi.org/10.1016/0012-821X\(84\)90089-X](https://doi.org/10.1016/0012-821X(84)90089-X)
- Cerling, T. E. (1991). Carbon dioxide in the atmosphere: Evidence from cenozoic and Mesozoic paleosols. *American Journal of Science*, 291, 377–400. <https://doi.org/10.2475/ajs.291.4.377>
- Cerling, T. E. (1992). Use of carbon isotopes in paleosols as an indicator of the $p(\text{CO}_2)$ of the paleoatmosphere. *Global Biogeochemical Cycles*, 6(3), 307–314. <https://doi.org/10.1029/92GB01102>
- Cerling, T. E., Harris, J. M., MacFadden, B. J., Leakey, M. G., Quade, J., Eisenmann, V., & Ehleringer, J. R. (1997). Global vegetation change through the Miocene/Pliocene boundary. *Nature*, 389, 153–158. <https://doi.org/10.1038/38229>
- Cerling, T. E., Wynn, J. G., Andanje, S. A., Bird, M. I., Korir, D. K., Levin, N. E., et al. (2011). Woody cover and hominin environments in the past 6 million years. *Nature*, 476, 51–56. <https://doi.org/10.1038/nature10306>
- Cermeño, O., Falkowski, P. G., Romerod, O. E., Schaller, M. F., & Vallina, S. M. (2015). Continental erosion and the Cenozoic rise of marine diatoms. *Proceedings of the National Academy of Sciences of the United States of America*, 112, 4239–4244. <https://doi.org/10.1073/pnas.1412883112>
- Cervato, C., & Burckle, L. (2003). Pattern of first and last appearance in diatoms: Oceanic circulation and the position of polar fronts during the Cenozoic. *Paleoceanography*, 18(2), 1055. <https://doi.org/10.1029/2002PA000805>
- Čerňanský, A., Szyndlar, Z., & Mörs, T. (2017). Fossil squamate faunas from the Neogene of Hambach (northwestern Germany). *Palaeobiodiversity and Palaeoenvironments*, 97(2), 329–354. <https://doi.org/10.1007/s12549-016-0252-1>
- Chaisson, W. P., & Ravelo, A. C. (2000). Pliocene development of the east-west hydrographic gradient in the equatorial Pacific. *Paleoceanography*, 15(5), 497–505. <https://doi.org/10.1029/1999PA000442>
- Charles-Dominique, T., Davies, T. J., Hempson, G. P., Bezeng, B. S., Daru, B. H., Kabongo, R. M., et al. (2016). Spiny plants, mammal browsers, and the origin of African savannas. *Proceedings of the National Academy of Sciences*, 113(38), E5572–E5579. <https://doi.org/10.1073/pnas.1607493113>
- Chase, C. G., Gregory-Wodzicki, K. M., Parrish, J. T., & DeCelles, P. G. (1998). Topographic history of the western Cordillera of North America and controls on climate. *Oxford Monographs on Geology and Geophysics*, 39, 73–99. <https://doi.org/10.2475/02.2012.05>
- Chen, C., Bai, Y., Fang, X., Guo, H., Meng, Q., Zhang, W., et al. (2019). A late miocene terrestrial temperature history for the northeastern Tibetan plateau's period of tectonic expansion. *Geophysical Research Letters*, 46, 8375–8386. <https://doi.org/10.1029/2019gl082805>
- Chen, S. T., Smith, S. Y., Sheldon, N. D., & Strömberg, C. A. E. (2015). Regional-scale variability in the spread of grasslands in the late Miocene. *Palaeogeography Palaeoclimatology Palaeoecology*, 437, 42–52. <https://doi.org/10.1016/j.palaeo.2015.07.020>
- Christensen, B. A., Renema, W., Henderiks, J., De Vleeschouwer, D., Groeneveld, J., Castañeda, I. S., et al. (2017). Indonesian through-flow drove Australian climate from humid Pliocene to arid Pleistocene. *Geophysical Research Letters*, 44(13), 6914–6925. <https://doi.org/10.1002/2017GL072977>
- Christin, P. A., Besnard, G., Samaritani, E., Duvall, M. R., Hodkinson, T. R., Savolainen, V., & Salamin, N. (2008). Oligocene CO₂ decline promoted C₄ photosynthesis in grasses. *Current Biology*, 18(1), 37–43. <https://doi.org/10.1016/j.cub.2007.11.058>
- Christin, P.-A., Spriggs, E., Osborne, C. P., Strömberg, C. A. E., Salamin, N., & Edwards, E. J. (2014). Molecular dating, evolutionary rates, and the age of the grasses. *Systematic Biology*, 63(2), 153–165. <https://doi.org/10.1093/sysbio/syt072>
- Churchill, M., Boessenecker, R. W., & Clementz, M. T. (2014). Colonization of the Southern Hemisphere by Fur seals and sea lions (Carnivora: Otariidae) revealed by combined evidence phylogenetic and Bayesian biogeographic analysis. *Zoological Journal of the Linnean Society*, 172, 200–225. <https://doi.org/10.1111/zoj.12163>
- Clift, P. D., Wan, S., & Blusztajn, J. (2014). Reconstructing chemical weathering, physical erosion and monsoon intensity since 25 Ma in the northern South China sea: A review of competing proxies. *Earth-Science Reviews*, 130, 86–102. <http://dx.doi.org/10.1016/j.earscirev.2014.01.002>
- Clift, P. D., & Webb, A. A. G. (2019). *Himalayan tectonics: A modern synthesis*. In P. J. Treloar, & M. P. Searle (Eds.), *A history of the Asian monsoon and its interactions with solid Earth tectonics in Cenozoic South Asia*. (pp. 631–652). London: Special Publications. <https://doi.org/10.1144/SP483.1>
- Cohen, K. M., Finney, S. C., Gibbard, P. L., & Fan, J.-X. (2013, updated v2020/01). The ICS international chronostratigraphic Chart. *Epiisodes*, 36(3), 199–204. <https://doi.org/10.18814/epiiugs/2013/v36i3/002>
- Colleoni, F., De Santis, L., Montoli, E., Olivo, E., Sorlien, C. C., Bart, P. J., et al. (2018). Past continental shelf evolution increased Antarctic ice sheet sensitivity to climatic conditions. *Scientific Reports*, 8(1), 11323. <https://doi.org/10.1038/s41598-018-29718-7>
- Colleoni, F., De Santis, L., Siddoway, C. S., Bergamasco, A., Golledge, N. R., Lohmann, G., et al. (2018). Spatio-temporal variability of processes across Antarctic ice-bed-ocean interfaces. *Nature Communications*, 9(1), 1–14. <https://doi.org/10.1038/s41467-018-04583-0>
- Collins, M., Knutti, R., Arblaster, J., Dufresne, J.-L., Fichefet, T., Friedlingstein, P., et al. (2013). Long-term climate change: Projections, Commitments and Irreversibility. In T. F. Stocker, et al. (Eds.), *Climate change 2013: The physical science Basis. Contribution of working group I to the Fifth assessment report of the Intergovernmental Panel on climate change*. Cambridge, United Kingdom and New York, NY, USA: Cambridge University Press.
- Collinson, M. E., Andrews, P., & Bamford, M. K. (2009). Taphonomy of the early miocene flora, Hiwegi formation, Rusinga island, Kenya. *Journal of Human Evolution*, 57, 149–162. <https://doi.org/10.1016/j.jhevol.2009.02.010>
- Compton, J. S., Hodell, D. A., Garrido, J. R., & Mallinson, D. J. (1993). Origin and age of phosphorite from the south-central Florida Platform: Relation of phosphogenesis to sea-level fluctuations and $\delta^{13}\text{C}$ excursion. *Geochimica et Cosmochimica Acta*, 57, 131–146. [https://doi.org/10.1016/0016-7037\(93\)90474-B](https://doi.org/10.1016/0016-7037(93)90474-B)
- Compton, J. S., Snyder, S. W., & Hodell, D. A. (1990). Phosphogenesis and weathering of shelf sediments from the southeastern United States: Implications for Miocene $\delta^{13}\text{C}$ excursions and global cooling. *Geology*, 18, 1227–1230. [https://doi.org/10.1130/0091-7613\(1990\)018<1227:PAWOSS>2.3.CO;2](https://doi.org/10.1130/0091-7613(1990)018<1227:PAWOSS>2.3.CO;2)

- Corfield, R. M., & Norris, R. D. (1996). Deep water circulation in the Paleocene ocean. *Geological Society*, 101(1), 443–456. <https://doi.org/10.1144/GSL.SP.1996.101.01.21>
- Cotton, J. M., Hyland, E. G., & Sheldon, N. D. (2014). Multi-proxy evidence for tectonic control on the expansion of C₄ grasses in northwest Argentina. *Earth and Planetary Science Letters*, 395, 41–50. <https://doi.org/10.1016/j.epsl.2014.03.014>
- Cotton, J. M., & Sheldon, N. D. (2012). New constraints on using paleosols to reconstruct atmospheric pCO₂. *GSA Bulletin*, 124(9/10), 1411–1423. <https://doi.org/10.1130/B30607.1>
- Couvering, V. J. A., Castradori, D., Cita, M. B., Hilgen, F. J., & Rio, D. (2000). The base of the Zanclean stage and of the Pliocene series. *Episodes*, 23, 179–187. <http://episodes.org/journal/view.html?doi=10.18814/epiugs/2000/v23i3/005>
- Couzens, A. M. C., & Prideaux, G. J. (2018). Rapid Pliocene adaptive radiation of modern kangaroos. *Science*, 362(6410), 72. <https://doi.org/10.1038/s41561-018-0069-9>
- Cowman, P. F., & Bellwood, D. R. (2013). The historical biogeography of coral reef fishes: Global patterns of origination and dispersal. *Journal of Biogeography*, 40, 209–224. <https://doi.org/10.1111/jbi.12003>
- Coxall, H. K., Huck, C. E., Huber, M., Lear, C. H., Legarda-Lisarrri, A., O'Regan, M., et al. (2018). Export of nutrient rich Northern Component Water preceded early Oligocene Antarctic glaciation. *Nature Geoscience*, 11, 190–196. <https://www.nature.com/articles/s41561-018-0069-9>
- Coxall, H. K., Wilson, P. A., Palike, H., Lear, C. H., & Backman, J. (2005). Rapid stepwise onset of Antarctic glaciation and deeper calcite compensation in the Pacific Ocean. *Nature*, 433, 53–57. <https://doi.org/10.1038/nature03135>
- Cramer, B. S., Miller, K. G., Barrett, P. J., & Wright, J. D. (2011). Late Cretaceous–Neogene trends in deep ocean temperature and continental ice volume: Reconciling records of benthic foraminiferal geochemistry ($\delta^{18}\text{O}$ and Mg/Ca) with sea level history. *Journal of Geophysical Research: Oceans*, 116(C12), C12023. <https://doi.org/10.1029/2011JC007255>
- Cramer, B. S., Toggweiler, J. R. T., Wright, J. D., Katz, M. E., & Miller, G. H. (2009). Ocean overturning since the Late Cretaceous: Inferences from a new benthic foraminiferal isotope compilation. *Paleoceanography*, 24, PA4216. <https://doi.org/10.1029/2008PA001683>
- Crampton, J. S., Foote, M., Beu, A. G., Maxwell, P. A., Cooper, R. A., Matcham, I., et al. (2006). The ark was full! Constant to declining Cenozoic shallow marine biodiversity on an isolated midlatitude continent. *Paleobiology*, 32(4), 509–532. <https://doi.org/10.1666/06014.1>
- Cui, Y., & Schubert, B. A. (2016). Quantifying uncertainty of past pCO₂ determined from changes in C₃ plant carbon isotope fractionation. *Geochimica et Cosmochimica Acta*, 172, 127–138. <https://doi.org/10.1016/j.gca.2015.09.032>
- Cui, Y., Schubert, B. A., & Jähren, A. H. (2020). A 23 m.y. record of low atmospheric CO₂. *Geology*, 48, 888–892. <https://doi.org/10.1130/G47681.1>
- Curran, E. D., Jacobs, B. F., Bush, R. T., Novello, A., Feseha, M., Grímsson, F., et al. (2019). Ecological dynamic equilibrium in an early Miocene (21.73 Ma) forest, Ethiopia. *Palaeogeography Palaeoclimatology Palaeoecology*, 539, 109425. <https://doi.org/10.1016/j.palaeo.2019.109425>
- Currie, B. S., Rowley, D. B., & Tabor, N. J. (2005). Middle Miocene paleoaltimetry of southern Tibet: Implications for the role of mantle thickening and delamination in the Himalayan orogen. *Geology*, 33(3), 181–184. <https://doi.org/10.1130/G21170.1>
- Dalsätt, J., Mörs, T., & Ericson, P. G. P. (2006). Fossil birds from the miocene and Pliocene of Hambach (NW Germany). *Palaeontographica Abteilung A*, 277(1–6), 113–121.
- Damuth, J., & Janis, C. M. (2011). On the relationship between hypsodonty and feeding ecology in ungulate mammals, and its utility in palaeoecology. *Biological Reviews*, 86(3), 733–758. <Go to ISI>://WOS:000292845500010
- Dausmann, V., Frank, M., Gutjahr, M., & Rickli, J. (2017). Glacial reduction of AMOC strength and long-term transition in weathering inputs into the Southern Ocean since the mid-Miocene: Evidence from radiogenic Nd and Hf isotopes. *Paleoceanography*, 32(3), 265–283. <https://doi.org/10.1002/2016PA003056>
- Dayem, K. E., Noone, D. C., & Molnar, P. (2007). Tropical western Pacific warm pool and maritime continent precipitation rates and their contrasting relationships with the Walker Circulation. *Journal of Geophysical Research*, 112(D6), D06101. <https://doi.org/10.1029/2006JD007870>
- de Boer, B., van de Wal, R., Bintanja, R., Lourens, L. J., & Tuenter, E. (2010). Cenozoic global ice-volume and temperature simulations with 1-D ice-sheet models forced by benthic $\delta^{18}\text{O}$ records. *Annals of Glaciology*, 51(55), 23–33. <https://doi.org/10.3189/172756410791392736>
- DeConto, R., Lear, C., Pagani, M., Pollard, D., Wilson, P., & Palike, H. (2008). Thresholds for Cenozoic bipolar glaciation. *Nature*, 455, 652–657. <https://doi.org/10.1038/nature07337>
- Degrange, F. J., Eddy, D., Puerta, P., & Clarke, J. (2019). New skull remains of *Phorusrhacos longissimus* (Aves, Cariamiformes) from the miocene of Argentina: Implications for the morphology of Phorusrhacidae. *Journal of Paleontology*, 93(6), 1221–1233. <https://doi.org/10.1017/jpa.2019.53>
- Dekens, P. S., Ravelo, A. C., & McCarthy, M. D. (2007). Warm upwelling regions in the Pliocene warm period. *Paleoceanography*, 22(3), PA3211. <https://doi.org/10.1029/2006PA001394>
- De La Rocha, C. L., Nowald, N., & Passow, U. (2008). Interactions between diatom aggregates, minerals, particulate organic carbon, and dissolved organic matter: Further implications for the ballast hypothesis. *Global Biogeochemical Cycles*, 22, GB4005. <https://doi.org/10.1029/2007GB003156>
- Denk, T., Grimm, G. W., Grímsson, F., & Zetter, R. (2013). Evidence from “Köppen signatures” of fossil plant assemblages for effective heat transport of Gulf Stream to subarctic North Atlantic during Miocene cooling. *Biogeosciences*, 10(12), 13563–13601. <https://doi.org/10.5194/bg-10-7927-2013>
- Denk, T., Grímsson, F., & Zetter, R. (2010). Episodic migration of oaks to Iceland: Evidence for a North Atlantic “land bridge” in the latest Miocene. *American Journal of Botany*, 97(2), 276–287. <https://doi.org/10.3733/ajb.0900195>
- Denk, T., Güner, H. T., & Bouchal, J. M. (2019). Early Miocene climate and biomes of Turkey: Evidence from leaf fossils, dispersed pollen, and petrified wood. *Palaeogeography Palaeoclimatology Palaeoecology*, 530, 236–248. <https://doi.org/10.1016/j.palaeo.2019.05.042>
- Denk, T., Güner, T. H., Kvaček, Z., & Bouchal, J. M. (2017). The early miocene flora of Güvem (central Anatolia, Turkey): A window into early neogene vegetation and environments in the eastern Mediterranean. *Acta Palaeobotanica*, 57(2), 237–338. <https://doi.org/10.1515/acpa-2017-0011>
- Denk, T., Zohner, C. M., Grimm, G. W., & Renner, S. S. (2018). Plant fossils reveal major biomes occupied by the late Miocene Old-World Pliocene fauna. *Nature Ecology & Evolution*, 2(12), 1864–1870. <https://doi.org/10.1038/s41559-018-0695-z>
- Dettman, D. L., & Lohmann, K. C. (2000). Oxygen isotope evidence for high-altitude snow in the Laramide Rocky Mountains of North America during the Late Cretaceous and Paleogene. *Geology*, 28(3), 243–246. [https://doi.org/10.1130/0091-7613\(2000\)28<243:OIEFHS>2.0.CO;2](https://doi.org/10.1130/0091-7613(2000)28<243:OIEFHS>2.0.CO;2)
- De Vleeschouwer, D., Vahlenkamp, M., Crucifix, M., & Pälike, H. (2017). Alternating Southern and Northern Hemisphere climate response to astronomical forcing during the past 35 m.y. *Geology*, 45(4), 375–378. <https://doi.org/10.1130/G38663.1>

- Dickens, G. R., & Owen, R. M. (1999). The latest miocene-early Pliocene biogenic bloom: A revised Indian ocean perspective. *Marine Geology*, 161(1), 75–91. [https://doi.org/10.1016/S0025-3227\(99\)00057-2](https://doi.org/10.1016/S0025-3227(99)00057-2)
- Diester-Haass, L., Billups, K., & Emeis, K. C. (2005). In search of the late Miocene–early Pliocene “biogenic bloom” in the Atlantic Ocean (ocean drilling program sites 982, 925, and 1088). *Paleoceanography*, 20, PA4001. <https://doi.org/10.1029/2005PA001139>
- Diester-Haass, L., Billups, K., Gröcke, D. R., Francois, L., Lefebvre, V., & Emeis, K. C. (2009). Mid-Miocene paleoproductivity in the Atlantic Ocean and implications for the global carbon cycle. *Paleoceanography*, 24, PA1209. <https://doi.org/10.1029/2008PA001605>
- Diester-Haass, L., Meyers, P. A., & Bickert, T. (2004). Carbonate crash and biogenic bloom in the late miocene: Evidence from ODP sites 1085, 1086, and 1087 in the Cape basin, southeast Atlantic ocean. *Paleoceanography*, 19, PA1007. <https://doi.org/10.1029/2003PA000933>
- Ding, L., Spicer, R. A., Yang, J., Xu, Q., Cai, F., Li, S., et al. (2017). Quantifying the rise of the Himalaya orogen and implications for the South Asian monsoon. *Geology*, 45(3), 215–218. <https://doi.org/10.1130/G38583.1>
- Dixon, J., Dietrich, J. R., & McNeil, D. H. (1992). *Upper cretaceous to pleistocene sequence stratigraphy of the beaufort-mackenzie and banks island areas, Northwest Canada*. Ottawa: Canada: Geological Survey of Canada.
- Domingo, L., Koch, P. L., Grimes, S. T., Morales, J., & Lopez-Martinez, N. (2012). Isotopic paleoecology of mammals and the middle miocene cooling event in the Madrid basin (Spain). *Palaeogeography Palaeoclimatology Palaeoecology*, 339, 98–113. <https://doi.org/10.1016/j.palaeo.2012.04.026>
- Domning, D. P. (1989). Kelp evolution: A comment. *Paleobiology*, 15, 53–56. <https://jstor.org/stable/2400908>
- Donders, T. H., Weijers, J. W. H., Munsterman, D. K., Kloosterboer-van Hoeve, M. L., Buckles, L. K., et al. (2009). Strong climate coupling of terrestrial and marine environments in the Miocene of northwest Europe. *Earth and Planetary Science Letters*, 281, 215–225. <https://doi.org/10.1016/j.epsl.2009.02.034>
- Dowsett, H. J., & Robinson, M. M. (2009). Mid-Pliocene equatorial sea surface temperature reconstruction: A multi-proxy perspective. *Philosophical Transactions of the Royal Society*, 367(1886), 109–125. <https://doi.org/10.1098/rsta.2008.0206>
- Dowsett, H. J., Robinson, M. M., Haywood, A. M., Hill, D. J., Dolan, A. M., Stoll, D. K., et al. (2012). Assessing confidence in Pliocene sea surface temperatures to evaluate predictive models. *Nature Climate Change*, 2(5), 365–371. <https://doi.org/10.1038/nclimate1455>
- Drury, A. J., John, C. M., & Shevenell, A. E. (2016). Evaluating climatic response to external radiative forcing during the late Miocene to early Pliocene: New perspectives from eastern equatorial Pacific (IODP U1338) and North Atlantic (ODP 982) locations. *Paleoceanography*, 31(1), 167–184. <https://doi.org/10.1002/2015PA002881>
- Drury, A. J., Lee, G. P., Gray, W. R., Lyle, M., Westerhold, T., Shevenell, A. E., & John, C. M. (2018). Deciphering the state of the late miocene to early Pliocene equatorial pacific. *Paleoceanography and Paleoclimatology*, 33, 246–263. <https://doi.org/10.1002/2017PA003245>
- Drury, A. J., Westerhold, T., Frederichs, T., Tian, J., Wilkens, R., Channell, J. E. T., et al. (2017). Late Miocene climate and time scale reconciliation: Accurate orbital calibration from a deep-sea perspective. *Earth and Planetary Science Letters*, 475, 254–266. <https://doi.org/10.1016/j.epsl.2017.07.038>
- Drury, A. J., Westerhold, T., Hodell, D., & Röhl, U. (2018). Reinforcing the north Atlantic backbone: Revision and extension of the composite splice at ODP site 982. *Climate of the Past*, 14, 321–338. <https://doi.org/10.5194/cp-14-321-2018>
- Dunkley Jones, T., Bown, P. R., Pearson, P. N., Wade, B. S., Coxall, H. K., & Lear, C. H. (2008). Major shifts in calcareous phytoplankton assemblages through the Eocene-Oligocene transition of Tanzania and their implications for low-latitude primary production. *Paleoceanography*, 23, PA4204. <https://doi.org/10.1029/2008PA001640>
- Dunn, R. E., Strömberg, C. A. E., Madden, R. H., Kohn, M. J., & Carlini, A. A. (2015). Linked canopy, climate and faunal change in the Cenozoic of Patagonia. *Science*, 347(6219), 258–261. <https://doi.org/10.1126/science.1260947>
- Dupont, L. M., Linder, H. P., Rommerskirchen, F., & Schefuß, E. (2011). Climate-driven rampant speciation of the Cape flora. *Journal of Biogeography*, 38(6), 1059–1068. <https://doi.org/10.1111/j.1365-2699.2011.02476.x>
- Dutton, J. F., & Barron, E. J. (1997). Miocene to present vegetation changes: A possible piece of the cenozoic cooling puzzle. *Geology*, 25(1), 39–41. [https://doi.org/10.1130/00917613\(1997\)025<0039:MTPVCA>2.3.CO;2](https://doi.org/10.1130/00917613(1997)025<0039:MTPVCA>2.3.CO;2)
- Edgar, K. M., Wilson, P. A., Sexton, P. F., & Suganuma, Y. (2007). No extreme bipolar glaciation during the main Eocene calcite compensation shift. *Nature*, 448, 908–911. <https://doi.org/10.1038/nature06053>
- Edwards, E. J., Osborne, C. P., Stromberg, C. A. E., Smith, S. A., & C4 Grasses Consortium (2010). The origins of C4 grasslands: Integrating evolutionary and ecosystem science. *Science*, 328, 587–591. <https://doi.org/10.1126/science.1177216>
- Edwards, E. J., & Smith, S. A. (2010). Phylogenetic analyses reveal the shady history of C-4 grasses. *Proceedings of the National Academy of Sciences of the United States of America*, 107, 2532–2537. <https://doi.org/10.1073/pnas.0909672107>
- Ehlers, B. M., & Jokat, W. (2013). Paleo-bathymetry of the northern North Atlantic and consequences for the opening of the Fram Strait. *Marine Geophysical Research*, 34(1), 25–43. <https://doi.org/10.1007/s11001-013-9165-9>
- Eisawi, A., & Schrank, E. (2008). Upper Cretaceous to neogene palynology of the Melut basin, southeast Sudan. *Palynology*, 32(1), 101–129. <https://doi.org/10.2113/gspalynol.32.1.101>
- El-Sorogy, A. S., Tsaparas, N., & Al-Kahtany, K. (2020). Middle miocene corals from Midyan area, northwestern Saudi Arabia. *Geological Journal*, 55, 5594–5605. <https://doi.org/10.1002/gj.3761>
- Eldrett, J. S., Harding, I. C., Wilson, P. A., Butler, E., & Roberts, A. P. (2007). Continental ice in Greenland during the Eocene and oligocene. *Nature*, 404, 91–127. <https://doi.org/10.1038/nature05591>
- Erdei, B., Dolezych, M., & Hably, L. (2009). The buried Miocene forest at Bükkábrány, Hungary. *Review of Palaeobotany and Palynology*, 155, 69–79. <https://doi.org/10.1016/j.revpalbo.2009.01.003>
- Escutia, C., DeConto, R. M., Dunbar, R., Santis, L. D., Shevenell, A., & Naish, T. (2019). Keeping an eye on antarctic ice sheet stability. *Oceanography*, 32(1), 32–46. <https://www.jstor.org/stable/26604948>
- Estes, J. A., Lindberg, D. R., & Wray, C. (2005). Evolution of large body size in abalones (*Haliotis*): Patterns and implications. *Paleobiology*, 31, 591–606. <https://doi.org/10.1666/04059.1>
- Estes, J. A., & Steinberg, P. D. (1988). Predation, herbivory, and kelp evolution. *Paleobiology*, 14, 19–36. <https://doi.org/10.1017/S0094837300011775>
- Evans, D., Müller, W., & Erez, J. (2018). Assessing foraminifera biomineralisation models through trace element data of cultures under variable seawater chemistry. *Geochimica et Cosmochimica Acta*, 236, 198–217. <https://doi.org/10.1016/j.gca.2018.02.048>
- Evenstar, L. A., Stuart, F. M., Hartley, A. J., & Tattitch, B. (2015). Slow cenozoic uplift of the western Andean Cordillera indicated by cosmogenic ³He in alluvial boulders from the pacific Planation surface. *Geophysical Research Letters*, 42(20), 8448–8455. <https://doi.org/10.1002/2015GL065959>
- Ezard, T. H. G., Aze, T., Pearson, P. N., & Purvis, A. (2011). Interplay between climate and species' ecology drives macroevolutionary dynamics. *Science*, 332, 349–351. <https://doi.org/10.1126/science.1203060>

- Falkowski, P. G., Katz, M. E., Knoll, A. H., Quigg, A., Raven, J. A., Schofield, O., & Taylor, F. J. R. (2004). The evolution of modern eukaryotic phytoplankton. *Science*, 305, 354–360. <https://doi.org/10.1126/science.1095964>
- Falkowski, P. G., Katz, M. E., Milligan, A. J., Fennel, K., Cramer, B. S., Aubry, M. P., et al. (2005). Evolution: The rise of oxygen over the past 205 million years and the evolution of large placental mammals. *Science*, 309, 2202–2204. <https://doi.org/10.1126/science.1116047>
- Fan, M., Heller, P., Allen, S. D., & Hough, B. G. (2014). Middle cenozoic uplift and concomitant drying in the central Rocky mountains and adjacent great plains. *Geology*, 42(6), 547–550. <https://doi.org/10.1130/G35444.1>
- Farnsworth, A., Lunt, D. J., Robinson, S. A., Valdes, P. J., Roberts, W. H. G., Clift, P. D., et al. (2019). Past East Asian monsoon evolution controlled by paleogeography, not CO₂. *Science Advances*, 5, eaax1697. <https://doi.org/10.1126/sciadv.aax1697>
- Farrell, J. W., Raffi, I., Janecek, I., Murray, D. W., Levitan, I., Dadey, K. A., et al. (1995). Late Neogene sedimentation patterns in the eastern equatorial Pacific. In N. G. Pisias, et al. (Eds.), *Proceedings of the ocean drilling program, scientific results*. Vol. 138 (pp. 717–756). College Station, TX: Ocean Drilling Program. <https://doi.org/10.2973/odp.proc.sr.138.143.1995>
- Favre, A., Päckert, M., Pauls, S. U., Jähnig, S. C., Uhl, D., Michalak, I., & Muellner-Riehl, A. N. (2015). The role of the uplift of the Qinghai-Tibetan Plateau for the evolution of Tibetan biotas. *Biological Reviews of the Cambridge Philosophical Society*, 90(1), 236–253. <https://doi.org/10.1111/brv.12107>
- Feakins, S. J., deMenocal, P. B., & Eglinton, T. J. (2005). Biomarker records of late neogene changes in east African vegetation. *Geology*, 33, 977–980. <https://doi.org/10.1073/pnas.1521267113>
- Feakins, S. J., Levin, N., Liddy, H., Sieracki, A., Eglinton, T., & Bonnefille, R. (2013). Northeast African vegetation change over 12 million years. *Geology*, 41, 295–298. <https://doi.org/10.1130/G33845.1>
- Feakins, S. J., Liddy, H. M., Tauxe, L., Galy, V., Feng, X., Tierney, J. E., et al. (2020). Miocene C₄ grassland expansion as recorded by the Indus Fan. *Paleoceanography and Paleoclimatology*, 35, e2020PA003856. <https://doi.org/10.1029/2020PA003856>
- Fedorov, A. V., Brierley, C. M., Lawrence, K. T., Liu, Z., Dekens, P. S., & Ravelo, A. C. (2013). Patterns and mechanisms of early Pliocene warmth. *Nature*, 496, 43–49. <https://doi.org/10.1038/nature12003>
- Fedorov, A., Dekens, P., McCarthy, M., Ravelo, A., deMenocal, P., Barreiro, M., et al. (2006). The Pliocene paradox (mechanisms for a permanent El Niño). *Science*, 312(5779), 1485–1489. <https://doi.org/10.1126/science.1122666>
- Fedorov, A., Pacanowski, R., Philander, S., & Boccaletti, G. (2004). The effect of salinity on the wind-driven circulation and the thermal structure of the upper ocean. *Journal of Physical Oceanography*, 34(9), 1949–1966. [https://doi.org/10.1175/1520-0485\(2004\)034<1949:TEOSOT>2.0.CO;2](https://doi.org/10.1175/1520-0485(2004)034<1949:TEOSOT>2.0.CO;2)
- Finkel, Z. V., Katz, M. E., Wright, J. D., Schofield, O. M. E., & Falkowski, P. G. (2005). Climatically driven macroevolutionary patterns in the size of marine diatoms over the Cenozoic. *Proceedings of the National Academy of Sciences of the United States of America*, 102(25), 8927–8932. <https://doi.org/10.1073/pnas.0409907102>
- Flecker, R., Krijgsman, W., Capella, W., de Castro Martins, C., Dmitrieva, E., Maysner, J. P., et al. (2015). Evolution of the Late Miocene Mediterranean–Atlantic gateways and their impact on regional and global environmental change. *Earth-Science Reviews*, 150, 365–392. <https://doi.org/10.1016/j.earscirev.2015.08.007>
- Florindo, F., Wilson, G. S., Roberts, A. P., Sagnotti, L., & Verosub, K. L. (2005). Magnetostratigraphic chronology of a late Eocene to early miocene glacial marine succession from the Victoria land basin, Ross Sea, Antarctica. *Global and Planetary Change*, 45(1–3), 207–236. <https://doi.org/10.1016/j.gloplacha.2004.09.009>
- Flower, B. P., & Kennett, J. P. (1993). Relations between Monterey formation deposition and middle miocene global cooling: Naples Beach section, California. *Geology*, 21(10), 877–880. [https://doi.org/10.1130/0091-7613\(1993\)021<0877:RBMFDA>2.3.CO;2](https://doi.org/10.1130/0091-7613(1993)021<0877:RBMFDA>2.3.CO;2)
- Flower, B. P., & Kennett, J. (1994). The middle Miocene climatic transition: East Antarctic ice sheet development, deep ocean circulation and global carbon cycling. *Palaeogeography Palaeoclimatology Palaeoecology*, 108(3–4), 537–555. [https://doi.org/10.1016/0031-0182\(94\)90251-8](https://doi.org/10.1016/0031-0182(94)90251-8)
- Fordyce, R. E. (2009). Cetacean fossil record. In W. F. Perrin, B. Würsig, & J. G. M. Thewissen (Eds.), *Encyclopedia of marine mammals* (2nd ed., pp. 207–215). Academic Press.
- Fordyce, R. E., & Marx, F. G. (2018). Gigantism precedes filter feeding in baleen whale evolution. *Current Biology*, 28(10), 1670–1676. <https://doi.org/10.1016/j.cub.2018.04.027>
- Fortelius, M., Eronen, J., Liu, L. P., Pushkina, D., Tesakov, A., Vislobokova, I., & Zhang, Z. Q. (2003). Continental-scale hypsodonty patterns, climatic paleobiogeography and dispersal of Eurasian Neogene large mammal herbivores. In J. W. F. Reumer, & W. Wessels (Eds.), *Distribution and migration of Tertiary mammals in Eurasia. A volume in honour of Hans de Bruijn*. Vol. 10 (pp. 1–11).
- Foster, G. L., Lear, C. H., & Rae, J. W. B. (2012). The evolution of pCO₂, ice volume and climate during the middle Miocene. *Earth and Planetary Science Letters*, 341, 243–254. <https://doi.org/10.1016/j.epsl.2012.06.007>
- Foster, G. L., & Rohling, E. J. (2013). Relationship between sea level and climate forcing by CO₂ on geological timescales. *Proceedings of the National Academy of Sciences of the United States of America*, 110(4), 1209–1214. <https://doi.org/10.1073/pnas.1216073110>
- Fox, D. L., Honey, J. G., Martin, R. A., & Pelaez-Campomanes, P. (2012). Pedogenic carbonate stable isotope record of environmental change during the Neogene in the southern Great Plains, southwest Kansas, USA: Carbon isotopes and the evolution of C₄-dominated grasslands. *The Geological Society of America Bulletin*, 124(3–4), 444–462. <https://doi.org/10.1130/B30401.1>
- Fox, D. L., & Koch, P. L. (2004). Carbon and oxygen isotopic variability in neogene paleosol carbonates: Constraints on the evolution of the C₄-grasslands of the great plains, USA. *Palaeogeography Palaeoclimatology Palaeoecology*, 207(3–4), 305–329. <https://doi.org/10.1016/j.palaeo.2003.09.030>
- Fox, L., Wade, B., Holbourn, A., Leng, M. A., & Bhatia, R. (2021). Temperature gradients across the pacific during the middle Miocene. *Paleoceanography and Paleoclimatology*. Manuscript submitted for publication.
- Franks, P. J., Royer, D. L., Beerling, D. J., Van de Water, P. K., Cantrill, D. J., Barbour, M. M., & Berry, J. A. (2014). New constraints on atmospheric CO₂ concentration for the Phanerozoic. *Geophysical Research Letters*, 41(13), 4685–4694. <https://doi.org/10.1002/2014GL060457>
- François, L., Utescher, T., Favre, E., Henrot, A.-J., Warnant, P., Micheels, A., et al. (2011). Modeling Late Miocene vegetation in Europe: Results of the CARAIB model and comparison with palaeovegetation data. *Palaeogeography Palaeoclimatology Palaeoecology*, 304(3), 359–378. <https://doi.org/10.1016/j.palaeo.2011.01.012>
- Fretwell, P., Pritchard, H. D., Vaughan, D. G., Bamber, J. L., Barrand, N. E., Bell, R., et al. (2013). Bedmap2: Improved ice bed, surface and thickness datasets for Antarctica. *The Cryosphere*, 7(1), 375–393. <https://doi.org/10.5194/tc-7-375-2013>
- Friedman, M., Keck, B. P., Dornburg, A., Eytan, R. I., Martin, C. H., Hulsey, C. D., et al. (2013). Molecular and fossil evidence place the origin of cichlid fishes long after Gondwanan rifting. *Proceedings of the Royal Society B*, 280, 20131733. <https://doi.org/10.1098/rspb.2013.1733>
- Frigola, A., Prange, M., & Schulz, M. (2018). Boundary conditions for the middle Miocene climate transition (MMCT v1.0). *Geoscientific Model Development*, 11(4), 1607–1626. <https://doi.org/10.5194/gmd-11-1607-2018>

- Frost, S. H. (1977). Cenozoic reef systems of Caribbean - prospects for paleoecologic synthesis: Modern and ancient reefs. *American Association of Petroleum Geology, Studies in Geology*, 4, 93–110. <https://doi.org/10.1306/St4393C8>
- Gabel, M. L., Backlund, D. C., & Haffner, J. (1998). The Miocene macroflora of the northern Ogallala Group, northern Nebraska and southern South Dakota. *Journal of Paleontology*, 72(2), 388–397. <https://www.jstor.org/stable/1306723>
- Galeotti, S., Von der Heydt, A., Huber, M., Bice, D., Dijkstra, H., Jilbert, T., et al. (2010). Evidence for active El Niño Southern Oscillation variability in the Late Miocene greenhouse climate. *Geology*, 38(5), 419–422. <https://doi.org/10.1130/G30629.1>
- Gallen, S. F., Wegmann, K. W., & Bohnenstiehl, D. R. (2013). Miocene rejuvenation of topographic relief in the southern Appalachians. *Geological Society of America Today*, 23(2), 4–10. <https://doi.org/10.1130/GSATG163A.1>
- Garric, G., & Huber, M. (2003). Quasi-decadal variability in paleoclimate records: Sunspot cycles or intrinsic oscillations? *Paleoceanography*, 18(3), 1068. <https://doi.org/10.1029/2002PA000869>
- Garzzone, C. N., Molnar, P., Libarkin, J. C., & MacFadden, B. J. (2006). Rapid late Miocene rise of the Bolivian Altiplano: Evidence for removal of mantle lithosphere. *Earth and Planetary Science Letters*, 241(3–4), 543–556. <https://doi.org/10.1016/j.epsl.2005.11.026>
- Garzzone, C. N., Quade, J., DeCelles, P. G., & English, N. B. (2000). Predicting paleoelevation of Tibet and the Himalaya from $\delta^{18}\text{O}$ vs. altitude gradients in meteoric water across the Nepal Himalaya. *Earth and Planetary Science Letters*, 183, 215–229. [https://doi.org/10.1016/S0012-821X\(00\)00252-1](https://doi.org/10.1016/S0012-821X(00)00252-1)
- Gasson, E., DeConto, R., & Pollard, D. (2015). Antarctic bedrock topography uncertainty and ice sheet stability. *Geophysical Research Letters*, 42(13), 5372–5377. <https://doi.org/10.1002/2015GL064322>
- Gasson, E., DeConto, R. M., Pollard, D., & Levy, R. H. (2016). Dynamic Antarctic ice sheet during the early to mid-Miocene. *Proceedings of the National Academy of Sciences*, 113(13), 3459–3464. <https://doi.org/10.1073/pnas.1516130113>
- Gasson, E., Lunt, D. J., DeConto, R., Goldner, A., Heinemann, M., Huber, M., et al. (2014). Uncertainties in the modeled CO_2 threshold for Antarctic glaciation. *Climate of the Past Discussion*, 10, 451–466. <https://doi.org/10.5194/cp-10-451-2014>
- Ghosh, P., Garzzone, C. N., & Eiler, J. M. (2006). Rapid uplift of the Altiplano revealed through ^{13}C - ^{18}O bonds in paleosol carbonates. *Science*, 311(5760), 511–515. <https://doi.org/10.1126/science.1119365>
- Gladenkov, A. Y., & Gladenkov, Y. B. (2004). Onset of connections between the Pacific and Arctic oceans through the Bering Strait in the Neogene. *Stratigraphy and Geological Correlation*, 12(2), 175–187.
- Gladstone, R., Flecker, R., Valdes, P., Lunt, D., & Markwick, P. (2007). The Mediterranean hydrologic budget from a Late Miocene global climate simulation. *Palaogeography Palaeoclimatology Palaeoecology*, 251(2), 254–267. <https://doi.org/10.1016/j.palaeo.2007.03.050>
- Göhlich, U. B. (2007). The oldest fossil record of the extant penguin genus *Spheniscus* - a new species from the Miocene of Peru. (2007). *Acta Palaeontologica Polonica*, 52, 285–298. <http://app.pan.pl/acta52/app52-285.pdf>
- Goldner, A., Herold, N., & Huber, M. (2014a). The challenge of simulating the warmth of the mid-Miocene climatic optimum in CESM1. *Climate of the Past*, 10(2), 523–536. <https://doi.org/10.5194/cp-10-523-2014>
- Goldner, A., Herold, N., & Huber, M. (2014b). Antarctic glaciation caused ocean circulation changes at the Eocene–Oligocene transition. *Nature*, 511, 574–577. <https://doi.org/10.1038/nature13597>
- Goldner, A., Huber, M., & Caballero, R. (2013). Does Antarctic glaciation cool the world?. *Climate of the Past*, 9, 173–189. <https://doi.org/10.5194/cp-9-173-2013>
- Graham, A. (1998). Studies in neotropical paleobotany. XI. Late Tertiary vegetation and environments of southeastern Guatemala: Palynofloras from the Mio-Pliocene Padre Miguel group and the Pliocene Herreria formation. *American Journal of Botany*, 85(10), 1409–1425. <https://doi.org/10.2307/2446399>
- Graham, A. (1999). *Late Cretaceous and Cenozoic history of north American vegetation*. Oxford: Oxford University Press.
- Graham, A., Gregory-Wodzicki, K. M., & Wright, K. L. (2001). Studies in neotropical paleobotany. XV. A Mio-Pliocene palynoflora from the eastern Cordillera, Bolivia: Implications for the uplift history of the central Andes. *American Journal of Botany*, 88(9), 1545–1557. <https://doi.org/10.2307/3558398>
- Grant, K. M., & Dickens, G. R. (2002). Coupled productivity and carbon isotope records in the southwest Pacific Ocean during the late Miocene - early Pliocene biogenic bloom. *Palaogeography, Palaeoclimatology, Palaeoecology*, 187, 61–82. [https://doi.org/10.1016/S0031-0182\(02\)00508-4](https://doi.org/10.1016/S0031-0182(02)00508-4)
- Greenop, R., Foster, G. L., Wilson, P. A., & Lear, C. H. (2014). Middle-Miocene climate instability associated with high-amplitude CO_2 variability. *Paleoceanography*, 29, 845–853. <https://doi.org/10.1002/2014PA002653>
- Greenop, R., Sossian, S. M., Henehan, M. J., Wilson, P. A., Lear, C. H., & Foster, G. L. (2019). Orbital forcing, ice volume, and CO_2 across the Oligocene-Miocene transition. *Paleoceanography and Paleoclimatology*, 34, 316–328. <https://doi.org/10.1029/2018PA003420>
- Gregory-Wodzicki, K. M. (2002). A late Miocene subtropical-dry flora from the northern Altiplano, Bolivia. *Palaogeography Palaeoclimatology Palaeoecology*, 180(4), 331–348. [https://doi.org/10.1016/S0031-0182\(01\)00434-5](https://doi.org/10.1016/S0031-0182(01)00434-5)
- Grein, M., Oehm, C., Konrad, W., Utescher, T., Kunzmann, L., & Roth-Nebelsick, A. (2013). Atmospheric CO_2 from the Late Oligocene to early Miocene based on photosynthesis data and fossil leaf characteristics. *Palaogeography Palaeoclimatology Palaeoecology*, 374, 41–51. <https://doi.org/10.1016/j.palaeo.2012.12.025>
- Grimsson, F., & Denk, T. (2007). Floristic turnover in Iceland from 15 to 6 Ma—extracting biogeographical signals from fossil floral assemblages. *Journal of Biogeography*, 34(9), 1490–1504. <https://doi.org/10.1111/j.1365-2699.2007.01712.x>
- Grimsson, F., Denk, T., & Simonarson, L. A. (2007). Middle Miocene floras of Iceland—the early colonization of an island?. *Review of Palaeobotany and Palynology*, 144(3–4), 181–219. <https://doi.org/10.1016/j.revpalbo.2006.07.003>
- Groenewald, J., Steph, S., Tiedemann, R., Garbe-Schonberg, D., Nurnberg, D., & Sturm, A. (2006). Pliocene mixed-layer oceanography for site 1241, using combined Mg/Ca and delta ^{18}O analyses of Globigerinoides sacculifer. In R. Tiedemann, A. Mix, C. Richter, & W. Rudiman (Eds.), *Proceedings of the Ocean Drilling Program, Scientific Results*, (p. 202. College Station, TX.
- Guinot, G., & Cavin, L. (2016). ‘Fish’ (Actinopterygii and Elasmobranchii) diversification patterns through deep time. *Biological Reviews*, 91, 950–981. <https://doi.org/10.1111/brv.12203>
- Gutián, J., Jones, T. D., Hernández-Almeida, I., Löffel, T., & Stoll, H. (2020). Adaptations of coccolithosphere size to selective pressures during the Oligocene - Early Miocene high CO_2 world. *Paleoceanography and Paleoclimatology*, 35, e2020PA003918. <https://doi.org/10.1029/2020PA003918>
- Gutián, J., Phelps, S., Polissar, P. J., Ausín, B., Eglinton, T. I., & Stoll, H. M. (2019). Midlatitude temperature variations in the Oligocene to early Miocene. *Paleoceanography and Paleoclimatology*, 34(8), 1328–1343. <https://doi.org/10.1029/2019PA003638>
- Gulick, S. P. S., Shevenell, A. E., Montelli, A., Fernandez, R., Smith, C., Warny, S., et al. (2017). Initiation and long-term instability of the east Antarctic ice sheet. *Nature*, 552, 225–229. <https://doi.org/10.1038/nature25026>
- Gupta, A. K., Yuvaraja, A., Prakasam, M., Clemens, S. C., & Velu, A. (2015). Evolution of the south Asian monsoon wind system since the late middle Miocene. *Palaogeography Palaeoclimatology Palaeoecology*, 438, 160–167. <https://doi.org/10.1016/j.palaeo.2015.08.006>

- Habeck-Fardy, A., & Nanson, G. C. (2014). Environmental character and history of the Lake Eyre Basin, one seventh of the Australian continent. *Earth-Science Reviews*, 132, 39–66. <https://doi.org/10.1016/j.earscirev.2014.02.003>
- Hague, A. M., Thomas, D. J., Huber, M., Korty, R., Woodard, S. C., & Jones, L. B. (2012). Convection of north pacific deep water during the early Cainozoic. *Geology*, 40(6), 527–530. <https://doi.org/10.1130/G32886.1>
- Halfar, J., & Mutti, M. (2005). Global dominance of coralline red-algal facies: A response to Miocene oceanographic events. *Geology*, 33, 481–484. <https://doi.org/10.1130/G21462>
- Hamon, N., Sepulchre, P., Donnadiou, Y., Henrot, A. J., François, L., Jaeger, J. J., & Ramstein, G. (2012). Growth of subtropical forests in Miocene Europe: The roles of carbon dioxide and Antarctic ice volume. *Geology*, 40, 567–570. <https://doi.org/10.1130/G32990.1>
- Hamon, N., Sepulchre, P., Lefebvre, V., & Ramstein, G. (2013). The role of eastern Tethys seaway closure in the middle Miocene climatic transition (ca. 14 Ma). *Climate of the Past*, 9(6), 2687–2702. <https://doi.org/10.5194/cp-9-2687-2013>
- Hannisdal, B., Henderiks, J., & Liow, L. H. (2012). Long-term evolutionary and ecological responses of calcifying phytoplankton to changes in atmospheric CO₂. *Global Change Biology*, 18(12), 3504–3516. <https://doi.org/10.1111/gcb.12007>
- Hao, Q., & Guo, Z. (2007). Magnetostratigraphy of an early-middle Miocene loess-soil sequence in the western Loess Plateau of China. *Geophysical Research Letters*, 34, L18305. <https://doi.org/10.1029/2007GL031162>
- Haq, B., Gorini, C., Baur, J., Moneron, J., & Rubino, J. L. (2020). Deep Mediterranean's Messinian evaporite giant: How much salt? *Global and Planetary Change*, 184, 103052. <https://doi.org/10.1016/j.gloplacha.2019.103052>
- Haq, B. U. (1980). Biogeographic history of Miocene calcareous nannoplankton and paleoceanography of the Atlantic Ocean. *Micropaleontology*, 26(4), 414–443. <https://doi.org/10.2307/1485353>
- Harper, H. E., & Knoll, A. J. (1975). Silica, diatoms, and Cenozoic radiolarian evolution. *Geology*, 3, 175–177. [https://doi.org/10.1130/0091-7613\(1975\)3<175:SDACRE>2.0.CO;2](https://doi.org/10.1130/0091-7613(1975)3<175:SDACRE>2.0.CO;2)
- Harris, E. B., Kohn, M. J., & Strömberg, C. A. E. (2020). Stable isotope compositions of herbivore teeth indicate climatic stability leading into the middle Miocene in Idaho. *Palaeogeography Palaeoclimatology Palaeoecology*, 546, 109610. <https://doi.org/10.1016/j.palaeo.2020.109610>
- Harris, E. B., Strömberg, C. A. E., Sheldon, N. D., Smith, S. Y., & Vilhena, D. (2017). Vegetation response during the lead-up to the middle Miocene warming event in the Northern Rocky Mountains. *Palaeogeography Palaeoclimatology Palaeoecology*, 485, 401–415. <https://doi.org/10.1016/j.palaeo.2017.06.029>
- Harzhauser, M., Mandic, O., & Zuschin, M. (2003). Changes in Paratethyan marine molluscs at the early/middle Miocene transition: Diversity, paleogeography and palaeoclimate. *Acta Geologica Polonica*, 53, 323–339.
- Harzhauser, M., Piller, W. E., & Steininger, F. (2002). Circum-Mediterranean Oligo-Miocene biogeographic evolution - the gastropods' point of view. *Palaeogeography Palaeoclimatology Palaeoecology*, 183(1–2), 103–133. [https://doi.org/10.1016/S0031-0182\(01\)00464-3](https://doi.org/10.1016/S0031-0182(01)00464-3)
- Haug, G. H., & Tiedemann, R. (1998). Effect of the formation of the isthmus of Panama on Atlantic Ocean thermohaline circulation. *Nature*, 393(6686), 673–676. <https://doi.org/10.1038/31447>
- Haug, G. H., Tiedemann, R., Zahn, R., & Ravelo, A. C. (2001). Role of Panama uplift on oceanic freshwater balance. *Geology*, 29(3), 207–210. [https://doi.org/10.1130/0091-7613\(2001\)029<0207:ROPUOO>2.0.CO;2](https://doi.org/10.1130/0091-7613(2001)029<0207:ROPUOO>2.0.CO;2)
- Haupt, B. J., & Seidov, D. (2012). Modeling geologically abrupt climate changes in the Miocene: Potential effects of high-latitude salinity changes. *Natural Science*, 4, 149–158. <https://doi.org/10.4236/ns.2012.43022>
- Hausfather, Z., & Peters, G. P. (2020). Emissions – the ‘business as usual’ story is misleading. *Nature*, 577, 618–620. <https://doi.org/10.1038/d41586-020-00177-3>
- Hayes, D. E., Frakes, L. A., Barrett, P. J., Burns, D. A., Chen, P.-H., Ford, A. B., et al. (1975). *Initial reports of the deep sea drilling project*. Washington, DC: US Government Printing Office.
- Haywood, A., Hill, D., Dolan, A., Otto-Bliesner, B., Bragg, F., Chan, W., et al. (2012). Large-scale features of Pliocene climate: Results from the Pliocene model intercomparison project. *Climate of the Past Discussions*, 8, 2969–3013. <https://doi.org/10.5194/cp-9-191-2013>
- Haywood, A., Valdes, P., & Sellwood, B. (2000). Global scale palaeoclimate reconstruction of the middle Pliocene climate using the UKMO GCM: Initial results. *Global and Planetary Change*, 25(3–4), 239–256. [https://doi.org/10.1016/S0921-8181\(00\)00028-X](https://doi.org/10.1016/S0921-8181(00)00028-X)
- Haywood, A. M., Dowsett, H. J., & Dolan, A. M. (2016). Integrating geological archives and climate models for the mid-Pliocene warm period. *Nature Communications*, 7, 10646. <https://www.nature.com/articles/ncomms10646>
- Haywood, A. M., Dowsett, H. J., Otto-Bliesner, B., Chandler, M. A., Dolan, A. M., Hill, D. J., et al. (2010). Pliocene model intercomparison project (pliomip): Experimental design and boundary conditions (experiment 1). *Geoscientific Model Development*, 3(1), 227–242. <https://doi.org/10.5194/gmd-3-227-2010>
- Haywood, A. M., Dowsett, H. J., Robinson, M. M., Stoll, D. K., Dolan, A. M., Lunt, D. J., et al. (2011). Pliocene model intercomparison project (pliomip): Experimental design and boundary conditions (experiment 2). *Geoscientific Model Development*, 4(3), 571–577. <https://doi.org/10.5194/gmd-4-571-2011>
- Haywood, A. M., Hill, D. J., Dolan, A. M., Otto-Bliesner, B. L., Bragg, F., Chan, W.-L., et al. (2013). Large-scale features of Pliocene climate: Results from the Pliocene Model Intercomparison Project. *Climate of the Past*, 9, 191–209. <https://doi.org/10.5194/cp-9-191-2013>
- Henderiks, J., Bartol, M., Pige, N., Karatsolis, B.-T., & Lougheed, B. C. (2020). Shifts in phytoplankton composition and stepwise climate change during the middle Miocene. *Paleoceanography and Paleoclimatology*, 35, e2020PA003915. <https://doi.org/10.1029/2020PA003915>
- Henderiks, J., & Pagani, M. (2008). Coccolithophore cell size and the Paleogene decline in atmospheric CO₂. *Earth and Planetary Science Letters*, 269, 575–583. <https://doi.org/10.1016/j.epsl.2008.03.016>
- Henrot, A.-J., François, L., Favre, E., Butzin, M., Ouberdous, M., & Munhoven, G. (2010). Effects of CO₂, continental distribution, topography and vegetation changes on the climate at the middle Miocene: A model study. *Climate of the Past*, 6, 675–694. <https://doi.org/10.5194/cp-6-675-2010>
- Henrot, A. J., Utescher, T., Erdei, B., Dury, M., Hamon, N., Ramstein, G., et al. (2017). Middle Miocene climate and vegetation models and their validation with proxy data. *Palaeogeography Palaeoclimatology Palaeoecology*, 467, 95–119. <https://doi.org/10.1016/j.palaeo.2016.05.026>
- Herbert, T. D., et al. (2020). Bi-hemispheric warming in the miocene climatic optimum as seen from the Danish North Sea. *Paleoceanography and Paleoclimatology*, 35, e2020PA003935. <https://doi.org/10.1029/2020PA003935>
- Herbert, T. D., Lawrence, K. T., Tzanova, A., Peterson, L. C., Caballero-Gill, R., & Kelly, C. S. (2016). Late Miocene global cooling and the rise of modern ecosystems. *Nature Geoscience*, 9, 843–847. <https://doi.org/10.1029/2020PA003956>
- Herbert, T. D., & Schuffert, J. D. (1998). Alkenone unsaturation estimates of late Miocene through late Pliocene sea surface temperatures at Site 958. *Proceedings of the Ocean Drilling Program Scientific Results*, 159T, 17–21. <https://doi.org/10.2973/odp.proc.sr.159T.063.1998>

- Herbert, T. D., Rose, R., Dybkjaer, K., Rasmussen, E. S., & Śliwińska, K. K. (2020). Bihemispheric warming in the Miocene climatic optimum as seen from the Danish North Sea. *Paleoceanography and Paleoclimatology*, 35(10), e2020PA003935. <https://doi.org/10.1029/2020PA003935>
- Herman, A. B., Spicer, R. A., Aleksandrova, G. N., Yang, J., Kodrul, T. M., Maslova, N. Pet al. (2017). Eocene-early oligocene climate and vegetation change in southern China: Evidence from the Maoming basin. *Palaeogeography Palaeoclimatology Palaeoecology*, 429, 126–137. <https://doi.org/10.1016/j.palaeo.2017.04.023>
- Herman, F., Seward, D., Valla, P. G., Carter, A., Kohn, B., Willett, S. D., & Ehlers, T. A. (2013). Worldwide acceleration of mountain erosion under a cooling climate. *Nature*, 504, 423–426. <https://doi.org/10.1175/2011JCLI4035.1>
- Herold, N., Huber, M., & Müller, R. D. (2011a). Modeling the miocene climatic optimum. Part I: Land and atmosphere. *Journal of Climate*, 24(24), 6353–6373. <https://doi.org/10.1038/nature12877>
- Herold, N., Huber, M., Müller, R. D., & Seton, M. (2012). Modeling the Miocene climatic optimum: Ocean circulation. *Paleoceanography*, 27(1), PA1209. <https://doi.org/10.1029/2010pa002041>
- Herold, N., Müller, R. D., & Seton, M. (2010). Comparing early to middle Miocene terrestrial climate simulations with geological data. *Geosphere*, 6(6), 952–961. <https://doi.org/10.1130/GES00544.1>
- Herold, N., Seton, M., Müller, R. D., You, Y., & Huber, M. (2008). Middle Miocene tectonic boundary conditions for use in climate models. *Geochemistry Geophysics Geosystems*, 9(10), Q10009. <https://doi.org/10.1029/2008gc002046>
- Herold, N., Huber, M., Greenwood, D. R., Müller, R. D., & Seton, M. (2011b). Early to middle Miocene monsoon climate in Australia. *Geology*, 39, 3–6. <https://doi.org/10.1130/G31208.1>
- Herrera, N. D., Poorten, T. J. J., Bieler, R., Mikkelsen, P. M., Strong, E. E., Jablonski, D., & Stepan, S. J. (2015). Molecular phylogenetics and historical biogeography amid shifting continents in the cockles and giant clams (Bivalvia: Cardiidae). *Molecular Phylogenetics and Evolution*, 93, 94–106. <https://doi.org/10.1016/j.ympev.2015.07.013>
- Hickey, L. J., Johnson, K. R., & Dawson, M. R. (1988). The stratigraphy, sedimentology, and fossils of the Houghton formation: A post-impact crater-fill, Devon island, NWT, Canada. *Meteoritics*, 23(3), 221–231. <https://doi.org/10.1111/j.1945-5100.1988.tb01284.x>
- Hierholzer, E., & Mörs, T. (2003). Cypriniden-Schlundzähne (Osteichthyes: Teleostei) aus dem Tertiär von Hambach (Niederrheinische Bucht, NW-Deutschland). *Palaeontographica Abteilung A*, 269(1–3), 1–38.
- Hilgen, F. J., et al. (2020). Should unit-stratotypes and astrochronozones be formally defined? A dual proposal (including postscriptum). *Newsletters on Stratigraphy*, 53(1), 19–39. <https://doi.org/10.1127/nos/2019/0514>
- Hilgen, F. J., Lourens, L. J., & Van Dam, J. A. (2012). The neogene period. In F. M. Gradstein, J. G. Ogg, M. D. Schmitz, & G. M. Ogg (Eds.), *The geologic timescale 2012* (pp. 923–978) Elsevier.
- Ho, S. L., & Laepple, T. (2016). Flat meridional temperature gradient in the early Eocene in the subsurface rather than surface ocean. *Nature Geoscience*, 9(8), 606–610. <https://doi.org/10.1038/ngeo2763>
- Hodell, D. A., & Woodruff, F. (1994). Variations in the strontium isotopic ratio of seawater during the Miocene: Stratigraphic and geochemical implications. *Paleoceanography*, 9(3), 405–426. <https://doi.org/10.1029/94PA00292>
- Hoetzal, S., Dupont, L. M., & Wefer, G. (2015). Miocene–Pliocene vegetation change in south-western Africa (ODP Site 1081, offshore Namibia). *Palaeogeography Palaeoclimatology Palaeoecology*, 423, 102–108. <https://doi.org/10.1016/j.palaeo.2015.02.002>
- Hohbein, M. W., Sexton, P. F., & Cartwright, J. A. (2012). Onset of North Atlantic Deep Water production coincident with inception of the Cenozoic global cooling trend. *Geology*, 40, 255–258. <https://doi.org/10.1130/G32461.1>
- Holbourn, A. E., Kuhnt, W., Clemens, S. C., Kochhann, K. G. D., Jöhncck, J., Lübbers, J., & Andersen, N. (2018). Late Miocene climate cooling and intensification of southeast Asian winter monsoon. *Nature Communications*, 9, 1584. <https://doi.org/10.1038/s41467-018-03950-1>
- Holbourn, A. E., Kuhnt, W., Clemens, S. C., Prell, W., & Andersen, N. (2013). Middle to late Miocene stepwise climate cooling: Evidence from a high-resolution deep-water isotope curve spanning 8 million years. *Paleoceanography*, 28(4), 688–699. <https://doi.org/10.1002/2013PA002538>
- Holbourn, A. E., Kuhnt, W., Frank, M., & Haley, B. (2013). Changes in Pacific Ocean circulation following the Miocene onset of permanent Antarctic ice cover. *Earth and Planetary Science Letters*, 365, 38–50. <https://doi.org/10.1016/j.epsl.2013.01.020>
- Holbourn, A. E., Kuhnt, W., Kochhann, K. G. D., Andersen, N., & Meier, K. J. S. (2015). Global perturbation of the carbon cycle at the onset of the Miocene climatic optimum. *Geology*, 43, 123–126. <https://doi.org/10.1130/G36317.1>
- Holbourn, A. E., Kuhnt, W., Lyle, M., Schneider, L., Romero, O., & Andersen, N. (2014). Middle Miocene climate cooling linked to intensification of eastern equatorial Pacific upwelling. *Geology*, 42, 19–22. <https://doi.org/10.1130/G34890.1>
- Holbourn, A. E., Kuhnt, W., Regenberg, M., Schulz, M., Mix, A., & Andersen, N. (2010). Does Antarctic glaciation force migration of the tropical rain belt?. *Geology*, 38, 783–786. <https://doi.org/10.1130/G31043.1>
- Holbourn, A. E., Kuhnt, W., Schulz, M., & Erlenkeuser, H. (2005). Impacts of orbital forcing and atmospheric carbon dioxide on Miocene ice-sheet expansion. *Nature*, 438(7067), 483–487. <https://doi.org/10.1038/nature04123>
- Holbourn, A. E., Kuhnt, W., Schulz, M., Flores, J.-A., & Andersen, N. (2007). Orbitally-paced climate evolution during the middle Miocene “Monterey” carbon-isotope excursion. *Earth and Planetary Science Letters*, 261, 534–550. <http://dx.doi.org/10.1016/j.epsl.2007.07.026>
- Holbourn, A. E., Kuhnt, W., Simo, J. A., & Li, Q. (2004). Middle Miocene isotope stratigraphy and paleoceanographic evolution of the northwest and southwest Australian margins (Wombat Plateau and Great Australian Bight). *Palaeogeography Palaeoclimatology Palaeoecology*, 208, 1–22. <https://doi.org/10.1016/j.palaeo.2004.02.003>
- Hollis, C. J., Jones, T. D., Anagnostou, E., Bijl, P. K., Cramwinckel, M. J., Cui, Y., et al. (2019). The DeepMIP contribution to PMIP4: Methodologies for selection, compilation and analysis of latest Paleocene and early Eocene climate proxy data, incorporating version 0.1 of the DeepMIP database. *Geoscientific Model Development*, 12(7), 3149–3206. <https://doi.org/10.5194/gmd-12-3149-2019>
- Horton, T. W., Sjostrom, D. J., Abruzzese, M. J., Poage, M. A., Waldbauer, J. R., Hren, M., et al. (2004). Spatial and temporal variation of cenozoic surface elevation in the great Basin and Sierra Nevada. *American Journal of Science*, 304, 862–888. <https://doi.org/10.2475/ajs.304.10.862>
- Hossain, A., Knorr, G., Jokat, & Lohmann, G. (2021). Opening of the Fram Strait led to the establishment of a modern-like three-layer stratification in the Arctic Ocean during the Miocene. *Arktos*. <https://doi.org/10.1007/s41063-020-00079-8>
- Hossain, A., Knorr, G., Lohmann, G., Stärr, M., & Jokat, W. (2020). Simulated thermohaline fingerprints in response to different Greenland-Scotland Ridge and Fram Strait subsidence histories. *Paleoceanography and Paleoclimatology*, 35, e2019PA003842. <https://doi.org/10.1029/2019PA003842>
- Howell, F. W., Haywood, A. M., Dowsett, H. J., Francis, J. E., Hill, D. J., et al. (2014). Can uncertainties in sea ice albedo reconcile patterns of data- model discord for the Pliocene and 20th/21st centuries?. *Geophysical Research Letters*, 41, 2011–2018. <https://doi.org/10.1002/2013GL058872>

- Hsü, K. J., Ryan, W. B., & Cita, M. B. (1973). Late miocene desiccation of the Mediterranean. *Nature*, 242(5395), 240–244. <https://doi.org/ezp.sub.su.se/10.1038/242240a0>
- Huang, X., Stürz, M., Gohl, K., Knorr, G., & Lohmann, G. (2017). Impact of Weddell Sea shelf progradation on Antarctic bottom water formation during the Miocene. *Paleoceanography*, 32(3), 304–317. <https://doi.org/10.1002/2016PA002987>
- Huang, Y., Clemens, S. C., Liu, W., Wang, Y., & Prell, W. L. (2007). Large-scale hydrological change drove the late Miocene C₄ plant expansion in the Himalayan foreland and Arabian Peninsula. *Geology*, 35, 531–534. <https://doi.org/10.1130/G23666A>
- Huber, M. (2013). A sensitivity to history. *Nature Geoscience*, 6, 15–16. <https://doi.org/10.1038/ngeo1695>
- Huber, M., & Caballero, R. (2003). Eocene el niño: Evidence for robust tropical dynamics in the “hothouse”. *Science*, 299(5608), 877–881. <https://doi.org/10.1126/science.1078766>
- Huber, M., & Goldner, A. (2012). Eocene monsoons. *Journal of Asian Earth Sciences*, 44, 3–23. <https://doi.org/10.1016/j.jseas.2011.09.014>
- Huber, M., & Sloan, L. C. (2001). Heat transport, deep waters, and thermal gradients: Coupled simulation of an Eocene greenhouse climate. *Geophysical Research Letters*, 28(18), 3481–3484. <https://doi.org/10.1029/2001GL012943>
- Huber, M., Sloan, L. C., & Shellito, C. (2003). Early Paleogene oceans and climate: A fully coupled modeling approach using the NCAR CCSM. In S. L. Wing, P. D. Gingerich, B. Schmitz, & E. Thomas (Eds.), *Causes and consequences of globally warm climates in the Early Paleogene*. Boulder: Geological Society of America Special Paper.
- Hughes, L. C., Orti, G., Huang, Y., Sun, Y., Baldwin, C. C., Thompson, A. W., et al. (2018). Comprehensive phylogeny of ray-finned fishes (Actinopterygii) based on transcriptomic and genomic data. *Proceedings of the National Academy of Sciences of the United States of America*, 115(24), 6249–6254. <https://doi.org/10.1073/pnas.1719358115>
- Hui, Z., Zhang, J., Ma, Z., Li, X., Peng, T., Li, J., & Wang, B. (2018). Global warming and rainfall: Lessons from an analysis of Mid-Miocene climate data. *Palaeogeography Palaeoclimatology Palaeoecology*, 512, 106–117. <https://doi.org/10.1016/j.palaeo.2018.10.025>
- Hüsing, S., Hilgen, F., Abdul Aziz, H., & Krijgsman, W. (2007). Completing the Neogene geological time scale between 8.5 and 12.5 Ma. *Earth and Planetary Science Letters*, 253, 340–358. <https://doi.org/10.1016/j.epsl.2006.10.036>
- Hüsing, S. K., Kuiper, K. F., Link, W., Hilgen, F. J., & Krijgsman, W. (2009). The upper Tortonian - lower Messinian at Monte dei Corvi (Northern Apennines, Italy): Completing a Mediterranean reference section for the Tortonian Stage. *Earth and Planetary Science Letters*, 282, 140–157. <https://doi.org/10.1016/j.epsl.2009.03.010>
- Huybrechts, P. (1993). Glaciological modeling of the late cenozoic East Antarctic ice sheet: Stability or dynamism?. *Geografiska Annaler - Series A: Physical Geography*, 75(4), 221. <https://doi.org/10.2307/521202>
- Hyland, E. G., Sheldon, N. D., Smith, S. Y., & Strömberg, C. A. (2018). Late Miocene rise and fall of C₄ grasses in the western United States linked to aridification and uplift. *The Geological Society of America Bulletin*, 131(1–2), 224–234. <https://doi.org/10.1130/B32009.1>
- Imai, R., Farida, M., Sato, T., & Iryu, Y. (2015). Evidence for eutrophication in the northwestern Pacific and eastern Indian oceans during the Miocene to Pleistocene based on the nannofossil accumulation rate. *Marine Micropaleontology*, 116, 15–27. <https://doi.org/10.1016/j.marmicro.2015.01.001>
- Inglis, G. N., Bragg, F., Burls, N., Evans, D., Foster, G. L., Huber, M., et al. (2020). Global mean surface temperature and climate sensitivity of the EECO, PETM and latest Paleocene. *Climate of the Past*, 16, 1953–1968. <https://doi.org/10.5194/cp-2019-167>
- Ivanov, D., Utescher, T., Mosbrugger, V., Syabryaj, S., Djordjević-Milutinović, D., & Molchanoff, S. (2011). Miocene vegetation and climate dynamics in eastern and central Paratethys (southeastern Europe). *Palaeogeography Palaeoclimatology Palaeoecology*, 304(3–4), 262–275. <https://doi.org/10.1016/j.palaeo.2010.07.006>
- Jablonski, D., Roy, K., & Valentine, D. L. (2006). Out of the tropics: Evolutionary dynamics of the latitudinal diversity gradient. *Science*, 314, 102–106. <https://doi.org/10.1126/science.1130880>
- Jacobs, B. F., & Deino, A. L. (1996). Test of climate-leaf physiognomy regression models, their application to two Miocene floras from Kenya, and 40Ar/39Ar dating of the Late Miocene Kapturo site. *Palaeogeography Palaeoclimatology Palaeoecology*, 123(1–4), 259–271. [https://doi.org/10.1016/0031-0182\(96\)00102-2](https://doi.org/10.1016/0031-0182(96)00102-2)
- Jacobs, B. F., Pan, A., & Scotese, C. R. (2010). A review of Cenozoic vegetation history of Africa. In L. Werdelin, & W. J. Sanders (Eds.), *Cenozoic mammals of africa* (pp. 57–72). University of California Press.
- Jadwiszczak, P., & Mörs, T. (2011). Aspects of diversity in early Antarctic penguins. *Acta Palaeontologica Polonica*, 56(2), 269–277. <http://dx.doi.org/10.4202/app.2009.1107>
- Jakobsson, M., Backman, J., Rudels, B., Nycander, J., Frank, M., Mayer, L., et al. (2007). The early Miocene onset of a ventilated circulation regime in the Arctic Ocean. *Nature*, 447(7147), 986. <https://doi.org/10.1038/nature05924>
- Janis, C. M. (1993). Tertiary mammal evolution in the context of changing climates, vegetation, and tectonic events. *Annual Review of Ecology and Systematics*, 24(1), 467–500. <https://doi.org/10.1146/annurev.es.24.110193.002343>
- Janis, C. M., Gunnell, G. F., & Uhen, M. (2008). *Evolution of Tertiary mammals of north America. Volume 2: Small mammals, xenarthrans, and marine mammals*. Cambridge: University <https://doi.org/10.1146/annurev.es.24.110193.002343>
- Janis, C. M., Scott, K. M., & Jacobs, L. L. (1998). *Evolution of Tertiary mammals of north America. Volume 1: Terrestrial carnivores. Ungulates, and Ungulate-like mammals*. Cambridge: Cambridge University.
- Jaramillo, C., Sepulchre, P., Cardenas, D., Correa-Metrio, A., Moreno, J. E., Trejos, R., et al. (2020). Drastic vegetation change in the La Guajira Peninsula (Colombia) during the Neogene. *Paleoceanography and Paleoclimatology*, 35. <https://doi.org/10.1029/2020PA003933>
- Jardine, P. E., Janis, C. M., Sahney, S., & Benton, M. J. (2012). Grit Not Grass: Concordant patterns of early origin of hypsodonty in Great Plains ungulates and Glires. *Palaeogeography, Palaeoclimatology, Palaeoecology*, 365–366, 1–10. <https://doi.org/10.1016/j.palaeo.2012.09.001>
- Ji, S., Nie, J., Lechler, A., Huntington, K. W., Heitmann, E. O., & Breecker, D. O. (2018). A symmetrical CO₂ peak and asymmetrical climate change during the middle Miocene. *Earth and Planetary Science Letters*, 499, 134–144. <https://doi.org/10.1016/j.epsl.2018.07.011>
- Jiménez-Moreno, G., Fauquette, S., & Suc, J.-P. (2008). Vegetation, climate and palaeoaltitude reconstructions of the Eastern Alps during the Miocene based on pollen records from Austria, Central Europe. *Journal of Biogeography*, 35(9), 1638–1649. <https://doi.org/10.1111/j.1365-2699.2008.01911.x>
- Jiménez-Moreno, G., & Suc, J.-P. (2007). Middle Miocene latitudinal climatic gradient in Western Europe: Evidence from pollen records. *Palaeogeography Palaeoclimatology Palaeoecology*, 253(1–2), 208–225. <https://doi.org/10.1016/j.palaeo.2007.03.040>
- John, C. M., Karner, G. D., Browning, E., Leckie, R. M., Mateo, Z., Carson, B., & Lowery, C. (2011). Timing and magnitude of Miocene eustasy derived from the mixed siliciclastic-carbonate stratigraphic record of the northeastern Australian margin. *Earth and Planetary Science Letters*, 304(3–4), 455–467. <https://doi.org/10.1016/j.epsl.2011.02.013>
- John, C. M., Karner, G. D., & Mutti, M. (2004). δ¹⁸O and Marion Plateau backstripping: Combining two approaches to constrain late middle Miocene eustatic amplitude. *Geology*, 32(9), 829. <https://doi.org/10.1130/G20580.1>

- Jöhnck, et al. (2020). Variability of the Indian monsoon in the Andaman sea across the miocene-Pliocene transition (6.2 to 4.9 Ma), *Paleoceanography and Paleoclimatology*, 359, e2020PA003923. <https://doi.org/10.1029/2020PA003923>
- Johnson, K. G., Budd, A. F., & Stemann, T. A. (1995). Extinction selectivity and ecology of Neogene Caribbean reef corals. *Paleobiology*, 21, 52–73. <https://www.jstor.org/stable/2401139>
- Joyce, W. G., Klein, N., & Mörs, T. (2004). Carettochelyine turtle from the neogene of Europe. *Copeia*, 2004(2), 406–411. <https://doi.org/10.1643/CH-03-172R>
- Jung, G., & Prange, M. (2020). The effect of mountain uplift on eastern boundary currents and upwelling systems. *Climate of the Past*, 16, 161–181. <https://doi.org/10.5194/cp-16-161-2020>
- Kafanov, A. I., & Volvenko, I. V. (1997). Bivalve molluscs and Cenozoic paleoclimatic events in the northwestern Pacific Ocean. *Palaeogeography Palaeoclimatology Palaeoecology*, 129, 119–153. [https://doi.org/10.1016/S0031-0182\(96\)00057-0](https://doi.org/10.1016/S0031-0182(96)00057-0)
- Kameo, K., & Sato, T. (2000). Biogeography of Neogene calcareous nannofossils in the Caribbean and the eastern equatorial Pacific - floral response to the emergence of the Isthmus of Panama. *Marine Micropaleontology*, 39, 201–218. [https://doi.org/10.1016/S0377-8398\(00\)00021-9](https://doi.org/10.1016/S0377-8398(00)00021-9)
- Kaplan, J. (2001). *Geophysical applications of vegetation modeling*. Lund: Lund University.
- Karp, A. T., Behrensmeier, A. K., & Freeman, K. H. (2018). Grassland fire ecology has roots in the late Miocene. *Proceedings of the National Academy of Sciences of the United States of America*, 115, 12130–12135. <https://doi.org/10.1073/pnas.1809758115>
- Kasbohm, J., & Schoene, B. (2018). Rapid eruption of the River flood basalt and correlation with the mid-Miocene climate optimum. *Science Advances*, 4(9), eaat8223. <https://doi.org/10.1126/sciadv.aat8223>
- Katz, M. E., Wright, J. D., Miller, K. G., Cramer, B. S., Fennel, K., & Falkowski, P. G. (2005). Biological overprint of the geological carbon cycle. *Marine Geology*, 217, 323–338. [10.1016/j.margeo.2004.08.005](https://doi.org/10.1016/j.margeo.2004.08.005)
- Kay, R. F., & Madden, R. H. (1997). Mammals and rainfall: Paleoeecology of the middle miocene at La Venta (Colombia, south America). *Journal of Human Evolution*, 32(2–3), 161–199. <https://doi.org/10.1006/jhev.1996.0104>
- Kay, R. F., Madden, R. H., Cifelli, R. L., & Flynn, J. J. (1997). *Vertebrate Paleontology in the neotropics. The Miocene fauna of La Venta, Colombia*. Washington and London: Smithsonian Institution. <https://doi.org/10.1086/420076>
- Keigwin, L. (1982). Isotopic paleoceanography of the Caribbean and east pacific: Role of Panama uplift in late neogene time. *Science*, 217(4557), 350–353. <https://doi.org/10.1126/science.217.4557.350>
- Kemp, A. E. S., & Baldauf, J. G. (1993). Vast Neogenelaminated diatom mat deposits from the eastern equatorial Pacific Ocean. *Nature*, 362, 141–144. <https://doi.org/10.1038/362141a0>
- Kemp, A. E. S., Baldauf, J. G., Pearce, R. B., & Piasias, N. G. (1995). Origins and paleoceanographic significance of laminated diatom ooze from the eastern equatorial Pacific Ocean. In N. G., L. A. Mayer, T. R. Janecek, A. Palmer-Julson, & T. H. van Andel (Eds.), *Proceedings ODP, Science Results*. (pp. 641–645). College Station, TX: Ocean Drilling Program. <https://doi.org/10.2973/odp.proc.sr.138.134.1995>
- Kender, S., Bogus, K. A., Cobb, T. D., & Thomas, D. J. (2018). Neodymium evidence for increased Circumpolar deep water flow to the north pacific during the middle miocene climate transition. *Paleoceanography and Paleoclimatology*, 33(7), 672–682. <https://doi.org/10.1029/2017PA003309>
- Kender, S., & Kaminski, M. A. (2013). Arctic Ocean foraminiferal faunal change associated with the onset of perennial sea ice in the middle Miocene. *Journal of Foraminiferal Research*, 43, 99–119. <https://doi.org/10.2113/gsjfr.43.1.99>
- Kennedy, A. T., Farnsworth, A., Lunt, D. J., Lear, C. H., & Markwick, P. J. (2015). Atmospheric and oceanic impacts of Antarctic glaciation across the Eocene–Oligocene transition. *Philosophical Transactions of the Royal Society A: Mathematical Physical and Engineering Sciences*, 373, 2054. <https://doi.org/10.1098/rsta.2014.0419>
- Kennedy-Asser, A. T., Lunt, D. J., Farnsworth, A., & Valdes, P. J. (2019a). Assessing mechanisms and uncertainty in modeled climatic change at the Eocene-oligocene transition. *Paleoceanography and Paleoclimatology*, 34, 16–34. <https://doi.org/10.1029/2018PA003380>
- Kennedy-Asser, A. T., Lunt, D. J., Valdes, P. J., Ladant, J. B., Frieling, J., & Laurentano, V. (2019b). Changes in the high latitude southern hemisphere through the Eocene-oligocene transition: A model-data comparison. *Climate of the Past*, 2019, 1–26. <https://doi.org/10.5194/cp-2019-112>
- Kern, A., Harzhauser, M., Mandic, O., Roetzel, R., Ćorić, S., Bruch, A. A., & Zuschin, M. (2011). Millennial-scale vegetation dynamics in an estuary at the onset of the Miocene Climate Optimum. *Palaeogeography Palaeoclimatology Palaeoecology*, 304(3–4), 247–261. <https://doi.org/10.1016/j.palaeo.2010.07.014>
- Kiehl, J. T., & Shields, C. A. (2013). Sensitivity of the Palaeocene–Eocene thermal maximum climate to cloud properties. *Philosophical Transactions of the Royal Society A: Mathematical, Physical & Engineering Sciences*, 371(2001), 20130093. <https://doi.org/10.1098/rsta.2013.0093>
- Kiel, S., & Taviani, M. (2018). Chemosymbiotic bivalves from the late Pliocene Stirone River hydrocarbon seep complex in northern Italy. *Acta Palaeontologica Polonica*, 63, 557–568. <https://doi.org/10.4202/app.00473.2018>
- Kirilova, V., Osborne, A. H., Störling, T., & Frank, M. (2019). Miocene restriction of the Pacific-North Atlantic throughflow strengthened Atlantic overturning circulation. *Nature Communications*, 10(1), 1–7. <https://doi.org/10.1038/s41467-019-12034-7>
- Kirschner, J. A., & Hoorn, C. (2020). The onset of grasses in the Amazon drainage basin, evidence from the fossil record. *Frontiers of Biogeography*, 12(2), e44827. <https://doi.org/10.21425/F5FBG44827>
- Klocker, A., Prange, M., & Schulz, M. (2005). Testing the influence of the central american seaway on orbitally forced northern hemisphere glaciation. *Geophysical Research Letters*, 32(3), L03703. <https://doi.org/10.1029/2004GL021564>
- Knies, J., Mattingsdal, R., Fabian, K., Grösfeld, K., Baranwal, S., Husum, K., et al. (2014). Effect of early Pliocene uplift on late Pliocene cooling in the Arctic–Atlantic gateway. *Earth and Planetary Science Letters*, 387, 132–144. <https://doi.org/10.1016/j.epsl.2013.11.007>
- Knorr, G., Butzin, M., Micheels, A., & Lohmann, G. (2011). A warm Miocene climate at low atmospheric CO₂ levels. *Geophysical Research Letters*, 38(20), L20701. <https://doi.org/10.1029/2011GL048873>
- Knorr, G., & Lohmann, G. (2014). Climate warming during Antarctic ice sheet expansion at the Middle Miocene transition. *Nature Geoscience*, 7, 376–381. <https://doi.org/10.1038/ngeo2119>
- Knutti, R., Rugenstein, M. A. A., & Hegerl, G. C. (2017). Beyond equilibrium climate sensitivity. *Nature Geoscience*, 10(10), 727–736. <https://doi.org/10.1038/ngeo3017>
- Kochhann, K. G. D., Holbourn, A. E., Kuhnt, W., Channell, J. E. T., Lyle, M., Shackford, J. K., et al. (2016). Eccentricity pacing of eastern equatorial Pacific carbonate dissolution cycles during the Miocene Climatic Optimum. *Paleoceanography*, 31, 1176–1192. <https://doi.org/10.1002/2016PA002988>
- Kochhann, K. G. D., Holbourn, A. E., Kuhnt, W., & Xu, J. (2017). Eastern equatorial Pacific benthic foraminiferal distribution and deep water temperature changes during the early to middle Miocene. *Marine Micropaleontology*, 133, 28–39. <https://doi.org/10.1016/j.marmicro.2017.05.002>

- Kohn, M. J., Strömberg, C. A. E., Madden, R. H., Dunn, R. E., Evans, S., Palacios, A., & Carlini, A. A. (2015). Quasi-static Eocene-Oligocene climate in Patagonia promotes slow faunal evolution and mid-Cenozoic global cooling. *Palaeogeography Palaeoclimatology Palaeoecology*, 435, 24–37. <https://doi.org/10.1016/j.palaeo.2015.05.028>
- Kominz, M. A., Browning, J. V., Miller, K. G., Sugarman, P. J., Mizintseva, S., & Scotese, C. R. (2008). Late Cretaceous to Miocene sea-level estimates from the New Jersey and Delaware coastal plain coreholes: An error analysis. *Basin Research*, 20(2), 211–226. <https://doi.org/10.1111/j.1365-2117.2008.00354.x>
- Kominz, M. A., Miller, K. G., Browning, J. V., Katz, M. E., & Mountain, G. S. (2016). Miocene relative sea level on the New Jersey shallow continental shelf and coastal plain derived from one-dimensional backstripping: A case for both eustasy and epeirogeny. *Geosphere*, 12, 1437–1456. <https://doi.org/10.1130/GES01241.1>
- Konrad, W., Katul, G., Roth-Nebelsick, A., & Grein, M. (2017). A reduced order model to analytically infer atmospheric CO₂ concentration from stomatal and climate data. *Advances in Water Resources*, 104, 145–157. <https://doi.org/10.1016/j.advwatres.2017.03.018>
- Konrad, W., Royer, D., Franks, P. J., & Roth-Nebelsick, A. (2020). Quantitative critique of leaf-based paleo-CO₂ proxies: Consequences for their reliability and applicability. *Geological Journal*, 2020, 1–7. <https://doi.org/10.1002/gj.3807>
- Korasidis, V. A., Wallace, M. W., Wagstaff, B. E., & Holdgate, G. R. (2017). Oligo-Miocene peatland ecosystems of the Gippsland Basin and modern analogs. *Global and Planetary Change*, 149, 91–104. <https://doi.org/10.1016/j.gloplacha.2017.01.003>
- Koretsky, I. A., & Barnes, L. G. (2006). Pinniped evolutionary history and paleobiogeography. In Z. Csiki (Ed.), *Mesozoic and Cenozoic vertebrates and paleoenvironments, Tributes to the career of Professor dan Grigorescu* (pp. 143–153). Bucharest: Ars Docendi.
- Koretsky, I. A., & Domning, D. P. (2014). One of the oldest seals (Carnivora, Phocidae) from the old world. *Journal of Vertebrate Paleontology*, 34, 224–229. <https://doi.org/10.1080/02724634.2013.787428>
- Kotrc, B., & Knoll, A. H. (2015). Morphospaces and databases: Diatom diversification through time. In C. Hamm (Ed.), *Evolution of light-weight structures* (pp. 17–37). https://doi.org/10.1007/978-94-017-9398-8_2
- Kotthoff, U., Greenwood, D. R., McCarthy, F. M. G., Müller-Navarra, K., Prader, S., & Hesselbo, S. P. (2014). Late Eocene to middle Miocene (33 to 13 million years ago) vegetation and climate development on the north American Atlantic coastal plain (IODP expedition 313, site M0027). *Climate of the Past*, 10, 1523–1539. <https://doi.org/10.5194/cp-10-1523-2014>
- Kováč, M., Král', J., Márton, E., Plašienka, D., & Uher, P. (1994). Alpine uplift history of the central western Carpathians: Geochronological, paleomagnetic, sedimentary and structural data. *Geologica Carpathica*, 45(2), 83–96.
- Kovar-Eder, J., Jechorek, H., Kvaček, Z., & Parashiv, V. (2008). The integrated plant record: An essential tool for reconstructing neogene zonal vegetation in Europe. *PALAIOS*, 23(2), 97–111. <https://doi.org/10.2110/palo.2006.p06-039r>
- Krammer, R., Baumann, K.-H., & Henrich, R. (2006). Middle to late Miocene fluctuations in the incipient Benguela Upwelling System revealed by calcareous nannofossil assemblages (ODP Site 1085A). *Palaeogeography Palaeoclimatology Palaeoecology*, 230(3–4), 319–334. <https://doi.org/10.1016/j.palaeo.2005.07.022>
- Krapp, M., & Jungclauss, J. H. (2011). The Middle Miocene climate as modeled in an atmosphere-ocean-biosphere model. *Climate of the Past*, 7(4), 1169–1188. <https://doi.org/10.5194/cp-7-1169-2011>
- Krapp, M., & Jungclauss, J. H. (2015). Pacific variability under present-day and Middle Miocene boundary conditions. *Climate Dynamics*, 44(9), 2609–2621. <https://doi.org/10.1007/s00382-014-2456-2>
- Krijgsman, W., Capella, W., Simon, D., Hilgen, F. J., Kouwenhoven, T. J., Meijer, P. T., et al. (2018). The Gibraltar corridor: Watergate of the Messinian salinity crisis. *Marine Geology*, 403, 238–246. <https://doi.org/10.1016/j.margeo.2018.06.008>
- Krijgsman, W., Langereis, C. G., Daams, R., & van der Meulen, A. J. (1994). Magnetostratigraphic dating of the middle Miocene climate change in the continental deposits of the Aragonian type area in the Calatayud-Teruel basin (Central Spain). *Earth and Planetary Science Letters*, 128, 513–526. [https://doi.org/10.1016/0012-821X\(94\)90167-8](https://doi.org/10.1016/0012-821X(94)90167-8)
- Kroon, D., Steens, T., & Troelstra, S. R. (1991). Onset of Monsoonal related upwelling in the western Arabian Sea as revealed by planktonic foraminifers. In W. Prell, & N. Niitsuma (Eds.), *Proceedings of the ocean drilling program, scientific results*. (pp. 257–263). College Station, TX: Ocean Drilling Program.
- Krylov, A. A., Andreeva, I. A., Vogt, C., Backman, J., Krupskaya, V. V., Grikurov, G. E., et al. (2008). A shift in heavy and clay mineral provenance indicates a middle Miocene onset of a perennial sea ice cover in the Arctic Ocean. *Paleoceanography*, 23, PA1S06. <https://doi.org/10.1029/2007PA001497>
- Kuhnt, W., Holbourn, A. E., Hall, R., Zuvela, M., & Käse, R. (2004). Neogene history of the Indonesian throughflow. Continent-Ocean Interactions within East Asian Marginal Seas. *Geophysical Monograph*, 149, 299–320. <https://doi.org/10.1029/149GM16>
- Kump, L. R., & Pollard, D. (2008). Amplification of Cretaceous warmth by biological cloud feedbacks. *Science*, 320, 195. <https://doi.org/10.1126/science.1153883>
- Kürschner, W. M., Kvaček, Z., & Dilcher, D. L. (2008). The impact of Miocene atmospheric carbon dioxide fluctuations on climate and the evolution of terrestrial ecosystems. *Proceedings of the National Academy of Sciences of the United States of America*, 105, 449–453. <https://doi.org/10.1073/pnas.0708588105>
- Kürschner, W. M., van der Burgh, J., Visscher, H., & Dilcher, D. (1996). Oakleaves as biosensors of late Neogene and early Pleistocene paleoatmospheric CO₂ concentrations. *Marine Micropaleontology*, 27(1–4), 299–213. [https://doi.org/10.1016/0377-8398\(95\)00067-4](https://doi.org/10.1016/0377-8398(95)00067-4)
- Ladant, J.-B., Donnadieu, Y., Lefebvre, V., & Dumas, C. (2014). The respective role of atmospheric carbon dioxide and orbital parameters on ice sheet evolution at the Eocene-Oligocene transition. *Paleoceanography*, 29, 810–823. <https://doi.org/10.1002/2013PA002593>
- Lagabrielle, Y., Goddérís, Y., Donnadieu, Y., Malavieille, J., & Suarez, M. (2009). The tectonic history of Drake Passage and its possible impacts on global climate. *Earth and Planetary Science Letters*, 279(3–4), 197–211. <https://doi.org/10.1016/j.epsl.2008.12.037>
- Langebroek, P. M., Paul, A., & Schulz, M. (2009). Antarctic ice-sheet response to atmospheric CO₂ and insolation in the Middle Miocene. *Climate of the Past*, 5(4), 633–646. <https://doi.org/10.5194/cp-5-633-2009>
- Langebroek, P. M., Paul, A., & Schulz, M. A. (2010). Simulating the sea level imprint on marine oxygen isotope records during the middle Miocene using an ice sheet-climate model. *Paleoceanography*, 25(4), 1–12. <https://doi.org/10.1029/2008PA001704>
- LaRivière, J. P., Ravelo, A. C., Crimmins, A., Dekens, P. S., Ford, H. L., Lyle, M., & Wara, M. W. (2012). Late Miocene decoupling of oceanic warmth and atmospheric carbon dioxide forcing. *Nature*, 486, 97–100. <https://doi.org/10.1038/nature11200>
- Larsen, H. C., Saunders, A. D., Clift, P. D., Beget, J., Wei, W., & Spezzaferri, S. (1994). Seven million years of glaciation in Greenland. *Science*, 264(5161), 952–955. <https://doi.org/10.1126/science.264.5161.952>
- Laskar, J., Robutel, P., Joutel, F., Gastineau, M., Correia, A. C. M., & Levrard, B. (2004). A long-term numerical solution for the insolation quantities of the Earth. *Astronomy & Astrophysics*, 428, 261–285. <https://doi.org/10.1051/0004-6361>
- Lawrence, K. T., Pearson, A., Castañeda, I. S., Laddow, C., Peterson, L. C., & Lawrence, C. E. (2020). Comparison of late Neogene U^k₃₇ and TEX₈₆ paleotemperature records from the eastern equatorial Pacific at orbital resolution. *Paleoceanography and Paleoclimatology*, 35, e2020PA003858. <https://doi.org/10.1029/2020PA003858>

- Lazarus, D., Barron, J., Renaudie, J., Diver, P., & Türke, A. (2014). Cenozoic planktonic marine diatom diversity and correlation to climate change. *PLoS One*, 9, e84857. <https://doi.org/10.1371/journal.pone.0084857>
- Lazarus, D. B. (2002). Environmental controls on diversity, evolutionary rates and taxa longevities in Antarctic Neogene radiolarian. *Palaeontologia Electronica*, 5, 32. https://palaeo-electronica.org/2002_1/antarct/issue1_02.htm
- Lazarus, D. B., Kotrc, B., Wulf, G., & Schmidt, D. N. (2009). Radiolarians decreased silicification as an evolutionary response to Cenozoic ocean silica availability. *Proceedings of the National Academy of Sciences of the United States of America*, 106(23), 9333–9338. <https://doi.org/10.1073/pnas.0812979106>
- Lear, C. H., Elderfield, H., & Wilson, P. (2000). Cenozoic deep-sea temperatures and global ice volumes from Mg/Ca in benthic foraminiferal calcite. *Science*, 287, 269–272. <https://doi.org/10.1126/science.287.5451.269>
- Lear, C. H., Coxall, H. K., Foster, G. L., Lunt, D. J., Mawbey, E., Rosenthal, Y., et al. (2015). Neogene ice volume and ocean temperatures: Insights from infaunal foraminiferal Mg/Ca paleothermometry. *Paleoceanography*, 30(11), 1437–1454. <https://doi.org/10.1002/2015PA002833>
- Lear, C. H., Mawbey, E. M., & Rosenthal, Y. (2010). Cenozoic benthic foraminiferal Mg/Ca and Li/Ca records: Toward unlocking temperatures and saturation states. *Paleoceanography*, 25(4), 1–11. <https://doi.org/10.1029/2009PA001880>
- Lear, C. H., Rosenthal, Y., Coxall, H. K., & Wilson, P. A. (2004). Late Eocene to early Miocene ice-sheet dynamics and the global carbon cycle. *Paleoceanography*, 19(4) PA4015. <https://doi.org/10.1029/2004PA001039>
- Lear, C. H., Rosenthal, Y., & Slowey, N. (2002). Benthic foraminiferal Mg/Ca-paleothermometry: A revised core-top calibration. *Geochimica et Cosmochimica Acta*, 66(19), 3375–3387. [https://doi.org/10.1016/S0016-7037\(02\)00941-9](https://doi.org/10.1016/S0016-7037(02)00941-9)
- Lear, C. H., Rosenthal, Y., & Wright, J. D. (2003). The closing of a seaway: Ocean water masses and global climate change. *Earth and Planetary Science Letters*, 210(3–4), 425–436. [https://doi.org/10.1016/S0012-821X\(03\)00164-X](https://doi.org/10.1016/S0012-821X(03)00164-X)
- Lebatard, A.-E., Bourlès, D. L., Düringer, P., Jolivet, M., Braucher, R., Carcaillet, J., et al. (2008). Cosmogenic nuclide dating of *Sahelanthropus tchadensis* and *Australopithecus bahrelghazali*: Mio–Pliocene hominids from Chad. *Proceedings of the National Academy of Sciences of the United States of America*, 105(9), 3226–3231. <https://doi.org/10.1073/pnas.0708015105>
- Leigh, E. G., O’Dea, A., & Vermeij, G. J. (2014). Historical biogeography of the Isthmus of Panama. *Biological Reviews*, 89, 148–172. <https://doi.org/10.1111/brv.12048>
- Leopold, E. B., & Denton, M. F. (1987). Comparative age of grassland and steppe east and west of the northern Rocky Mountains. *Annals of the Missouri Botanical Garden*, 74, 841–867. <https://doi.org/10.2307/2399452>
- Leopold, E. B., Liu, G. W., & Clay-Poole, C. (1992). Low-biomass vegetation in the oligocene?. In *Eocene-Oligocene climatic and biotic evolution* (pp. 399–420). Princeton University Press.
- Levy, R., Harwood, D., Florindo, F., Sangiorgi, F., Tripathi, R., von Eynatten, H., et al. (2016). Antarctic ice sheet sensitivity to atmospheric CO₂ variations in the early to mid-Miocene. *Proceedings of the National Academy of Sciences of the United States of America*, 113(13), 3453–3458. <https://doi.org/10.1073/pnas.1516030113>
- Levy, R. H., Meyers, S. R., Naish, T. R., Golledge, N. R., McKay, R. M., Crampton, J. S., et al. (2019). Antarctic ice-sheet sensitivity to obliquity forcing enhanced through ocean connections. *Nature Geoscience*, 12, 132–137. <https://doi.org/10.1038/s41561-018-0284-4>
- Lewis, A. R., Marchant, D. R., Ashworth, A. C., Hedenäs, L., Hemming, S. R., Johnson, J. V., et al. (2008). Mid-Miocene cooling and the extinction of tundra in continental Antarctica. *Proceedings of the National Academy of Sciences*, 105(31), 10676–10680. <https://doi.org/10.1073/pnas.0802501105>
- Lewitus, E., Bittner, L., Malvlya, S., Bowler, C., & Morlon, H. (2018). Clade-specific diversification dynamics of marine diatoms since the Jurassic. *Nature Ecology and Evolution*, 2, 1715–1723. <https://doi.org/10.1038/s41559-018-0691-3>
- Lhomme, N., Clarke, G. K. C., & Ritz, C. A. (2005). Global budget of water isotopes inferred from polar ice sheets. *Geophysical Research Letters*, 32(20), 1–4. <https://doi.org/10.1029/2005GL023774>
- Li, L., Li, Q., Tian, J., Wang, P., Wang, H., & Liu, Z. (2011). A 4-Ma record of thermal evolution in the tropical western Pacific and its implications on climate change. *Earth and Planetary Science Letters*, 309, 10–20. <https://doi.org/10.1016/j.epsl.2011.04.016>
- Licht, A., Van Cappelle, M., Abels, H. A., Ladant, J. B., Trabucho-Alexandre, J., France-Lanord, et al. (2014). Asian monsoons in a late Eocene greenhouse world. *Nature*, 513(7519), 501–506. <https://doi.org/10.1038/nature13704>
- Liebrand, D., Beddow, H. M., Lourens, L. J., Pälike, H., Raffi, I., Bohaty, S. M., et al. (2016). Cyclostratigraphy and eccentricity tuning of the early oligocene through early miocene (30.1–17.1 Ma): *Cibicides mundulus* stable oxygen and carbon isotope records from Walvis Ridge site 1264. *Earth and Planetary Science Letters*, 450, 392–405. <https://doi.org/10.1016/j.epsl.2016.06.007>
- Liebrand, D., de Bakker, A. T. M., Beddow, H. M., Wilson, P. A., Bohaty, S. M., Ruessink, G., et al. (2017). Evolution of the early antarctic ice ages. *Proceedings of the National Academy of Sciences*, 114, (15),3867. <https://doi.org/10.1073/pnas.1615440114>
- Liebrand, D., Lourens, L. J., Hodell, D. A., De Boer, B., Van de Wal, R. S. W., & Pälike, H. (2011). Antarctic ice sheet and oceanographic response to eccentricity forcing during the early Miocene. *Climate of the Past*, 7(3), 869–880. <https://doi.org/10.5194/cp-7-869-2011>
- Linnemann, U., Su, T., Kunzmann, L., Spicer, R. A., Ding, W.-N., Spicer, T. E. V., Zieger, J., et al. (2018). New U-Pb dates show a Paleogene origin for the modern Asian biodiversity hot spots. *Geology*, 46(1), 3–6. <https://doi.org/10.1130/G39693.1>
- Lisiecki, L. E., & Raymo, M. E. (2005). A Pliocene–Pleistocene stack of 57 globally distributed benthic ¹⁸O records. *Paleoceanography*, 20, PA1003. <https://doi.org/10.1029/2004PA001071>
- Liu, Y.-S., Utescher, T., Zhou, Z., & Sun, B. (2011). The evolution of Miocene climates in North China: Preliminary results of quantitative reconstructions from plant fossil records. *Palaeogeography Palaeoclimatology Palaeoecology*, 304(3), 308–317. <https://doi.org/10.1016/j.palaeo.2010.07.004>
- Liu, Z., He, X., Jiang, Y., Wang, H., Bohaty, S. M., & Wilson, P. A. (2018). Transient temperature asymmetry between hemispheres in the Palaeogene Atlantic ocean. *Nature Geoscience*, 11, 656–660. <https://doi.org/10.1038/s41561-018-0182-9>
- Loch, C., Buono, M., Kalthoff, D. C., Mörs, T., & Fernandez, M. (2019). Enamel microstructure in Eocene cetaceans from Antarctica (Archaeoceti and Mysticeti). *Journal of Mammalian Evolution*, 27, 289–298. <https://doi.org/10.1007/s10914-018-09456-3>
- Loughney, K. M., Hren, M. T., Smith, S. Y., & Pappas, J. L. (2020). Vegetation and habitat change in southern California through the Middle Miocene Climatic Optimum: Paleoenvironmental records from the Barstow Formation, Mojave Desert, USA. *GSA Bulletin*, 123, 113–129. <https://doi.org/10.1130/B35061.1>
- Lohmann, G. P., & Carlson, J. J. (1981). Oceanographic significance of pacific late miocene calcareous nannoplankton. *Marine Micropaleontology*, 6, 553–579. [https://doi.org/10.1016/0377-8398\(81\)90021-9](https://doi.org/10.1016/0377-8398(81)90021-9)
- Lomax, B. H., Lake, J. A., Leng, M. J., & Jardine, P. E. (2019). An experimental evaluation of the use of ¹³C as a proxy for palaeoatmospheric CO₂. *Geochimica et Cosmochimica Acta*, 247, 162–174. <https://doi.org/10.1016/j.gca.2018.12.026>

- Londoño, L., Royer, D. L., Jaramillo, C., Escobar, J., Foster, D. A., Cárdenas-Rozo, A. L., & Wood, A. (2018). Early Miocene CO₂ estimates from a Neotropical fossil leaf assemblage exceed 400 ppm. *American Journal of Botany*, *105*, 1929–1937. <https://doi.org/10.1002/ajb2.1187>
- Long, J. A. (2011). *The rise of fishes*. Baltimore: Johns Hopkins University.
- Long, J. A., & Archer, M. (2002). *Prehistoric mammals of Australia and new Guinea: One Hundred million Years of evolution*. Sidney: UNSW.
- Lourens, L. J., Hilgen, F. J., Laskar, J., Shackleton, N. J., & Wilson, D. (2004). The Neogene period. In F. M. Gradstein, J. G. Ogg, & A. G. Smith (Eds.), *A geologic time scale 2004*. Cambridge: Cambridge University Press. <https://doi.org/10.1017/CBO9780511536045>
- Lozouet, P. (2014). Temporal and latitudinal trends in the biodiversity of European Atlantic Cenozoic gastropod (Mollusca) faunas. A base for the history of biogeographic provinces. *Carnets de Géologie*, *14*, 273–314. <http://paleopolis.rediris.es/cg/1414/>
- Luebbbers, J., Kuhn, W., Holbourn, A. E., Bolton, C. T., Gray, E., Usui, Y., et al. (2019). The middle to late miocene “carbonate crash” in the equatorial Indian ocean. *Paleoceanography and Paleoclimatology*, *34*(5), 813–832. <https://doi.org/10.1029/2018PA003482>
- Lunt, D. J., Flecker, R., Valdes, P. J., Salzmann, U., Gladstone, R., & Haywood, A. M. (2008a). A methodology for targeting palaeo proxy data acquisition: A case study for the terrestrial late miocene. *Earth and Planetary Science Letters*, *271*(1), 53–62. <https://doi.org/10.1016/j.epsl.2008.03.035>
- Lunt, D. J., Haywood, A. M., Foster, G. L., & Stone, E. J. (2009). The arctic cryosphere in the mid- Pliocene and the future. *Philosophical Transactions of the Royal Society A: Mathematical, Physical & Engineering Sciences*, *367*(1886), 49–67. <https://doi.org/10.1098/rsta.2008.0218>
- Lunt, D. J., Valdes, P. J., Haywood, A., & Rutt, I. (2008b). Closure of the Panama seaway during the Pliocene: Implications for climate and northern hemisphere glaciation. *Climate Dynamics*, *30*, 1–18.
- Lüthi, D., Le Floch, M., Bereiter, B., Blunier, T., Barnola, J.-M., Siegenthaler, U., et al. (2008). High-resolution carbon dioxide concentration record 650,000–800,000 years before present. *Nature*, *453*(7193), 379–382. <https://doi.org/10.1038/nature06949>
- Lyle, M., & Baldauf, J. (2015). Biogenic sediment regimes in the Neogene equatorial Pacific, IODP Site U1338: Burial, production, and diatom community. *Palaeogeography Palaeoclimatology Palaeoecology*, *433*, 106–128. <https://doi.org/10.1016/j.palaeo.2015.04.001>
- Lyle, M., Barron, J., Bralower, T. J., Huber, M., Lyle, A. O., Ravelo, A. C., et al. (2008). Pacific ocean and cenozoic evolution of climate. *Reviews of Geophysics*, *46*(2), RG2002. <https://doi.org/10.1029/2005RG000190>
- Lyle, M., Dadey, K. A., & Farrell, J. W. (1995). The Late Miocene (11–8 Ma) Eastern Pacific Carbonate Crash: Evidence for reorganization of deep-water Circulation by the closure of the Panama Gateway. *Proceedings of the ocean Drilling Program, Scientific Results* (Vol. 138). <http://dx.doi.org/10.2973/odp.proc.sr.138.157.1995>
- Lyle, M., Drury, A. J., Tian, J., Wilkens, R., & Westerhold, T. (2019). Late miocene to Holocene high-resolution eastern equatorial pacific carbonate records: Stratigraphy linked by dissolution and paleoproductivity. *Climate of the Past*, *15*(5), 1715–1739. <https://www.clim-past.net/15/1715/2019/>
- Ma, X., Tian, J., Ma, W., Li, K., & Yu, J. (2018). Changes of deep Pacific overturning circulation and carbonate chemistry during middle Miocene East Antarctic ice sheet expansion. *Earth and Planetary Science Letters*, *484*, 253–263. <https://doi.org/10.1016/j.epsl.2017.12.002>
- MacFadden, B. J. (2005). Fossil horses – evidence for evolution. *Science*, *307*, 1728–1730. <https://doi.org/10.1126/science.1105458>
- Macgregor, D. (2015). History of the development of the east African Rift system: A series of interpreted maps through time. *Journal of African Earth Sciences*, *101*, 232–252. <https://doi.org/10.1016/j.jafrearsci.2014.09.016>
- Mackensen, A. (2008). Biogeochemical controls on paleoceanographic environmental proxies. In W. E. N. Austin, & R. H. James (Eds.), *On the use of benthic foraminiferal δ¹³C in paleoceanography: Constraints from primary proxy relationships*. Vol. 303 (pp. 121–133), Geological Society - Special Publications. <https://doi.org/10.1144/SP303.9>
- Macphail, M. K. (2007). Australian palaeoclimates: Cretaceous to Tertiary A review of palaeobotanical and related evidence to the year 2000. *CRC LEME Open File Report*, *151*, 1–279. <http://hdl.handle.net/1885/35585>
- MacRae, R. A., Fensome, R. A., & Williams, G. L. (1996). Fossil dinoflagellate diversity, originations, and extinctions and their significance. *Canadian Journal of Biology*, *74*, 1687–1694. <https://doi.org/10.1139/b96-205>
- Maier-Reimer, E., Mikolajewicz, U., & Crowley, T. (1990). ocean general circulation model sensitivity experiment with an open central American isthmus. *Paleoceanography*, *5*(3), 349–366. <https://doi.org/10.1029/PA005i003p00349>
- Mamani, M., Wörner, G., & Sempere, T. (2010). Geochemical variations in igneous rocks of the Central Andean orocline (13 S to 18 S): Tracing crustal thickening and magma generation through time and space. *GSA Bulletin*, *122*(1–2), 162–182. <https://doi.org/10.1130/B26538.1>
- Markwick, P. J. (2007). The paleogeographic and paleoclimatic significance of climate proxies for data–model comparisons. In M. Williams, A. M. Haywood, F. J. Gregory, & D. N. Schmidt (Eds.), *Deep-time perspectives on climate change: Marrying the signal from computer models and biological proxies* (pp. 251–312). The Micropaleontological Society Special Publications. The Geological Society.
- Markwick, P. J., & Valdes, P. J. (2004). Palaeo-digital elevation models for use as boundary conditions in coupled ocean-atmosphere GCM experiments: A Maastrichtian (late Cretaceous) example. *Paleogeography Paleoclimatology Palaeoecology*, *2013*, 37–63. <https://doi.org/10.1016/j.palaeo.2004.06.015>
- Marlow, J. R., Lange, C., Wefer, G., & Rosell-Mele, A. (2000). Upwelling intensification as part of the Pliocene-Pleistocene climate transition. *Science*, *290*(5500), 2288–2291. <https://doi.org/10.1126/science.290.5500.2288>
- Martin, H. A. (2006). Cenozoic climatic change and the development of the arid vegetation in Australia. *Journal of Arid Environments*, *66*, 533–563. <https://doi.org/10.1016/j.jaridenv.2006.01.009>
- Martinetto, E., Momohara, A., Bizzarri, R., Baldanza, A., Delfino, M., Esu, D., & Sardella, R. (2017). Late persistence and deterministic extinction of “humid thermophilous plant taxa of East Asian affinity” (HUTEA) in southern Europe. *Palaeogeography Palaeoclimatology Palaeoecology*, *467*, 211–231. <https://doi.org/10.1016/j.palaeo.2015.08.015>
- Marx, F. G., & Fordyce, R. E. (2015). Baleen boom and bust: A synthesis of mysticete phylogeny, diversity and disparity. *Royal Society Open Science*, *2*(4), 140434. <https://doi.org/10.1098/rsos.140434>
- Marx, F. G., & Uhen, M. D. (2010). Climate, critters, and cetaceans: Cenozoic drivers of the evolution of modern whales. *Science*, *327*(5968), 993–996. <https://doi.org/10.1126/science.1185581>
- Marzocchi, A., Flecker, R., Lunt, D. J., Krijgsman, W., & Hilgen, F. J. (2019). Precessional drivers of late miocene Mediterranean sedimentary sequences: African summer monsoon and Atlantic winter storm tracks. *Paleoceanography and Paleoclimatology*, *34*(12), 1980–1994. <https://doi.org/10.1029/2019PA003721>
- Marzocchi, A., Lunt, D. J., Flecker, R., Bradshaw, C. D., Farnsworth, A., & Hilgen, F. J. (2015). Orbital control on late miocene climate and the north African monsoon: Insight from an ensemble of sub-precessional simulations. *Climate of the Past*, *11*(10), 1271–1295. <https://doi.org/10.5194/cp-11-1271-2015>

- Mathew, M., Makhankova, A., Menier, D., Sautter, B., Betzler, C., & Pierson, B. (2020). The emergence of Miocene reefs in South China Sea and its resilient adaptability under varying eustatic, climatic and oceanographic conditions. *Scientific Reports*, *10*, 7141. [10.1038/s41598-020-64119-9](https://doi.org/10.1038/s41598-020-64119-9)
- Matthews, J. V., Jr, Telka, A., & Kuzmina, S. A. (2019). Late neogene insect and other invertebrate fossils from Alaska and arctic/subarctic Canada. *Invertebrate Zoology*, *16*, 126–153. [10.15298/invertzool.16.2.03](https://doi.org/10.15298/invertzool.16.2.03)
- Mawbey, E. M., & Lear, C. H. (2013). Carbon cycle feedbacks during the Oligocene-Miocene transient glaciation. *Geology*, *41*(9), 963–966. <https://doi.org/10.1130/G34422.1>
- Maxbauer, D. P., Peppe, D. J., Bamford, M., McNulty, K. P., Harcourt-Smith, W. E., & Davis, L. E. (2013). A morphotype catalog and palaeoenvironmental interpretations of early Miocene fossil leaves from the Hiwegi Formation, Rusinga Island, Lake Victoria, Kenya. *Palaeontologia Electronica*, *16*, 28. <https://doi.org/10.26879/342>
- Mayer, L. A., Shipley, T. H., & Winterer, E. L. (1986). Equatorial Pacific seismic reflectors as indicators of global oceanographic events. *Science*, *233*(4765), 761–764. <https://doi.org/10.1126/science.233.4765.761>
- Mayer, L. A., Theyer, F., Barron, J. A., Dunn, D. A., Handyside, T., Hills, S., et al. (1985). *Initial reports of the deep sea drilling project*. Washington: U.S. Government Printing. <https://doi.org/10.2973/dsdp.proc.85.1985>
- Mayr, G. (2009). *Paleogene fossil birds*. Frankfurt am Main: Springer.
- Mayr, G., & Goedert, J. L. (2018). First record of a tarsometatarsus of *Tonsala hildegardae* (Plotopteridae) and other avian remains from the late Eocene/early Oligocene of Washington State (USA). *Geobios*, *51*(1), 51–59. <https://doi.org/10.1016/j.geobios.2017.12.006>
- Mayr, G., & Göhlich, U. B. (2004). A new parrot from the Miocene of Germany, with comments on the variation of hypotarsus morphology in some Psittaciformes. *Belgian Journal of Zoology*, *134*(1), 47–54.
- McCaffrey, J. C., Wallace, M. W., & Gallagher, S. J. (2020). A Cenozoic great barrier reef on Australia's north west shelf. *Global and Planetary Change*, *184*, 103048. [10.1016/j.gloplacha.2019.103048](https://doi.org/10.1016/j.gloplacha.2019.103048)
- McElwain, J. C., & Chaloner, W. G. (1995). Stomatal density and index of fossil plants track atmospheric carbon-dioxide in the Paleozoic. *Annals of Botany*, *76*, 389–395. <https://doi.org/10.1006/anbo.1995.1112>
- McElwain, J. C., & Steinthorsdottir, M. (2017). Paleoeology, ploidy, palaeoatmospheric composition and developmental biology: A review of the multiple uses of fossil stomata. *Plant Physiology*, *174*, 650–664. <https://doi.org/10.1104/pp.17.00204>
- McInerney, F. A., Strömberg, C. A. E., & White, J. W. C. (2011). The Neogene transition from C₃ to C₄ grasslands in North America: Stable carbon isotope ratios of fossil phytoliths. *Paleobiology*, *37*(1), 23–49. <https://doi.org/10.1666/09068.1>
- McKay, R. M., De Santis, L., & Kulhanek, D. K. (2018). *Expedition 374 preliminary report: Ross sea west antarctic ice sheet history*. College Station: International Ocean Discovery Program. <https://doi.org/10.14379/iodp.pr.374.2018>
- McKinley, C. C., Thomas, D. J., LeVay, L. J., & Rolewicz, Z. (2019). Nd isotopic structure of the Pacific Ocean 40–10 Ma, and evidence for the reorganization of deep North Pacific Ocean circulation between 36 and 25 Ma. *Earth and Planetary Science Letters*, *521*, 139–149. <https://doi.org/10.1016/j.epsl.2019.06.009>
- Medina-Elizalde, M., Lea, D. W., & Fantle, M. S. (2008). Implications of seawater Mg/Ca variability for Plio-Pleistocene tropical climate reconstruction. *Earth and Planetary Science Letters*, *269*(3–4), 584–594. <https://doi.org/10.1016/j.epsl.2008.03.014>
- Médus, J., Popoff, M., Fournanier, E., & Sowunmi, M. A. (1988). Sedimentology, pollen, spores and diatoms of a 148 m deep Miocene drill hole from Oku Lake, east central Nigeria. *Palaeogeography Palaeoclimatology Palaeoecology*, *68*(1), 79–94. [https://doi.org/10.1016/0031-0182\(88\)90018-1](https://doi.org/10.1016/0031-0182(88)90018-1)
- Mejia, L. M., Méndez-Vicente, A., Abrevaya, L., Lawrence, K. T., Ladlow, C., Bolton, C., et al. (2017). A diatom record of CO₂ decline since the late Miocene. *Earth and Planetary Science Letters*, *479*, 18–33. <https://doi.org/10.1016/j.epsl.2017.08.034>
- Meulenkamp, J. E., & Sissingh, W. (2003). Tertiary paleogeography and tectonostratigraphic evolution of the Northern and Southern Peri-Tethys platforms and the intermediate domains of the African–Eurasian convergent plate boundary zone. *Palaeogeography Palaeoclimatology Palaeoecology*, *196*(1–2), 209–228. [https://doi.org/10.1016/S0031-0182\(03\)00319-5](https://doi.org/10.1016/S0031-0182(03)00319-5)
- Micheels, A., Bruch, A. A., Eronen, J., Fortelius, M., Harzhauser, M., Utescher, T., & Mosbrugger, V. (2011). Analysis of heat transport mechanisms from a Late Miocene model experiment with a fully-coupled atmosphere–ocean general circulation model. *Palaeogeography Palaeoclimatology Palaeoecology*, *304*(3), 337–350. <https://doi.org/10.1016/j.palaeo.2010.09.021>
- Micheels, A., Bruch, A. A., Uhl, D., Utescher, T., & Mosbrugger, V. (2007). A Late Miocene climate model simulation with ECHAM4/ML and its quantitative validation with terrestrial proxy data. *Palaeogeography Palaeoclimatology Palaeoecology*, *253*(1), 251–270. <https://doi.org/10.1016/j.palaeo.2007.03.042>
- Michel, L. A., Peppe, D. J., Lutz, J. A., Driese, S. G., Dunsworth, H. M., Harcourt-Smith, W. E., et al. (2014). Remnants of an ancient forest provide ecological context for Early Miocene fossil apes. *Nature Communications*, *5*, 3236. <https://doi.org/10.1038/ncomms4236>
- Mihlbachler, M. C., Rivals, F., Solounias, N., & Semperebon, G. M. (2011). Dietary change and evolution of horses in North America. *Science*, *331*, 1178–1181. <https://doi.org/10.1126/science.1196166>
- Mikolajewicz, U., & Crowley, T. J. (1997). Response of a coupled ocean/energy balance model to restricted flow through the Central American Isthmus. *Paleoceanography*, *12*(3), 429–441. <https://doi.org/10.1029/96PA03542>
- Miller, K. G. (2005). The Phanerozoic record of global sea-level change. *Science*, *310*(5752), 1293–1298. <https://doi.org/10.1126/science.1116412>
- Miller, K. G., Browning, J. V., Schmelz, W. J., Kopp, R. E., Mountain, G. S., & Wright, J. D. (2020). Cenozoic sea-level and cryospheric evolution from deep-sea geochemical and continental margin records: *Science Advances*, *6*(20), eaaz1346. [10.1126/sciadv.aaz1346](https://doi.org/10.1126/sciadv.aaz1346)
- Miller, K. G., & Katz, M. E. (1987). Oligocene to Miocene benthic foraminiferal and abyssal circulation changes in the North Atlantic. *Micropaleontology*, *33*, 97–149. www.jstor.org/stable/1485489
- Miller, K. G., Wright, J., & Fairbanks, R. (1991). Unlocking the ice house: Oligocene-Miocene oxygen isotopes, eustasy, and margin erosion. *Journal of Geophysical Research*, *96*, 6829–6848. <https://doi.org/10.1029/90JB02015>
- Miller, K. G., & Wright, J. D. (2017). Success and failure in Cenozoic global correlations using golden spikes: A geochemical and magnetostratigraphic perspective. *Episodes*, *40*, 8–21. <http://dx.doi.org/10.18814/epiiugs/2017/v40i1/017003>
- Modestou, S. E., Leutert, T. J., Fernandez, A., Lear, C. H., & Meckler, A. N. (2020). Warm middle Miocene Indian Ocean bottom water temperatures: Comparison of clumped isotope and Mg/Ca-based estimates. *Paleoceanography and Paleoclimatology*, *35*(11), e2020PA003927. <https://doi.org/10.1029/2020PA003927>
- Molnar, P., & Cane, M. A. (2002). El Niño's tropical climate and teleconnections as a blueprint for pre-Ice Age climates. *Paleoceanography*, *17*(2), 11. <https://doi.org/10.1029/2001PA000663>
- Molnar, P., & Cane, M. A. (2007). Early Pliocene (pre-ice age) el Niño-like global climate: Which el Niño?. *Geosphere*, *3*(5), 337–365. <https://doi.org/10.1130/GES00103.1>

- Mondal, S., & Harries, P. J. (2016). The effect of taxonomic corrections on Phanerozoic generic richness trends in marine bivalves with a discussion on the clade's overall history. *Paleobiology*, *42*, 157–171. <https://doi.org/10.1017/pab.2015.35>
- Montaggione, L. F., & Braithwaite, C. J. R. (2009). *Quaternary coral reef systems: History, development processes and controlling factors*. Amsterdam: Elsevier.
- Montes, C., Cardona, A., Jaramillo, C., Pardo, A., Silva, J. C., Valencia, V., et al. (2015). Middle Miocene closure of the central American seaway. *Science*, *348*(6231), 226–229. <https://doi.org/10.1126/science.aaa2815>
- Morales-García, N. M., Säilä, L. K., & Janis, C. M. (2020). The neogene savannas of north America: A retrospective analysis on artiodactyl faunas. *Frontiers of Earth Science*, *8*, 191. <https://doi.org/10.3389/feart.2020.00191>
- Morley, R. J., & Richards, K. (1993). Gramineae cuticle: A key indicator of late cenozoic climatic change in the Niger delta. *Review of Palaeobotany and Palynology*, *77*(1), 119–127. [https://doi.org/10.1016/0034-6667\(93\)90060-8](https://doi.org/10.1016/0034-6667(93)90060-8)
- Mörs, T. (2002). Biostratigraphy and paleoecology of continental Tertiary vertebrate faunas in the lower rhine Embayment (NW-Germany). *Netherlands Journal of Geosciences*, *81*(2), 177–183. <https://doi.org/10.1017/S0016774600022411>
- Mourik, A. A., Bijkerk, J. F., Cascella, A., Hüsing, S. K., Hilgen, F. J., Lourens, L. J., & Turco, E. (2010). Astronomical tuning of the La Vedova high cliff section (Ancona, Italy) - implications of the middle Miocene climate transition for Mediterranean sapropel formation. *Earth and Planetary Science Letters*, *297*, 249–261. <https://doi.org/10.1016/j.epsl.2010.06.026>
- Mucina, L., & Geldenhuys, C. J. (2006). *The vegetation of South Africa, Lesotho and Swaziland*. Pretoria: South African National Biodiversity Institute. <http://hdl.handle.net/20.500.11937/11564>
- Mudelsee, M., Bickert, T., Lear, C. H., & Lohmann, G. (2014). Cenozoic climate changes: A review based on time series analysis of marine benthic $\delta^{18}\text{O}$ records. *Reviews of Geophysics*, *52*, 333–374. <https://doi.org/10.1002/2013RG000440>
- Mudie, P. J., De Vernal, A., & Head, M. J. (1990). Neogene to recent Palynostratigraphy of circum-arctic basins: Results of ODP leg 104, Norwegian sea, leg 105, Baffin Bay, and DSDP site 611, Irminger sea. In Bliel, U., & Thiede, J. (Eds.) *Geological history of the polar oceans: Arctic versus antarctic* (pp. 609–646). https://doi.org/10.1007/978-94-009-2029-3_33
- Mudie, P. J., Fensome, R. A., Rochon, A., & Bakrač, K. (2019). The dinoflagellate cysts *Thalassiphora subreticulata* n. sp. and *Thalassiphora balcanica*: Their taxonomy, ontogenetic variation and evolution. *Palynology*, *44*(2), 237–269. <https://doi.org/10.1080/01916122.2019.1567614>
- Nairn, M. G., Lear, C. H., Sosdian, S. M., Bailey, T. R., & Beavington-Penney, S. (2021). Tropical sea surface temperatures following the middle Miocene climate transition from laser-ablation ICP-MS analysis of glassy foraminifera. *Paleoceanography and Paleoclimatology*, *36*, e2020PA004165. <https://doi.org/10.1029/2020PA004165>
- Nakov, T., Beaulieu, J. M., & Alverson, A. J. (2018). Accelerated diversification is related to life history and locomotion in a hyperdiverse lineage of microbial eukaryotes (Diatoms, Bacillariophyta). *New Phytologist*, *219*, 462–473. <https://doi.org/10.1111/nph.15137>
- Neumann, F. H., & Bamford, M. K. (2015). Shaping of modern southern African biomes: Neogene vegetation and climate changes. *Transactions of the Royal Society of South Africa*, *70*(3), 195–212. <https://doi.org/10.1080/0035919X.2015.1072859>
- Nielsen, S. N., & Glodny, J. (2009). Early Miocene subtropical water temperatures in the southeast Pacific. *Palaeogeography Palaeoclimatology Palaeoecology*, *280*(3–4), 480–488. <https://doi.org/10.1016/j.palaeo.2009.06.035>
- Nisancioglu, K. H., Raymo, M. E., & Stone, P. H. (2003). Reorganization of Miocene deep water circulation in response to the shoaling of the Central American Seaway. *Paleoceanography*, *18*(1), 6–1. <https://doi.org/10.1029/2002PA000767>
- O'Brien, C. L., Foster, G. L., Martínez-Botí, M. A., Abell, R., Rae, J. W., & Pancost, R. D. (2014). High sea surface temperatures in tropical warm pools during the Pliocene. *Nature Geoscience*, *7*(8), 606–611. <https://doi.org/10.1038/ngeo2194>
- O'Dea, A., Lessios, H. A., Coates, A. G., Eytan, R. I., Restrepo-Moreno, S. A., Cione, A. L., et al. (2016). formation of the isthmus of Panama. *Science Advances*, *2*(8), e1600883. <https://doi.org/10.1126/sciadv.1600883>
- Oerlemans, J. (1991). The role of ice sheets in the Pleistocene climate. *Norsk Geologisk Tidsskrift*, *71*, 155–161.
- Oerlemans, J. (2002). Global dynamics of the Antarctic ice sheet. *Climate Dynamics*, *19*, 85–93. <https://doi.org/10.1007/s00382-001-0210-z>
- Ohneiser, C., Florindo, F., Stocchi, P., Roberts, A. P., DeConto, R. M., & Pollard, D. (2015). Antarctic glacio-eustatic contributions to late Miocene Mediterranean desiccation and reflooding. *Nature Communications*, *6*, 8765. <https://doi.org/10.1038/ncomms9765>
- Olson, D. M., Dinerstein, E., Wikramanayake, E. D., Burgess, N. D., Powell, G. V. N., Underwood, E. C., et al. (2001). Terrestrial Ecoregions of the world: A new Map of life on Earth. *BioScience*, *51*, 933–938. [https://doi.org/10.1641/0006-3568\(2001\)051\[0933:TEOTWA\]2.0.CO;2](https://doi.org/10.1641/0006-3568(2001)051[0933:TEOTWA]2.0.CO;2)
- Olson, S. L. (1985). Psittaciformes. In D. S. Farner, J. R. King, K. C. Parkes, & C. Kenneth (Eds.), *Avian Biology*, Vol. 8 (pp. 120–121). New York, NY: Academic Press. <https://doi.org/10.1016/B978-0-12-249408-6.X5001-8>
- Opdyke, B. N., & Wilkinson, B. H. (1988). Surface area control of shallow cratonic to deep marine carbonate accumulation. *Paleoceanography*, *3*(6), 685–703. <https://doi.org/10.1029/PA003i06p0685>
- O'Regan, A. M., Williams, C. J., Frey, K. E., & Jakobsson, M. (2011). A Synthesis of the long-term paleoclimatic evolution of the Arctic. *Oceanography*, *24*, 66–80. <https://doi.org/10.5670/oceanog.2011.57>
- Osborne, C. P. (2008). Atmosphere, ecology and evolution: What drove the Miocene expansion of C-4 grasslands?. *Journal of Ecology*, *96*, 35–45. <https://doi.org/10.1111/j.1365-2745.2007.01323.x>
- Osborne, C. P., & Freckleton, R. P. (2009). Ecological selection pressures for C-4 photosynthesis in the grasses. *Proceedings of the Royal Society B: Biological Sciences*, *276*(1663), 1753–1760. <https://doi.org/10.1098/rspb.2008.1762>
- Otero, R. A., Jimenez-Huidobro, P., Soto-Acuña, S., & Yury-Yáñez, R. E. (2014). Evidence of a giant helmeted frog (Australobatrachia, Calyptocephalellidae) from Eocene levels of the Magallanes basin, southernmost Chile. *Journal of South American Earth Sciences*, *55*, 133–140. <https://doi.org/10.1016/j.jsames.2014.06.010>
- Owen-Smith, N. (1987). Pleistocene extinctions: The pivotal role of megaherbivores. *Paleobiology*, *13*(3), 351–362. <https://doi.org/10.1017/S0094837300008927>
- Pagani, M. (2002). The alkenone-CO₂ proxy and ancient atmospheric carbon dioxide. *Philosophical Transactions of the Royal Society of London*, *360*, 609–632. <https://doi.org/10.1098/rsta.2001.0959>
- Pagani, M., Arthur, M. A., & Freeman, K. H. (1999a). Miocene evolution of atmospheric carbon dioxide. *Paleoceanography*, *14*(3), 273–292. <https://doi.org/10.1029/1999PA900006>
- Pagani, M., Arthur, M. A., & Freeman, K. H. (2000). Variations in Miocene phytoplankton growth rates in the southwest Atlantic: Evidence for changes in ocean circulation. *Paleoceanography*, *15*(5), 486–496. <https://doi.org/10.1029/1999PA000484>
- Pagani, M., Freeman, K. H., & Arthur, M. A. (1999b). Late Miocene atmospheric CO₂ concentrations and the expansion of C₄ grasses. *Science*, *285*, 876–879. <https://doi.org/10.1126/science.285.5429.876>
- Pagani, M., Liu, Z., Larivieri, J., & Ravelo, A. C. (2010). High Earth-system climate sensitivity determined from Pliocene carbon dioxide concentrations. *Nature Geoscience*, *3*, 27–30. <https://doi.org/10.1038/ngeo724>

- Pagani, M., Zachos, J. C., Freeman, K. H., Tipple, B., & Bohaty, S. (2005). Marked decline in atmospheric carbon dioxide concentrations during the Paleogene. *Science*, 309(5734), 600–603. <https://doi.org/10.1126/science.1110063>
- Palazzesi, L., & Barreda, V. (2007). Major vegetation trends in the Tertiary of Patagonia (Argentina): A qualitative paleoclimatic approach based on palynological evidence. *Flora-Morphology, Distribution, Functional Ecology of Plants*, 202(4), 328–337. <https://doi.org/10.1016/j.flora.2006.07.006>
- Palazzesi, L., & Barreda, V. (2012). Fossil pollen records reveal a late rise of open-habitat ecosystems in Patagonia. *Nature Communications*, 3(1), 1–6. <https://doi.org/10.1038/ncomms2299>
- Pälike, H., Norris, R. D., Herrle, J. O., Wilson, P. A., Coxall, H. K., Lear, C. H., et al. (2006). The heartbeat of the Oligocene climate system. *Science*, 314, 1894–1898. <https://doi.org/10.1126/science.1133822>
- Parker, W. C., Feldman, A., & Arnold, A. J. (1999). Paleobiogeographic patterns in the morphological diversification of Neogene planktonic foraminifera. *Palaeoogeography Palaeoclimatology Palaeoecology*, 152(1–2), 1–14. [https://doi.org/10.1016/S0031-0182\(99\)00049-8](https://doi.org/10.1016/S0031-0182(99)00049-8)
- Passchier, S., Browne, G., Field, B., Fielding, C. R., Krissek, K., Pekar, S. F., & ANDRILL-SMS Science Team (2011). Early and middle Miocene Antarctic glacial history from the sedimentary facies distribution in the AND-2A drill hole, Ross Sea, Antarctica. *GSA Bulletin*, 123(11–12), 2352–2365. <https://doi.org/10.1130/B30334.1>
- Paul, H. A., Zachos, J. C., Flower, B. P., & Tripati, A. (2000). Orbitally induced climate and geochemical variability across the Oligocene/Miocene boundary. *Paleoceanography*, 15(5), 471–485. <https://doi.org/10.1029/1999PA000443>
- Paxman, G. J. G., Jamieson, S. S. R., Ferraccioli, F., Bentley, M. J., Ross, N., Armadillo, et al. (2018). Bedrock erosion surfaces record former East Antarctic ice sheet extent. *Geophysical Research Letters*, 45, 4114–4123. <https://doi.org/10.1029/2018GL077268>
- Paxman, G. J. G., Jamieson, S. S. R., Hochmuth, K., Gohl, K., Bentley, M. J., Leitchenkov, G., & Ferraccioli, F. (2019). Reconstructions of antarctic topography since the Eocene–Oligocene boundary. *Palaeoogeography Palaeoclimatology Palaeoecology*, 535, 109346. <https://doi.org/10.1016/j.palaeo.2019.109346>
- Pazzaglia, F. J., & Gardner, T. W. (1994). Late Cenozoic flexural deformation of the middle US Atlantic passive margin. *Journal of Geophysical Research: Solid Earth*, 99(B6), 12143–12157. <https://doi.org/10.1038/35021000>
- Pearson, P. N., & Palmer, M. R. (2000). Atmospheric carbon dioxide concentrations over the past 60 million years. *Nature*, 406, 695–699. <https://doi.org/10.1038/35021000>
- Pearson, P. N., Shackleton, N. J., & Hall, M. A. (1997). Stable isotopic evidence for the sympatric divergence of *Globigerinoides trilobus* and *Orbulina universa* (planktonic foraminifera). *Journal of the Geological Society*, 154, 295–302. <https://doi.org/10.1144/gsjgs.154.2.0295>
- Pedersen, V. K., Larsen, N. K., & Egholm, D. L. (2019). The timing of fjord formation and early glaciations in North and Northeast Greenland. *Geology*, 47(7), 682–686. <https://doi.org/10.1130/G46064.1>
- Pekar, S. F., & DeConto, R. M. (2007). High-resolution ice-volume estimates for the early Miocene: Evidence for a dynamic ice sheet in Antarctica. *Palaeoogeography Palaeoclimatology Palaeoecology*, 231(1–2), 101–109. <https://doi.org/10.1016/j.palaeo.2005.07.027>
- Perrin, C. (2002). Tertiary: The emergence of modern reef ecosystems. In Flügel E., Kiessling W. & Golonka J. (Eds.), *Phanerozoic reef patterns*, SEPM, (pp. 587–618), SEPM Special Publication n°72. <https://doi.org/10.2110/pec.02.72.0587>
- Petersen, S. V., & Schrag, D. P. (2015). Antarctic ice growth before and after the Eocene–Oligocene transition: New estimates from clumped isotope paleothermometry. *Paleoceanography*, 30(10), 1305–1317. <https://doi.org/10.1002/2014PA002769>
- Peterson, L. C., Murray, D. W., Ehrmann, W. U., & Hempel, P. (1992). Cenozoic carbonate accumulation and compensation depth changes in the Indian Ocean. *Synthesis of Results from Scientific Drilling in the Indian Ocean*, 70, 311–333. <https://doi.org/10.1029/GM070p0311>
- Pfuhl, H. A., & McCave, I. N. (2007). *The oligocene–Miocene boundary – cause and consequence from a Southern Ocean perspective, deep-time perspectives on climate change: Marrying the signal from computer models and biological proxies*, Micropalaeontological society, special publication, 2. Geological Society of London. <https://doi.org/10.1144/TMS002.17>
- Philander, S. G., & Fedorov, A. V. (2003). Role of tropics in changing the response to Milankovitch forcing some three million years ago. *Paleoceanography*, 18, 1045. <https://doi.org/10.1029/2002PA000837>
- Pierce, E. L., van de Flierdt, T., Williams, T., Hemming, S. R., Cook, C. P., & Passchier, S. (2017). Evidence for a dynamic East Antarctic ice sheet during the mid-Miocene climate transition. *Earth and Planetary Science Letters*, 478, 1–13. <https://doi.org/10.1016/j.epsl.2017.08.011>
- Pierrehumbert, R. (2000). Climate change and the tropical Pacific: The sleeping dragon wakes. *Proceedings of the National Academy of Sciences of the United States of America*, 97(4), 1355–1358. <https://doi.org/10.1073/pnas.97.4.1355>
- Pike, J., & Kemp, A. E. S. (1999). Diatoms mats from Gulf of California: Implications for silica burial and paleoenvironmental interpretation of laminated sediments. *Geology*, 27, 311–314. [https://doi.org/10.1130/0091-7613\(1999\)027<0311:DMIGOC>2.3.CO;2](https://doi.org/10.1130/0091-7613(1999)027<0311:DMIGOC>2.3.CO;2)
- Pimiento, C., Griffin, J. N., Clements, C. F., Silvestro, D., Varela, S., Uhen, M. D., & Jaramillo, C. (2017). The Pliocene marine megafauna extinction and its impact on functional diversity. *Nature Ecology and Evolution*, 1(8), 1100–1106. <https://doi.org/10.1038/s41559-017-0223-6>
- Pineker, P., & Mörs, T. (2011). Neocometes (Rodentia: Platacanthomyiinae) from the early Miocene of Echzell, Germany. *Geobios*, 44(2–3), 279–287. <http://dx.doi.org/10.1016/j.geobios.2010.12.001>
- Pinet, P. R., Popenoe, P., & Nelligan, D. F. (1981). Gulf Stream: Reconstruction of cenozoic flow patterns over the Blake plateau. *Geology*, 9, 266–270. [https://doi.org/10.1130/0091-7613\(1981\)9<266:GSROCF>2.0.CO;2](https://doi.org/10.1130/0091-7613(1981)9<266:GSROCF>2.0.CO;2)
- Planderová, E. (1971). Contribution à l'étude palynologique des sédiments Tertiaires de la Tunisie. *Geologické Práce, Zprávy*, 56, 199–216.
- Polissar, P. J., Rose, C., Uno, K. T., Phelps, S. R., & deMenocal, P. (2019). Synchronous rise of African C₄ ecosystems 10 million years ago in the absence of aridification. *Nature Geoscience*, 12, 657–660. <https://doi.org/10.1038/s41561-019-0399-2>
- Pollard, D., & DeConto, R. (2005). Hysteresis in cenozoic antarctic ice-sheet variations. *Global and Planetary Change*, 45(1–3), 9–21. <https://doi.org/10.1016/j.gloplacha.2004.09.011>
- Pollard, D., DeConto, R. M., & Alley, R. B. (2015). Potential Antarctic Ice Sheet retreat driven by hydrofracturing and ice cliff failure. *Earth and Planetary Science Letters*, 412, 112–121. <https://doi.org/10.1016/j.epsl.2014.12.035>
- Poore, H. R., Samworth, R., White, N. J., Jones, S. M., & McCave, I. N. (2006). Neogene overflow of northern component water at the Greenland-Scotland Ridge. *Geochemistry Geophysics Geosystems*, 7, Q06010. <https://doi.org/10.1029/2005GC001085>
- Porter, A. S., Evans-FitzGerald, C., Yiotis, C., Montañez, I. P., & McElwain, J. C. (2019). Testing the accuracy of new palaeoatmospheric CO₂ proxies based on plant stable carbon isotopic composition and stomatal traits in a range of simulated palaeoatmospheric O₂/CO₂ ratios. *Geochimica et Cosmochimica Acta*, 259, 69–90. <https://doi.org/10.1016/j.gca.2019.05.037>
- Potter, P. E., & Szatmari, P. (2009). Global Miocene tectonics and the modern world. *Earth-Science Reviews*, 96(4), 279–295. <https://doi.org/10.1016/j.earscirev.2009.07.003>
- Poulsen, C. J., Ehlers, T. A., & Insel, N. (2010). Onset of convective rainfall during gradual late Miocene rise of the central Andes. *Science*, 328, 490–493. <https://doi.org/10.1126/science.1185078>

- Poumot, C. (1989). Palynological evidence for eustatic events in the tropical Neogene. *Bulletin des Centres de Recherches Exploration-Production Elf-Aquitaine*, 13(2), 437–453. <https://doi.org/10.12691/aees-3-3-1>
- Pound, M. J., Haywood, A. M., Salzmann, U., & Riding, J. B. (2012). Global vegetation dynamics and latitudinal temperature gradients during the Mid to Late Miocene (15.97–5.33Ma). *Earth-Science Reviews*, 112(1), 1–22. <https://doi.org/10.1016/j.earscirev.2012.02.005>
- Pound, M. J., Haywood, A. M., Salzmann, U., Riding, J. B., Lunt, D. J., & Hunter, S. J. (2011). A Tortonian (late Miocene, 11.61–7.25 Ma) global vegetation reconstruction. *Palaeogeography Palaeoclimatology Palaeoecology*, 300, 29–45. <https://doi.org/10.1016/j.palaeo.2010.11.029>
- Pound, M. J., & Riding, J. B. (2016). Palaeoenvironment, palaeoclimate and age of the Brassington formation (Miocene) of Derbyshire, UK. *Journal of the Geological Society*, 173, 306–319. <https://doi.org/10.1144/jgs2015-050>
- Prasad, V., Strömberg, C. A. E., Leache, A., Samant, B. P., Tang, L., et al. (2011). Late Cretaceous origin of the rice tribe. *Nature Communications*, 2, 480. <https://doi.org/10.1038/ncomms1482>
- Preiss-Daimler, I. V., Henrich, R., & Bickert, T. (2013). The final Miocene carbonate crash in the Atlantic: Assessing carbonate accumulation, preservation and production. *Marine Geology*, 343, 39–46. <https://doi.org/10.1016/j.margeo.2013.06.010>
- Prell, W. L., Murray, D. W., Clemens, S. C., & Anderson, D. M. (1992). Evolution and variability of the Indian ocean summer monsoon: Evidence from the western Arabian Sea drilling program. In R. A. Duncan, D. K. Rea, R. B. Kidd, U. Von Rad, & J. K. Weissel (Eds.), *Synthesis of results from scientific drilling in the Indian Ocean*. American Geophysical Union, Geophysical Monographs <https://doi.org/10.1029/GM070p0447>
- Pyens, N. D. (2017). The ecological rise of whales chronicled by the fossil record. *Current Biology*, 27, R558–R564. <https://doi.org/10.1016/j.cub.2017.05.001>
- Quade, J., Cater, J. M. L., Ojha, T. P., Adam, J., & Harrison, T. M. (1995). Late Miocene environmental change in Nepal and the northern Indian subcontinent; stable isotopic evidence from paleosols. *Geological Society of America Bulletin*, 107(12), 1381–1397.
- Quade, J., & Cerling, T. E. (1995). Expansion of C₄ grasses in the late Miocene of northern Pakistan: Evidence from stable isotopes in paleosols. *Palaeogeography Palaeoclimatology Palaeoecology*, 115(1–2), 91–116. [https://doi.org/10.1016/0031-0182\(94\)00108-K](https://doi.org/10.1016/0031-0182(94)00108-K)
- Quade, J., Leary, R., Dettlinger, M. P., Orme, D., Krupa, A., DeCelles, P. G., et al. (2020). Resetting Southern Tibet: The serious challenge of obtaining primary records of Paleotemperature. *Global and Planetary Change*, 191, 103194. <https://doi.org/10.1016/j.gloplacha.2020.103194>
- Quan, C., Liu, Y. S., & Utescher, T. (2011). Paleogene evolution of precipitation in northeastern China supporting the middle Eocene intensification of the east Asian monsoon. *Palaios*, 26, 743–753. <https://doi.org/10.2110/palo.2011.p11-019>
- Quental, T. B., & Marshall, C. R. (2010). Diversity dynamics: Molecular phylogenies need the fossil record. *Trends in Ecology & Evolution*, 8, 434–441. <https://doi.org/10.1016/j.tree.2010.05.002>
- Rabowsky, D. L., & Sorhannus, U. (2009). Diversity dynamics of marine planktonic diatoms across the Cenozoic. *Nature*, 457, 183–186. <https://doi.org/10.1038/nature07435>
- Raffi, I., Backman, J., Fornaciari, E., Pälike, H., Rio, D., Lourens, L., & Hilgen, F. (2006). A review of calcareous nannofossil astrochronology encompassing the past 25 million years. *Quaternary Science Reviews*, 25, 3113–3137. <https://doi.org/10.1016/j.quascirev.2006.07.007>
- Ramstein, G., Fluteau, F., Besse, J., & Joussaume, S. (1997). Effect of orogeny, plate motion and land–sea distribution on Eurasian climate change over the past 30 million years. *Nature*, 386(6627), 788–795. <https://doi.org/10.1038/386788a0>
- Raymo, M. E., Kozdon, R., Evans, D., Lisiecki, L., & Ford, H. L. (2018). The accuracy of mid-Pliocene $\delta^{18}\text{O}$ -based ice volume and sea level reconstructions. *Earth-Science Reviews*, 177, 291–302. <https://doi.org/10.1016/j.earscirev.2017.11.022>
- Reghellin, D., Dickens, G. R., Coxall, H. K., & Backman, J. (2020). Understanding bulk sediment stable isotope records in the Eastern Equatorial Pacific, from seven million years ago to present-day. *Paleoceanography and Paleoclimatology*, 35(2), pa003586. <https://doi.org/10.1029/2019pa003586>
- Reichenbacher, B., Böhme, M., Heissig, K., Prieto, J., & Kossler, A. (2004). New approach to assess biostratigraphy, paleoecology and past climate in the south German Molasse basin during the early Miocene (Ottangian, Karpatian). *Courier Forschungsinstitut Senckenberg*, 249, 71–89.
- Reichgelt, T., D'Andrea, W. J., & Fox, B. R. S. (2016). Abrupt plant physiological changes in southern New Zealand at the termination of the Mi-1 event reflect shifts in hydroclimate and pCO₂. *Earth and Planetary Science Letters*, 455, 115–124. <http://dx.doi.org/10.1016/j.epsl.2016.09.026>
- Reichgelt, T., Kennedy, E. M., Conran, J. G., Lee, W. G., & Lee, D. E. (2019). The presence of moisture deficits in Miocene New Zealand. *Global and Planetary Change*, 172, 268–277. <https://doi.org/10.1016/j.gloplacha.2018.10.013>
- Reichgelt, T., Kennedy, E. M., Mildenhall, D. C., Conran, J. G., Greenwood, D. R., & Lee, D. E. (2013). Quantitative palaeoclimate estimates for early Miocene southern New Zealand: Evidence from Foulden maar. *Palaeogeography Palaeoclimatology Palaeoecology*, 378, 36–44. <https://doi.org/10.1016/j.palaeo.2013.03.019>
- Reidel, S. P. (2015). The Columbia River basalt group: A flood basalt province in the Pacific Northwest, USA. *Geoscience Canada*, 42, 151–168. <http://dx.doi.org/10.12789/geocanj.2014.41.061>
- Reinink-Smith, L. M., & Leopold, E. B. (2005). Warm climate in the Late Miocene of the south coast of Alaska and the occurrence of Podocarpaceae pollen. *Palynology*, 29, 205–262. <https://www.jstor.org/stable/3687806>
- Reinink-Smith, L. M., Zaborac-Reed, S., & Leopold, E. B. (2018). Clamgulchian (Miocene–Pliocene) pollen assemblages of the Kenai lowland, Alaska, and the persistence of the family Podocarpaceae. *Palynology*, 42, 66–101. <https://doi.org/10.1080/01916122.2017.1310767>
- Renaudie, J. (2016). Quantifying the cenozoic marine diatom deposition history: Links to the C and Si cycles. *Biogeosciences*, 13(21), 6003–6014. <https://doi.org/10.5194/bg-13-6003-2016>
- Renema, W., Bellwood, D. R., Braga, J. C., Bromfield, K., Hall, R., Johnson, K. G., et al. (2008). Hopping Hotspots: Global shifts in marine biodiversity. *Science*, 321, 654–657. <https://doi.org/10.1126/science.1155674>
- Retallack, G. J., & Kirby, M. X. (2007). Middle Miocene global change and paleogeography of Panama. *Palaios*, 22(6), 667–679. <https://doi.org/10.2110/palo.2006.p06-130r>
- Reyes-Bonilla, H., & Jordán-Dahlgren, E. (2017). Caribbean coral reefs: Past, present, and insights into the future. In *Marine animal forests* (pp. 31–32). Cham, Springer Link: Springer. https://doi-org.ezp.sub.su.se/10.1007/978-3-319-21012-4_2
- Rickaby, R., & Halloran, P. (2005). Cool La Niña during the warmth of the Pliocene?. *Science*, 307(5717), 1948–1952. <https://doi.org/10.1126/science.1104666>
- Roberts, C. D., LeGrande, A. N., & Tripathi, A. K. (2009). Climate sensitivity to Arctic seaway restriction during the early Paleogene. *Earth and Planetary Science Letters*, 286(3–4), 576–585. <https://doi.org/10.1016/j.epsl.2009.07.026>
- Rögl, F. (1999). Mediterranean and Paratethys. Facts and hypotheses of an Oligocene to Miocene paleogeography (short overview). *Geologica Carpathica*, 50(4), 339–349.
- Rohling, E. J., Sluijs, A., Dijkstra, H. A., Köhler, P., van de Wal, R. S., von der Heydt, A. S., et al. (2012). Making sense of palaeoclimate sensitivity. *Nature*, 491(7426), 683.

- Rohrman, A., Sachse, D., Mulch, A., Pingel, H., Tofelde, S., Alonso, R. N. & Strecker, M. R. (2016). Miocene orographic uplift forces rapid hydrological change in the southern central Andes. *Scientific Reports*, 6, 35678. <https://doi.org/10.1038/srep35678>
- Rosenberg, R., Kirby, E., Aslan, A., Karlstrom, K., Heizler, M., & Ouimet, W. (2014). Late Miocene erosion and evolution of topography along the western slope of the Colorado Rockies. *Geosphere*, 10(4), 641–663. <https://doi.org/10.1130/GES00989.1>
- Rosenthal, Y., Holbourn, A. E., Kulhanek, D. K., Aiello, I. W., Babila, T. L., Bayon, G., et al. (2018). Western Pacific warm pool. In Y. Rosenthal, A. E. Holbourn, & D. K. Kulhanek (Eds.), *Proceedings of the International Ocean Discovery program*, 363. College Station, TX: International Ocean Discovery Program. <https://doi.org/10.14379/iodp.proc.363.101.2018>
- Rössner, G. E., & Heissig, K. (1999). *The Miocene land mammals of Europe*. Munich: Pfeil.
- Rossouw, L., Stynder, D. D., & Haarhof, P. (2010). Evidence for opal phytolith preservation in the Langebaanweg 'E' Quarry Varswater Formation and its potential for palaeohabitat reconstruction. *South African Journal of Science*, 5, 105223. <https://doi.org/10.4102/sajs.v105i5/6.95>
- Roth-Nebelsick, A., Utescher, T., Mosbrugger, V., Diester-Haass, L., & Walthert, H. (2012). Changes in atmospheric CO₂ concentrations and climate from the late Eocene to early Miocene: Palaeobotanical reconstruction based on fossil floras from Saxony, Germany. *Palaeogeography Palaeoclimatology Palaeoecology*, 205, 43–67. <https://doi.org/10.1016/j.palaeo.2003.11.014>
- Roth, J., Droxler, A. W., & Kameo, K. (2000). The Caribbean carbonate crash at the middle to late Miocene transition: Linkage to the establishment of the modern global ocean conveyor. In R. M. Leckie, H. Sigurdsson, G. D. Acton, & G. Draper (Eds.), *Proceedings of the ocean drilling program, scientific results*. College Station, TX: Ocean Drilling Program. <https://doi.org/10.2973/odp.proc.sr.165.013.2000>
- Roveri, M., Flecker, R., Krijgsman, W., Lofi, J., Lugli, S., Manzi, V., et al. (2014). The Messinian salinity crisis: Past and future of a great challenge for marine sciences. *Marine Geology*, 352, 25–58. <https://doi.org/10.1016/j.margeo.2014.02.002>
- Rowley, D. B., & Garzzone, C. N. (2007). Stable isotope-based paleoaltimetry. *Annual Review of Earth and Planetary Sciences*, 35, 463–508. <https://doi.org/10.1146/annurev.earth.35.031306.140155>
- Royer, D. L. (2001). Stomatal density and stomatal index as indicators of paleoatmospheric CO₂ concentration. *Review of Palaeobotany and Palynology*, 114, 1–28. [https://doi.org/10.1016/S0034-6667\(00\)00074-9](https://doi.org/10.1016/S0034-6667(00)00074-9)
- Ruddiman, W. F., Kutzbach, J. E., & Prentice, I. C. (1997). Testing the climatic effects of orography and CO₂ with general circulation and biome models. In W. F. Ruddiman (Ed.), *Tectonic uplift and climate change* (pp. 204–235). Plenum.
- Ruddiman, W. F., Raymo, M. E., Lamb, H. H., Andrews, J. T., Shackleton, N. J., West, R. G., & Bowen, B. Q. (1988). Northern hemisphere climate regimes during the past 3 Ma: Possible tectonic connections. *Philosophical Transactions of the Royal Society of London B Biological Sciences*, 318, 411–430. <https://www.jstor.org/stable/2396614>
- Ryan, W. B. F. (1973). Geodynamic responses to a two-step model of the Messinian salinity crisis. *Bulletin de la Societe Geologique de France*, 182, 73–78. <https://doi.org/10.2113/gssgfbull.182.2.73>
- Sagoo, N., Valdes, P., Flecker, R., & Gregoire, L. J. (2013). The early Eocene equable climate problem: Can perturbations of climate model parameters identify possible solutions?. *Philosophical Transactions of the Royal Society A: Mathematical, Physical & Engineering Sciences*, 371, 20130123. <https://doi.org/10.1098/rsta.2013.0123>
- Salzmann, U., Dolan, A. M., Haywood, A. M., Chan, W.-L., Voss, J., Hill, D. J., et al. (2013). Challenges in quantifying Pliocene terrestrial warming revealed by data-model discord. *Nature Climate Change*, 3, 969–974. <https://doi.org/10.1038/nclimate2008>
- Sanchez-Villagra, M. R., & Aguilera, O. A. (2006). Neogene vertebrates from Urumaco, Falcón state, Venezuela: Diversity and significance. *Journal of Systematic Palaeontology*, 4(3), 213–220. <https://doi.org/10.1017/S1477201906001829>
- Sangiorgi, F., Bijl, P. K., Passchier, S., Salzmann, U., Schouten, S., McKay, R., et al. (2018). Southern Ocean warming and Wilkes Land ice sheet retreat during the mid-Miocene. *Nature Communications*, 9, 317. <https://doi.org/10.1038/s41467-017-02609-7>
- Sanyal, A., Hemming, N. G., Hanson, G. N., & Broecker, W. S. (1995). Evidence for a higher pH in the glacial ocean from boron isotopes in foraminifera. *Nature*, 373, 324–326. <https://doi.org/10.1038/373234a0>
- Savin, S. M., Abel, L., Barrera, E., Hodell, D., Keller, G., Kennett, J. P., et al. (1985). The evolution of Miocene surface and near-surface marine temperatures: Oxygen isotopic evidence. In J. P. Kennett (Ed.), *The Miocene ocean: Paleoceanography and Biogeography*. Boulder: The Geological Society of America. <https://doi.org/10.1130/MEM163-p49>
- Saylor, J. E., & Horton, B. K. (2014). Nonuniform surface uplift of the Andean plateau revealed by deuterium isotopes in Miocene volcanic glass from southern Peru. *Earth and Planetary Science Letters*, 387, 120–131. <https://doi.org/10.1016/j.epsl.2013.11.015>
- Scheiter, S., Higgins, S. I., Osborne, C. P., Bradshaw, C., Lunt, D., Ripley, B. S., et al. (2012). Fire and fire-adapted vegetation promoted C₄ expansion in the late Miocene. *New Phytologist*, 195(3), 653–666. <https://doi.org/10.1111/j.1469-8137.2012.04202.x>
- Schellnhuber, H. J., Rahmstorf, S., & Winkelmann, R. (2016). Why the right climate target was agreed in Paris. *Nature Climate Change*, 6(7), 649–653. <https://doi.org/10.1038/nclimate3013>
- Scher, H. D., & Martin, E. E. (2008). Oligocene deep water export from the North Atlantic and the development of the Antarctic Circumpolar Current examined with neodymium isotopes. *Paleoceanography*, 23(1), PA1205. <https://doi.org/10.1029/2006PA001400>
- Schmidt, D. N., Lazarus, D., Young, J. R., & Kucera, M. (2006). Biogeography and evolution of body size in marine plankton. *Earth-Science Reviews*, 78(3–4), 239–266. <https://doi.org/10.1016/j.earscirev.2006.05.004>
- Schmidt, D. N., Thierstein, H. R., & Bollmann, J. (2004). The evolutionary history of size variation of planktic foraminiferal assemblages in the Cenozoic. *Palaeogeography Palaeoclimatology Palaeoecology*, 212, 159–180. <https://doi.org/10.1016/j.palaeo.2004.06.002>
- Schneider, G., & Marais, C. (2005). *Passage through time. The Fossils of Namibia*. Windhoek: Gamsberg Macmillan.
- Schubert, B. A., & Jahren, A. H. (2012). The effect of atmospheric CO₂ concentration on carbon isotope fractionation in C₃ land plants. *Geochimica et Cosmochimica Acta*, 96, 29–43. <https://doi.org/10.1016/j.gca.2012.08.003>
- Schubert, B. A., & Jahren, A. H. (2015). Global increase in plant carbon isotope fractionation following the Last Glacial Maximum caused by increase in atmospheric pCO₂. *Geology*, 43, 435–438. <https://doi.org/10.1130/G36467.1>
- Schuster, M., Düringer, P., Ghienne, J.-F., Vignaud, P., Mackaye, H. T., Likius, A., & Brunet, M. (2006). The age of the Sahara desert. *Science*, 311, 821. <https://doi.org/10.1126/science.1120161>
- Scroxton, N., Bonham, S. G., Rickaby, R. E. M., Lawrence, S. H. F., Hermoso, M., & Haywood, A. M. (2011). Persistent el Niño–southern oscillation variation during the Pliocene epoch. *Paleoceanography*, 26, 2. <https://doi.org/10.1029/2010PA002097>
- Semprebon, G. M., Rivals, F., & Janis, C. M. (2019). The role of grass versus Exogenous Abrasives in the Paleodietary patterns of north American ungulates. *Frontiers in Ecology and Evolution*, 7, 65. <https://doi.org/10.3389/fevo.2019.00065>
- Semprebon, G. M., Rivals, F., Solounias, N., & Hulbert, R. C. (2016). Paleodietary reconstruction of fossil horses from the Eocene through Pleistocene of North America. *Palaeogeography, Palaeoclimatology, Palaeoecology*, 442, 110–127. <https://doi.org/10.1016/j.palaeo.2015.11.004>
- Senut, B., & Ségalen, L. (2014). Neogene palaeoenvironments of the Namib desert: A brief synthesis. *Transactions of the Royal Society of South Africa*, 69(3), 205–211. <https://doi.org/10.1080/0035919X.2014.958605>

- Sepulchre, P., Arsouze, T., Donnadiou, Y., Dutay, J.-C., Jaramillo, C., Bras, J. L., et al. (2014). Consequences of shoaling of the Central American Seaway determined from modeling Nd isotopes. *Paleoceanography*, 29(3), 176–189. <https://doi.org/10.1002/2013PA002501>
- Shackleton, N. J., Crowhurst, S. J., Hagelberg, T., Pisias, N. G., & Schneider, D. A. (1995). A new late neogene time scale: Application to leg 138 sites. In N. G. Pisias, L. A. Mayer, T. R. Janecek, A. Palmer-Julson, & T. H. van Andel (Eds.), *Proceedings of the ocean drilling program*. Vol. 138 (pp. 73–110) <https://doi.org/10.2973/odp.proc.sr.138.106.1995>
- Shackleton, N. J., Crowhurst, S. J., Weedon, G. P., & Laskar, J. (1999). Astronomical calibration of Oligocene-Miocene time. *Philosophical Transactions of the Royal Society A, London*, 357, 1907–1929. <https://doi.org/10.1098/rsta.1999.0407>
- Shackleton, N. J., & Hall, M. A. (1997). The late Miocene stable isotope record, Site 926. In N. J. Shackleton, W. B. Curry, C. Richter, & T. J. Bralower (Eds.), *Proceedings of the Ocean Drilling Program, Scientific Results*. http://www-odp.tamu.edu/Publications/154_SR24_CHAP.PDF
- Shackleton, N. J., Hall, M. A., & Pate, D. (1995). Pliocene stable isotope stratigraphy of Site 846. In N. G. Pisias, L. A. Mayer, T. R. Janecek, A. Palmer-Julson, & T. H. van Andel (Eds.), *Proceedings of the ocean drilling program, scientific results 138* (pp. 337–355). Ocean Drilling Program.
- Shakun, J. D., Corbett, L. B., Bierman, P. R., Underwood, K., Rizzo, D. M., & Zimmerman, S. R. (2018). Minimal East Antarctic Ice Sheet retreat onto land during the past eight million years. *Nature*, 588, 284–287. <https://doi.org/10.1038/s41586-018-0155-6>
- Sharp, Z. D., Masson, H., & Lucchini, R. (2005). Stable isotope geochemistry and formation mechanisms of quartz veins; extreme paleolatitudes of the Central Alps in the Neogene. *American Journal of Science*, 305(3), 187–219. <https://doi.org/10.2475/ajs.305.3.187>
- Shevenell, A. E., & Kennett, J. P. (2007). Cenozoic Antarctic cryosphere evolution: Tales from deep-sea sedimentary records. *Deep-Sea Research II*, 54, 2308–2324. <https://doi.org/10.1016/j.dsr2.2007.07.018>
- Shevenell, A. E., Kennett, J. P., & Lea, D. W. (2004). Middle Miocene Southern Ocean cooling and antarctic cryosphere expansion. *Science*, 305(5691), 1766–1770. <https://doi.org/10.1126/science.1100061>
- Shevenell, A. E., Kennett, J. P., & Lea, D. W. (2008). Middle Miocene ice sheet dynamics, deep-sea temperatures, and carbon cycling: A Southern Ocean perspective. *Geochemistry, Geophysics, Geosystems*, 9(2), Q02006. <https://doi.org/10.1029/2007GC001736>
- Si, W., & Rosenthal, Y. (2019). Reduced continental weathering and marine calcification linked to late Neogene decline in atmospheric CO₂. *Nature Geoscience*, 12, 833–838. <https://doi.org/10.1038/s41561-019-0450-3>
- Sibert, E., Norris, R., Cuevas, J., & Graves, L. (2016). Eighty-five million years of Pacific Ocean gyre ecosystem structure: Long-term stability marked by punctuated change. *Proceedings of the Royal Society B: Biological Sciences*, 283, 20160189. <http://dx.doi.org/10.1098/rspb.2016.0189>
- Simon, D., Marzocchi, A., Flecker, R., Lunt, D. J., Hilgen, F. J., & Meijer, P. T. (2017). Quantifying the Mediterranean freshwater budget throughout the late Miocene: New implications for sapropel formation and the Messinian salinity crisis. *Earth and Planetary Science Letters*, 472, 25–37. <https://doi.org/10.1016/j.epsl.2017.05.013>
- Simon, D., Palcu, D., Meijer, P., & Krijgsman, W. (2018). The sensitivity of middle Miocene paleoenvironments to changing marine gateways in Central Europe. *Geology*, 47(1), 35–38. <https://doi.org/10.1130/G45698.1>
- Simon, P., Caratini, C., Charpy, N., & Tissot, C. (1984). Sédimentologie et palynologie du Crétacé terminal et du Tertiaire de la région de Bonoua (Côte d'Ivoire). *Geologie Méditerranéenne*, 11(1), 77–85. <https://doi.org/10.3406/geolm.1984.1291>
- Singh, R. J., Gupta, A. K., & Das, M. (2012). Paleoceanographic significance of deep-sea benthic foraminiferal species diversity at south-eastern Indian Ocean Hole 752A during the Neogene. *Palaeogeography Palaeoclimatology Palaeoecology*, 361–362, 94–103. <http://dx.doi.org/10.1016/j.palaeo.2012.08.008>
- Siqueira, A. C., Morais, R. A., Bellwood, D. R., & Cowman, P. F. (2020). Trophic innovations fuel reef fish diversification. *Nature Communications*, 11, 2669. [10.1038/s41467-020-16498-w](https://doi.org/10.1038/s41467-020-16498-w)
- Sjostrom, D. J., Hren, M. T., Horton, T. W., Waldbauer, J. R., & Chamberlain, C. P. (2006). Stable isotopic evidence for a pre-late Miocene elevation gradient in the Great Plains-Rocky Mountain region, USA. *Geological Society of America Special Papers*, 398, 309–319. [https://doi.org/10.1130/2006.2398\(19\)](https://doi.org/10.1130/2006.2398(19))
- Smart, C. W., Thomas, E., & Ramsay, A. T. S. (2007). Middle-late Miocene benthic foraminifera in a western equatorial Indian Ocean depth transect: Paleoceanographic implications. *Palaeogeography Palaeoclimatology Palaeoecology*, 247, 402–420. <https://doi.org/10.1016/j.palaeo.2006.11.003>
- Smiley, T. M., Hyland, E. G., Cotton, J. M., & Reynolds, R. E. (2018). Evidence of early C₄ grasses, habitat heterogeneity, and faunal response during the Miocene Climatic Optimum in the Mojave Region. *Palaeogeography Palaeoclimatology Palaeoecology*, 490, 415–430. <https://doi.org/10.1016/j.palaeo.2017.11.020>
- Soliman, A., & Riding, J. B. (2017). Late Miocene (Tortonian) gonyaulacacean dinoflagellate cysts from the Vienna basin, Austria. *Review of Palaeobotany and Palynology*, 244, 325–346. <https://doi.org/10.1016/j.revpalbo.2017.02.003>
- Sosdian, S. M., Babila, T. L., Greenop, R., Foster, G. L., & Lear, C. H. (2020). ocean carbon storage across the middle Miocene: A new interpretation for the Monterey event. *Nature Communications*, 11, 134. <https://doi.org/10.1038/s41467-019-13792-0>
- Sosdian, S. M., Greenop, R., Hain, M. P., Foster, G. L., Pearson, P. N., & Lear, C. H. (2018). Constraining the evolution of Neogene ocean carbonate chemistry using the boron isotope pH proxy. *Earth and Planetary Science Letters*, 498, 362–376. <https://doi.org/10.1016/j.epsl.2018.06.017>
- Sosdian, S. M., & Lear, C. H. (2020). Initiation of the Western Pacific warm pool at the middle miocene climate transition? *Paleoceanography and Paleoclimatology*, 35(12). doi.org/10.1029/2020PA003920
- Spicer, R. A. (2017). Tibet, the Himalaya, Asian monsoons and biodiversity – in what ways are they related?. *Plant Diversity*, 39(5), 233–244. <https://doi.org/10.1016/j.pld.2017.09.001>
- Spicer, R. A., Su, T., Valdes, P. J., Farnsworth, A., Wu, F. X., Shi, G., et al. (2020). Why the 'uplift of the Tibetan plateau' is a myth. *National Science Review*, nwa091. <https://doi.org/10.1093/nsr/nwaa091>
- Spicer, R. A., Yang, J., Herman, A. B., Kodrul, T., Maslova, N., Spicer, T. E., et al. (2016). Asian Eocene monsoons as revealed by leaf architectural signatures. *Earth and Planetary Science Letters*, 449, 61–68. <http://dx.doi.org/10.1016/j.epsl.2016.05.036>
- Spray, J. F., Bohaty, S. M., Davies, A., Bailey, I., Romans, B. W., Cooper, M. J., et al. (2019). North Atlantic evidence for a unipolar ice-house climate state at the Eocene–oligocene transition. *Paleoceanography and Paleoclimatology*, 34, 1124–1138. <https://doi.org/10.1029/2019PA003563>
- Srifer, R. L., & Huber, M. (2010). Modeled sensitivity of upper thermocline properties to tropical cyclone winds and possible feedbacks on the hadley circulation. *Geophysical Research Letters*, 37(8), L08704. <https://doi.org/10.1029/2010GL042836>
- Stap, L. B., Knorr, G., & Lohmann, G. (2020). Anti-phased miocene ice volume and CO₂ changes by transient Antarctic ice sheet variability. *Paleoceanography and Paleoclimatology*, 35(11). doi.org/10.1029/2020PA003971

- Stap, L. B., Sutter, J., Knorr, G., Stürz, M., & Lohmann, G. (2019). Transient variability of the Miocene Antarctic ice sheet smaller than equilibrium differences. *Geophysical Research Letters*, *46*(8), 4288–4298. <https://doi.org/10.1029/2019GL082163>
- Stap, L. B., van de Wal, R. S. W., De Boer, B., Bintanja, R., & Lourens, L. J. (2016). The MMCO-EOT conundrum: Same benthic $\delta^{18}\text{O}$, different CO_2 . *Paleoceanography*, *31*(9), 1270–1282. <https://doi.org/10.1002/2016PA002958>
- Stürz, M., Jokat, W., Knorr, G., & Lohmann, G. (2017). Threshold in north Atlantic-arctic ocean circulation controlled by the subsidence of the Greenland-Scotland Ridge. *Nature Communications*, *8*(1), 15681. <https://doi.org/10.1038/ncomms15681>
- Stein, R., Fahl, K., Gierz, P., Niessen, F., & Lohmann, G. (2017). Arctic Ocean sea ice cover during the penultimate glacial and the last interglacial. *Nature Communications*, *8*(1), 373. <https://doi.org/10.1038/s41467-017-00552-1>
- Stein, R., Fahl, K., Schreck, M., Knorr, G., Niessen, F., Forwick, M., et al. (2016). Evidence for ice-free summers in the late Miocene central Arctic Ocean. *Nature Communications*, *7*, 1–13. <https://doi.org/10.1038/ncomms11148>
- Steininger, F. F., Aubry, M.-P., Berggren, W. A., Biolzi, M., Borsetti, A. M., Cartlidge, J. E., et al. (1997). The global Stratotype section and point (GSSP) for the base of the neogene. *Episodes*, *20*(1), 23–28.
- Steinthorsdottir, M., Jardine, P. E., & Rember, W. C. (2020). Near-Future $p\text{CO}_2$ during the hot Miocene Climatic Optimum. *Paleoceanography and Paleoclimatology*, *36*, e2020PA003900. <https://doi.org/10.1029/2020PA003900>
- Steinthorsdottir, M., Vajda, V., & Pole, M. (2019). Significant transient $p\text{CO}_2$ perturbation across the New Zealand Oligocene–Miocene transition recorded by fossil plants. *Palaeogeography Palaeoclimatology Palaeoecology*, *515*, 152–161. <https://doi.org/10.1016/j.palaeo.2018.01.039>
- Steph, S., Tiedemann, R., Prange, M., Groeneveld, J., Nürnberg, D., Reuning, L., et al. (2006). Changes in Caribbean surface hydrography during the Pliocene shoaling of the Central American Seaway. *Paleoceanography*, *21*, 4. <https://doi.org/10.1029/2004PA001092>
- Steph, S., Tiedemann, R., Prange, M., Groeneveld, J., Schulz, M., Timmermann, A., et al. (2010). Early Pliocene increase in thermohaline overturning: A precondition for the development of the modern equatorial Pacific cold tongue. *Paleoceanography*, *25*(2), PA2202. <https://doi.org/10.1029/2008PA001645>
- Steppuhn, A., Micheels, A., Bruch, A. A., Uhl, D., Utescher, T., & Mosbrugger, V. (2007). The sensitivity of ECHAM4/ML to a double CO_2 scenario for the Late Miocene and the comparison to terrestrial proxy data. *Global and Planetary Change*, *57*(3), 189–212. <https://doi.org/10.1016/j.gloplacha.2006.09.003>
- Steppuhn, A., Micheels, A., Geiger, G., & Mosbrugger, V. (2006). Reconstructing the Late Miocene climate and oceanic heat flux using the AGCM ECHAM4 coupled to a mixed-layer ocean model with adjusted flux correction. *Palaeogeography Palaeoclimatology Palaeoecology*, *238*(1), 399–423. <https://doi.org/10.1016/j.palaeo.2006.03.037>
- Stewart, D. R. M., Pearson, P. N., Ditchfield, P. W., & Singano, J. M. (2004). Miocene tropical Indian ocean temperatures: Evidence from three exceptionally preserved foraminiferal assemblages from Tanzania. *Journal of African Earth Sciences*, *40*(3–4), 173–190. <https://doi.org/10.1016/j.jafrearsci.2004.09.001>
- Stewart, K. M. (2001). The freshwater fish of neogene Africa (Miocene–Pleistocene): Systematics and biogeography. *Fish and Fisheries*, *2*(3), 177–230. <https://doi.org/10.1046/j.1467-2960.2001.00052.x>
- Stoll, D. K., Guitian, J., Hernandez-Almeida, I., Mejia, L. M., Phelps, S., Polissar, P., et al. (2019). Upregulation of phytoplankton carbon concentrating mechanisms during low CO_2 glacial periods and implications for the phytoplankton $p\text{CO}_2$ proxy. *Quaternary Science Reviews*, *208*, 1–20. <https://doi.org/10.1016/j.quascirev.2019.01.012>
- Stover, L. E., Brinkhuis, H., Damassa, S. P., de Verteuil, L., Helby, R. J., Monteil, et al. (1996). Chapter 19. Mesozoic–Tertiary dinoflagellates, acritarchs and prasinophytes. In J. Jansoni, & D. C. McGregor (Eds.), *Palynology: Principles and applications*. Vol. 2 (pp. 641–750) American Association of Stratigraphic Palynologists Foundation.
- Strömberg, C. A. E. (2005). Decoupled taxonomic radiation and ecological expansion of open-habitat grasses in the Cenozoic of North America. *Proceedings of the National Academy of Sciences of the United States of America*, *102*(34), 11980–11984. <https://doi.org/10.1073/pnas.0505700102>
- Strömberg, C. A. E. (2006). The evolution of hypsodonty in equids: testing a hypothesis of adaptation. *Paleobiology*, *32*(2), 236–258.
- Strömberg, C. A. E. (2011). Evolution of grasses and grassland ecosystems. *Annual Review of Earth and Planetary Sciences*, *39*, 517–544. <https://doi.org/10.1146/annurev-earth-040809-152402>
- Strömberg, C. A. E., Dunn, R. E., Madden, R. H., Kohn, M. J., & Carlini, A. A. (2013). Decoupling the spread of grasslands from the evolution of grazer-type herbivores in South America. *Nature Communications*, *4*, 1478. <https://doi.org/10.1038/ncomms2508>
- Strömberg, C. A. E., & McInerney, F. A. (2011). The neogene transition from C_3 to C_4 grasslands in north America: Assemblage analysis of fossil phytoliths. *Paleobiology*, *37*, 50–71. <https://doi.org/10.1666/09067.1>
- Strömberg, C. A. E., Werdelin, L., Friis, E. M., & Saraç, G. (2007). The spread of grass-dominated habitats in Turkey and surrounding areas during the Cenozoic: Phytolith evidence. *Palaeogeography Palaeoclimatology Palaeoecology*, *250*(1), 18–49. <https://doi.org/10.1016/j.palaeo.2007.02.012>
- Stults, D. Z., Wagner-Cremer, F., & Axsmith, B. J. (2011). Atmospheric paleo- CO_2 estimates based on *Taxodium distichum* (Cupressaceae) fossils from the Miocene and Pliocene of eastern North America. *Palaeogeography Palaeoclimatology Palaeoecology*, *309*, 327–332. <https://doi.org/10.1016/j.palaeo.2011.06.017>
- Suchéras-Marx, B., & Henderiks, J. (2014). Downsizing the pelagic carbonate factory: Impacts of calcareous nannoplankton evolution on carbonate burial over the past 17 million years. *Global and Planetary Change*, *123*(A), 97–109. <https://doi.org/10.1016/j.gloplacha.2014.10.015>
- Summerhayes, C. P., Prell, W. L., & Emeis, K. C. (1992). Evolution of upwelling systems since the early Miocene. *Geological Society of London Special Publication*, *64*, 1–5. <https://doi.org/10.1144/GSL.SP.1992.064.01.01>
- Sun, J., & Liu, T. (2006). The age of the Taklimakan Desert. *Science*, *312*, 1621. <https://doi.org/10.1126/science.1124616>
- Sun, X., & Wang, P. (2005). How old is the Asian monsoon system? Palaeobotanical records from China. *Palaeogeography Palaeoclimatology Palaeoecology*, *222*(3), 181–222. <https://doi.org/10.1016/j.palaeo.2005.03.005>
- Sun, J., Zhang, Z., & Zhang, L. (2009). New evidence on the age of the Taklimakan Desert. *Geology*, *37*(2), 159–162. <https://doi.org/10.1130/G25338A.1>
- Super, J. R., Thomas, E., Pagani, M., Huber, M., O'Brien, C., & Hull, P. M. (2018). North Atlantic temperature and $p\text{CO}_2$ coupling in the early-middle Miocene. *Geology*, *46*(6), 519–522. <https://doi.org/10.1130/G40228.1>
- Super, J. R., Thomas, E., Pagani, M., Huber, M., O'Brien, C. L., & Hull, P. M. (2020). Miocene Evolution of North Atlantic Sea Surface Temperature. *Paleoceanography and Paleoclimatology*, *35*(5). <https://doi.org/10.1029/2019PA003748>
- Suto, I. (2006). The explosive diversification of the diatom genus *Chaetoceros* across the Eocene/Oligocene and Oligocene/Miocene boundaries in the Norwegian Sea. *Marine Micropaleontology*, *58*, 259–269. <https://doi.org/10.1016/j.marmicro.2005.11.004>

- Tada, R., Zheng, H., & Clift, P. D. (2016). Evolution and variability of the Asian monsoon and its potential linkage with uplift of the Himalaya and Tibetan Plateau. *Progress in Earth and Planetary Science*, 3, 1–26. <https://doi.org/10.1186/s40645-016-0080-y>
- Tang, Z.-H., & Ding, Z.-L. (2013). A palynological insight into the Miocene aridification in the Eurasian interior. *Palaeoworld*, 22(3–4), 77–85. <https://doi.org/10.1016/j.palwor.2013.05.001>
- Tanner, T., Hernández-Almeida, I., Drury, A. J., Guitián, J., & Stoll, H. (2020). Decreasing atmospheric CO₂ during the late miocene cooling. *Paleoceanography and Paleoclimatology*, 35(12), e2020PA003925. <https://doi.org/10.1029/2020PA003925>
- Tauxe, L., & Feakins, S. J. (2020). A reassessment of the chronostratigraphy of late miocene C3–C4 transitions. *Paleoceanography and Paleoclimatology*, 35(7), e2020PA003857. <https://doi.org/10.1029/2020PA003857>
- Taylor, F. J. R., Hoppenrath, M., & Saldarriaga, J. F. (2007). Dinoflagellate diversity and distribution. *Biodiversity & Conservation*, 17(2), 407–418. <https://doi.org/10.1007/s10531-007-9258-3>
- Taylor, S. H., Ripley, B. S., Martin, T., De-Wet, L. A., Woodward, F. I., & Osborne, C. P. (2014). Physiological advantages of C₄ grasses in the field: A comparative experiment demonstrating the importance of drought. *Global Change Biology*, 20(6), 1992–2003. <https://doi.org/10.1111/gcb.12498>
- Tesfamichael, T., Jacobs, B., Tabor, N., Michel, L., Currano, E., Feseha, M., et al. (2017). Settling the issue of “decoupling” between atmospheric carbon dioxide and global temperatures: [CO₂]_{atm} reconstructions across the warming Paleogene–neogene divide. *Geology*, 45(11), 999–1002. <https://doi.org/10.1130/G39048.1>
- Thiede, J., Jessen, C., Knutz, P. C., Kuijpers, A., Mikkelsen, N., Nørgaard-Pedersen, N., & Spielhagen, R. F. (2011). Millions of Years of Greenland ice sheet history recorded in ocean sediments. *Polarforschung*, 80, 141–159. <https://doi.org/10.2312/polarforschung.80.3.141>
- Thomas, D. J., Korty, R., Huber, M., Schubert, J. A., & Haines, B. (2014). Nd isotopic structure of the Pacific Ocean 70–30 Ma and numerical evidence for vigorous ocean circulation and ocean heat transport in a greenhouse world. *Paleoceanography*, 29(5), 454–469. <https://doi.org/10.1002/2013PA002535>
- Thomas, D. J., & Via, R. K. (2007). Neogene evolution of Atlantic thermohaline circulation: Perspective from Walvis Ridge, southeastern Atlantic ocean. *Paleoceanography*, 22(2), PA2212. <https://doi.org/10.1029/2006PA001297>
- Thompson, B., Nilsson, J., Nycander, J., Jakobsson, M., & Döös, K. (2010). Ventilation of the Miocene Arctic Ocean: An idealized model study. *Paleoceanography and Paleoclimatology*, 25(4), 1–19. <https://doi.org/10.1029/2009PA001883>
- Thomasson, J. R., Zakrzewski, R. J., LaGarry, H. E., & Mergen, D. E. (1990). A late Miocene (late early Hemphillian) biota from northwestern Kansas. *National Geographic Research*, 6(2), 231–244. <https://doi.org/10.2307/3627997>
- Tian, J., Ma, X., Zhou, J., Jiang, X., Lyle, M., Shackford, J., & Wilkens, R. (2018). Paleoceanography of the east equatorial Pacific over the past 16 Myr and Pacific–Atlantic comparison: High resolution benthic foraminiferal δ¹⁸O and δ¹³C records at IODP Site U1337. *Earth and Planetary Science Letters*, 499, 185–196. <https://doi.org/10.1016/j.epsl.2018.07.025>
- Tian, J., Yang, M., Lyle, M. W., Wilkens, R., & Shackford, J. K. (2013). Obliquity and long eccentricity pacing of the Middle Miocene climate transition. *Geochemistry Geophysics Geosystems* 14(6), 1740–1755. <https://doi.org/10.1002/ggge.20108>
- Tierney, J. E., Haywood, A. M., Feng, R., Bhattacharya, T., & Otto-Bliesner, B. L. (2019). Pliocene warmth consistent with greenhouse gas forcing. *Geophysical Research Letters*, 46, 9136–9144. <https://doi.org/10.1029/2019GL083802>
- Tipple, B. J., & Pagani, M. (2010). A 35 Myr North American leaf-wax compound-specific carbon and hydrogen isotope record: Implications for C₄ grasslands and hydrologic cycle dynamics. *Earth and Planetary Science Letters*, 299, 250–262. <https://doi.org/10.1016/j.epsl.2010.09.006>
- Todd, J. A., Jackson, J. B. C., Johnson, K. G., Fortunato, H. M., Heitz, A., Alvarez, M., & Jung, P. (2002). The ecology of extinction: Molluscan feeding and faunal turnover in the Caribbean neogene. *Proceedings of the Royal Society B: Biological Sciences*, 269, 571–577. <https://doi.org/10.1098/rspb.2001.1923>
- Tong, J. A., You, Y., Müller, R. D., & Seton, M. (2009). Climate model sensitivity to atmospheric CO₂ concentrations for the middle Miocene. *Global and Planetary Change*, 67(3), 129–140. <https://doi.org/10.1016/j.gloplacha.2009.02.001>
- Trayler, R., Kohn, M. J., Bargo, M. S., Cuitino, J. I., Kay, R. F., Strömberg, C. A. E., & Vizcaino, S. F. (2020). Patagonian aridification at the onset of the mid-miocene climatic optimum. *Paleoceanography and Paleoclimatology*, 35. doi.org/10.1029/2020PA003956
- Tréguer, P., Bowler, C., Moriceau, B., Dutkiewicz, S., Gehlen, M., Aumont, O., et al. (2017). Influence of diatom diversity on the ocean biological carbon pump. *Nature Geoscience*, 11, 27–37. <https://doi.org/10.1038/s41561-017-0028-x>
- Tripathi, A., & Darby, D. (2018). Evidence for ephemeral middle Eocene to early Oligocene Greenland glacial ice and pan-Arctic sea ice. *Nature Communications*, 9(1038). <https://doi.org/10.1038/s41467-018-03180-5>
- Tucholke, B. E., & Mountain, G. S. (1985). Mesozoic and Cenozoic geology of the U.S. Atlantic continental slope and rise. In W. Poag (Ed.), *The Western North Atlantic region of north America* (pp. 293–341). New York, NY: Nostrand Reinhold.
- Turco, E., Hüsing, S., Hilgen, F., Cascella, A., Gennari, R., Iaccarino, S. M., & Sagnotti, L. (2018). Astronomical tuning of the La Vedova section between 16.3 and 15.0 Ma. Implications for the origin of megabeds and the Langhian GSSP. *Newsletters on Stratigraphy*, 50(1), 1–29. <https://doi.org/10.1127/nos/2016/0302>
- Tütken, T., Vennemann, T. W., Janz, H., & Heizmann, E. P. J. (2006). Palaeoenvironment and palaeoclimate of the middle Miocene lake in the Steinheim basin, SW Germany: A reconstruction from C, O, and Sr isotopes of fossil remains. *Palaeoecology Palaoclimatology Palaeoecology*, 241(3–4), 457–491. <https://doi.org/10.1016/j.palaeo.2006.04.007>
- Tziperman, E., & Farrell, B. F. (2009). The Pliocene equatorial temperature—lessons from atmospheric superrotation. *Paleoceanography*, 24, PA1101. <https://doi.org/10.1029/2008PA001652>
- Uenzelmann-Neben, G., & Gruetzner, J. (2018). Chronology of Greenland Scotland Ridge overflow: What do we really know?. *Marine Geology*, 406, 109–118. <https://doi.org/10.1016/j.margeo.2018.09.008>
- Unger, N., & Yue, X. (2014). Strong chemistry-climate feedbacks in the Pliocene. *Geophysical Research Letters*, 41(2), 527–533. <https://doi.org/10.1002/2013GL058773>
- Uno, K. T., Cerling, T. E., Harris, J. M., Kunitatsu, Y., Leakey, M. G., Nakatsukasa, M., & Nakaya, H. (2011). Late Miocene to Pliocene carbon isotope record of differential diet change among East African herbivores. *Proceedings of the National Academy of Sciences of the United States of America*, 108, 6509–6514. <https://doi.org/10.1073/pnas.1018435108>
- Uno, K. T., Polissar, P. J., Jackson, K. E., & deMenocal, P. B. (2016). Neogene biomarker record of vegetation change in eastern Africa. *Proceedings of the National Academy of Sciences of the United States of America*, 113, 6355–6363. <https://doi.org/10.1073/pnas.1521267113>
- Urban, M. A., Nelson, D. M., Jimenez-Moreno, G., Chateaufort, J. J., Pearson, A., & Hu, F. S. (2010). Isotopic evidence of C-4 grasses in southwestern Europe during the early oligocene-middle Miocene. *Geology*, 38, 1091–1094. <https://doi.org/10.1130/g31117.1>
- Utescher, T., Bruch, A. A., Micheels, A., Mosbrugger, V., & Popova, S. (2011). Cenozoic climate gradients in Eurasia—a palaeo-perspective on future climate change?. *Palaeoecology Palaoclimatology Palaeoecology*, 304(3–4), 351–358. <https://doi.org/10.1016/j.palaeo.2010.09.031>

- Utescher, T., Erdei, B., Hably, L., & Mosbrugger, V. (2017). Late Miocene vegetation of the Pannonian basin. *Palaeogeography Palaeoclimatology Palaeoecology*, *467*, 131–148. <https://doi.org/10.1016/j.palaeo.2016.02.042>
- Utescher, T., Mosbrugger, V., & Ashraf, A. R. (2000). Terrestrial climate evolution in northwest Germany over the last 25 million Years. *Palaaios*, *15*(5), 430–449. [https://doi.org/10.1669/0883-1351\(2000\)015<0430:TCEING>2.0.CO;2](https://doi.org/10.1669/0883-1351(2000)015<0430:TCEING>2.0.CO;2)
- van Dam, J. A., & Reichart, G. J. (2009). Oxygen and carbon isotope signatures in late Neogene horse teeth from Spain and application as temperature and seasonality proxies. *Palaeogeography Palaeoclimatology Palaeoecology*, *274*(1–2), 64–81. <https://doi.org/10.1016/j.palaeo.2008.12.022>
- van de Flierdt, T., Griffiths, A. M., Lambelet, M., Little, S. H., Stichel, T., & Wilson, D. J. (2016). Neodymium in the oceans: A global database, a regional comparison and implications for paleoceanographic research. *Philosophical Transactions of the Royal Society A: Mathematical, Physical & Engineering Sciences*, *374*, 2081. <https://doi.org/10.1098/rsta.2015.0293>
- Van Der Burgh, J., Visscher, H., Dilcher, D. L., & Kürschner, W. M. (1993). Paleoatmospheric signatures in Neogene fossil leaves. *Science*, *260*, 1788–1790. <https://doi.org/10.1126/science.260.5115.1788>
- Via, R. K., & Thomas, D. J. (2006). Evolution of Atlantic thermohaline circulation. Early Oligocene onset of deep-water production in the North Atlantic. *Geology*, *34*, 441–444. <https://doi.org/10.1130/G22545.1>
- Vickers-Rich, P., & Rich, T. H. (1993). *Wildlife of Gondwana*. Chatswood: Reed.
- Vieira, M., Pound, M. J., & Pereira, D. I. (2018). The late Pliocene palaeoenvironments and palaeoclimates of the western Iberian Atlantic margin from the Rio Maior flora. *Palaeogeography Palaeoclimatology Palaeoecology*, *495*, 245–258. <https://doi.org/10.1016/j.palaeo.2018.01.018>
- Vincent, E., & Berger, W. H. (1985). Carbon dioxide and polar cooling in the Miocene: The Monterey hypothesis. In W. S. Broecker, & E. T. Sundquist (Eds.), *The carbon cycle and atmospheric CO₂. Natural variations Archaean to present*. Vol. 32 (pp. 455–468). Washington: American Geophysical Union, Geophysical Monograph Series. <https://doi.org/10.1029/GM032p0455>
- Vizcaino, S. F., Kay, R. F., & Bargo, S. (2012). *Early Miocene paleobiology in Patagonia. High-latitude paleocommunities of the Santa Cruz formation*. Cambridge: Cambridge University.
- Volkova, V. S. (2011). Paleogene and Neogene stratigraphy and paleotemperature trend of West Siberia (from palynologic data). *Russian Geology and Geophysics*, *52*(7), 709–716. <https://doi.org/10.1016/j.rgg.2011.06.003>
- von der Heydt, A., & Dijkstra, H. A. (2005). Flow reorganizations in the Panama seaway: A cause for the demise of Miocene corals? *Geophysical Research Letters*, *32*(2), L02609. <https://doi.org/10.1029/2004GL020990>
- von der Heydt, A., & Dijkstra, H. A. (2006). Effect of ocean gateways on the global ocean circulation in the late Oligocene and early Miocene. *Paleoceanography*, *21*(1), PA1011. <https://doi.org/10.1029/2005PA001149>
- von der Heydt, A. S., & Dijkstra, H. A. (2011). The impact of ocean gateways on ENSO variability in the Miocene. *Geological Society Special Publication*, *355*, 305–318. <https://doi.org/10.1144/SP355.15>
- Wade, B. S., Pearson, P. N., Olsson, R. K., Premoli Silva, I., Berggren, W. A., Spezzaferri, S., et al. (2018). Taxonomy, biostratigraphy and diversity of Oligocene and early Miocene planktonic foraminifera. In B. S. Wade et al. (Eds.), *Atlas of Oligocene planktonic foraminifera*. Vol. 46 (pp. 1–28) Cushman Foundation for Foraminiferal Research Special Publication.
- Wan, S., Kürschner, W. M., Cliff, P. D., & Li, T. (2009). Extreme weathering/erosion during the miocene climatic optimum: Evidence from sediment record in the South China Sea. *Geophysical Research Letters*, *36*, 1–5. <https://doi.org/10.1029/2009GL040279>
- Wang, C. S., Dai, J., Zhao, X., Li, Y., Graham, S. A., He, D., et al. (2014). Outward-growth of the Tibetan plateau during the cenozoic: A review. *Tectonics*, *62*(1), 1–43. <https://doi.org/10.1016/j.tecto.2014.01.036>
- Wang, X., Flynn, L. J., & Fortelius, M. (2013). *Neogene terrestrial mammalian Biostratigraphy and chronology of Asia*. New York, NY: Columbia University. <https://doi.org/10.7312/wang15012>
- Wang, Y., Momohara, A., Wang, L., Lebreton-Anberrée, J., & Zhou, Z. (2015). Evolutionary history of atmospheric CO₂ during the late cenozoic from fossilized *Metasequoia* needles. *PLoS ONE*, *10*(7), e013eLocator941. <https://doi.org/10.1371/journal.pone.0130941>
- Wang, W., Zhang, P.-Z., Kirby, E., Wang, L.-H., Zhang, G.-L., Zheng, D.-W., & Chai, C.-Z. (2011). A revised chronology for Tertiary sedimentation in the Sikouzi basin: Implications for the tectonic evolution of the northeastern corner of the Tibetan Plateau. *Tectonophysics*, *505*(1–4), 100–114. <https://doi.org/10.1016/j.tecto.2011.04.006>
- Wara, M., Ravelo, A., & Delaney, M. (2005). Permanent el niño-like conditions during the Pliocene Warm Period. *Science*, *309*(5735), 758–761. <https://doi.org/10.1126/science.1112596>
- Warny, S., Askin, R., Hannah, M., Mohr, B., Raine, J., Harwood, D., et al. (2009). Palynomorphs from a sediment core reveal a sudden remarkably warm Antarctica during the middle Miocene. *Geology*, *37*, 955–958. <https://doi.org/10.1130/G30139A.1>
- Watanabe, T., Suzuki, A., Minobe, S., Kawashima, T., Kameo, K., Minoshima, K., et al. (2011). Permanent El Niño during the Pliocene warm period not supported by coral evidence. *Nature*, *471*, 209–211. <https://doi.org/10.1038/nature09777>
- Wei, K.-Y., & Kennett, J. P. (1986). Taxonomic evolution of Neogene planktonic foraminifera and paleoceanographic relations. *Paleoceanography*, *1*, 67–84. <https://doi.org/10.1029/PA001i001p00067>
- Weller, P., & Stein, R. (2008). Paleogene biomarker records from the central Arctic Ocean (Integrated Ocean Drilling Program Expedition 302): Organic carbon sources, anoxia, and sea surface temperature. *Paleoceanography*, *23*(1), 1–15. <https://doi.org/10.1029/2007PA001472>
- Werdelin, L., & Sanders, W. J. (2010). *Cenozoic mammals of Africa*. Los Angeles, CA: University of California.
- Westerhold, T., Röhl, U., & Laskar, J. (2012). Time scale controversy: Accurate orbital calibration of the early Paleogene. *Geochemistry Geophysics Geosystems*, *13*, Q06015. <https://doi.org/10.1029/2012GC004096>
- Wheeler, E. A., Wiemann, M. C., & Fleagle, J. G. (2007). Woods from the Miocene Bakate Formation, Ethiopia: Anatomical characteristics, estimates of original specific gravity and ecological inferences. *Review of Palaeobotany and Palynology*, *146*(1), 193–207. <https://doi.org/10.1016/j.revpalbo.2007.04.002>
- White, J. M., Ager, T. A., Adam, D. P., Leopold, E. B., Liu, G., Jette, H., & Schweger, C. E. (1997). An 18 million year record of vegetation and climate change in northwestern Canada and Alaska: Tectonic and global climatic correlates. *Palaeogeography Palaeoclimatology Palaeoecology*, *130*(1–4), 293–306. [https://doi.org/10.1016/S0031-0182\(96\)00146-0](https://doi.org/10.1016/S0031-0182(96)00146-0)
- Wilkinson, B. H. (2005). Humans as geologic agents: A deep-time perspective. *Geology*, *33*(3), 161–164. <https://doi.org/10.1130/G21108.1>
- Williams, C. J., Mendell, E. K., Murphy, J., Court, W. M., Johnson, A. H., & Richter, S. L. (2008). Paleoenvironmental reconstruction of a middle Miocene forest from the western Canadian arctic. *Palaeogeography Palaeoclimatology Palaeoecology*, *261*, 160–176. <https://doi.org/10.1016/j.palaeo.2008.01.014>
- Williams, S. T., & Duda, T. F. J. (2008). Did tectonic activity stimulate Oligo–Miocene speciation in the Indo-west pacific?. *Evolution*, *62*, 1618–1634. <https://doi.org/10.1111/j.1558-5646.2008.00399.x>
- Willis, K., & McElwain, J. (2014). *The evolution of plants*. Oxford University Press.

- Wilson, M. E. J., & Rosen, B. R. (1998). Implications of paucity of corals in the Paleogene of SE Asia: plate tectonics or center of origin. In R. Hall, & J. D. Holloway (Eds.), *Biogeography and geological evolution of SE Asia* (pp. 165–195). Leiden: Backhuys Publishers.
- Wolf-Welling, T. C., Cremer, M., O'Connell, S., Winkler, A., & Thiede, J. (1996). Cenozoic Arctic gateway paleoclimate variability: Indications from changes in coarse-fraction composition. In *Proceedings of the Ocean Drilling Program*, Scientific results. National Science Foundation. <https://doi.org/10.2973/odp.proc.sr.151.139.1996>
- Wolfe, J. A. (1985). Distribution of major vegetational types during the Tertiary. In E. T. Sundquist, & W. S. Broecker (Eds.), *The carbon cycle and atmospheric CO₂: natural variations Archean to present*. Vol. 32 (pp. 357–375). Washington, DC: American Geophysical Union. <https://doi.org/10.1029/GM032p0357>
- Wolfe, J. A. (1994). Tertiary climatic changes at middle latitudes of western North America. *Palaeogeography Palaeoclimatology Palaeoecology*, 108(3–4), 195–205. [https://doi.org/10.1016/0031-0182\(94\)90233-X](https://doi.org/10.1016/0031-0182(94)90233-X)
- Wolfe, J. A., Schorn, H. E., Forest, C. E., & Molnar, P. (1997). Paleobotanical evidence for high altitudes in Nevada during the Miocene. *Science*, 276(5319), 1672–1675. <https://doi.org/10.1126/science.276.5319.1672>
- Woodruff, F., & Savin, S. M. (1989). Miocene deepwater oceanography. *Paleoceanography*, 4(1), 87–140. <https://doi.org/10.1029/PA004i001p00087>
- Woodruff, F., & Savin, S. M. (1991). Mid-Miocene isotope stratigraphy in the deep sea: High-resolution correlations, paleoclimatic cycles, and sediment preservation. *Paleoceanography*, 6(6), 755–806. <https://doi.org/10.1029/91PA02561>
- Woodward, F. I. (1987). Stomatal numbers are sensitive to increase in CO₂ from pre-industrial levels. *Nature*, 327, 617–618. <https://doi.org/10.1038/327617a0>
- Worthy, T. H., Handley, W. D., Archer, M., & Hand, S. J. (2016). The extinct flightless mihirungs (Aves, Dromornithidae): Cranial anatomy, a new species, and assessment of Oligo–Miocene lineage diversity. *Journal of Vertebrate Paleontology*, 36(3), e1031345. <https://doi.org/10.1080/02724634.2015.1031345>
- Worthy, T. H., Tennyson, A. J. D., Archer, M., & Scofield, R. P. (2010). First record of Palaelodus (Aves: Phoenicopteriformes) from New Zealand. *Records of the Australian Museum*, 62, 77–88. <https://doi.org/10.3853/j.0067-1975.62.2010.1545>
- Worthy, T. H., Tennyson, A. J. D., & Scofield, R. P. (2011). An early Miocene diversity of parrots (Aves, Strigopidae, Nestorinae) from New Zealand. *Journal of Vertebrate Paleontology*, 31(5), 1102–1116. <https://doi.org/10.1080/02724634.2011.595857>
- Wright, J. D., & Miller, K. G. (1996). Control of north Atlantic deep water circulation by the Greenland-Scotland Ridge. *Paleoceanography*, 11, 157–170. <https://doi.org/10.1029/95PA03696>
- Wright, J. D., Miller, K. G., & Fairbanks, R. G. (1992). Early and middle Miocene stable isotopes: Implications for deepwater circulation and climate. *Paleoceanography*, 7(3), 357–389. <https://doi.org/10.1029/92PA00760>
- Wu, F., Gao, S., Tang, F., Meng, Q., & An, C. (2019). A late Miocene–early Pleistocene palynological record and its climatic and tectonic implications for the Yunnan Plateau, China. *Palaeogeography Palaeoclimatology Palaeoecology*, 530, 190–199. <https://doi.org/10.1016/j.palaeo.2019.05.037>
- Wunsch, C. (2009). A perpetually running ENSO in the Pliocene?. *Journal of Climate*, 22(12), 3506–3510. <https://doi.org/10.1175/2009JCLI2925.1>
- Xu, J.-X., Ferguson, D. K., Li, C.-S., & Wang, Y.-F. (2008). Late Miocene vegetation and climate of the Lühe region in Yunnan, southwestern China. *Review of Palaeobotany and Palynology*, 148, 36–59. <https://doi.org/10.1016/j.revpalbo.2007.08.004>
- Yang, X., Groeneveld, J., Jian, Z., Steinke, S., & Giosan, L. (2020). Middle Miocene Intensification of South Asian Monsoonal Rainfall. *Paleoceanography and Paleoclimatology*, 35(12), e2020PA003853. <https://doi.org/10.1029/2020PA003853>
- Yao, Y.-F., Bruch, A. A., Mosbrugger, V., & Li, C.-S. (2011). Quantitative reconstruction of Miocene climate patterns and evolution in Southern China based on plant fossils. *Palaeogeography Palaeoclimatology Palaeoecology*, 304(3), 291–307. <https://doi.org/10.1016/j.palaeo.2010.04.012>
- You, Y., Huber, M., Müller, R. D., Poulsen, C. J., & Ribbe, J. (2009). Simulation of the middle Miocene climate optimum. *Geophysical Research Letters*, 36, L04702. <https://doi.org/10.1029/2008GL036571>
- Young, J. (1990). Size variation of neogene *Reticulofenestra* coccoliths from Indian ocean DSDP cores. *Journal of Micropaleontology*, 9(1), 71–86. <https://doi.org/10.1144/jm.9.1.71>
- Zachos, J. C., Dickens, G. R., & Zeebe, R. E. (2008). An early Cenozoic perspective on greenhouse warming and carbon-cycle dynamics. *Nature*, 451(7176), 279–283. <https://doi.org/10.1038/nature06588>
- Zachos, J. C., Shackleton, N. J., Revenaugh, J. S., Palike, H., & Flower, B. P. (2001). Climate response to orbital forcing across the Oligocene–Miocene boundary. *Science*, 292(5515), 274–278. <https://doi.org/10.1126/science.1058288>
- Zeeden, C., Hilgen, F. J., Husing, S. K., & Lourens, L. L. (2014). The Miocene astronomical time scale 9–12 Ma: New constraints on tidal dissipation and their implications for paleoclimatic investigations. *Paleoceanography*, 29, 296–307. <https://doi.org/10.1002/2014PA002615>
- Zelenkov, N. V. (2016). The first fossil parrot (Aves, Psittaciformes) from Siberia and its implications for the historical biogeography of Psittaciformes. *Biology Letters*, 12(10), 20160717. <https://doi.org/10.1098/rsbl.2016.0717>
- Zelenkov, N. V., Lavrov, A. V., Startsev, D. B., Vislobokova, I. A., & Lopatin, A. V. (2019). A giant early Pleistocene bird from eastern Europe: Unexpected component of terrestrial faunas at the time of early Homo arrival. *Journal of Vertebrate Paleontology*, 39(2), e1605521. <https://doi.org/10.1080/02724634.2019.1605521>
- Zhai, L., Wan, S., Colin, C., Zhao, D., Ye, Y., Song, Z., et al. (2021). Deep-water formation in the North Pacific during the late Miocene global cooling. *Paleoceanography and Paleoclimatology*, 36, e2020PA003946. <https://doi.org/10.1029/2020PA003946>
- Zhang, Y. G., Henderiks, J., & Liu, X. (2020). Refining the alkenone-*p*CO₂ method II: Toward resolving the physiological parameter 'b'. *Geochimica et Cosmochimica Acta*, 281, 118–134. <https://doi.org/10.1016/j.gca.2020.05.002>
- Zhang, Y. G., Pagani, M., & Liu, Z. (2014). A 12-million-year temperature history of the tropical Pacific Ocean. *Science*, 344(6179), 84–87. <https://doi.org/10.1126/science.1246172>
- Zhang, Y. G., Pagani, M., Liu, Z., Bohaty, S., & DeConto, R. (2013). A 40-million-year history of atmospheric CO₂. *Philosophical Transactions of the Royal Society of London - B*, 371, 20130096. <https://doi.org/10.1098/rsta.2013.0096>
- Zhang, Y. G., Pearson, A., Benthien, A., Dong, L., Huybers, P., Liu, X., & Pagani, M. (2019). Refining the alkenone-*p*CO₂ method I: Lessons from the Quaternary glacial cycles. *Geochimica et Cosmochimica Acta*, 260, 177–191. <https://doi.org/10.1016/j.gca.2019.06.032>
- Zhang, Z., Ramstein, G., Schuster, M., Li, C., Contoux, C., & Yan, Q. (2014). Aridification of the Sahara desert caused by tethys Sea shrinkage during the late Miocene. *Nature*, 513, 401–404. <https://doi.org/10.1038/nature13705>
- Zhang, Z. S., Nisancioglu, K. H., Chandler, M. A., Hayward, A. M., Otto-Bliessner, B. L., Ramstein, G., et al. (2013). Mid-Pliocene Atlantic meridional overturning circulation not unlike modern. *Climate of the Past*, 9(4), 1495–1504. <https://doi.org/10.5194/cp-9-1495-2013>

- Zhou, H., Helliker, B. R., Huber, M., Dicks, A., & Akçay, E. (2018). C₄ photosynthesis and climate through the lens of optimality. *Proceedings of the National Academy of Sciences*, 115(47), 12057–12062. <https://doi.org/10.1073/pnas.1718988115>
- Zhu, J., Poulsen, C. J., & Tierney, J. E. (2019). Simulation of Eocene extreme warmth and high climate sensitivity through cloud feedbacks. *Science Advances*, 5(9), eaax1874. <https://doi.org/10.1126/sciadv.aax1874>